WRDC-TR-89-4027

THERMAL MECHANICAL FATIGUE OF COATED BLADE MATERIALS

J. E. Heine
J. R. Warren
B. A. Cowles

United Technologies Corporation
Pratt & Whitney
Advanced Engineering Operations
P. O. Box 109600, West Palm Beach, Florida 33410-9600

27 June 1989

Final Report for Period 1 August 1984 through 30 September 1988

Materials Laboratory
Wright Research Development Center
Air Force Systems Command
Wright-Patterson Air Force Base, Ohio 45433-6533

UNCLASSIFIED

SECURITY CLASSIFICATION OF THIS PAGE

REPORT DOCUMENTATION PAGE

Form Approved OMB No. 0704-0188

1a. REPORT SECURITY CLASSIFICATION UNCLASSIFIED	1b. RESTRICTIVE MARKINGS NONE
2a. SECURITY CLASSIFICATION AUTHORITY	3. DISTRIBUTION/AVAILABILITY OF REPORT Approved for public release; distribution unlimited
2b. DECLASSIFICATION/DOWNGRADING SCHEDULE	
4. PERFORMING ORGANIZATION REPORT NUMBER(S) P&W/FL/FR-20505	5. MONITORING ORGANIZATION REPORT NUMBER(S) WRDC-TR-89-4027
6a. NAME OF PERFORMING ORGANIZATION United Technologies Corporation Pratt & Whitney/Materials Engineering 6b. OFFICE SYMBOL (If applicable)	7a. NAME OF MONITORING ORGANIZATION Wright Research Development Center
6c. ADDRESS (City, State, and ZIP Code) P.O. Box 109600 West Palm Beach FL 33410-9600	7b. ADDRESS (City, State, and ZIP Code) Materials Laboratory Wright-Patterson AFB, OH 45433-6533 Attn: WRDC/MLLN L.P. Zawada
8a. NAME OF FUNDING/SPONSORING ORGANIZATION WRDC/MLLN 8b. OFFICE SYMBOL (If applicable)	9. PROCUREMENT INSTRUMENT IDENTIFICATION NUMBER F33615-84-C-5027
8c. ADDRESS (City, State, and ZIP Code) Wright-Patterson AFB, Ohio 45433-6533	10. SOURCE OF FUNDING NOS. PROGRAM ELEMENT NO.: 62102F PROJECT NO.: 2420 TASK NO.: 01 WORK UNIT ACCESSION NO.: 55
11. TITLE (Include Security Classification) Thermal Mechanical Fatigue of Coated Blade Materials	
12. PERSONAL AUTHOR(S) J.E. Heine, J.R. Warren, B.A. Cowles	
13a. TYPE OF REPORT Final 13b. TIME COVERED FROM 84-08-01 TO 88-09-30	14. DATE OF REPORT (Year, Month, Day) 1989 June 27 15. PAGE COUNT 193
16. SUPPLEMENTARY NOTATION	

17. COSATI CODES			18. SUBJECT TERMS (Continue on reverse if necessary and identify by block number)
FIELD	GROUP	SUB. GR.	Thermal Mechanical Fatigue, Crack Initiation, Aluminide Coatings, Overlay Coatings, Single Crystal, Life Prediction, TURBINE AIR-FOIL

19. ABSTRACT (Continue on reverse if necessary and identify by block number)

A model capable of predicting thermal mechanical fatigue (TMF) crack initiation and propagation in coated advanced blade materials, with emphasis on crack initiation, was developed and demonstrated. The experimental program included isothermal baseline and TMF tests on one alloy and two coating materials to evaluate the effects of mean stress, frequency, hold periods, and maximum temperature on the TMF life of a coated system.

Task I, Definition of TMF Conditions, was completed using the results of a separately funded program evaluating current and advanced airfoil conditions.

Task II, Alloy/Coating Selection and Isothermal Properties, generated monotonic data for uncoated PWA 1480, freestanding PWA 276 overlay coating, and PWA 275 aluminide coating.

20. DISTRIBUTION/AVAILABILITY OF ABSTRACT ☒ UNCLASSIFIED/UNLIMITED ☐ SAME AS RPT. ☐ DTIC USERS	21. ABSTRACT SECURITY CLASSIFICATION UNCLASSIFIED

22a. NAME OF RESPONSIBLE INDIVIDUAL	22b. TELEPHONE (Include Area Code)	22c. OFFICE SYMBOL
Jennifer E. Heine	(513) 255-1350	WRDC/MLLN

DD Form 1473, JUN 86 *Previous editions are obsolete.* UNCLASSIFIED

SECURITY CLASSIFICATION OF THIS PAGE

Task III, Experimental Program, used the results of Task I to review and revise the TMF test matrices. Data in argon and air were generated according to these matrices to support the model development.

Task IV, Metallurgical Evaluation, examined the failed specimens of Task III to determine the effect of cycle type and time at elevated temperature on the failure mechanisms in order to determine an environmental effect.

Task V, Model Development, consolidated coated and uncoated TMF data from Task III using the two bar hysteretic energy model. Three interrelated techniques were developed to evaluate the required parameters of the model. The environmental damage parameter, proposed at the outset of this program, was found to be a negligible effect and was discontinued as a viable damage parameter.

Task VI, Model Demonstration, selected two quadrilateral cycles with holds at different temperatures to demonstrate the life prediction capabilities of the two bar hysteretic energy model. Actual cycles to failure fell within $\pm 2.5\times$ of the predicted life.

ACKNOWLEDGEMENTS

Acknowledgement is gratefully given to the following within ME&T for their contribution to this program.

The technicians of the Thermal Mechanical Fatigue Group: DuWayne Brudnicki, Jean Lieske, Marcelino Maldonado, and Douglas Shoemaker. The technicians and engineers of Low Cycle Fatigue, Metallography, Mechanical Properties, and Coatings Development, and for assistance with computer programming, Thomas Watkins.

Special recognition is given for the contributions made by Paul Pejsa and John Wall as Principal Investigators and to Richard Barkalow for the valuable technical assistance in the evaluation and interpretation of failure mechanisms.

TABLE OF CONTENTS

Section			*Page*
1.0		INTRODUCTION AND BACKGROUND	1
	1.1	Introduction	1
2.0		TECHNICAL PROGRAM AND RESULTS	5
	2.1	Definition of TMF Conditions	5
	2.2	Alloy/Coating Selection and Isothermal Properties	13
		2.2.1 Alloy/Coating Selection and Procurement	13
		2.2.2 Isothermal Properties of PWA 286	13
		2.2.3 Isothermal Properties of PWA 275	14
		2.2.4 Coating — Substrate Comparison	16
		2.2.5 Isothermal Properties of PWA 1480	16
	2.3	Thermal Mechanical Fatigue Experimental Program	31
		2.3.1 Task Objectives	31
		2.3.2 Mean Stress Effects	32
		2.3.3 Frequency Effects	32
		2.3.4 Hold Time Effects	33
		2.3.5 Shutdown Cycle Effects	33
		2.3.6 In-Phase Cycles	33
		2.3.7 Quadrilateral Cycles	34
		2.3.8 Temperature Range Effects	34
		2.3.9 Coating Effects	35
		2.3.10 Inert Environment Testing	35
	2.4	Metallurgical Evaluation	75
		2.4.1 Oxidation	75
		2.4.2 Long Exposure Time Effects	75
		2.4.3 Fracture Modes of Air Tests	76
		2.4.4 Inert Environment Effects	76
		2.4.5 Purified Inert Environment Effects	77
		2.4.6 Fracture Modes for Inert Environment Tests	77
		2.4.7 TMF Temperature Range Comparisons for Coated PWA 1480	78
		2.4.8 Substrate Failure Modes	79
		2.4.9 Environment Effect	81
	2.5	Model Development	121
		2.5.1 Modeling Approach	121
		2.5.2 Two-Bar Model	122
		2.5.3 Hysteretic Energy	124
		2.5.4 Incremented Inelastic Strain Technique	125
		2.5.5 Plastic Strain Balancing Technique	125
		2.5.6 Simplified Constitutive Technique	126
		2.5.7 Octahedral Normal Stress Factor	127
		2.5.8 Optimum Life Prediction Model	128
	2.6	Model Demonstration	178

TABLE OF CONTENTS (Continued)

Section			*Page*
3.0	DISCUSSION OF RESULTS AND RECOMMENDATIONS	.....	185
	3.1 Model Characteristics	.....	185
	3.2 Life Prediction Model Results	.....	187
	3.3 Model Testing Requirements	.....	188
	3.4 Recommendations	.....	191
4.0	CONCLUSIONS	.....	193
REFERENCES		.....	195

LIST OF ILLUSTRATIONS

Figure		*Page*
1	Typical Distress Areas for Coated Airfoils	2
2	Relationship Between Simple Cycles and Engine Transient Cycles	3
3	Program Plan	3
4	Typical Out-of-Phase TMF Cycle	7
5	Typical Quadrilateral TMF Cycle	8
6	Ductility Versus Temperature for Aluminide and Overlay Coatings	8
7	Creep Rupture Behavior for PWA 1480	9
8	Relaxed Centrifugal Stress Versus Average Metal Temperature. Local Metal Temperature = 927°C (1700°F)	9
9	Relaxed Centrifugal Stress Versus Average Metal Temperature. Local Metal Temperature = 982°C (1800°F)	10
10	Relaxed Centrifugal Stress Versus Average Metal Temperature. Local Metal Temperature = 1038°C (1900°F)	10
11	Relaxed Centrifugal Stress Versus Average Metal Temperature. Local Metal Temperature = 1093°C (2000°F)	11
12	Schematic Hysteresis Loops for a Type 1 TMF Test Showing the Effect of Maximum Temperature	11
13	Range of Relaxed Stress at Tmax TMF Lab Testing and Analytical Predictions	12
14	Mean Coefficient of Thermal Expansion, PWA 276 Bulk Coating Material	18
15	Elastic Modulus Versus Temperature, PWA 276 Bulk Coating Material	19
16	Yield and Ultimate Strength Versus Temperature, PWA 276 Bulk Coating Material	19
17	Monotonic Test Specimen for PWA 275	20
18	Monotonic Tensile Test Curve for PWA 1480 and PWA 275 Coated System ($\leq$49°C$\leq$1200°F)	21
19	Monotonic Tensile Test Curve for PWA 1480 and PWA 275 Coated System ($\leq$871°C/$\leq$1600°F)	21

LIST OF ILLUSTRATIONS (Continued)

Figure		*Page*
20	Extrapolation of the Effective Elastic Modulus of PWA 275 (Includes Coating and Diffusion Layers)	22
21	Effective Elastic Modulus of PWA 275 (Includes Coating and Diffusion Layers)	22
22	Post Test Measurement of Substrate and Coating Thickness	23
23	Representative Longitudinal Cross Section of Monotonic Test Specimen Showing Coating/Substrate System	23
24	Elastic Modulus Comparison of Coating and Substrate Materials	24
25	Ductility Versus Temperature for Aluminide and Overlay Coatings (Data Not Generated Under This Contract)	24
26	Thermal Expansion Data for Aluminide Coatings, Overlay Coatings, and PWA 1480 (Data Not Generated Under This Contract)	25
27	Yield Strength Versus Temperature for PWA 1480, PWA 275, and PWA 276	26
28	Inelastic Strain Versus Stress Range for PWA 1480	27
29	Inelastic Strain Versus Stress Range for PWA 1480 (Representative Data Points)	28
30	Monotonic Tensile Data for PWA 1480	28
31	Inelastic Strain Versus Stress Range for PWA 1480 (0.2% Inelastic Strain)	29
32	Elastic Modulus Data for PWA 1480	29
33	Primary Creep Stress Relaxation Data for PWA 1480	30
34	Primary Creep Stress Relaxation Data With Model for PWA 1480	30
35	Mechanical Strain Range Versus Fatigue Life for All Uncoated PWA 1480 TMF Tests	47
36	Mechanical Strain Range Versus Fatigue Life for All PWA 275 Coated PWA 1480 TMF Tests	47
37	Mechanical Strain Range Versus Fatigue Life for All PWA 286 Coated PWA 1480 TMF Tests	48
38	Controlled Minimum Stress Effects on Uncoated PWA 1480 (Out-of-Phase TMF Cycle, 1 cpm, 427-927°C (800-1700°F))	48

LIST OF ILLUSTRATIONS (Continued)

Figure		*Page*
39	Controlled Minimum Stress Effects on Uncoated PWA 1480 (Out-of-Phase TMF Cycle, 1 cpm, 427-1038°C (800-1900°F))	49
40	Controlled Minimum Stress Effects on Uncoated PWA 1480 (Out-of-Phase TMF Cycle, 0.5 cpm, 427-1093°C (800-2000°F))	49
41	Controlled Minimum Stress Effects on PWA 275 Coated PWA 1480 (Out-of-Phase TMF Cycle, 1 cpm, 427-927°C (800-1700°F))	50
42	Controlled Minimum Stress Effects on PWA 275 Coated PWA 1480 (Out-of-Phase TMF Cycle, 1 cpm, 427-1038°C (800-1900°F))	50
43	Controlled Minimum Stress Effects on PWA 275 Coated PWA 1480 (Out-of-Phase TMF Cycle, 0.5 cpm, 427-1093°C (800-2000°F))	51
44	Controlled Minimum Stress Effects on PWA 286 Coated PWA 1480 (Out-of-Phase TMF Cycle, 1 cpm, 427-927°C (800-1700°F))	51
45	Controlled Minimum Stress Effects on PWA 286 Coated PWA 1480 (Out-of-Phase TMF Cycle, 1 cpm, 427-1038°C (800-1900°F))	52
46	Controlled Minimum Stress Effects on PWA 286 Coated PWA 1480 (Out-of-Phase TMF Cycle, 0.5 cpm, 427-1093°C (800-2000°F))	52
47	Effects of Mean Stress on TMF Mechanical Behavior	53
48	Cyclic Frequency Effects on TMF for Uncoated PWA 1480 (Out-of-Phase Cycle, 427-1093°C (800-1900°F))	53
49	Cyclic Frequency Effects on TMF for PWA 275 Coated PWA 1480 (Out-of-Phase Cycle, 427-1038°C (800-1900°F))	54
50	Cyclic Frequency Effects on TMF for PWA 286 Coated PWA 1480 (Out-of-Phase Cycle, 427-1038°C (800-1900°F))	54
51	Hold Time Effects on TMF for Uncoated PWA 1480 (Type 1 Cycle, 1 cpm, 427-1038°C (800-1900°F))	55
52	Hold Time Effects on TMF for PWA 275 Coated PWA 1480 (Type 1 Cycle, 1 cpm, 427-1038°C (800-1900°F))	55
53	Hold Time Effects on TMF for PWA 286 Coated PWA 1480 (Type 1 Cycle, 1 cpm, 427-1038°C (800-1900°F))	56
54	Typical Out-of-Phase and Shutdown TMF Cycles	56
55	Shutdown Cycle Effect on TMF Testing of Uncoated PWA 1480	57

LIST OF ILLUSTRATIONS (Continued)

Figure		*Page*
56	Shutdown Cycle Effect on TMF Testing of PWA 275 Coated PWA 1480	57
57	Shutdown Cycle Effect on TMF Testing of PWA 286 Coated PWA 1480	58
58	Typical In-Phase Cycle (Type 2 Cycle)	58
59	In-Phase Versus Out-of-Phase Cycles for Uncoated PWA 1480 (1 cpm (427-1038°C (800-1900°F))	59
60	In-Phase Versus Out-of-Phase Cycles for PWA 275 Coated PWA 1480 (1.0 cpm, 427-1038°C (800-1900°F))	59
61	In-Phase Versus Out-of-Phase Cycles for PWA 286 Coated PWA 1480 (1.0 cpm (427-1038°C (800-1900°F))	60
62	Quadrilateral and Out-of-Phase TMF Cycle Descriptions	60
63	Quadrilateral Cycle Comparison for TMF Testing of Uncoated PWA 1480, (0.5 cpm, 427-1093°C (800-2000°F))	61
64	Quadrilateral Cycle Comparison for TMF Testing of PWA 275 Coated PWA 1480, (0.5 cpm, 427-1093°C (800-2000°F))	62
65	Quadrilateral Cycle Comparison for TMF Testing of PWA 286 Coated PWA 1480, (0.5 cpm, 427-1093°C (800-2000°F))	63
66	Quadrilateral Cycle Comparison of All Coating Systems on Coated PWA 1480, (0.5 cpm, 427-1093°C (800-2000°F))	63
67	Effect of Maximum Temperature on the TMF Behavior of Uncoated PWA 1480 (Type 1 Cycle, 1 cpm)	64
68	Effect of Maximum Temperature on the Behavior of PWA 275 Coated PWA 1480 (Type 1 Cycle, 1 cpm)	64
69	Effect of Maximum Temperature on the Behavior of PWA 286 Coated PWA 1480 (Type 1 Cycle, 1 cpm)	65
70	Coating Effects on TMF Testing of PWA 1480 (Type 1 Cycle, 1 cpm, 427-927°C (800-1700°F))	65
71	Coating Effects on TMF Testing of PWA 1480 (Type 1 Cycle, 1 cpm, 427-1037°C (800-1900°F))	66
72	Coating Effects on TMF Testing of PWA 1480 (Type 1 Cycle, .5 cpm, 427-1093°C (800-2000°F))	66

LIST OF ILLUSTRATIONS (Continued)

Figure		*Page*
73	Coating Effects on TMF Testing of PWA 1480 (Shutdown Cycles, 427-1093°C (800-2000°F), 0.3 cpm)	67
74	Coating Effects on TMF Testing of PWA 1480 (Quadrilateral Cycles, 427-1093°C (800-2000°F), 0.5 cpm)	67
75	TMF Test in Progress in Argon Chamber	68
76	Schematic of Inert Environment Gas Purification System	68
77	Inert Environment TMF Test Results for Uncoated PWA 1480 (Various Cycles)	69
78	Inert Environment TMF Test Results for PWA 275 Coated PWA 1480 (Various Cycles)	70
79	Inert Environment TMF Test Results for PWA 286 Coated PWA 1480 (Various Cycles)	71
80	Inert Environment Testing of PWA 1480 (Type 1, 0.6 Strain Range, 800-1900°F, and 1 cpm) (Unless so indicated)	72
81	Inert Environment Testing Within the Scatter of All TMF Tests for Uncoated PWA 1480	73
82	Inert Environment Testing Within the Scatter of All TMF Tests for PWA 275 Coated PWA 1480	73
83	Inert Environment Testing Within the Scatter of All TMF Tests for PWA 286 Coated PWA 1480	74
84	Oxidation Behavior of Nickel-Base Superalloys Showing Initiation and Propagation Stages	82
85	Test Frequency Effect on Microstructure of Uncoated PWA 1480	83
86	Secondary Crack for Uncoated PWA 1480 Initiated on ID (Type 1 Cycle, $\Delta\varepsilon$ = 0.4%, ΔT = 427-1038°C (800-1900°F), 1 cpm, N_f = 41906)	84
87	Secondary Crack for PWA 275 Coated PWA 1480 Initiated on OD (Type 1 Cycle, $\Delta\varepsilon$ = 0.8%, ΔT = 427-1038°C (800-1900°F), 1 cpm, N_f = 718)	85
88	Secondary Crack for PWA 286 Coated PWA 1480 Initiated on OD (Type 1 Cycle, $\Delta\varepsilon$ = 0.6%, ΔT = 427-1038°C (800-1900°F), 1 cpm, N_f = 4729)	86

LIST OF ILLUSTRATIONS (Continued)

Figure		*Page*
89	Typical Surface Oxidation of Uncoated PWA 1480 Tested In Air Type 1, ΔT = 427-1038°C (800-1900°F), $\Delta\varepsilon$ = 0.4%, 1 cpm N_f = 41906)	87
90	Secondary Crack for Uncoated PWA 1480 Tested in Argon Environment (Type 1 Cycle, $\Delta\varepsilon$ = 0.6%, ΔT ε 427-1038°C (ȣ00-1900°F), 1 cpm, N_f = 9658)	87
91	Secondary Crack for PWA 275 Coated PWA 1480 Tested in Argon Environment (Type 1 Cycle, $\Delta\varepsilon$ = 0.4%, ΔT = 427-1038°C (800-1900°F), 1 cpm, N_f = 26809)	88
92	Metallography of a PWA 275 Coated PWA 1480 LATMF Specimen Tested in Argon (Type 1, ΔT = 800-1900°F, $\Delta\varepsilon$ = 0.6%, 1 cpm, N_f = 5,720)	89
93	Surface Oxidation of Uncoated PWA 1480 Tested in Reduced Partial Pressure Oxygen Environment (≤1.0 ppm) (Type 1, ΔT = 427-1038°C (800-1900°F), $\Delta\varepsilon$ = 0.8%, 1 cpm, N_f = 3069)	90
94	Comparison of Uncoated Internal Diameter Surfaces In Ambient Air and Inert Environment. Test Cycle Was 427-1038°C (800-1900°F) Out-of-Phase TMF, 1 cpm, With No Hold Time For Both Examples (a) Ambient Air Test Showing Extreme Surface Oxidation Indicated By the Rough Texture and Thick Al Depleted Zone (b) Inert Environment Test Showing No Significant Amounts of Oxidation or Depleted Zone .	91
95	Ambient Air Out-of-Phase TMF Test on PWA 275 Coated PWA 1480 (Type 1, 1 cpm, ΔT = 427-1038°C (800-1900°F), $\Delta\varepsilon$ = 0.6%, N_f = 3180)	92
96	Increased Purity Inert Environment Out-of-Phase TMF on PWA 275 Coated PWA 1480 (Type 1, 1 cpm, ΔT = 427-1038°C (800-1900°F), $\Delta\varepsilon$ = 0.6%, N_f = 8000-Contamination) (a) Specimen Gage Section Showing Superficial Discoloration and Two Large Secondary Cracks (Specimen Failure Occurred Out of Gage) (b) Sectioned Photomicrograph of Secondary Crack Shown in View (a). Coating Shows No Discernable Oxidation; However, Secondary Crack Is Oxidized in the Substrate Material (Noncontinuous Alumina Subscale β Arrows)	93
97	Typical Secondary Crack of PWA 275 Coated PWA 1480 in Out-of-Phase Test in Inert Environment (Type 1, 1 cpm). Characterized by Very Tight Crack Propagation into the Substrate	94

LIST OF ILLUSTRATIONS (Continued)

Figure		*Page*
98	Comparison of PWA 275 Coated PWA 1480 Secondary Cracks in Ambient Air and Inert Environment (Cycle Type: Out-of-Phase, 427-1038°C (800-1900°F), 1 cpm, With 30-Second Hold at Tmax) (a) Ambient Air Test Showing Many Large Secondary Cracks (b) Inert Environment Test Showing Smaller, Tighter Secondary Cracks. Note the Orientation of the Eutectic Gamma Prime Strings Indicate the Crystal Axis Could Be Off by Approximately 10°	95
99	Secondary Cracks of Ambient Air Tested PWA 275 Coated PWA 1480 (Cycle Type: Out-of-Phase, 427-1038°C (800-1900°F), 1 cpm, With 30-Second Hold at Tmax). Note Extreme Width of Cracks With Heavy Denuded Zone Along Crack Sides. Both Photographs Have Same Magnification	96
100	Secondary Cracks of Inert Environment Tested PWA 275 Coated PWA 1480 (Cycle Type: Out-of-Phase, 427-1038°C (800-1900°F), 1 cpm, With 30-Second Hold at Tmax). Crack Widths Are Approximately ¼ the Width of the Similar Ambient Air Test (Figure 99). Higher Magnification (Views b and c) Are of Crack Shown on Left Side of View (a)	97
101	Fracture Face of PWA 275 Coated PWA 1480 Specimen Tested in Ambient Air (Cycle Type: Out-of-Phase, 427-1038°C (800-1900°F), 1 cpm, With 30-Second Hold at Tmax). Fracture Face Shows Multiple Thumbnail Origins Covering 10-15% of Specimen Cross-Sectional Area	98
102	Fracture Face of PWA 275 Coated PWA 1480 Specimen Tested in an Inert Environment (Cycle Type: Out-of-Phase, 427-1038°C (800-1900°F), 1 cpm, With 30-Second Hold at Tmax). Fracture Face Shows Extremely Limited Stage II Crack Propagation (Less Than 3% of Specimen Cross-Sectional Area)	98
103	Fracture Morphology of PWA 275 Coated PWA 1480 (Out-of-Phase Cycle, $\Delta\varepsilon$ = 0.6%, 1 cpm, 427-927°C (800-1700°F))	99
104	Fracture Morphology of PWA 286 Coated PWA 1480 (Out-of-Phase Cycle, $\Delta\varepsilon$ = 0.6%, 1 cpm, 427-927°C (800-1700°F))	100
105	Fracture Morphology of PWA 275 Coated PWA 1480 (Out-of-Phase Cycle, $\Delta\varepsilon$ = 0.6%, 0.5 cpm, 427-1093°C (800-2000°F))	101
106	Fracture Morphology of PWA 286 Coated PWA 1480 (Out-of-Phase Cycle, $\Delta\varepsilon$ = 0.6%, 0.5 cpm, 427-1093°C (800-2000°F))	102
107	(111) Octahedron With Corresponding Crystallographic Orientations in Single Crystal PWA 1480	103
108	(111) Octahedral Propagation Observed in PWA 275 Coated PWA 1480 In-Phase TMF Test (427-1038°C/800-1900°F)	104

LIST OF ILLUSTRATIONS (Continued)

Figure		*Page*
109	(111) Crack Propagation Plane Relative to Secondary Orientations Determined From Dendrite Arms (Photographs are Oriented With Respect to One Another)	105
110	(111) Octahedral Overstress Planes Observed in PWA 1480 Out-of-Phase TMF Test (427-1038°C/800-1900°F)	106
111	(111) Octahedral Overstress β Plane A	107
112	(111) Octahedral Overstress β Plane B	107
113	Typical Fracture Surface Side View for Type 1 Cycle, Uncoated PWA 1480 ($\Delta\varepsilon$ = 0.5%, 1 cpm, 427-1038°C (800-1900°F), S/N 2)	108
114	Typical Fracture Surface for Type 1 Cycle, Uncoated PWA 1480 ($\Delta\varepsilon$ = 0.5%, 1 cpm, 427-1038°C (800-1900°F), S/N 2), White Arrow Indicates Origin	109
115	SEM of Fracture Origin Showing Thumbnail for Type 1 Cycle, Uncoated PWA 1480 ($\Delta\varepsilon$ = 0.5%, 1 cpm, 427-1038°C (800-1900°F), S/N 2)	110
116	In-test Surface Conditions for Type 1 and Quadrilateral TMF Cycles	111
117	Typical Fracture Surface Side View for Quadrilateral Cycle PWA 286 Coated PWA 1480, $\Delta\varepsilon$ = (0.7%, 1 cpm, 427-1093°C (800-2000°F), S/N 31)	112
118	Typical Fracture Surface for Quadrilateral Cycle PWA 286 Coated PWA 1480, ($\Delta\varepsilon$ = 0.7%, 1 cpm, 427-1093°C (800-2000°F), S/N 31)	112
119	Typical Fracture Surface Showing Thumbnail Initiation for Quadrilateral Cycle, PWA 286 Coated PWA 1480 ($\Delta\varepsilon$ = 0.7%, 0.5 cpm, 427-1093°C (800-1900°F), S/N 31)	113
120	Typical Scale/Metal Interface for Uncoated PWA 1480, (Quadrilateral Cycle, $\Delta\varepsilon$ = 0.7%, ΔT = 427-1093°C (800-2000°F), 0.5 cpm)	114
121	Secondary Crack Along Octahedral Plane for Uncoated PWA 1480, (Quadrilateral Cycle, $\Delta\varepsilon$ = 1.05%, ΔT = 427-1093°C (800-2000°F), 0.5 cpm)	115
122	Complete Aluminide Coating (PWA 275) Loss Experienced on Quadrilateral Cycle (PWA 1480, $\Delta\varepsilon$ = 0.7%, 0.5 cpm, 427-1093°C (800-2000°F))	116
123	Initiation of Coating Degradation in PWA 275 Coated PWA 1480 (Quadrilateral Cycle, $\Delta\varepsilon$ = 0.7%, ΔT = 427-1093°C (800-2000°F), 0.5 cpm, S/N 11)	117

LIST OF ILLUSTRATIONS (Continued)

Figure		*Page*
124	Severe Bulk Substrate Damage Following Coating Spallation in PWA 275 Coated PWA 1480 (Quadrilateral Cycle, $\Delta\varepsilon$ = 0.7%, ΔT = 427-1093°C (800-2000°F),0.5 cpm, S/N 11)	118
125	Fracture Morphology of Overlay Coated (PWA 286) PWA 1480, Quadrilateral Cycle, (S/N 31, $\Delta\varepsilon$ = 0.7%, 0.5 cpm, 427-1093°C (800-2000°F))	119
126	Preferential Oxidation of the Beta-NiAl Phase in the PWA 286 Overlay Coating Which Contributes to Crack Propagation Into the Substrate Quadrilateral Cycle, (S/N 31, $\Delta\varepsilon$ = 0.7%, 0.5 cpm, 427-1093°C (800-2000°F))	120
127	TMF Life Prediction Data Input File	132
128	Computer Cycle Type Formats	133
129	Program Structure	134
130	Hysteretic Energy with Octahedral Normal Stress Factor Versus Cycles to Failure for PWA 1480, Strain Control LCF, $\Delta\varepsilon$ = 0.5-1.5%, 427°C (800°F), 760°C (1400°F), and 982°C (1800°F) from F33165-82-C-5109	135
131	Thermal Strains Produced in the Coating as a Result of Thermal Expansion Mismatch	136
132	Mechanically Applied Strain on the Coating/Substrate System	137
133	Ductility Versus Temperature for Aluminide and Overlay Coatings (Data Not Generated Under this Contract)	137
134	Stress Versus Strain Plot of PWA 275 Coating on PWA 1480 Substrate (Out-of-Phase Cycle, 427-1038°C (800-1900°F), $\Delta\varepsilon$ = 0.6%)	138
135	Stress Versus Strain Plot of PWA 275 Coating on PWA 1480 Substrate (Quadrilateral Cycle, 427-1093°C (800-2000°F), $\Delta\varepsilon$ = 0.7%)	138
136	Stress Versus Strain Plot of PWA 286 Coating on PWA 1480 Substrate (Out-of-Phase Cycle, 427-1038°C (800-1900°F), $\Delta\varepsilon$ = 0.6%)	139
137	Stress Versus Strain Plot of PWA 286 Coating on PWA 1480 Substrate (Quadrilateral Cycle, 427-1093°C (800-2000°F), $\Delta\varepsilon$ = 0.7%)	139
138	Coating Hysteresis Loops for PWA 275 Coating, Out-of-Phase Cycles, 0.8% Strain Range and Various Temperatures	140
139	Coating Hysteresis Loops for PWA 286 Coating, Out-of-Phase Cycles, 0.8% Strain Range and Various Temperatures	140

LIST OF ILLUSTRATIONS (Continued)

Figure		*Page*
140	Coating Hysteresis Loops for PWA 275 Coating, Out-of-Phase Cycles, 427-1037°C (800-1900°F) Temperature Range and Various Strain Ranges	141
141	Coating Hysteresis Loops for PWA 286 Coating, Out-of-Phase Cycles, 427-1038°C (800-1900°F) Temperature Range and Various Strain Ranges	141
142	Inelastic Strain Versus Cycles to Failure for Uncoated PWA 1480, All TMF Data (Incremented Inelastic Strain Method)	142
143	Inelastic Strain Versus Cycles to Failure for PWA 275 Coated PWA 1480, All TMF Data (Incremented Inelastic Strain Method)	142
144	Inelastic Strain Versus Cycles to Failure for PWA 286 Coated PWA 1480, All TMF Data	143
145	Hysteretic Energy Approach	143
146	Inelastic Strain Calculation (Incremented Inelastic Strain Method)	144
147	Substrate Hysteretic Energy Damage Function Versus Cycles to Failure, Uncoated PWA 1480, Incremented Inelastic Strain Method, Observed Tensile Stress from Test Data	145
148	Substrate Hysteretic Energy Damage Function Versus Cycles to Failure, Aluminide Coated (PWA 275) PWA 1480, Incremented Inelastic Strain Method, Observed Tensile Stress from Test Data	146
149	Substrate Hysteretic Energy Damage Function Versus Cycles to Failure, Overlay Coated (PWA 286) PWA 1480, Incremented Inelastic Strain Method, Observed Tensile Stress from Test Data	147
150	Substrate Hysteretic Energy Damage Function Versus Cycles to Failure, Uncoated PWA 1480, Incremented Inelastic Strain Method, Simplified Constitutive Tensile Stress	158
151	Substrate Hysteretic Energy Damage Function Versus Cycles to Failure, Aluminide Coated (PWA 275) PWA 1480, Incremented Inelastic Strain Method, Simplified Constitutive Tensile Stress	149
152	Substrate Hysteretic Energy Damage Function Versus Cycles to Failure, Overlay Coated (PWA 286) PWA 1480, Incremented Inelastic Strain Method, Simplified Constitutive Tensile Stress	150
153	Damage Parameter, ΔW, Calculation (Plastic Strain Balancing Method)	151

LIST OF ILLUSTRATIONS (Continued)

Figure		*Page*
154	Substrate Hysteretic Energy Damage Function Versus Cycles to Failure, Uncoated PWA 1480, Plastic Strain Balancing Method, Observed Tensile Stress from Test Data	152
155	Substrate Hysteretic Energy Damage Function Versus Cycles to Failure, Aluminide Coated (PWA 275) PWA 1480, Plastic Strain Balancing Method, Observed Tensile Stress from Test Data	153
156	Substrate Hysteretic Energy Damage Function Versus Cycles to Failure, Overlay Coated (PWA 286) PWA 1480, Plastic Strain Balancing Method, Observed Tensile Stress from Test Data	154
157	Substrate Hysteretic Energy Damage Function Versus Cycles to Failure, Uncoated PWA 1480, Plastic Strain Balancing Method for Stress and Strain	155
158	Substrate Hysteretic Energy Damage Function Versus Cycles to Failure, Aluminide Coated (PWA 275) PWA 1480, Plastic Strain Balancing Method for Stress and Strain	156
159	Substrate Hysteretic Energy Damage Function Versus Cycles to Failure, Overlay Coated (PWA 286) PWA 1480, Plastic Strain Balancing Method for Stress and Strain	157
160	Hysteresis Loop Calculation (Simplified Constitutive Method)	158
161	Actual Tensile Stress Versus Predicted Tensile Stress β Uncoated PWA 1480, [001] Orientation (Simplified Constitutive Method)	159
162	Actual Tensile Stress Versus Predicted Tensile Stress β PWA 275 Coated PWA 1480, [001] Orientation (Simplified Constitutive Method)	160
163	Actual Tensile Stress Versus Predicted Tensile Stress β PWA 286 Coated PWA 1480 [001] Orientation (Simplified Constitutive Method)	161
164	Actual Tensile Stress Versus Predicted Tensile Stress β PWA 1480 [111] Orientation, Simplified Constitutive Method (Data not Generated Under Current Contract)	162
165	Life Versus Damage Parameter ΔW, for Uncoated PWA 1480 (Simplified Constitutive Method)	163
166	Hysteretic Energy Damage Function Versus Cycles to Failure for Quadrilateral Cycles, Substrate dW Only (Observed Test Tensile Stress and Incremented Inelastic Strain Method)	164
167	Effective Hysteretic Energy Damage Function Versus Cycles to Failure for Uncoated PWA 1480 [001], Observed Tensile Stress	165

LIST OF ILLUSTRATIONS (Continued)

Figure		*Page*
168	Effective Hysteretic Energy Damage Function Versus Cycles to Failure for Aluminide Coated (PWA 275) PWA 1480 [001], Observed Tensile Stress	166
169	Effective Hysteretic Energy Damage Function Versus Cycles to Failure for Overlay Coated (PWA 286) PWA 1480 [001], Observed Tensile Stress	167
170	Effective Hysteretic Energy Damage Function Versus Cycles to Failure for PWA 1480 [111] With Various Coatings, Observed Tensile Stress	168
171	Effective Hysteretic Energy Damage Function Versus Cycles to Failure for Uncoated PWA 1480 [001], Constitutive Tensile Stress	169
172	Effective Hysteretic Energy Damage Function Versus Cycles to Failure for Aluminide Coated (PWA 275) PWA 1480 [001], Constitutive Tensile Stress	170
173	Effective Hysteretic Energy Damage Function Versus Cycles to Failure for Overlay Coated (PWA 286) PWA 1480 [001], Constitutive Tensile Stress	171
174	Effective Hysteretic Energy Damage Function Versus Cycles to Failure for PWA 1480 [111] With Various Coatings, Constitutive Tensile Stress	172
175	Actual Life Versus Predicted Life for Uncoated PWA 1480 [001] Observed Tensile Stress	172
176	Actual Life Versus Predicted Life for Aluminide Coated (PWA 275) PWA 1480 [001], Observed Tensile Stress	173
177	Actual Life Versus Predicted Life for Overlay Coated (PWA 286) PWA 1480 [001], Observed Tensile Stress	173
178	Actual Life Versus Predicted Life for PWA 1480 [111] With Various Coatings, Observed Tensile Stress	174
179	Actual Life Versus Predicted Life for Uncoated PWA 1480 [001] Constitutive Tensile Stress	174
180	Actual Life Versus Predicted Life for Aluminide Coated (PWA 275) PWA 1480 [001], Constitutive Tensile Stress	175
181	Actual Life Versus Predicted Life for Overlay Coated (PWA 286) PWA 1480 [001], Constitutive Tensile Stress	175
182	Actual Life Versus Predicted Life for PWA 1480 [111] With Various Coatings, Constitutive Tensile Stress	176

LIST OF ILLUSTRATIONS (Continued)

Figure		*Page*
183	Effective Hysteretic Energy Damage Function Versus Cycles to Failure for PWA 1480 With Various Coatings and Orientations, Observed Tensile Stress	176
184	Effective Hysteretic Energy Damage Function Versus Cycles to Failure for PWA 1480 With Various Coatings and Orientations, Constitutive Tensile Stress	177
185	TMF Model Demonstration Cycle 1 — Quadrilateral with Hold at Minimum Strain	180
186	TMF Model Demonstration Cycle 2 — Quadrilateral with Hold at Maximum Temperature	181
187	Demonstration Cycles: Actual Life Versus Predicted Life	182
188	Actual Versus Predicted Stresses for the Demonstration Cycles (Simplified Constitutive Technique)	183

LIST OF TABLES

Table		*Page*
1	Substrate Mechanical Properties	17
2	Coating Mechanical and Physical Properties Test	17
3	Cross-Sectional Area Ratios for Tubular Aluminide Coating Test Specimens (0.0051 cm [0.002-in.] Coating Assumed)	17
4	Elastic Modulus Test Results for PWA 1480/275	18
5	LATMF Test Matrix	36
6	SCTMF Test Matrix	37
7	Uncoated PWA 1480 TMF Test Results	38
8	PWA 1480/275 TMF Test Results	40
9	PWA 1480/286 TMF Test Results	42
10	Uncoated PWA 1480 TMF Test Results	44
11	PWA 1480/275 TMF Test Results	45
12	PWA 1480/286 TMF Test Results	46
13	Regression Results for the Incremented Inelastic Strain Technique	130
14	Regression Results for the Plastic Strain Balancing Technique	130
15	Regression Results for the Final Life Prediction Model $Log_{10}(N_f) = A + B\ Log_{10}(DW_{EFF})$	131
16	Life predictions for the PWA 1480 (001) Model Demonstration	179
17	Actual and Predicted Stresses for the PWA 1480 001 Model Demonstration	180
18	Life Prediction Model Testing Requirements	190

SECTION 1.0

INTRODUCTION AND BACKGROUND

1.1 INTRODUCTION

The most severe cyclic stresses that turbine airfoils encounter are thermally induced by extreme temperature gradients and transients. These thermally induced stresses, which combine with mechanically induced centrifugal and gas bending loads, produce thermal mechanical fatigue (TMF) of the airfoil, typically in locations illustrated in Figure 1. Strain range, temperature, mean stress, frequency and dwell time may all be important parameters affecting TMF life, just as they are for isothermal low cycle fatigue conditions. In addition, the overall cycle shape and phase angle between the cycling temperature and strain greatly affect TMF life. The temperature-strain phase angle may vary from 180 degrees out of phase, for fast transients at thermally responsive airfoil locations such as leading edges, to nearly in-phase for slow transients and less responsive locations, as illustrated in Figure 2. For a basic, simplified TMF cycle where cyclic strains and temperature are 180 degrees out-of-phase, the maximum tensile stress occurs at the minimum temperature. The maximum compressive stress occurs at high temperature, and the resultant creep-relaxation causes further increases in local peak stress at low temperature, which leads to coating cracking, followed by crack growth into the substrate. Blade life prediction for TMF cycles such as these has not, in general, been very successful when based upon isothermally generated laboratory data, and consequently TMF type laboratory data are required for airfoil life predictions.

Advanced military fighter engines in high thrust-to-weight ratio aircraft are subjected to many more rapid throttle movements than previous military or commercial engines. As a result, the turbine airfoils experience many more TMF cycles in these engines, and the cycles may vary considerably from the simple out-of-phase cycle (Type 1) which is currently used as the empirical basis for airfoil TMF life predictions.

Finally, both the airfoil alloys and their protective coatings have advanced dramatically in the past 15 years. The cast nickel-base alloys have progressed from equiaxed microstructure in the 1960's to directionally solidified (DS) materials in the 1970's, and finally to single-crystal alloys in the 1980's, with possibilities for wrought powder alloys in the future. Both the directionally solidified and single-crystal materials are highly anisotropic, which affords opportunities for optimizing properties, but which also complicates analysis for design and life prediction. Coatings have evolved from the original diffusion aluminides to current enhanced ductility aluminides and overlays, and development of thermal-barrier coatings is progressing rapidly. The coating plays a key role in the TMF failure process; consequently, the alloy and coating must be considered a system for TMF life evaluations.

Thermal mechanical fatigue lives are currently predicted on the basis of simple out-of-phase (Type 1 cycle) laboratory tests performed at a variety of strain ranges and maximum temperatures. The results are used for airfoil life prediction, as well as alloy and coating development and selection. Alloys, heat treatments, orientation effects (anisotropy), and coatings are all evaluated for TMF response, principally with the same simple TMF cycle. The laboratory tests are expensive and time consuming, and since the test cycle influences TMF life so strongly, selection of the appropriate cycle shape and test conditions is crucial for accurate assessment of engine service capability.

The objectives of this program were to attain a fundamental understanding of the TMF process and to develop a model capable of predicting thermal mechanical fatigue life for coated turbine airfoil materials over a range of engine representative conditions. Ideally the model

would be capable of predicting both crack initiation and propagation behavior in an anisotropic substrate/coating system for representative strain ranges, mean stresses and/or strains, temperatures, frequencies, hold times, and TMF cycle shapes. In actuality, a model which facilitated accurate life prediction of cycles to initiation of an engineering-size crack for a coating/substrate system with a minimum of experimental tests would represent significant improvement over the current empirical approach. These objectives were achieved under this program.

This program, conducted to meet the objective of developing and demonstrating a TMF life prediction model, was composed of six technical tasks and one reporting task as shown in Figure 3. The technical tasks included an assessment of blade operating conditions, basic substrate and coating property determinations, substantial thermal mechanical fatigue evaluations, metallography and fractography, TMF life model development, and a model demonstration task. The technical approach combined experimental and analytical efforts to develop a fundamental understanding of TMF behavior, principally crack initiation behavior, of coated airfoil materials. The alloy selected for evaluation was cast single-crystal PWA 1480 with both diffusion aluminide and overlay coatings.

The life prediction model selected for development was based on tensile hysteretic energy. This model was selected because it included strain range and mean stress effects explicitly, and had previously been shown to offer promise for TMF life prediction (References 1 and 2). Coating effects were assessed using a simple two-bar model to represent the coating and substrate materials. Both substrate and coating behavior were calculated using simple constitutive models based on isothermal data.

The technical program and results are described on a task-by-task basis in Section 2.0 following.

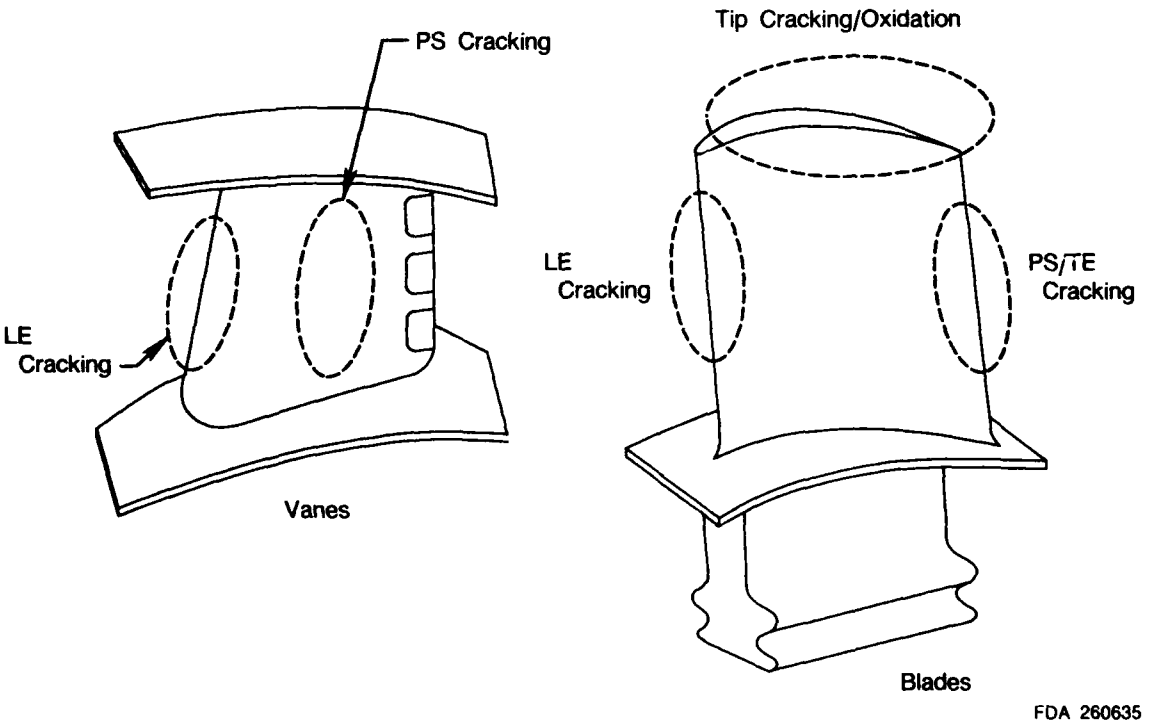

Figure 1. Typical Distress Areas for Coated Airfoils

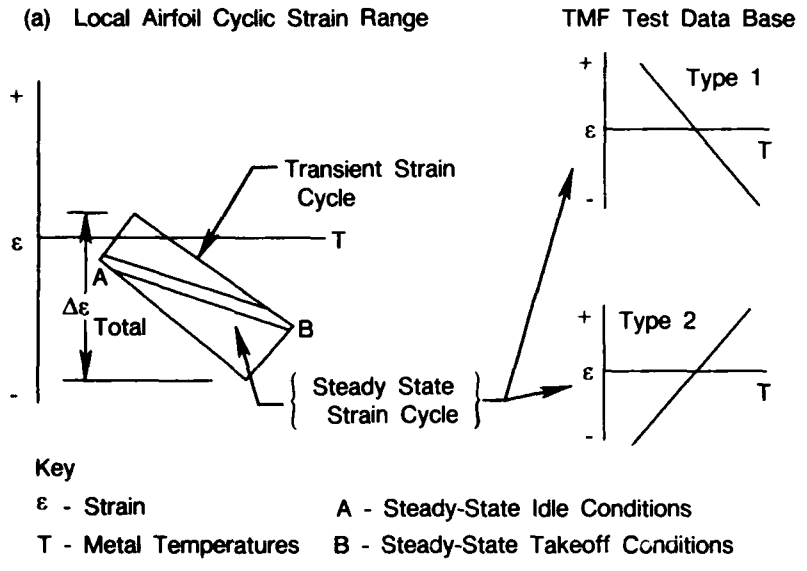

Figure 2. Relationship Between Simple Cycles and Engine Transient Cycles

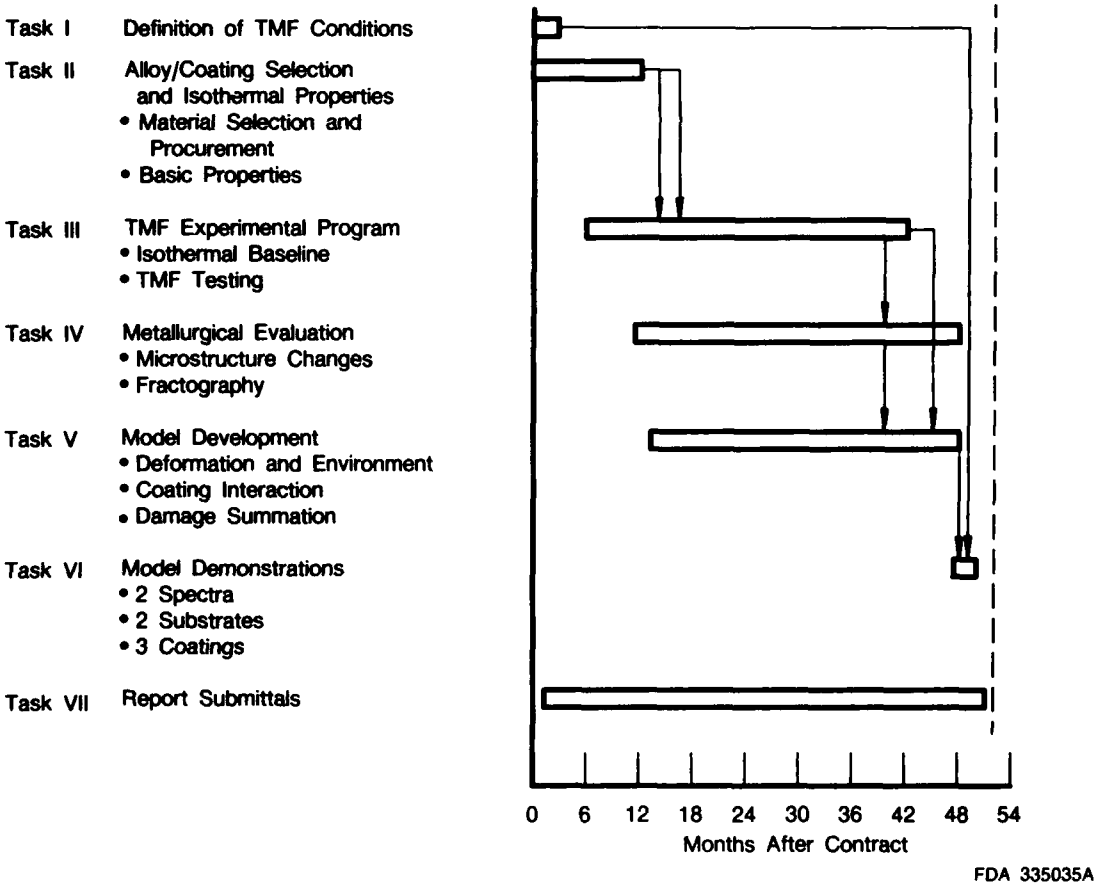

Figure 3. Program Plan

SECTION 2.0

TECHNICAL PROGRAM AND RESULTS

The technical program of this contract was conducted as a seven-task effort outlined below. Program activities are detailed on a task-by-task basis in the following subsections.

Task I — Definition of the thermal mechanical fatigue (TMF) conditions provided typical cycle types for laboratory TMF testing based upon evaluation of conditions expected to be encountered by engine operational blades.

Task II — Determination of the material properties for the alloy/coating system included the alloy and coating selection, alloy procurement, specimen manufacture, and coating and mechanical property testing of specimens under isothermal conditions.

Task III — Definition of the principal variables affecting TMF using the cycles established in Task I. This task generated specimen crack initiation and propagation data with emphasis on the former.

Task IV — Metallurgical evaluation of failed specimens identified the failure modes and mechanisms for selected TMF tests. These findings were utilized in the life prediction model.

Task V — Development of the TMF life prediction model utilized the results of Tasks II, III, and IV to predict crack initiation and propagation behavior for TMF of a constituent system.

Task VI — Demonstration of the TMF life prediction model used specimen TMF testing under selected conditions to verify the model predictions.

Task VII — Submittal of reports and compliance with Contract Data Requirement List (CDRL) Items in accordance with the contract requirements.

2.1 DEFINITION OF TMF CONDITIONS

The results of a separately funded program to evaluate current and advanced airfoil conditions were made available to this program to determine the range of laboratory thermal mechanical fatigue (TMF) test conditions needed to represent the range of engine operating conditions. The parameters that were examined for their effect on TMF behavior and, consequently, fatigue life included cycle type, hold period and frequency, changes in cyclic temperature endpoints, and mean stress.

Two primary cycle types were selected for examination in this study. The majority of testing was performed using the linear out-of-phase strain-temperature (Type 1) cycle shown in Figure 4. This cycle represents an intermediate limit of TMF response in the airfoil and corresponds to a slow transient. The other extreme of TMF response corresponds to a faster transient, which is represented best by an open quadrilateral cycle (Figure 5).

The frequency of a TMF cyclic waveform and hold periods may also have a significant effect on crack initiation life. The effect of either large changes in frequency or extended hold periods on life comprises a mechanical damage component and an environmental damage component. In order to separate these two forms of damage, a number of tests were attempted in

an inert environment. These tests also gave significant insight into the development of the life prediction model. Frequencies ranging from approximately 0.2 to 4 cpm were investigated. The former represents the minimum frequency at which tests can practically be conducted. The latter is near the limit of the testing equipment and approaches actual engine transient time. Hold periods up to 2 minutes in duration were used, representing the upper bound of dwell time in the engine.

Maximum cyclic temperatures of 927°C (1700°F), 1038°C (1900°F), and 1093°C (2000°F) were investigated. The majority of testing was conducted at 1038°C (1900°F). A minimum temperature of 427°C (800°F) was used in all tests since this is typical of in-service throttle excursions. In addition, selected tests were performed using a minimum temperature of approximately 38°C (100°F) to simulate the effect of an engine shutdown cycle. The shutdown cycle had an especially strong effect on the overlay coating, which experienced a continuous loss of ductility as temperature decreased from 427°C (800°F) to room temperature (Figure 6). In contrast, aluminides attained a minimum level of ductility at approximately 649°C (1200°F) and reductions in temperature in a TMF test below 427°C (800°F) did not produce a further debit in cyclic life.

Steady-state stress-temperature relationships have been developed for a range of current and advanced airfoil geometries and operating conditions. This information, combined with relaxed stress-maximum temperature data from past TMF test efforts, has been used to determine the range of TMF stress states that represent the full spectrum of predicted airfoil behavior (Reference 3).

For a given material, lines of constant creep life may be plotted as a function of steady stress and temperature. Figure 7 shows these relationships for PWA 1480. Combining this information with calculated centrifugal stress-average airfoil midspan temperature data results in relationships between creep life, relaxed centrifugal stress, and average metal temperature. Figures 8 through 11 present these relationships for local (i.e., leading edge) airfoil temperatures ranging from 927°C (1700°F) to 1093°C (2000°F), and three current and advanced airfoil geometries.

Current military engine airfoils operate at a midspan centrifugal stress of about 126 MPa (18.3 ksi), and advanced engine airfoils are expected to operate at stresses up to about 207 MPa (30 ksi). For a specified geometry, design life, and average metal temperature, the relaxed centrifugal stress may be calculated for critical locations on the airfoil.

Relaxed stresses observed in the laboratory, however, do not necessarily reflect airfoil behavior. Thermal mechanical fatigue testing has historically been based on cycle definitions in the form of strain-temperature histories. The cycle typically used to generate TMF data is a simple out-of-phase linear strain-temperature waveform (Type 1 cycle). Stress at the maximum temperature gradually relaxes during the shakedown of the specimen. The steady-state stress levels achieved are dependent only on the maximum temperature, creep strength, and the applied strain range. Schematic stress-strain hysteresis loops for a Type 1 cycle test are shown in Figure 12 for two different maximum temperature conditions. The figure shows that a tensile mean stress is developed in the test and increases as a result of stress relaxation at the maximum temperature of the cycle.

An analysis of blades run in a test engine shows that, due to stress redistribution across the airfoil, an all-tensile stress cycle is imposed on the material, as predicted above (Reference 3). At higher temperatures, correspondingly lower tensile mean stresses are predicted. In contrast, the simple cycle laboratory tests have tensile mean stresses which increase with increasing temperature and are significantly lower than predicted values. This difference is due to the ability to include net section and local stresses (at critical locations) in the analysis, while the laboratory test reflects transient strain-temperature effects on a single selected critical location.

A comparison between the relaxed stress at maximum temperature (from Type 1 cycle TMF data generated for PWA 1480) and the results of the analysis is presented in Figure 13 (curves presented show the range of stress at given temperatures). Tests conducted at maximum temperatures ranging from 927°C (1700°F) to 1093°C (2000°F) resulted in relaxed stresses (at the maximum temperature) ranging from an average of −207 MPa (−30 ksi) to an average of −69 MPa (−10 ksi), respectively. In contrast, predicted relaxed stresses decrease from an average of +167 MPa (+24 ksi) to an average of +55 MPa (+8 ksi) over the same temperature range for representative average metal temperatures. The TMF test stress state corresponds more directly to vane applications not subject to centrifugal forces. However, to better represent rotating hardware conditions, the effects of centrifugal loading should be taken into consideration. Tests were conducted to simulate this behavior in the laboratory.

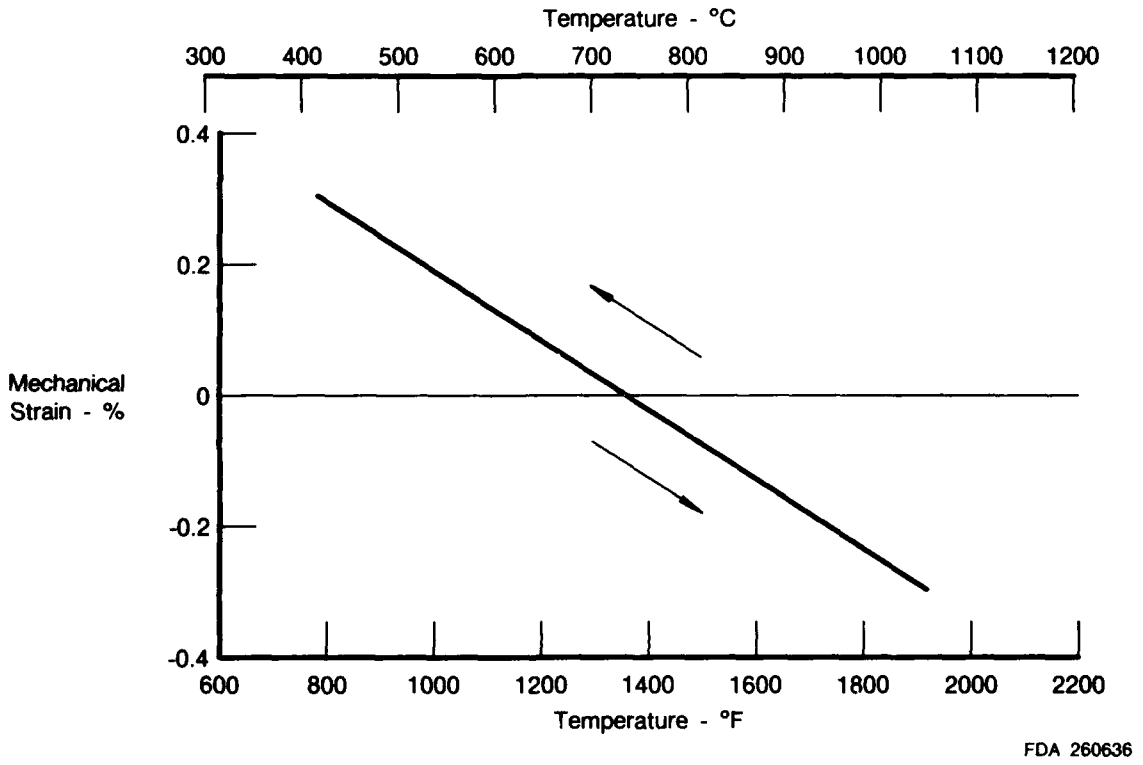

Figure 4. Typical Out-of-Phase TMF Cycle

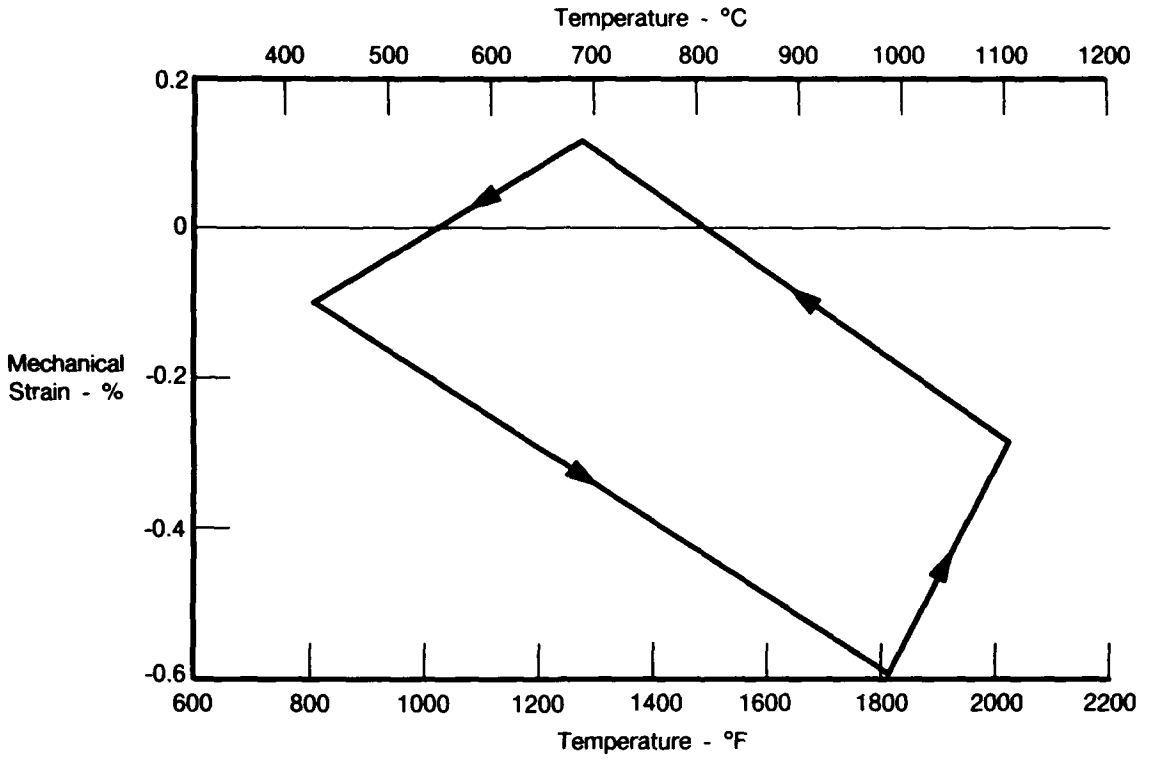

Figure 5. Typical Quadrilateral TMF Cycle

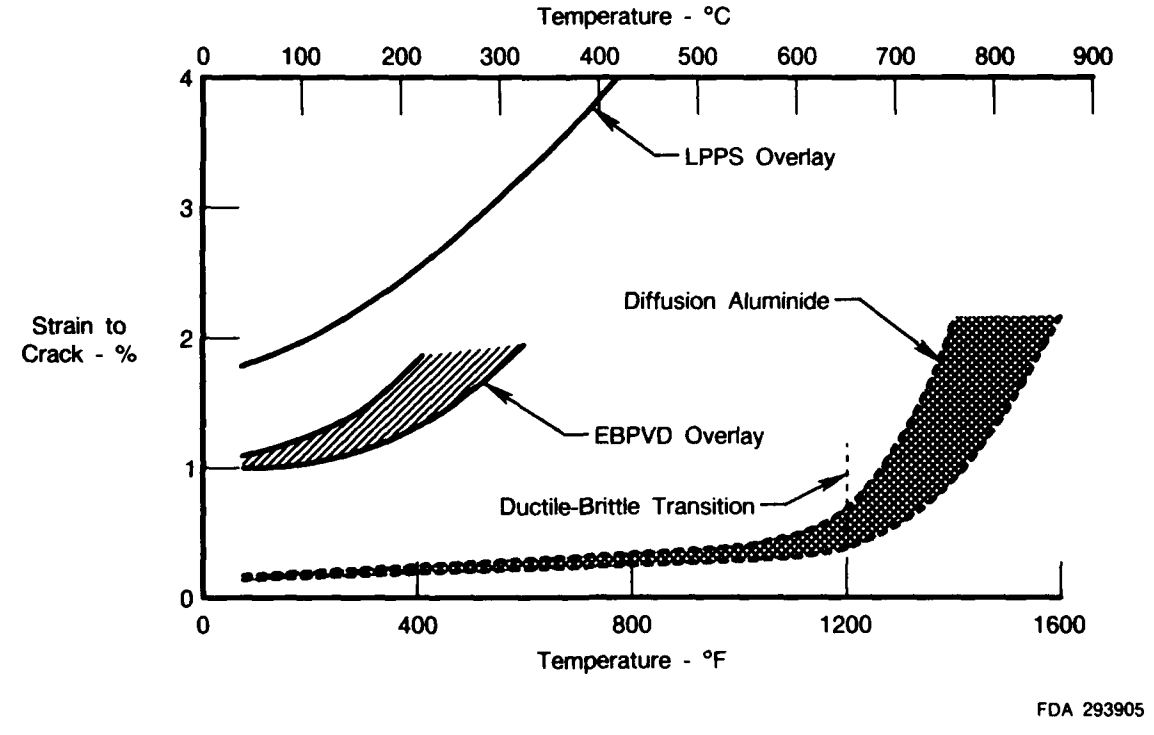

Figure 6. Ductility Versus Temperature for Aluminide and Overlay Coatings

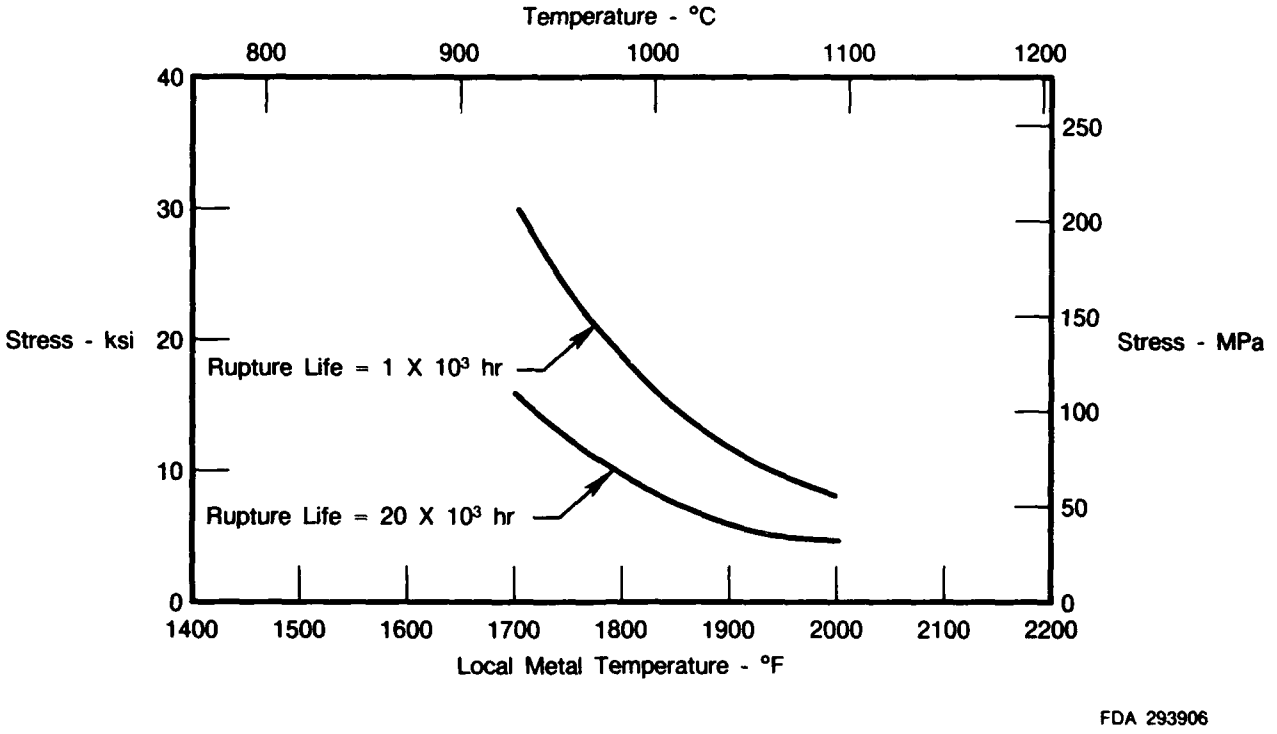

Figure 7. Creep Rupture Behavior for PWA 1480

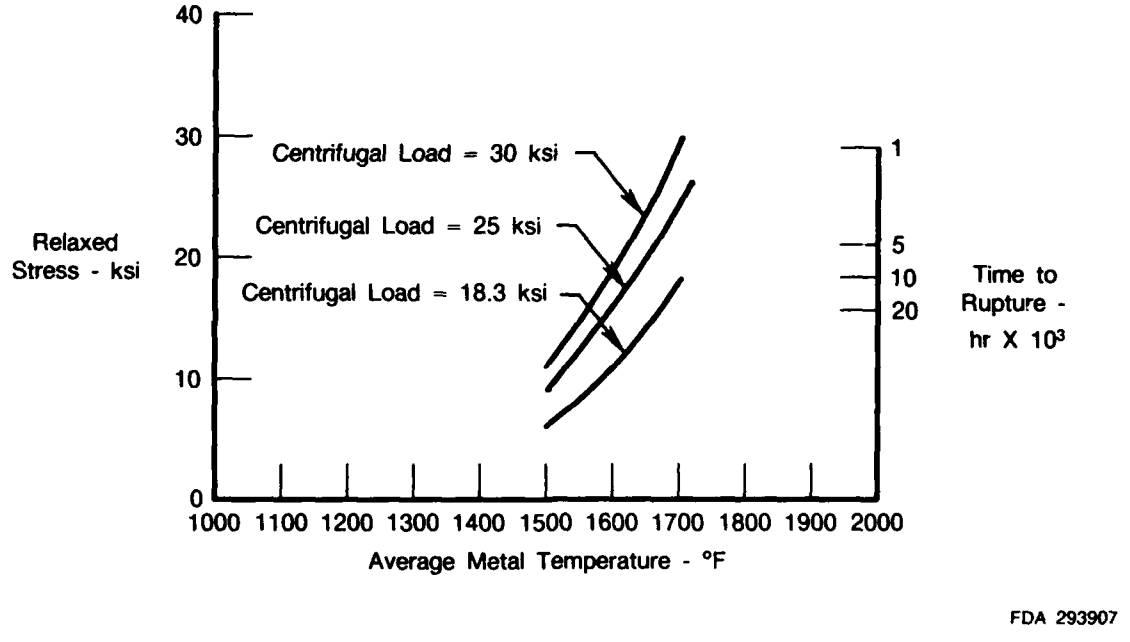

Figure 8. Relaxed Centrifugal Stress Versus Average Metal Temperature. Local Metal Temperature = 927°C (1700°F)

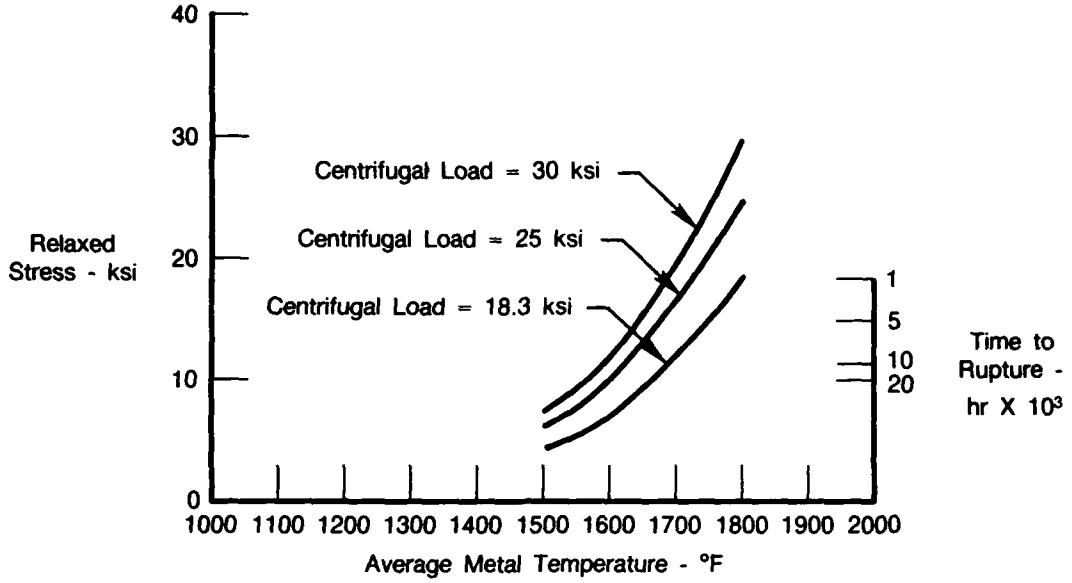

Figure 9. Relaxed Centrifugal Stress Versus Average Metal Temperature. Local Metal Temperature = 982°C (1800°F)

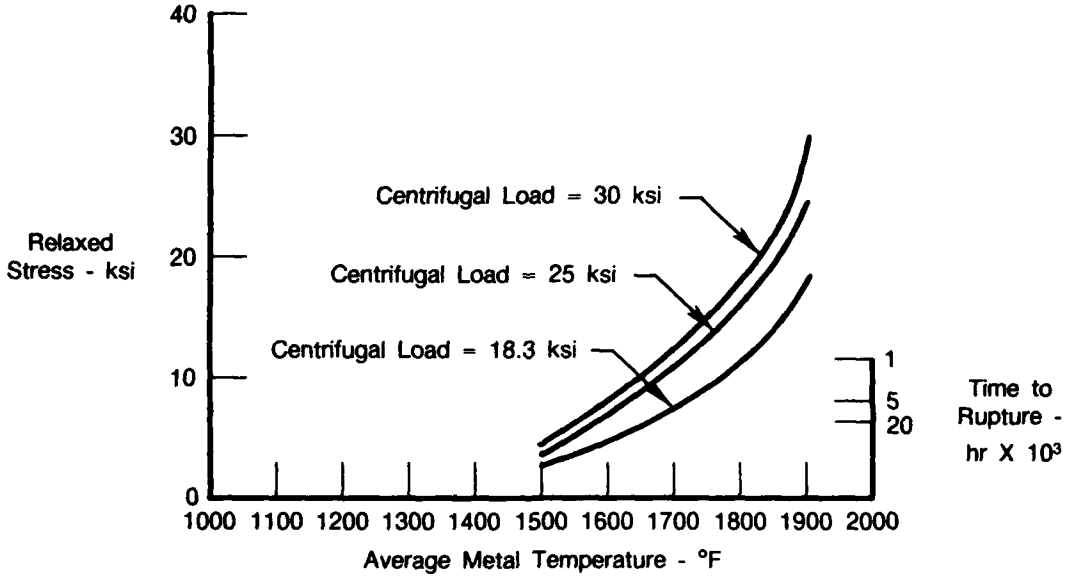

Figure 10. Relaxed Centrifugal Stress Versus Average Metal Temperature. Local Metal Temperature = 1038°C (1900°F)

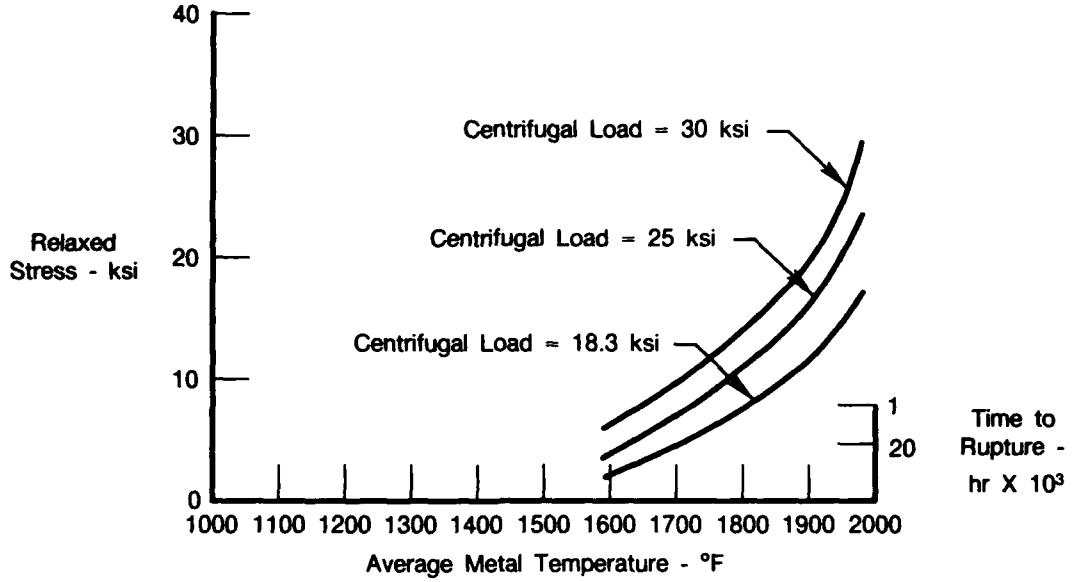

Figure 11. Relaxed Centrifugal Stress Versus Average Metal Temperature. Local Metal Temperature = 1093°C (2000°F)

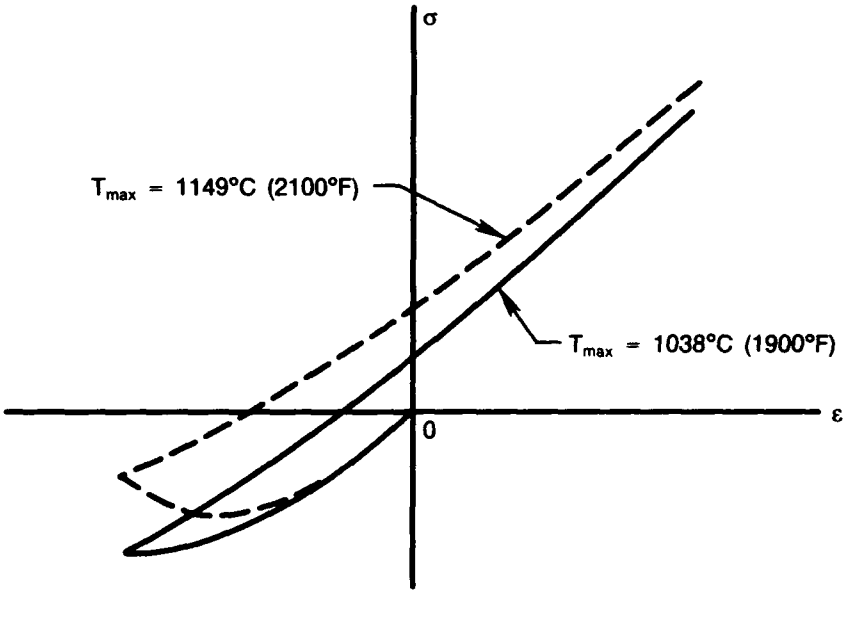

Figure 12. Schematic Hysteresis Loops for a Type 1 TMF Test Showing the Effect of Maximum Temperature

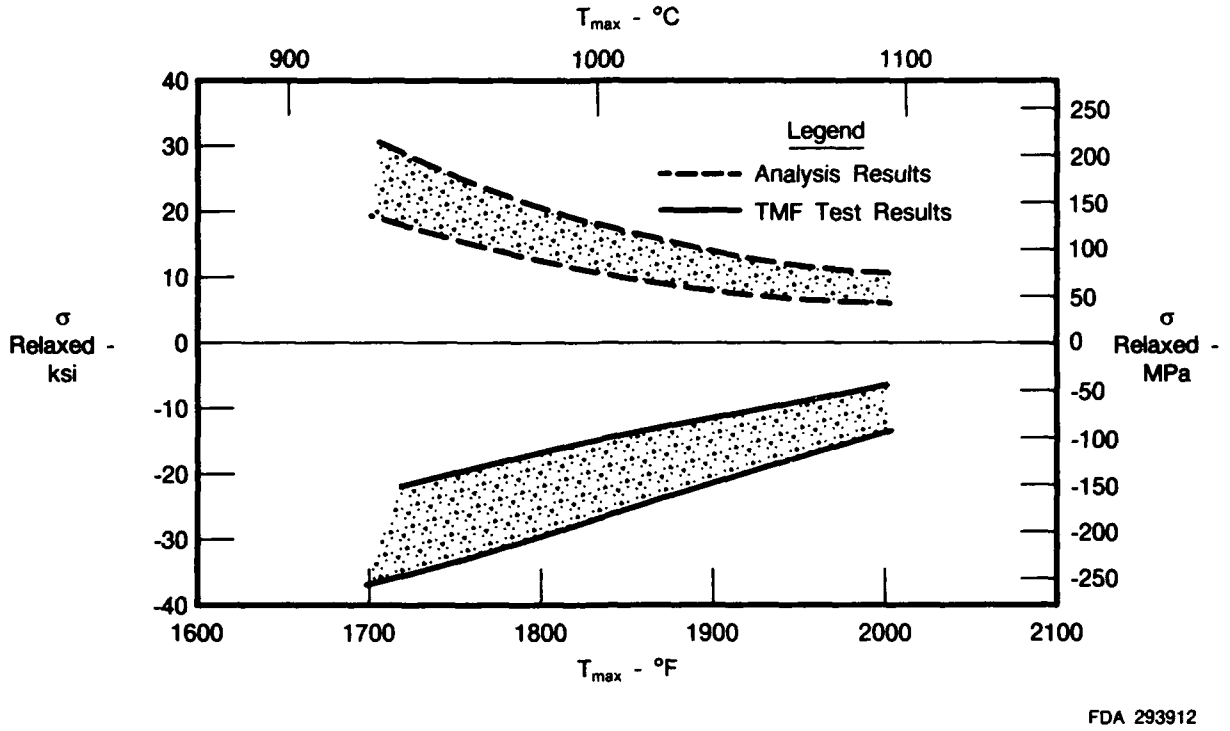

Figure 13. Range of Relaxed Stress at T_{max} TMF Lab Testing and Analytical Predictions

2.2 ALLOY/COATING SELECTION AND ISOTHERMAL PROPERTIES

The objectives of this task were to: (1) select and procure the alloy to be studied in the program, (2) select the aluminide and overlay coatings, and (3) perform tests to determine the basic properties of the material (alloy and coatings). The test matrices are presented in Tables 1 and 2. Data were generated over a range of engine-representative temperatures. Monotonic property determination, Table 1, included tensile and creep/stress rupture testing of PWA 1480. It is noted that the majority of this data was currently available. Coating mechanical and physical properties are essential to the successful description of coated system behavior. Table 2 presents the tests which were conducted to generate the required information.

Monotonic tests were performed under Task II using freestanding (or thin substrate coated) aluminide (PWA 275) and overlay (PWA 286) coatings. Properties that were tested included elastic modulus, thermal expansion, tensile ductility, stress-strain, and (under Task III) TMF. A discussion of test methods and specimens follows.

2.2.1 Alloy/Coating Selection and Procurement

PWA 1480 was selected as the alloy for study in the program. The aluminide and overlay coatings were selected as PWA 275 and PWA 286, respectively. Howmet was selected as the vendor for the test material. Cast bars were procured in four forms:

1. Round bars 1.6 cm (5/8-in.) diameter × 20.3 cm (8-in.) long (for tensile, creep, LCF, and load adjusted TMF specimens)

2. 2.5 cm (1-in.) diameter × 15.2 cm (6-in.) long (for SCTMF specimens)

3. Four slabs 3.2 cm (1¼-in.) thick × 10.8 cm (4¾-in.) long × 4.5 cm (1-¾-in.) wide (for coating property testing).

Cast bars were supplied in the macro grain etched condition and were visually inspected upon receipt for subgrains or other defects. Laue back reflection was performed by the vendor, and crystal orientations were called out not to exceed ±8 degrees from the primary [001] axis.

2.2.2 Isothermal Properties of PWA 286

With the concurrence of the Air Force project engineer, slabs of hot isostatically pressed (HIPed) PWA 276 coating were used to generate mechanical property data for PWA 286. The compositions of the two are identical (with the exception of small additions of Si and Hf in PWA 286), and the mechanical properties should be essentially the same. Monotonic tests were performed using standard test specimens. Results are presented in Figures 14 through 16.

The mean coefficient of thermal expansion from ambient temperature to 1093°C (2000°F) is shown in Figure 14. Two tests were conducted. After the first test run, a permanent hysteresis was observed in each specimen. No dimensional changes were observed for either specimen after the second test run, and these data are assumed to be the steady-state behavior of the material. There is a significant difference between the coefficient of thermal expansion of PWA 1480 and that of the coating, the latter being lower throughout the temperature range. It is felt that this difference results in a portion of the degradation of overlay coatings observed in TMF.

The elastic modulus of PWA 276 from ambient temperature to 1038°C (1900°F) is presented in Figure 15. Figure 16 presents yield strength and ultimate strength of the coating. The loss of strength and the sharp increase in ductility above 538°C (1000°F) indicates that the coating is in an essentially stress-free state at the higher cyclic temperatures of the TMF test,

which will have a significant impact on the stress-strain cycle that it experiences during a TMF cycle in a coated system.

2.2.3 Isothermal Properties of PWA 275

Since the production of an aluminide coating system requires a substrate material for the diffusion of aluminum to occur, a truly "freestanding" aluminide coating is unattainable. However, properties of the coating system may be approximated. Using hollow, tubular specimens with several different wall thicknesses and coated with PWA 275, mechanical property curves were generated for different coating/subtrate cross-sectional area ratios. Regression constants were then extrapolated to the zero substrate area condition, approximating the behavior of the coating. Three wall thicknesses were used, 0.102, 0.051, and 0.025 cm (0.040, 0.020, and 0.010 in.). Corresponding area ratios are presented in Table 3. Monotonic tests were performed using the specimen shown in Figure 17. Use of a tubular specimen has several advantages over methods involving strip or sheet specimens. First, the specimens may be tested using existing test equipment and heating methods. Secondly, tubular specimens may be loaded in compression, whereas strip or sheet specimens may only be loaded in tension. Lastly, a large data base currently exists for monotonic, and TMF of PWA 275 coated PWA 1480. This information was used to provide data for the lowest coating/substrate cross-sectional area ratio case.

PWA 275 coating was applied to both the inside and outside diameters to increase the coating area and, thereby, more accurately determine the physical properties of the coating. Measurement of the gage section inside and outside diameters were taken before and after coating.

Tensile tests were performed at four temperatures using each of the three wall thicknesses. For the lower temperature ($\leq$649°C/$\leq$1200°F) typical stress-strain behavior of the PWA 1480/275 specimens exhibited a modulus shift in the elastic portion of the curve, as shown in Figure 18. The initial modulus is a combined modulus of the coating and the substrate. This modulus is controlled by the individual moduli of the two materials at the given test temperature and by the relative percent of cross-sectional area of each material. The transition point and the secondary modulus represent yielding and then failure of the coating material. The higher temperature tests ($\geq$871°C/$\geq$1600°F) did not exhibit this modulus transition. These tensile stress-strain curves show a single modulus with typical yield and failure, as shown in Figure 19. The reason for this behavior is not entirely due to a reduced elastic modulus of the coating, but rather the dramatic loss in the coating yield strength and significantly increased coating ductility at the increased temperatures. Accurate measurement of the initial combined moduli is not possible with this method if the yield strength of the coating becomes very small with respect to the substrate. However, an effective secant modulus of the coating, which defines its total contribution to the system stiffness even during considerable plastic deformation, was determined and can be used in the two-bar model.

Coating percentage and combined modulus results for each test are listed in Table 4 and plotted in Figure 20. Data regressions for each test condition were performed and extrapolated to the 100 percent coating condition. These results are plotted in Figure 21.

Post test measurement of the substrate thickness and coating thickness was performed by sectioning the failed test specimens longitudinally (Figure 22). A longitudinal half and a transverse semi-circle, approximately 0.064 cm (0.025 in.) behind the fracture, were embedded in the same mount. The longitudinal sections were used to determine any coating thickness variation over the gage length. Results indicate the coatings were indeed uniform throughout. Coating/substrate thickness measurements were taken from the transverse section. Typical longitudinal coating section with 0.025 cm (0.010 in.) wall thickness is shown in Figure 23, which

is representative of a standard coating/diffusion zone/substrate system. The diffusion zone is considered a part of the coating due to the diffusion zone's similarity in composition and crack growth behavior. Typically, TMF cracks will initiate in the coating, propagate to the substrate/diffusion zone interface, where they will often stop, indicating significant material differences. Therefore, all calculations using the coating area include the diffusion zone.

As discussed previously, modulus calculations for the higher temperature tests ($\geq$871°C/$\geq$1600°F) may not accurately represent the true coating properties, due to a dramatic loss in yield strength. However, the values shown represent an effective modulus (i.e., substrate modulus plus the coating secant modulus) which contributes to the coating/substrate system. Results of the alternate coating strength calculations may aid in determining actual coating modulus.

Approximate stress-strain curves of the PWA 275 coating were determined using a method analogous to those employed for composite materials with longtudinally-oriented continuous fibers. Assuming that a 871°C (1600°F) and 1038°C (1900°F) the coating yields at very low stress (<69 MPa (10 ksi)) and continues to plastically deform with the substrate, a secant modulus was calculated for the coating to approximate coating stress at a given strain, where substrate physical properties are known. The secant modulus of the coating was calculated using the equilibrium relationship:

$$P = \sigma_s (A_s) + \sigma_c (A_c)$$

and the constitutive relationship:

$$\varepsilon_s = \sigma_s / E_s$$

and the compatability relationship:

$$\varepsilon_t = \varepsilon_s = \varepsilon_c$$

where the subscript "s" represents the substrate, subscript "c" represents the coating, and the subscript "t" represents the total (or combined) system:

$$P = \varepsilon_t E_s (A_s) + \sigma_c (A_c)$$

coating stress may then be calculated at a given strain:

$$\sigma_c = \frac{P}{A_c} - \varepsilon_t E_s \left(\frac{A_s}{A_c}\right)$$

An effort to determine approximate stress/strain behavior of the PWA 275 coating was performed. These investigations indicate that small deviations in the stress/strain behavior of the single crystal PWA 1480 substrate material (due to crystal orientation effects) result in magnified effects in the coating stress/strain property calculations. Additionally, some error may be produced by assuming an exactly uniform coating thickness throughout the gage section. These combined effects have precluded accurate determination of stress/strain curves for the PWA 275 coating at this time.

2.2.4 Coating — Substrate Comparison

A comparison plot shows the elastic modulus of PWA 1480, PWA 275 coating, and PWA 276 coating versus temperature is presented in Figure 24.

Ductility properties are shown in Figure 25 for the aluminide coating, overlay coating, and PWA 1480. Note that the diffusion aluminide coating has a ductile to brittle transition at approximately 649°C (1200°F). Above 649°C (1200°F) the coating exhibits increased plastic behavior, which explains the extreme loss of the yield strength.

Thermal expansion data for aluminide coating, overlay coating, and PWA 1480 are plotted in Figure 26. Two bar-model thermal expansion mismatch stresses are to be calculated from the data presented along with the ductility information (Figure 25) to determine temperature and stress levels critical to coating failure.

Yield strength results are shown in Figure 27 for the aluminide coating (PWA 275), overlay coating (PWA 276), and PWA 1480. These results will be used in the two-bar model and the simplified constitutive method to simulate the relaxation of stress due to yielding.

2.2.5 Isothermal Properties of PWA 1480

The isothermal properties of PWA 1480 include elastic modulus, ductility, thermal expansion, yield strength, cyclic stress-strain, and stress relaxation. The first four properties are compared to the same properties for the two coatings. All of these properties are used in the life prediction model.

Past inelastic strain calculations for modeling purposes were based on very limited cyclic stress/strain data, which also required extrapolation down to the stress ranges of interest to this program. Therefore, discretionary isothermal cyclic stress/strain tests of PWA 1480 have been performed throughout the TMF temperature range to increase the accuracy of this data base. Results of these tests are shown in Figure 28. Representative data points are shown for $\leq$760°C ($\leq$1400°F), 871°c (1600°F), 982°C (1800°F), and 1093°C (2000°F) in Figure 29 with the regressed lines. The lines were regressed using a Ramburg-Osgood type function.

The statistical correlation coefficient ("R" squared value) of the data at each test temperature varied from below 0.10 to more than 0.99. The lowest correlations were found at temperatures below 760°C (1400°F), which were caused when these tests were repeated to verify the cross-over reported in Interim FR-18645-6. When the tests were repeated, more scatter was introduced at 427°C (800°F), 538°C (1000°F), 649°C (1200°F), and 538°C (1400°F). These temperatures had the lowest correlation coefficients. The slopes of the lines at 27°C (80°F), 427°C (800°F), 528°C (1000°F), 649°C (1200°F), and 760°C (1400°F) were very similar and were, therefore, averaged to prevent the lines from crossing.

In addition, monotonic tensile data (Figure 30) indicates that the 0.2 percent yield strength decreases from 27°C (80°F) to 427°C (800°F) and then increases to 760°C (1400°F). Although cyclic stress/strain testing differs from monotonic tensile testing, due to the cyclic damage involved, the two properties are related. At the 0.2 percent inelastic strain level (Figure 31), the relative order of stress range closely corresponds to the tensile data. Elastic modulus checks were made prior to testing at each temperature and are in agreement with standard PWA 1480 modulus data (Figure 32). The specimens were submitted for Laue to determine if any significant deviation existed between the specimen axis and the [001] crystallographic primary orientation. Results indicate that deviations from the primary orientation were minimal ($\leq$8 degrees). Laboratory test material is generally controlled to within 8 degrees of casting bar orientation.

Discretionary testing of PWA 1480 to determine primary creep rates between 871°C (1600°F) and 1093°C (2000°F) has been performed. Results of these tests are shown in Figure 33. Positive values for the stress are required for the logarithmic regression of the stress relaxation curves. Therefore, the absolute value of the compressive data was used in the regression model. Representative data points and the stress relaxation model are shown in Figure 34. The statistical correlation coefficient ("R" squared value) for the data correlating the temperature, stress and time exceeds 0.95 indicating a good regression fit. These results were used in the later modelling effort by providing information on stress relaxation occurring during the cycle and during hold times.

TABLE 1. Substrate Mechanical Properties

		Number of Tests				
Alloy	*Type Test*	*at 427°C (800°F)*	*at 760°C (1400°F)*	*at 982°C (1800°F)*	*at 1038°C(1900°F) or 1093°C(2000°F)*	*Total*
PWA 1480	Tensile	2*	2*	2*	2	8
PWA 1480	Creep/SR		2*	2*	2	6

*Available from Contract F33615-82-C-5109
**Available from other P&W Sources

R20505/1

TABLE 2. Coating Mechanical and Physical Properties Test

Coating	*Temperature — °C (°F)*	*Elastic Modulus*	*Thermal Expansion (a)*	*Tensile Ductility*	*Stress-Strain*
Aluminide	427 (800)	X	X	X	X
Aluminide	649 (1200)	X	X	X	X
Aluminide	871 (1600)	X	X	X	X
Aluminide	1093 (2000)	X	X	X	X
Overlay	427 (800)	X	X	X	X
Overlay	649 (1200)	X	X	X	X
Overlay	871 (1600)	X	X	X	X
Overlay	1093 (2000)	X	X	X	X

Notes:
1. Substrate is PWA 1480 alloy, [001] orientation (where required).
2. Most test data available from other sources.

R20505/1

TABLE 3. Cross-Sectional Area Ratios for Tubular Aluminide Coating Test Specimens (0.0051 cm [0.002-in.] Coating Assumed)

Specimen ID cm(in.)	*Specimen OD — cm^2 (in.)*	*Specimen Area — cm^2 ($in.^2$)*	*Coating Area* — cm^2 ($in.^2$)*	*Coating Area/Substrate Area — %*
0.635(0.250)	0.686(0.270)	0.0527(0.00817)	0.0208(0.00323)	40
0.635(0.250)	0.737(0.290)	0.1087(0.0170)	0.0219(0.00340)	20
0.635(0.250)	0.838(0.330)	0.2348(0.0364)	0.0238(0.00369)	10
0.381(0.150)	0.635(0.250)	0.2026(0.0314)	0.0103(0.00160**)	5.1

* Coating on OD and ID
**Standard TMF Specimen — Coating on OD only

R20505/1

TABLE 4. Elastic Modulus Test Results for PWA 1480/275

Test Temperature °C (°F)	Coating Area / Total Gage Area — %	Combined Modulus** x 10^6 kPa (x 10^6 psi)
427 (800)	0*	113.1(16.4)
427 (800)	9.1	122.0(17.7)
427 (800)	13.2	128.2(18.6)
649 (1200)	0*	103.4(15.0)
649 (1200)	7.0	110.3(16.0)
649 (1200)	14.0	116.5(16.9)
649 (1200)	23.3	140 0(20.3)
871 (1600)	0*	91.0(13.2)
871 (1600)	7.1	86.9(12.6)
871 (1600)	13.4	100.0(14.5)
871 (1600)	31.4	89.6(13.0)
1038 (1900)	0*	81.4(11.8)
1038 (1900)	7.2	73.8(10.7)
1038 (1900)	16.8	72.4(10.5)
1038 (1900)	22.0	63.4(9.2)

*Corresponds to uncoated PWA 1480 baseline data.
**Modulus determined from combined area of coating and substrate material.

R20505/1

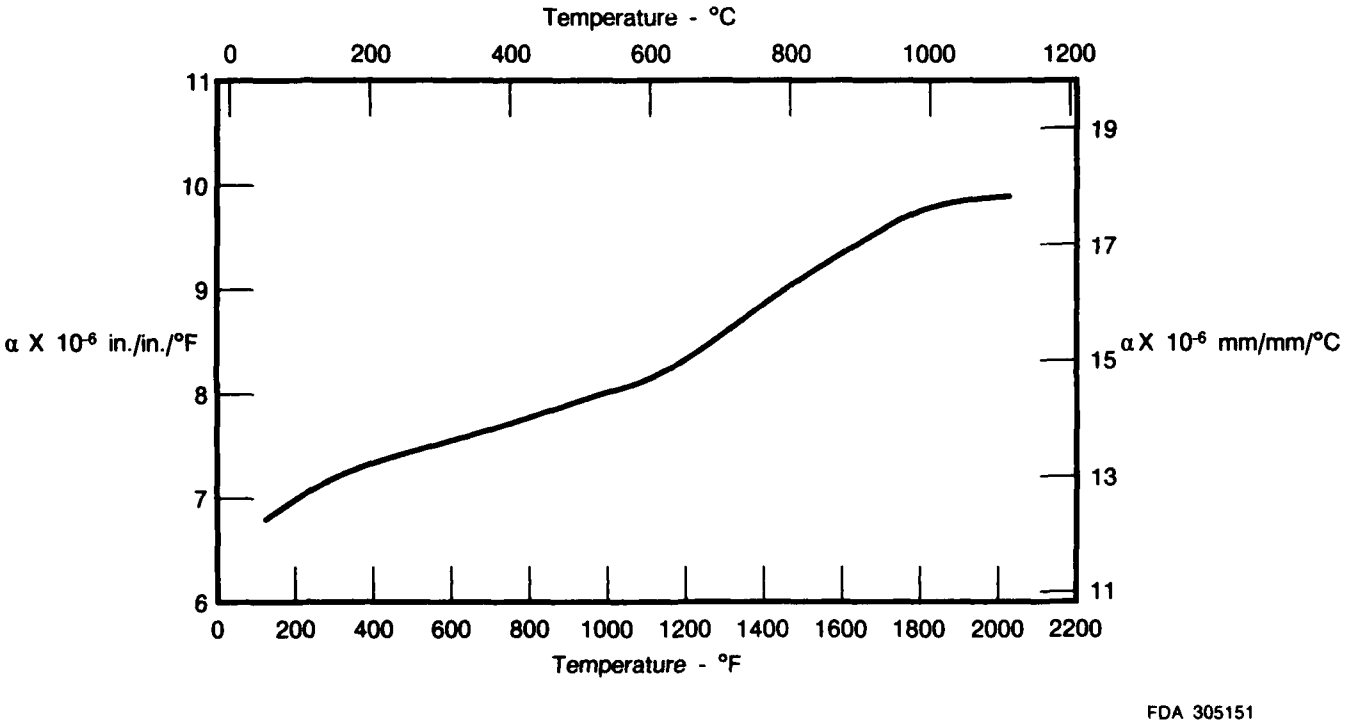

Figure 14. Mean Coefficient of Thermal Expansion, PWA 276 Bulk Coating Material

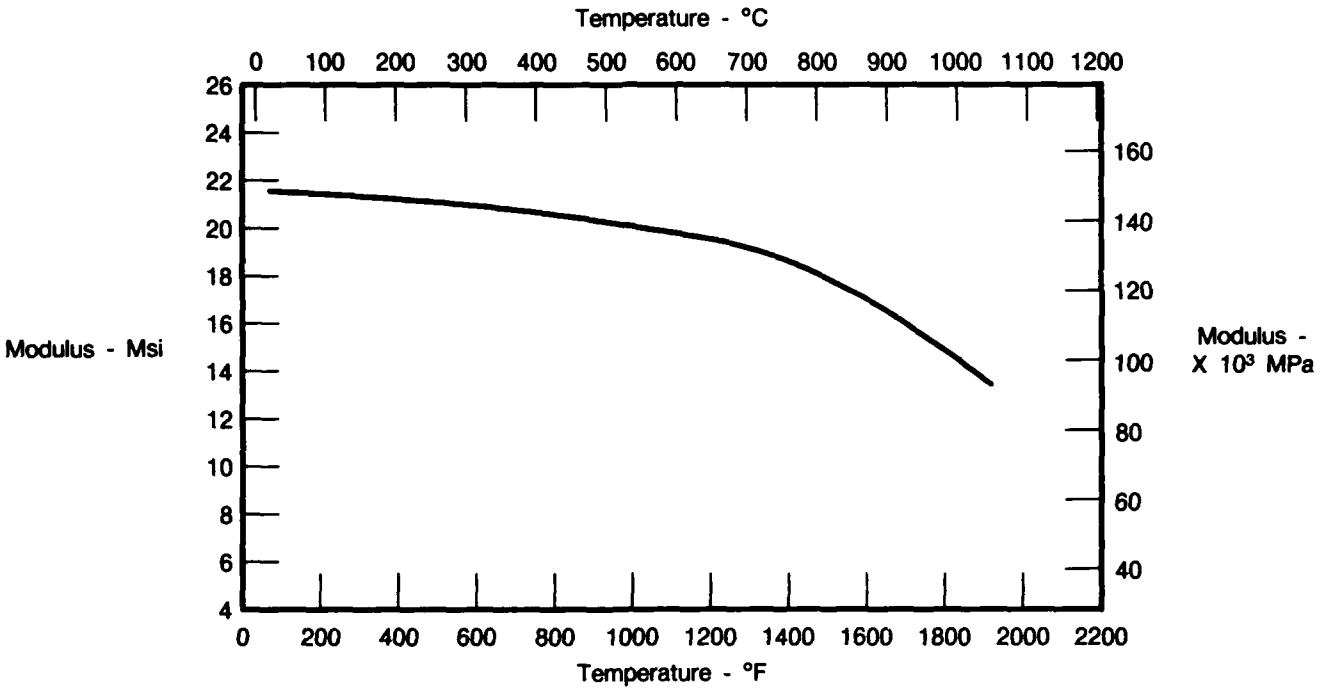

Figure 15. Elastic Modulus Versus Temperature, PWA 276 Bulk Coating Material

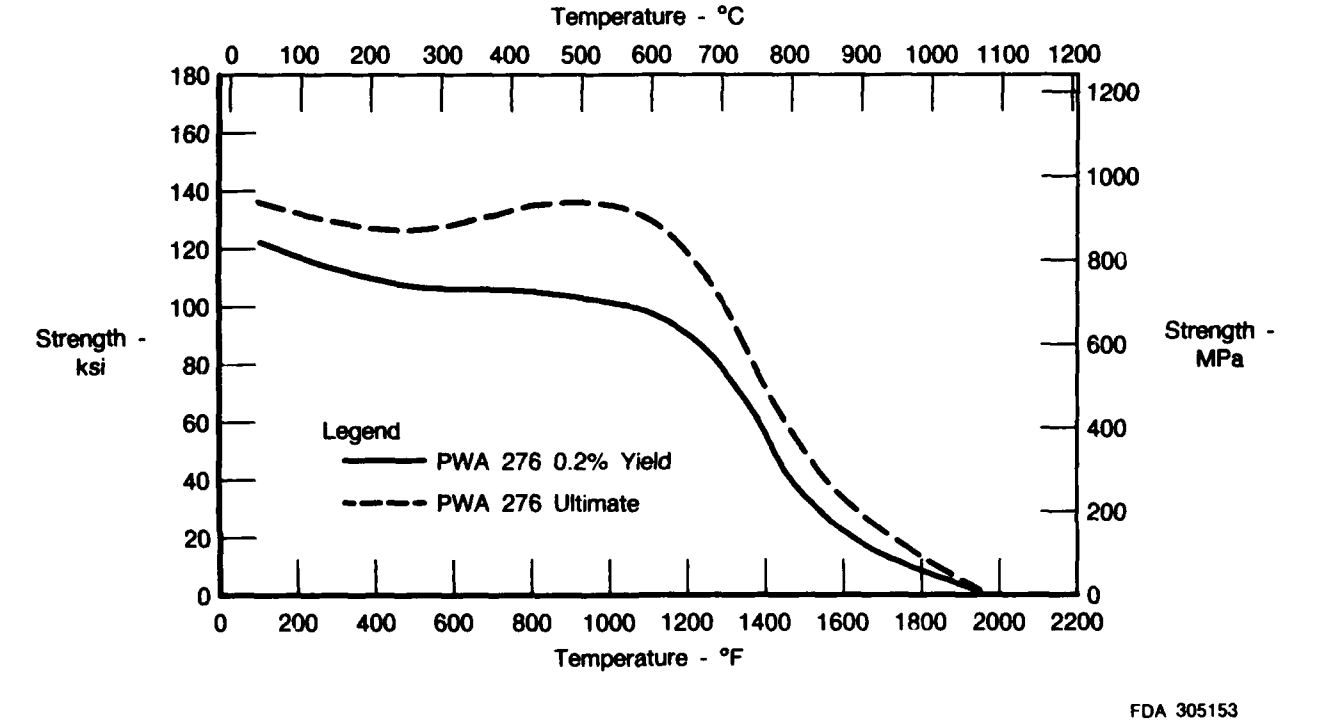

Figure 16. Yield and Ultimate Strength Versus Temperature, PWA 276 Bulk Coating Material

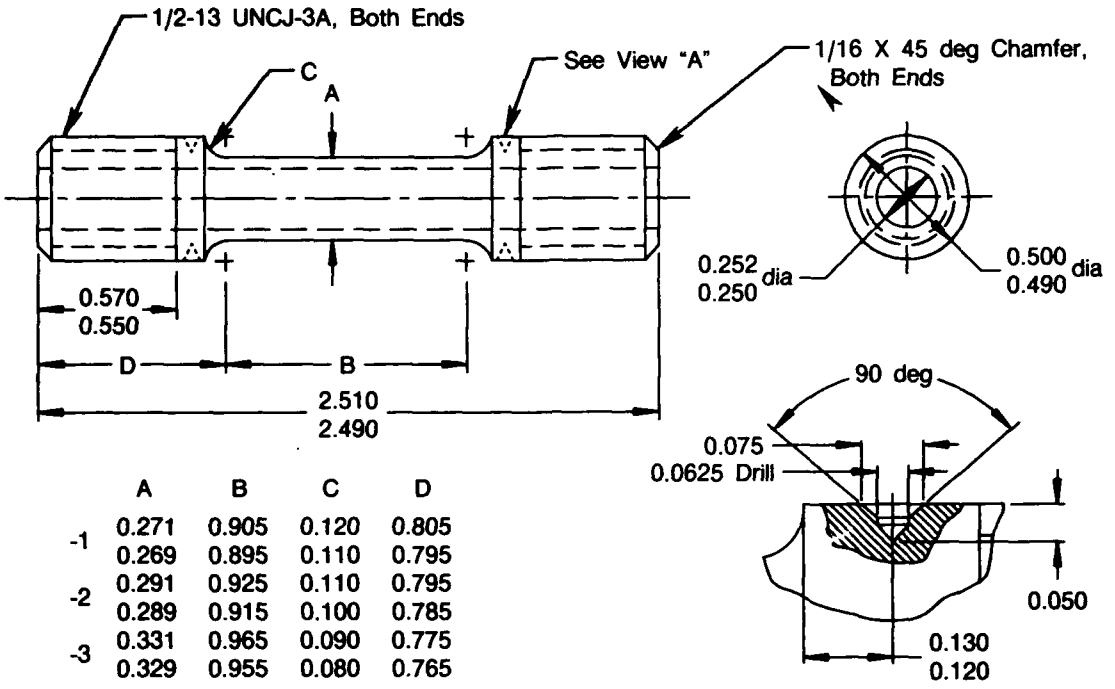

	A	B	C	D
-1	0.271 0.269	0.905 0.895	0.120 0.110	0.805 0.795
-2	0.291 0.289	0.925 0.915	0.110 0.100	0.795 0.785
-3	0.331 0.329	0.965 0.955	0.090 0.080	0.775 0.765

Notes

1. All dimensions in inches
2. All diameters concentric within 0.001 fir
3. Center of specimen to be 0.001 smaller than remainder of dimension "B". To be blended smoothly. No steps allowed
4. Identification marks permitted on ends of specimen only

Drill and C'sk 2 Holes 180 deg Apart (Both Sides)
Radial Alignment ± 00 deg 30 min
Axial Alignment ± 0.001

FDA 293914

Figure 17. Monotonic Test Specimen for PWA 275

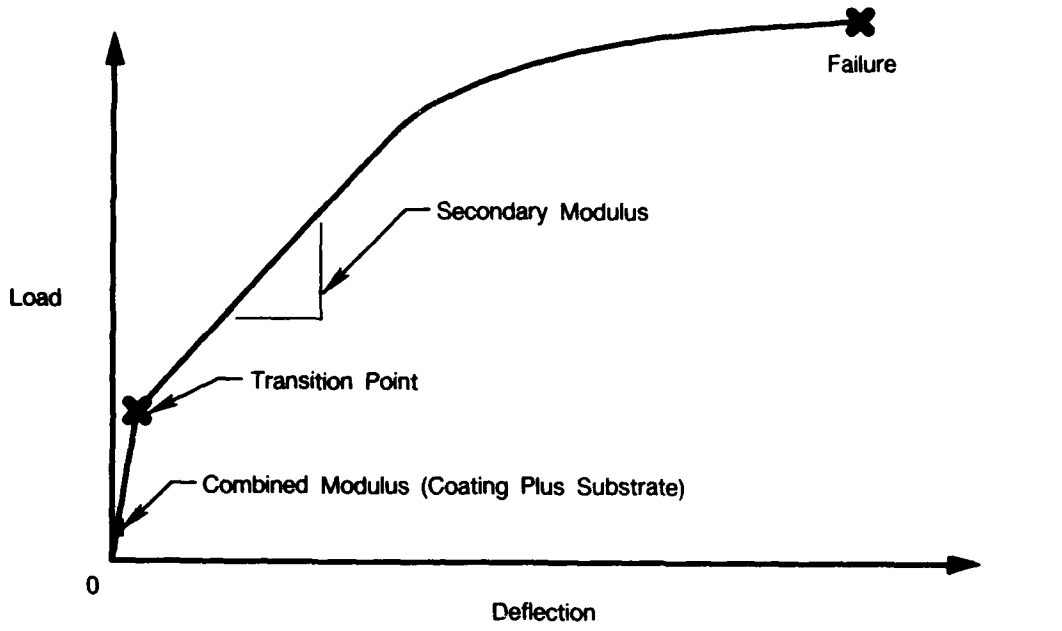

Figure 18. Monotonic Tensile Test Curve for PWA 1480 and PWA 275 Coated System (≤649°C/≤1200°F)

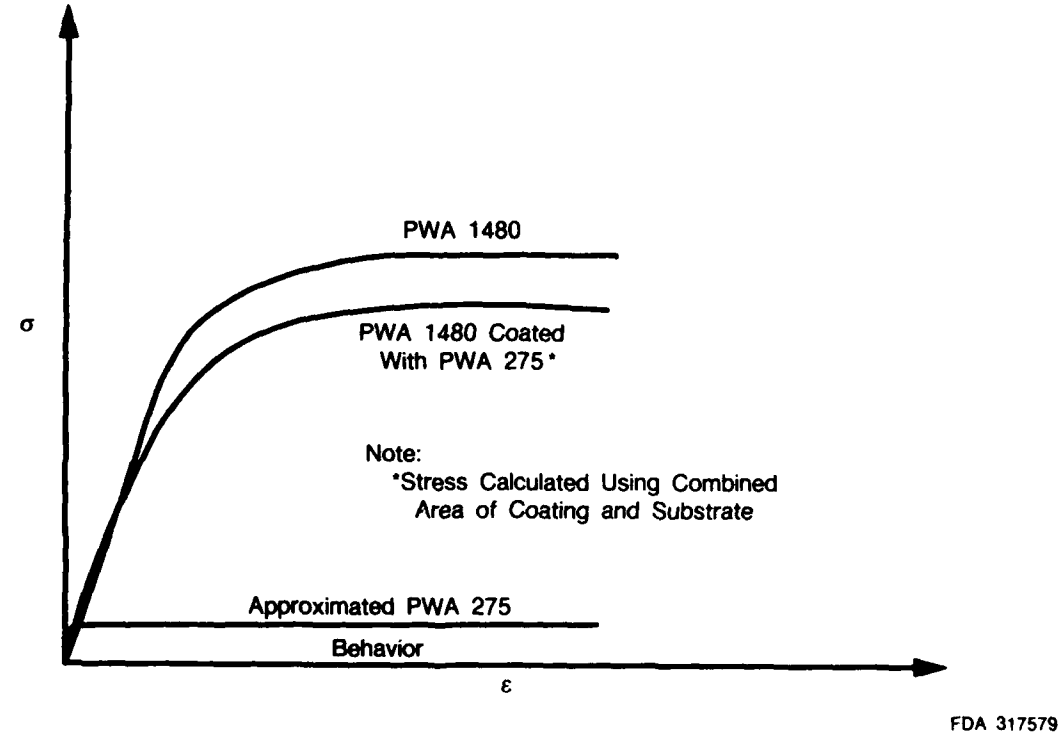

Figure 19. Monotonic Tensile Test Curve for PWA 1480 and PWA 275 Coated System (≥871°C/≥1600°F)

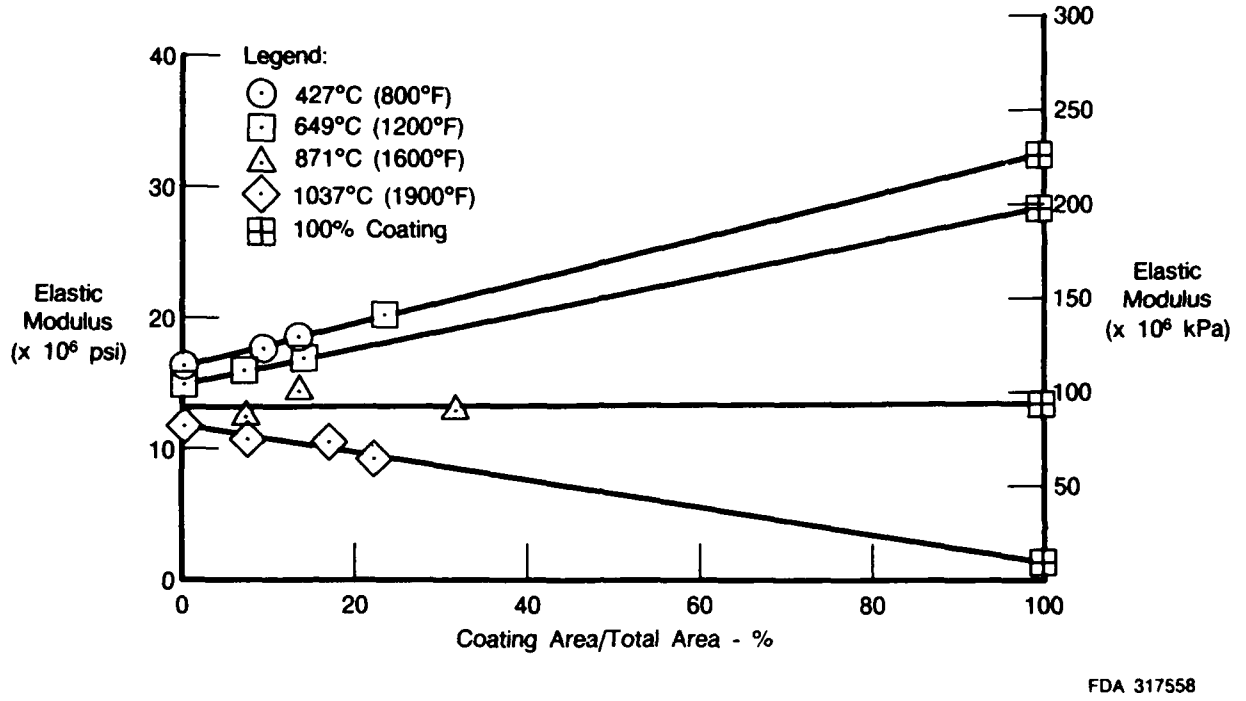

Figure 20. Extrapolation of the Effective Elastic Modulus of PWA 275 (Includes Coating and Diffusion Layers)

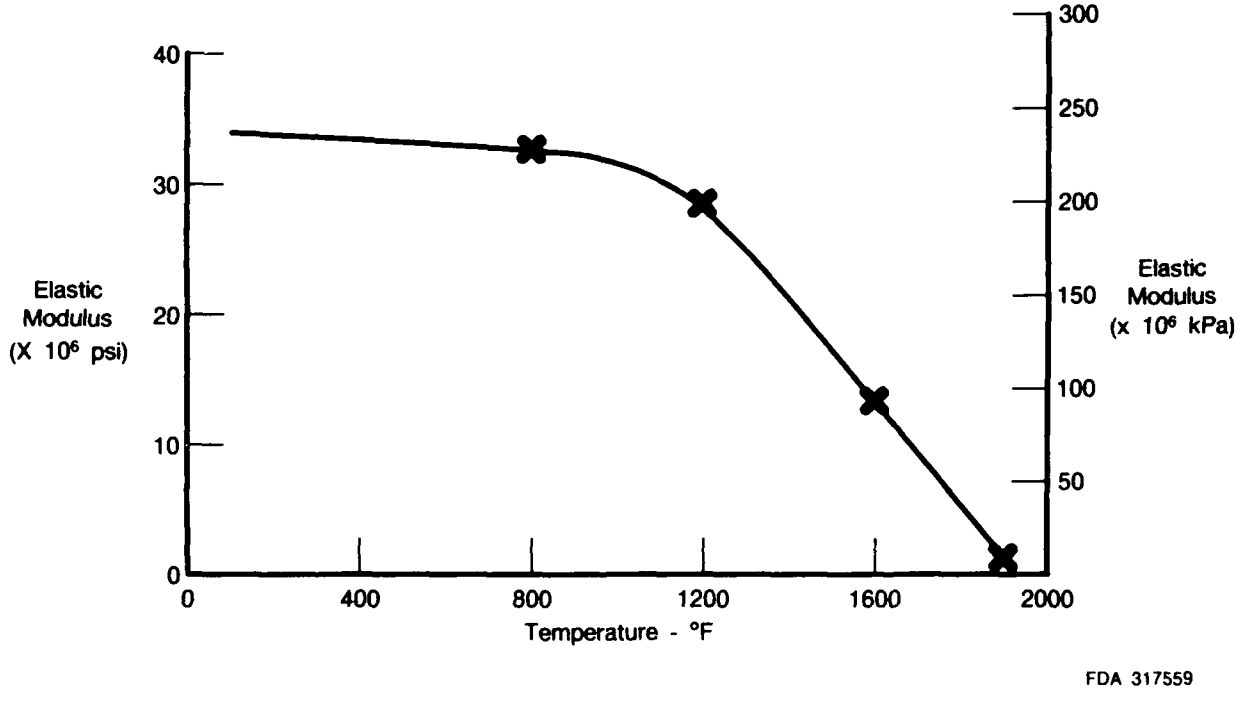

Figure 21. Effective Elastic Modulus of PWA 275 (Includes Coating and Diffusion Layers)

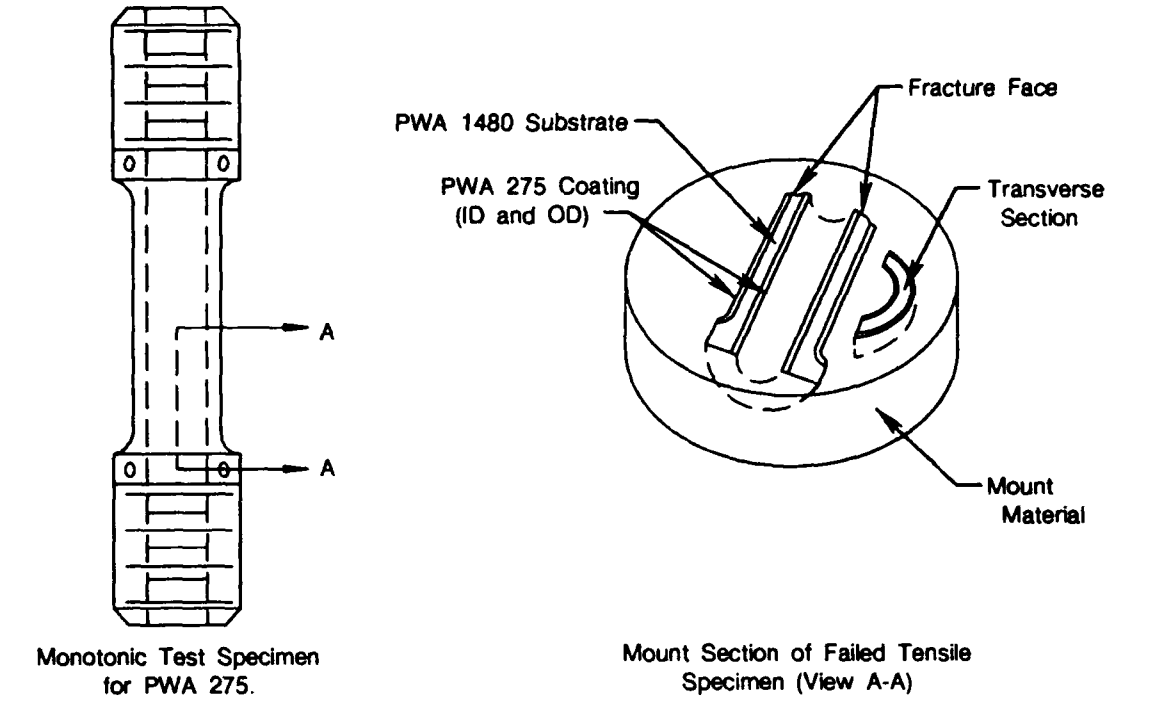

Figure 22. Post Test Measurement of Substrate and Coating Thickness

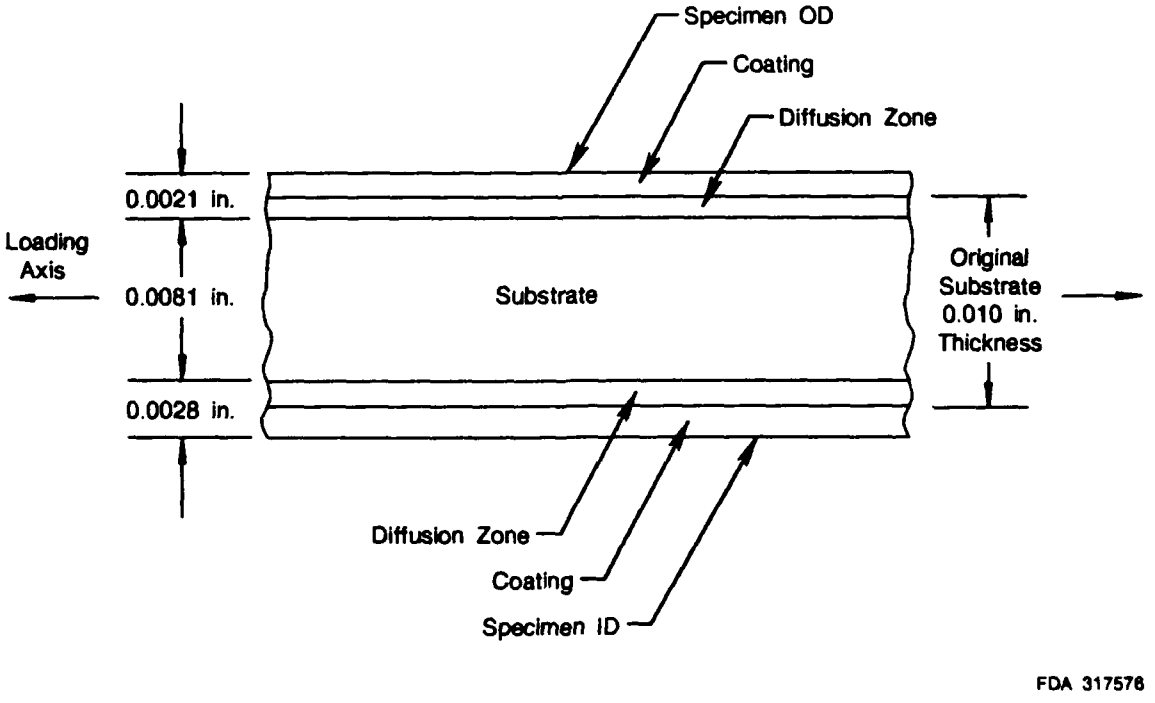

Figure 23. Representative Longitudinal Cross Section of Monotonic Test Specimen Showing Coating/Substrate System

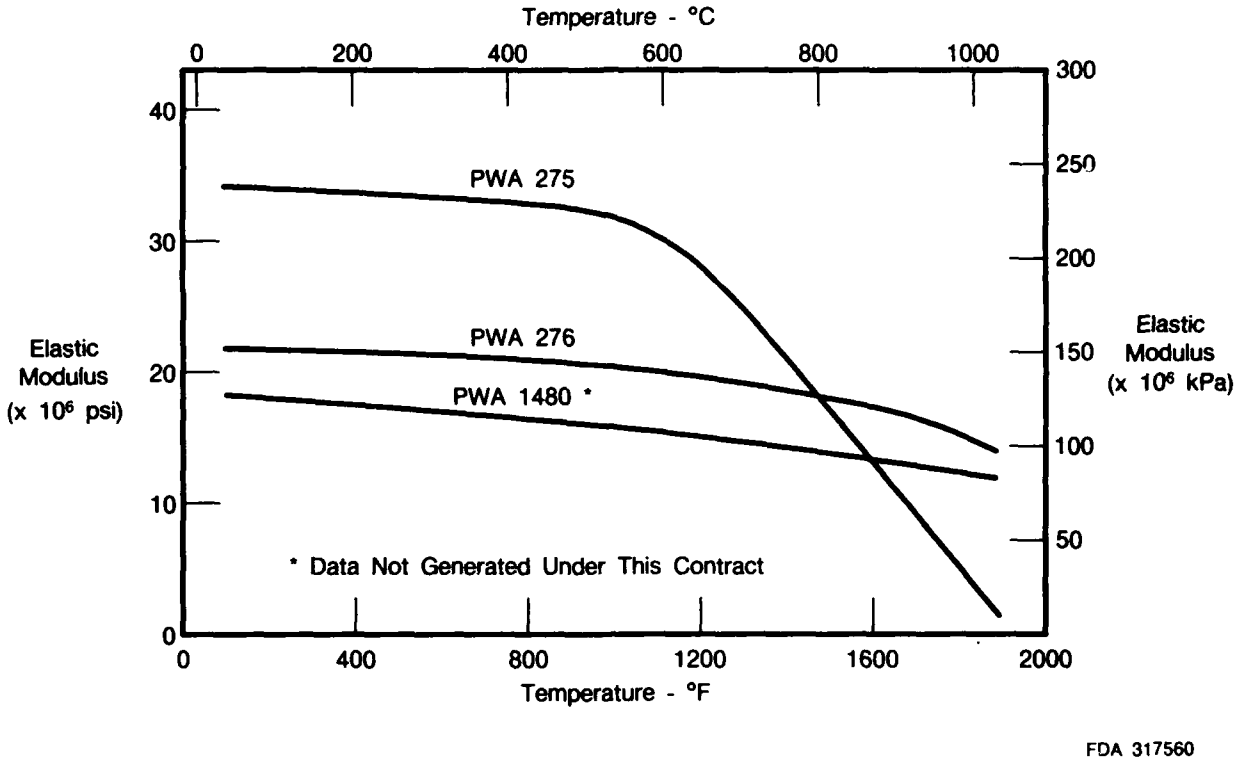

Figure 24. Elastic Modulus Comparison of Coating and Substrate Materials

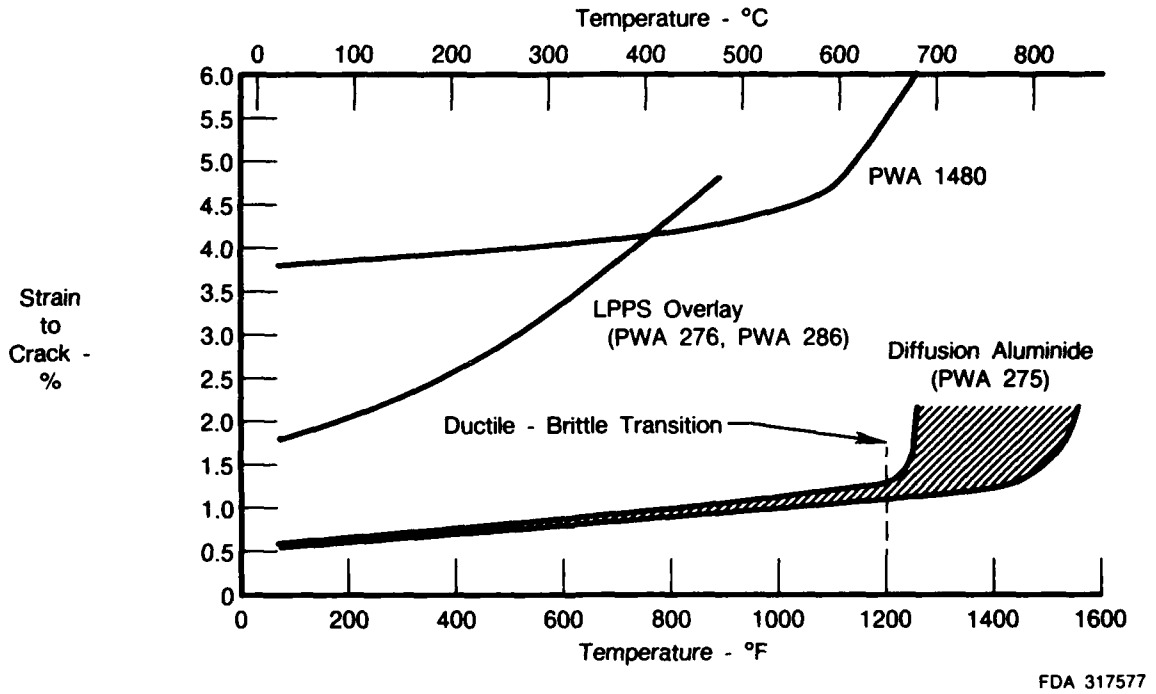

Figure 25. Ductility Versus Temperature for Aluminide and Overlay Coatings (Data Not Generated Under This Contract)

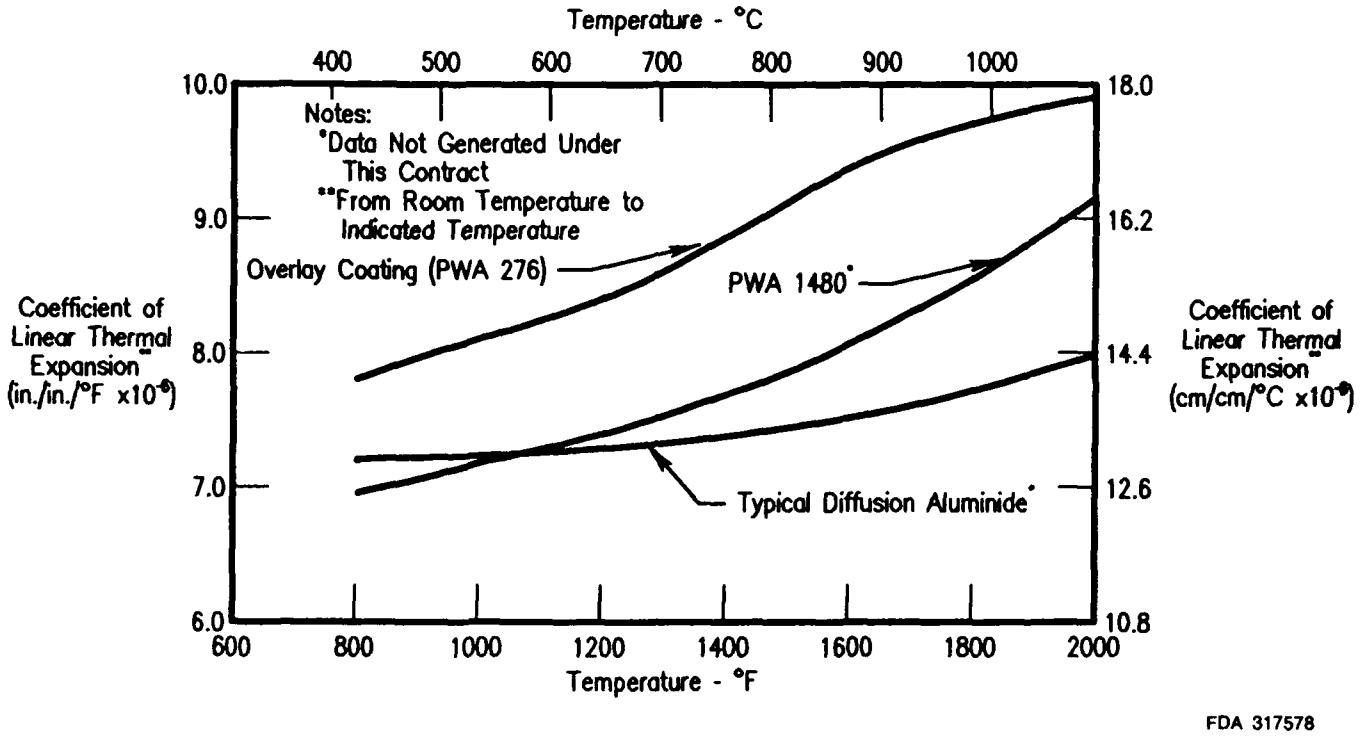

Figure 26. Thermal Expansion Data for Aluminide Coatings, Overlay Coatings, and PWA 1480 (Data Not Generated Under This Contract)

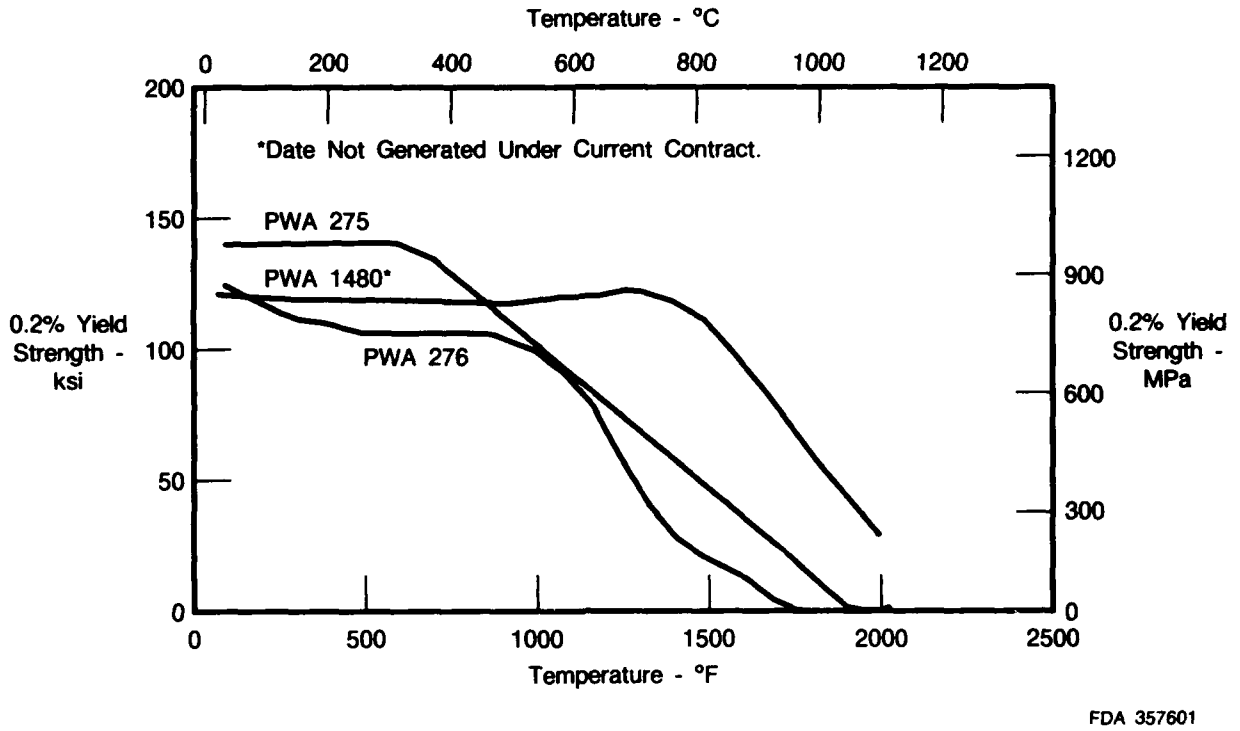

Figure 27. Yield Strength Versus Temperature for PWA 1480, PWA 275, and PWA 276

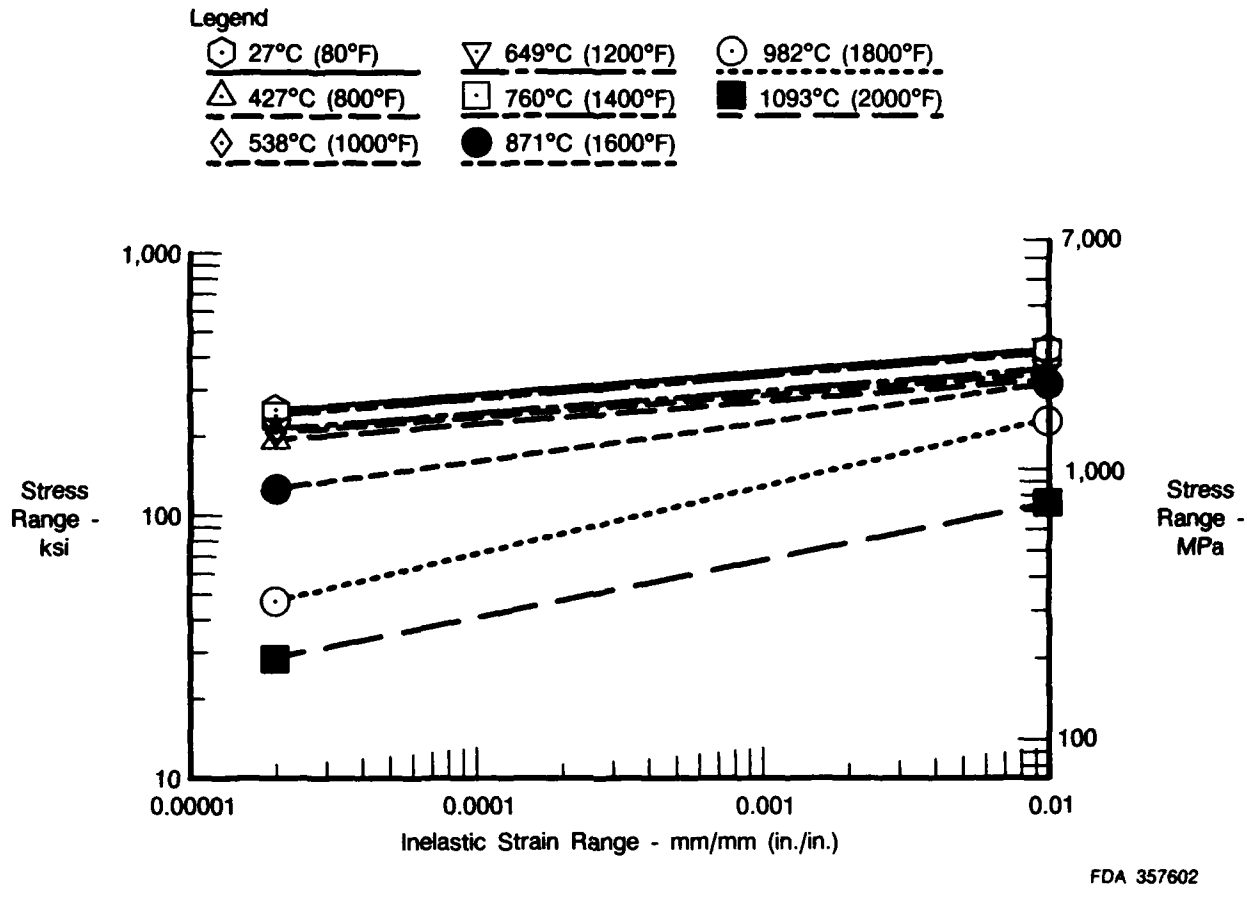

Figure 28. Inelastic Strain Versus Stress Range for PWA 1480

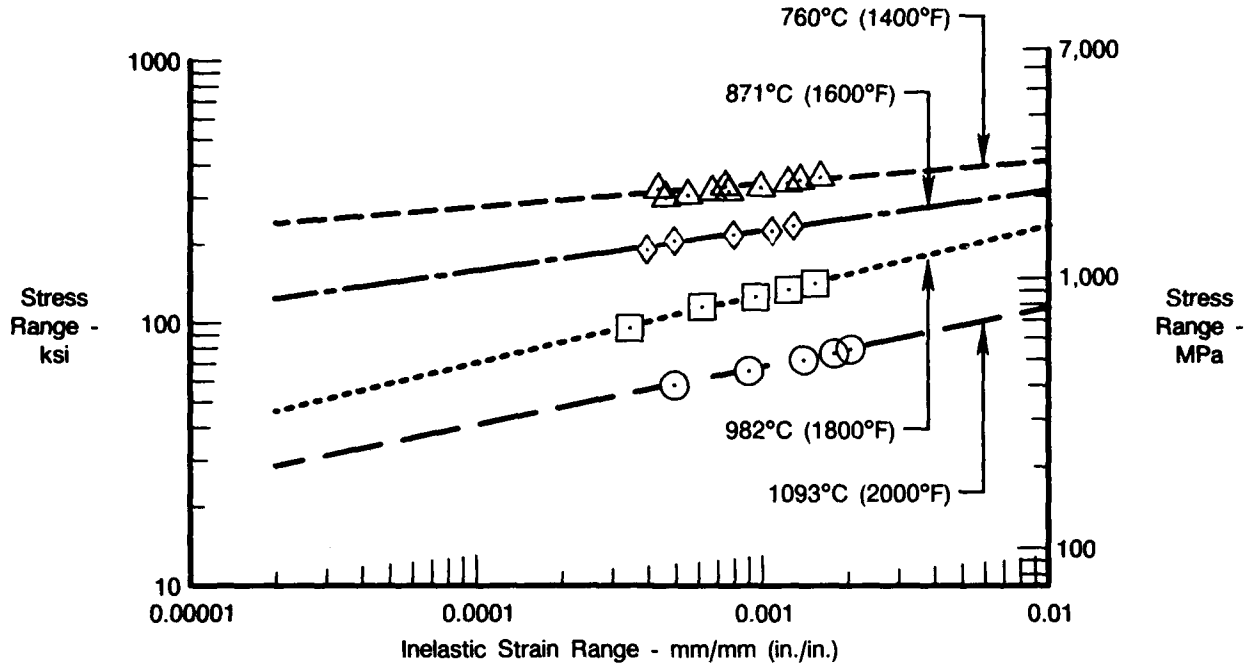

Figure 29. Inelastic Strain Versus Stress Range for PWA 1480 (Representative Data Points)

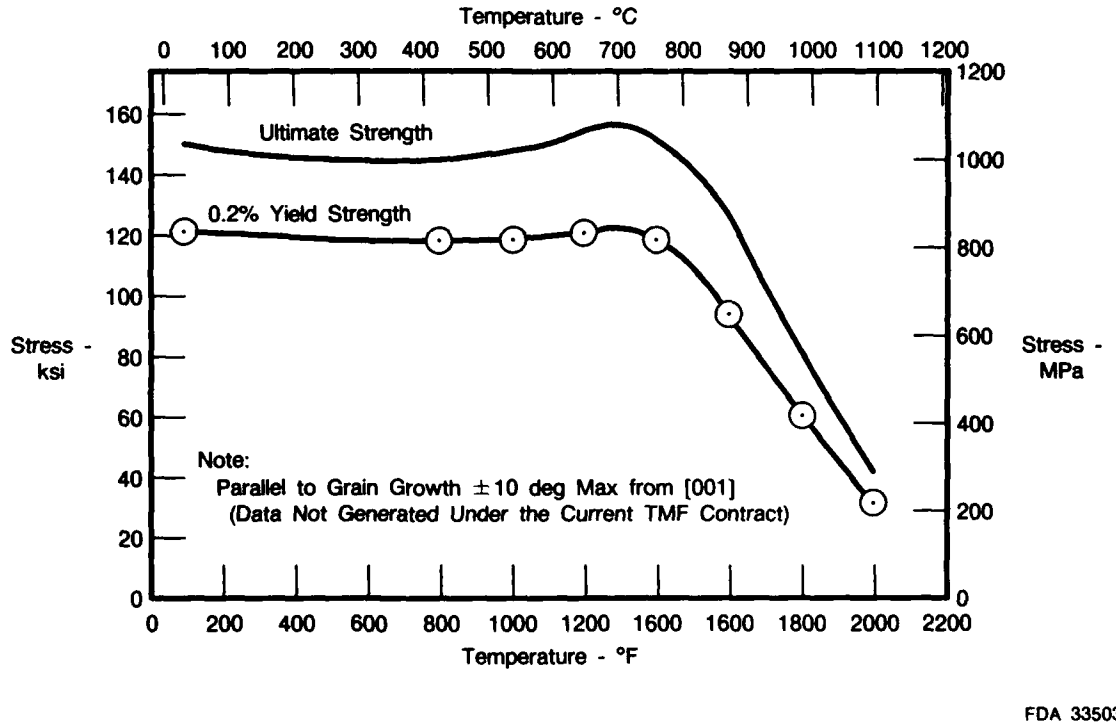

Figure 30. Monotonic Tensile Data for PWA 1480

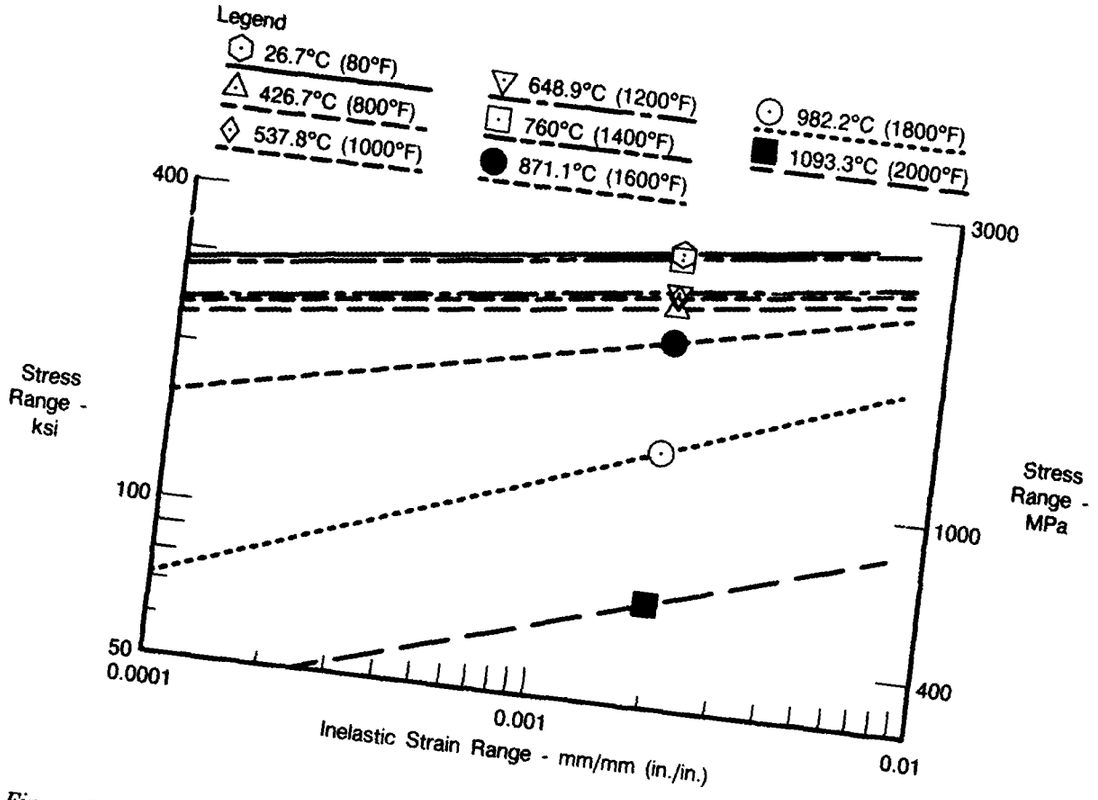

Figure 31. Inelastic Strain Versus Stress Range for PWA 1480 (0.2% Inelastic Strain)

FDA 357604

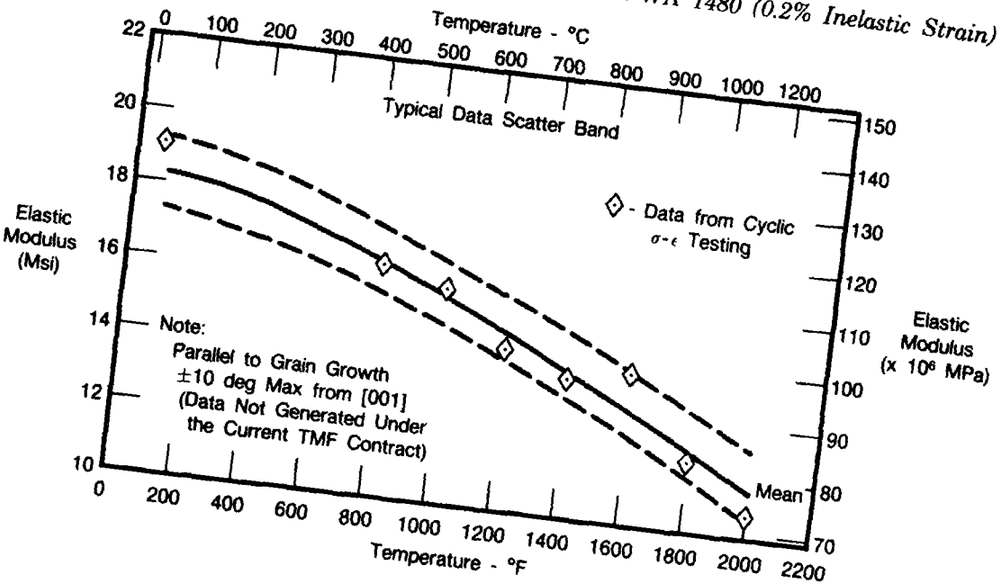

Figure 32. Elastic Modulus Data for PWA 1480

FDA 335040

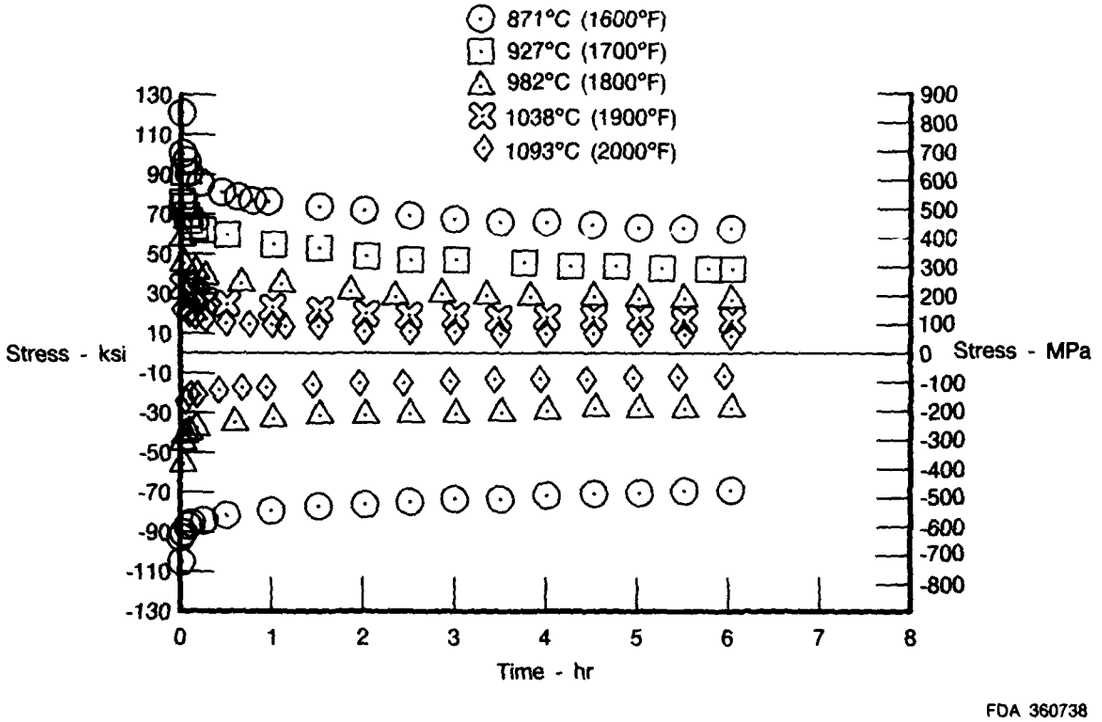

Figure 33. Primary Creep Stress Relaxation Data for PWA 1480

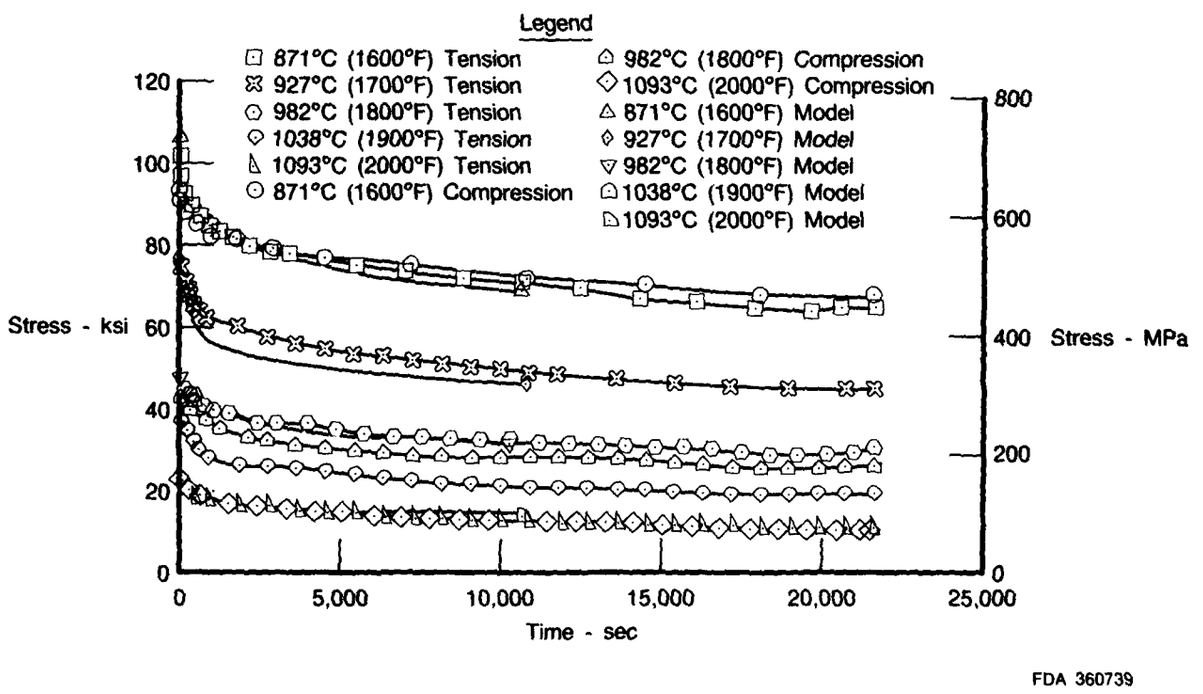

Figure 34. Primary Creep Stress Relaxation Data With Model for PWA 1480

2.3 THERMAL MECHANICAL FATIGUE EXPERIMENTAL PROGRAM

The test program conducted under this contract contains both monotonic and cyclic, isothermal and non-isothermal tests of PWA 1480 in coated and uncoated forms. A limited amount of testing was also performed on PWA 275 and PWA 286 coatings in freestanding or thin substrate coating form. The results of the monotonic and isothermal tests on the coatings and substrate were presented in Section 2.2. The TMF experimental program included the efforts of Task III described previously in Section 2.0. This effort was a parametric study of the variables that affect TMF as described by Task I. The TMF test program objectives and results are presented below.

2.3.1 Task Objectives

The objective of this task is to define the principal variables affecting thermal mechanical fatigue. Results of Task I indicated that the parameters that needed to be investigated for their effect on TMF crack initiation life include: temperature range, stress at maximum temperature, cyclic frequency, hold periods, and cycle type. Where more than one test was required for a particular set of conditions, the additional tests were performed at different strain ranges. Repeats of critical tests were run using the discretionary tests called out in each matrix.

The load adjusted TMF (LATMF) matrix is presented in the Table 5. This test method was used for parametric studies of the effects of stress at maximum temperature, cyclic frequency, hold periods, and cycle types. The stress at the maximum cyclic temperature was controlled in tests at 927°C (1700°F) and 1038°C (1900°F) to replicate predicted steady-state engine conditions. The out-of-phase cycle (Figure 4), with a minimum cyclic temperature of 427°C (800°F), was used for these tests, and for the majority of the TMF experimental program, since it is generically representative of an engine thermal-mechanical temperature excursion. Controlled stress testing was also conducted for a maximum cyclic temperature of 1093°C (2000°F). Due to the high temperatures and stresses (i.e., high inelastic strains), the majority of these tests were conducted in the strain-controlled mode. Cyclic frequency extremes of 4.0 cpm and 0.2 cpm were investigated. The former represents the maximum limit of TMF cyclic capability and approaches the actual engine transient time. The latter represents the minimum practical frequency at which tests could be conducted. Maximum temperature hold periods of 30 seconds and 2 minutes were investigated to simulate hold periods in engine operation, which range from 0 to 2 minutes. A shutdown cycle (a modified out-of-phase cycle incorporating an excursion to room temperature at constant mechanical strain) was also conducted. A quadrilateral type cycle (Figure 5) which represents predicted engine transient behavior, was conducted to generate baseline data for modeling. The majority of quadrilateral cycle testing was conducted using the strain control TMF (SCTMF) test method. In addition, a number of tests were conducted in inert (argon) environment. Tests were run both with and without a 2-minute hold. The results provided valuable information for the development of environmental damage modeling methodologies.

The SCTMF test matrix is presented in Table 6. SCTMF test methods were used to generate the majority of the baseline data and investigate complex cycles. Baseline tests were conducted for maximum cyclic temperatures of 927°C (1700°F), 1038°C (1900°F), and 1093°C (2000°F) using the out-of-phase cycle. A number of in-phase strain and temperature tests (Type 2 cycles) were run for use in the modeling effort. The 427° to 1093°C (800° to 2000°F) and some 427° to 1038°C (800° to 1900°F) controlled-stress tests were conducted in SCTMF, as previously discussed. Complex cycle tests were run both with and without the stress controlled at the maximum cyclic temperature.

The LATMF test results for uncoated, aluminide coated (PWA 275), and overlay coated (PWA 286) PWA 1480 are presented in Tables 7, 8, and 9, respectively. SCTMF test results for the uncoated, aluminide coated (PWA 275), and overlay coated (PWA 286) PWA 1480 are

presented in Tables 10, 11, and 12, respectively. Fatigue life versus mechanical strain range for uncoated, aluminide coated IPWA 275), and overlay coated (PWA 286) PWA 1480 are shown in Figures 35, 36, and 37, respectively. Both LATMF and SCTMF are shown in these figures.

2.3.2 Mean Stress Effects

To examine the effects of mean stress on TMF, out-of-phase tests were run with the minimum stress controlled to be constant at a higher stress than typically seen by Type I cycle that stress-relaxed naturally (baseline tests). For tests with maximum temperature at 827°C (1700°F), the minimum offset stress was held at 124 MPa (18.0 ksi), for 1038°C (1900°F) maximum temperature, the controlled minimum stress was 72 MPa (10.5 ksi), and for maximum temperature of 1093°C (2000°F), the minimum stress was 62 MPa (9.0 ksi). Comparison plots of uncoated PWA 1480 controlled stress test results with baseline out-of-phase (Type 1 cycle) test results are shown in Figures 38, 39, and 40, for the temperature ranges 427-827°C (800-1700°F), 427-1038°C (800-1900°F), and 427-1093°C (800-2000°F), respectively. Similarly, comparison plots of aluminide coated (PWA 275) and overlay coated (PWA 286) PWA 1480 over the same temperature ranges are shown in Figures 41, 42, and 43 for the aluminide coated material and Figures 44, 45, and 46 for the overlay coated material.

The decreased fatigue lives were expected due to the larger tensile stresses imposed in the stress-controlled tests, as compared to standard out-of-phase TMF test (Figure 47). The offset in the mean stress increases the tensile hysteretic energy imposed in the TMF cycle and causes a degradation in fatigue life, which the current energy model would predict.

The effect of the controlled minimum stress on the fatigue life of the uncoated PWA 1480 decreases with decreasing strain range. A 2X-life degradation is shown in the 0.6 percent strain range tests in all the temperature ranges tested. However, at the lower strain range tested (0.4 percent), this effect is reduced.

The aluminide coated (PWA 275) PWA 1480 shows much less effect on fatigue life due to the minimum stress control. The 427-1038°C (800-1900°F) out-of-phase cycle (Figure 43) shows the minimum stress effect on the fatigue life increases with decreasing strain. Time at temperature effects may be occurring due to the minimum stress being tensile rather than compressive at maximum temperature.

The effect of the minimum stress on fatigue life of the overlay coated (PWA 286) PWA 1480 decreases with increasing temperature range (increasing maximum test temperature). An approximate 4X-life degradation is exhibited at the 0.6 percent strain range for the 427-927°C (800-1700°F) temperature range (Figure 44). The 427-1038°C (800-1900°F) out-of-phase cycle shows the minimum stress produces an approximate 2X-life debit throughout the strain ranges tested (Figure 44). While the 427-1093°C (800-2000°F) temperature range exhibits no significant life degradation ($<\frac{1}{3}$X-cyclic life debit at 0.6 percent strain range). Uncoated and aluminide coated PWA 1480 do not experience this increased life degradation with decreasing temperature range. These results would indicate that the increased degradation shown in the overlay coated PWA 1480 is related to the coating behavior.

2.3.3 Frequency Effects

Testing for frequency effects was performed at 0.2, 1, and 4 cpm for uncoated, aluminide coated (PWA 275), and overlay coated (PWA 286) PWA 1480 as shown in Figures 48, 49, and 50, respectively. It was observed that there is little effect on life due to the factor-of-20 shift in cyclic frequency at the higher strain range tested (0.6 percent) for all the uncoated and coated tests. However, a 2X-life degradation is shown at the lower strain range tested (0.4 percent) for the aluminide and overlay coated tests for the 0.2 cpm frequency.

The degradation is related to both creep and environmental effects. Results of the hold time test comparisons between ambient air and the inert environments provided additional insight into the role of oxidation on cyclic life. The creep damage effect was addressed through stress relaxation tests that determined primary creep rates for PWA 1480.

2.3.4 Hold Time Effects

Another cycle type that significantly reduces TMF life compared to the 427°C (800°F) to 1038°C (1900°F) out-of-phase uncoated baseline was an out-of-phase cycle with a 30-second and 120-second hold at maximum cyclic temperature. Results of these hold time tests for uncoated, aluminide coated (PWA 275), and overlay coated (PWA 286) PWA 1480 are shown in Figures 51, 52, and 53, respectively.

The uncoated PWA 1480 did not exhibit a significant effect on life for the tests with 30-second hold times. The hold time of 120 seconds showed more of a life debit at 0.6% strain range but no debit at 0.4% strain range. It is assumed, therefore, that larger strain ranges and more than 30 seconds at the maximum temperature are required for significant damage to occur in uncoated PWA 1480.

The data for aluminide coated (PWA 275) PWA 1480 show a 2X-cyclic life degradation for the hold times of 30 seconds and 120 seconds at the maximum cyclic temperature. However, there is no significant life difference between the 30-second hold time and the 120-second hold time results. It is assumed that for the PWA 275 coated tests, the majority of the hold time compressive creep damage occurs within the first 30 seconds with a very reduced effect occurring in the following 90 seconds of hold time.

The data for overlay coated (PWA 286) PWA 1480 show a life degradation for both the 30-second and 120-second hold times. The difference in life exhibited by the two different hold times may be attributed to environmental effects. Further insight into creep and environmental damage may be gained from hold time tests in the inert environment.

2.3.5 Shutdown Cycle Effects

A modified out-of-phase cycle incorporating an excursion to room temperature at constant strain (referred to as a shutdown cycle (Figure 54) was performed on the aluminide and overlay coated PWA 1480 for a comparison to the standard 427-1038°C (800-1900°F) and 427-1093°C (800-2000°F) out-of-phase cycles. The excursion to room temperature at constant strain range was thought to have a significant effect on fatigue life of coated material systems. The coatings generally experience a loss of ductility at low temperature which can contribute to premature cracking and failure. The initial shutdown test cycle was a low strain range, all-tensile (tensile mean strain (Figure 54b) out-of-phase type cycle with a constant strain excursion to 38°C (100°F). The reasoning for the low strain range mean offset cycle was to possibly degrade the coating with maximum tensile strains during the excursion to 38°C (100°F). This cycle does not incorporate the high temperature compressive strain portion of the standard out-of-phase cycle as shown in Figure 54a. Results of these tests (for uncoated, PWA 275 and PWA 286 coated PWA 1480) showed no significant degradation due to the shutdown portion of the cycle or the mean offset strain (Figures 55, 56, and 57). However, the mean offset strain cycle may actually incorporate less cyclic damage due to the absence of the high temperature compressive strain portion of the cycle.

2.3.6 In-Phase Cycles

One in-phase (Type 2) cycle test, as shown in Figure 58, was performed for each uncoated, aluminide coated, and overlay coated PWA 1480 sample. The uncoated PWA 1480 was tested at

427-1038°C (800-1900°F), 0.6 percent strain range and 1 cpm frequency. The in-phase test was compared to the standard out-of-phase tests in Figure 59. The in-phase test does not exhibit a significant difference in fatigue life compared to the out-of-phase tests. For the PWA 1480 with coatings, in-phase tests were conducted at 472-1038°C (800-1900°F), 0.8 percent strain range and 1 cpm frequency in Figures 60 and 61. For both the aluminide (PWA 275) coated and the overlay (PWA 286) coated PWA 1480 there was a significant life benefit for the in-phase cycle. The in-phase cycle has the maximum stress at the maximum temperature. The life benefit of the coated material is due to the low mean stress of the cycle and the high ductility of the coating at the maximum temperature. The in-phase cycle incorporates less damage to the coating than the out-of-phase cycle. The uncoated material does not exhibit this drastic change in ductility at high temperatures and, therefore, does not demonstrate as significant a life benefit as the coated material.

2.3.7 Quadrilateral Cycles

The quadrilateral (quad) type cycle (Figure 62), which represents predicted engine transient behavior, has been used for testing uncoated, aluminide coated (PWA 275), and overlay coated (PWA 286) PWA 1480, and the results are plotted in Figures 63, 64, and 65, respectively. Baseline out-of-phase test results are also presented showing the large difference in cyclic life between the two cycle types (6× to 20×). The uncoated PWA 1480 low strain range quad (0.7 percent $\Delta\varepsilon$) has a cyclic life comparable to a 0.4 percent strain range standard out-of-phase cycle at the same temperature range (Figure 63). These differences appear larger in the case of the two coatings.

Even more interesting is that when all the coated system results for the quadrilateral cycle are plotted together, the differences in cyclic life are very small (Figure 66). Although the uncoated and aluminide coated (0.7 percent) quadrilateral tests resulted in no failure (due to control problems late in testing), the cyclic lives would probably have been similar. The aluminide coating (PWA 275) was so aggravated by this cycle type that at approximately 8000 cycles the coating had completely spalled off, essentially leaving an uncoated sample. The uncoated PWA 1480 tested with this cycle type appeared to go through an alternating series of first surface oxidation and subsequent spallation. Oxidation was severe enough to produce a substantial loss of cross-sectional area which lead to failure. The overlay coated (PWA 286) PWA 1480 sample that was tested similarly did not spall the coating off the substrate. However, the overlay coating did experience severe coating attack and oxidation which produced extreme coating cracking. This left the substrate without oxidation protection, again producing essentially an uncoated sample. The higher strain range (1.05 percent) quadrilateral cycle did not appear to degrade the coating as with the lower strain range. Apparently, the samples failed prior to the onset of extreme coating degradation. The higher strain range allowed coating cracks to propagate into the substrate producing ultimate failure.

2.3.8 Temperature Range Effects

Out-of-phase TMF test results for the uncoated material show that an increase in maximum cyclic temperature reduces cyclic life (Figure 67). Although high maximum cyclic temperature during compressive stress results in higher mean stress (due to stress relaxation) and an increased amount of mechanical damage, it is probable that there is also an environmental interaction. Similar results are shown for the aluminide coated (PWA 275) and overlay coated (PWA 286) PWA 1480, Figures 68 and 69, respectively. The maximum cyclic temperature comparisons of uncoated, PWA 275 coated, and coated (PWA 286) PWA 1480 provide the baseline temperature effects information necessary for the modeling effort.

2.3.9 Coating Effects

Comparison plots of uncoated, PWA 275 coated, and PWA 286 coated PWA 1480 out-of-phase TMF test results are shown in Figures 70, 71, and 72 for the temperature ranges studied, 427-927°C (800-1700°F), 427-1038°C (800-1900°F), and 427-1093°C (800-2000°F), respectively. Initially, the PWA 286 overlay coating was expected to exhibit a greater TMF debit than the PWA 275 aluminide coating. However, throughout the temperature ranges tested, the overlay coated (PWA 286) PWA 1480 consistently showed smaller TMF debits compared to the aluminide-coated (PWA 275) PWA 1480. Further information on coating degradation (both aluminide and overlay coatings) as a function of temperature range is presented in the metallurgical evaluation.

For shutdown cycles, the overlay (PWA 286) coated material has the largest life debit compared to the aluminide (PWA 275) coated and the uncoated PWA 1480 (Figure 73). This is because the overlay coating exhibits continuously decreasing ductility as the temperature decreases. As the temperature went from 427°C (800°F) to 38°C (100°F) the ductility of the PWA 286 decreases whereas the ductility of the PWA 275 aluminide coating remained essentially constant. The aluminide coating has no effect on the fatigue life compared to the uncoated PWA 1480. There was no significant effect of the coatings for quadrilateral cycles (Figure 74). This is due to the extreme coating degradation caused by the large compressive strains of the cycle, which results in essentially uncoated behavior.

2.3.10 Inert Environment Testing

Inert environment TMF tests have been conducted to determine the role of oxidation on cyclic life, possibly as an environmental damage term for the modeling effort. The inert environment test system used for this testing contained argon at 15 psig with a partial pressure of oxygen below 10^{-5} ppm 0_2 ($<10^{-11}$ atm.). The inert environment chamber and a basic schematic of the test system are shown in Figures 75 and 76. The system features the addition of an oxygen "gettering" furnace, a gas analyzer, and improved seal modifications.

The standard out-of-phase TMF cycle was used for preliminary inert environment tests for direct comparison to air testing. In addition, the standard out-of-phase cycle was used with a hold time at maximum cyclic temperature to further investigate creep and oxidation effects.

The uncoated PWA 1480 427-1037°C (800-1900°F) out-of-phase tests in argon showed that there exists no significant life benefit over the similar air environment out-of-phase cycle. The increase in life in the inert environment compared to the air environment is less than 1.5 times (Figure 77). The argon environment also had little effect on the life of the overlay (PWA 286) coated PWA 1480. This was true for all cases tested (Figures 78 and 79).

The inert environment had little effect on the life of the aluminide (PWA 275) coated PWA 1480 for out-of-phase tests at 427-1037°C (800-1900°F) with no hold times and with two-minute hold times. There were significant life benefits for the out-of-phase tests at 427-1037°C (800-1900°F) with a 30-second hold time (2.5× life increase) and out-of-phase tests at 427-1093°C (800-2000°F) with no hold (3.5× life increase), as shown in Figures 78 and 80. The only quad cycle tested in the argon environment was for the aluminide coated PWA 1480, which exhibited a slight life debit in argon as compared to the air environment. This is well within the scatter of the quad cycles.

The inert environment tests fall within the scatter of all of the tests for uncoated, PWA 275 coated, and PWA 286 coated PWA 1480 as shown in Figures 81, 82, and 83. This makes determining the true environment effect very difficult because, for all of the above cases, the tests in argon fall within the limits of the tests in air. Even though the PWA 275 coated 30-second

hold and the high temperature (427-1093°C (800-2000°F)) tests demonstrated a much greater life in argon than in air, there does not appear to be sufficient evidence of a trend. The fact that the environment does not appear to have an effect was unexpected. An environment term in the model would not be feasible at this time. Therefore, the environment effect was considered to be negligible.

TABLE 5. LATMF Test Matrix

Cycle Type	*Frequency cpm*	*Controlled Stress*	*ΔT-°C(°F)*	*Coating*		
				PWA 286	*PWA 275*	*Uncoated*
1 — (Controlled σ)	1	σ*1700	427 to 927 (800 to 1700)	2	2	2
1 — (Controlled σ)	1	σ*1900	427 to 1038 (800 to 1900)	2	2	2
1 — (Controlled σ)	0.5	σ*2000	427 to 1093 (800 to 2000)	1	1	
1 — (Frequency Effect)	4	—	427 to 1038 (800 to 1900)	2	2	2
1 — (Frequency Effect)	1	—	427 to 1038 (800 to 1900)	1*	*	2*
1 — (Frequency Effect)	0.2	—	427 to 1038 (800 to 1900)	2	2	2
1 — (30-sec Hold, T_{max})	1	—	427 to 1038 (800 to 1900)	2	2	
1 — (2-min Hold, T_{max})	1	—	427 to 1038 (800 to 1900)	2	2	2
1 — (Inert Environment)	1	—	427 to 1038 (800 to 1900)	2	2	2
1 — (Inert Environment 2-min Hold, T_{max})	1	—	427 to 1038 (800 to 1900)	2	2	2
Shutdown Cycle	0.3	—	RT to 1093 (RT to 2000)	2	1	1
Quadrilateral Cycle	0.5	—	427 to 1093 (800 to 2000)			1

*Determined from Task I results

56 Tests
Discretionary — 8
Total — 64

R20505/1

TABLE 6. SCTMF Test Matrix

Cycle Type	*Frequency — cpm*	*Controlled Stress*	*ΔT — °C (°F)*	*Coating*		
				PWA 286	*PWA 275*	*Uncoated*
1 — (Baseline)	1	—	427 to 927 (800 to 1700)	2	2	2
	1	—	427 to 1038 (800 to 1900)	3	2	2
	0.5	—	427 to 1093 (800 to 2000)	2	2	2
2 — (In-phase)	1	—	427 to 1038 (800 to 1900)	1	1	
1 — (Controlled σ)	1	σ*1900	427 to 1038 (800 to 1900)	1	1	1
1 — (Controlled σ)	0.5	σ*2000	427 to 1038 (800 to 2000)	2	2	2
Quadrilateral	0.5	—	427 to 1093 (800 to 2000)	2	2	2
Quadrilateral Cycle (Controlled Stress)	0.5	σ*2000	427 to 1093 (800 to 2000)	2	2	2

*From Task I results

42 Tests

Discretionary — 3

Total — 45

R20505/1

TABLE 7. Uncoated PWA 1480 TMF Test Results

Cycle Type	*Control Mode*	*ΔT,°C(°F)*	*Δε-%**	*Frequency cpm*	*Special Conditions*	*Δσ at $N_f/2$, MPa (ksi)*	*σ_{mean} at $N_f/2$, MPa (ksi)*	*N_f*
Out-of-Phase	LATMF	427-927 (800-1700)	0.6	1	Fixed $\sigma_{min} \approx$ 124 MPa (18 ksi)	661 (96)	455 (66)	16,440
Out-of-Phase	LATMF	427-927 (800-1700)	0.4	1	Fixed $\sigma_{min} \approx$ 124 MPa (18 ksi)	441 (64)	345 (50)	113,392
Out-of-Phase	LATMF	427-1038 (800-1900)	0.6	1	Fixed $\sigma_{min} \approx$ 72.4 MPa (10.5 ksi)	648 (94)	396 (58)	4,409
Out-of-Phase	LATMF	427-1038 (800-1900)	0.4	1	Fixed $\sigma_{min} \approx$ 79.3 MPa (11.5 ksi)	424 (62)	292 (42)	56,789
Out-of-Phase	LATMF	427-1038 (800-1900)	0.6	4	—	641 (93)	162 (24)	12,250
Out-of-Phase	LATMF	427-1038 (800-1900)	0.4	4	—	427 (62)	90 (13)	61,095
Out-of-Phase	LATMF	427-1038 (800-1900)	0.6	1	—	648 (94)	165 (24)	8,679
Out-of-Phase	LATMF	427-1038 (800-1900)	0.4	1	—	434 (63)	107 (16)	41,906
Out-of-Phase	LATMF	427-1038 (800-1900)	0.6	0.2	—	648 (94)	268 (39)	8,481
Out-of-Phase	LATMF	427-1038 (800-1900)	0.6	1	30 sec hold at T_{max}	648 (94)	186 (27)	9,095
Out-of-Phase	LATMF	427-1038 (800-1900)	0.4	1	30 sec hold at T_{max}	427 (62)	117 (17)	36,730
Out-of-Phase	LATMF	427-1038 (800-1900)	0.6	1	120 sec hold at T_{max}	648 (94)	220 (32)	3,612
Out-of-Phase	LATMF	427-1038 (800-1900)	0.4	1	120 sec hold at T_{max}	427 (62)	172 (25)	28,712
Out-of-Phase	LATMF	427-1038 (800-1900)	0.6	1	Inert Environment ($<10^{-5}$ ppm O_2)	648 (94)	165 (24)	9,658
Shutdown	LATMF	38-1093 (100-2000)	0.3	0.3	—	358 (52)	179 (26)	31,094
Quadrilateral	LATMF	427-1093 (800-2000)	0.7	0.5	—	683 (99)	114 (17)	9,849

* All tests $\bar{\varepsilon}_m = 0$, except tests with a fixed minimum stress.

TABLE 7. Uncoated PWA 1480 TMF Test Results (Continued)

Cycle Type	*Control Mode*	*ΔT,°C(°F)*	*Δε-%**	*Frequency cpm*	*Special Conditions*	*Δσ at $N_f/2$, MPa (ksi)*	*σ_{mean} at $N_f/2$, MPa (ksi)*	*N_f*
Out-of-Phase	LATMF	427-1038 (800-1900)	0.5	1	—	531 (77)	203 (30)	19,484
Out-of-Phase	LATMF	427-1038 (800-1900)	0.4	0.2	—	427 (62)	110 (16)	37,000
Out-of-Phase	LATMF	427-1038 (800-1900)	0.8	1	Inert Environment ($<10^{-5}$ ppm O_2)	841 (122)	290 (42)	3,069
Out-of-Phase	LATMF	427-1038 (800-1900)	0.6	1	Inert Environment ($<10^{-5}$ ppm O_2)	648 (94)	172 (25)	11,102
In-Phase	LATMF	427-1038 (800-1900)	0.6	1	—	648 (94)	−165 (−24)	13,343
Out-of-Phase	LATMF	427-927 (800-1700)	0.6	1	—	662 (96)	69 (10)	25,151
Out-of-Phase	LATMF	427-1093 (800-2000)	0.6	0.5	—	618 (90)	256 (37)	7,121

* All tests $\bar{\varepsilon}_m = 0$, except tests with a fixed minimum stress.

R20506/1

TABLE 8. PWA 1480/275 TMF Test Results

Cycle Type	*Control Mode*	*ΔT,°C(°F)*	*Δε-%**	*Frequency cpm*	*Special Conditions*	*Δσ at $N_f/2$, MPa (ksi)*	*σ_{mean} at $N_f/2$, MPa (ksi)*	*N_f*
Out-of-Phase	LATMF	427-927 (800-1700)	0.6	1	Fixed σ_{min} = 124 MPa (18 ksi)	648 (94)	448 (65)	4,328
Out-of-Phase	LATMF	427-1038 (800-1900)	0.6	1	Fixed σ_{min} = 72.4 MPa (10.5 ksi)	652 (95)	399 (58)	3,180
Out-of-Phase	LATMF	427-1038 (800-1900)	0.4	1	Fixed σ_{min} = 72.4 MPa (10.5 ksi)	445 (65)	295 (43)	19,444
Out-of-Phase	LATMF	427-1093 (800-2000)	0.4	0.5	Fixed σ_{min} = 62 MPa (9 ksi)	414 (60)	268 (39)	6,177
Out-of-Phase	LATMF	427-1038 (800-1900)	0.6	4		648 (94)	193 (28)	5,527
Out-of-Phase	LATMF	427-1038 (800-1900)	0.4	4		427 (62)	117 (17)	35,042
Out-of-Phase	LATMF	427-1038 (800-1900)	0.6	1		655 (95)	155 (23)	5,405
Out-of-Phase	LATMF	427-1038 (800-1900)	0.5	1		531 (77)	121 (18)	13,445
Out-of-Phase	LATMF	427-1038 (800-1900)	0.6	0.2		551 (94)	227 (33)	3,631
Out-of-Phase	LATMF	427-1038 (800-1900)	0.4	0.2		427 (62)	124 (18)	15,790
Out-of-Phase	LATMF	427-1038 (800-1900)	0.6	1	30-sec hold at T_{max}	648 (94)	241 (35)	3,297
Out-of-Phase	LATMF	427-1038 (800-1900)	0.4	1	30-sec hold at T_{max}	427 (62)	138 (20)	13,320
Out-of-Phase	LATMF	427-1038 (800-1900)	0.6	1	2-min hold at T_{max}	648 (94)	255 (37)	2,876
Out-of-Phase	LATMF	427-1038 (800-1900)	0.4	1	2-min hold at T_{max}	427 (62)	159 (23)	11,674
Out-of-Phase	LATMF	427-1038 (800-1900)	0.6	1	Inert Environment ($<10^{-5}$ ppm O_2)	655 (95)	197 (29)	8,000 (Contamination)

* All tests $\bar{\varepsilon}_m = 0$, except tests with a fixed minimum stress.

TABLE 8. PWA 1480/275 TMF Test Results (Continued)

Cycle Type	*Control Mode*	*ΔT,°C(°F)*	*Δε-%**	*Frequency cpm*	*Special Conditions*	*Δσ at $N_f/2$, MPa (ksi)*	*σ_{mean} at $N_f/2$, MPa (ksi)*	*N_f*
Out-of-Phase	LATMF	427-1038 (800-1900)	0.6	1	30-sec hold at T_{max}, Inert Environment ($<10^{-5}$ ppm O_2)	655 (95)	197 (29)	8,629
Out-of-Phase	LATMF	427-1038 (800-1900)	0.6	1	120-sec hold at T_{max}, Inert Environment ($<10^{-5}$ ppm O_2)	648 (94)	207 (30)	3,718
Shutdown	LATMF	38-1093 (100-2000)	0.3	0.3	Fixed σ_{min} = 0 MPa (0 ksi)	359 (52)	179 (26)	33,567
Shutdown	LATMF	38-1093 (100-2000)	0.6	0.3		696 (101)	279 (41)	3,242
Out-of-Phase	LATMF	427-1038 (800-1990)	0.6	1	Inert Environment ($<10^{-5}$ ppm O_2)	648 (94)	228 (33)	5,720
Out-of-Phase	LATMF	427-1038 (800-1990)	0.4	1	Inert Environment ($<10^{-5}$ ppm O_2)	427 (62)	131 (19)	26,809
Out-of-Phase	LATMF	427-1038 (800-1990)	0.6	1	Inert Environment ($<10^{-5}$ ppm O_2)	648 (94)	200 (29)	5,693
In-Phase	LATMF	427-1038 (800-1990)	0.8	1	Inert Environment ($<10^{-5}$ ppm O_2)	814 (118)	−179 (−26)	1,648
Out-of-Phase	LATMF	427-1038 (800-1990)	0 55	1	Inert Environment ($<10^{-5}$ ppm O_2)	600 (87)	141 (21)	13,864
Out-of-Phase	LATMF	427-1093 (800-2000)	0.6	0.5	Inert Environment ($<10^{-5}$ ppm O_2)	621 (90)	241 (35)	6,957
Quad	LATMF	427-1093 (800-2000)	0.7	1	Inert Environment ($<10^{-5}$ ppm O_2)	676 (98)	62 (9)	12,000 DNF

* All tests $\bar{\varepsilon}_m$ = 0, except tests with a fixed minimum stress.

R20505/1

TABLE 9. PWA 1480/286 TMF Test Results

Cycle Type	*Control Mode*	*ΔT,°C(°F)*	*Δε-%**	*Frequency cpm*	*Special Conditions*	*Δσ at $N_f/2$, MPa (ksi)*	*σ_{mean} at $N_f/2$, MPa (ksi)*	*N_f*
Out-of-Phase	LATMF	427-927 (800-1700)	0.6	1	Fixed σ_{min} = 124 MPa (18 ksi)	655 (95)	452 (66)	7,281
Out-of-Phase	LATMF	427-927 (800-1700)	0.4	1	Fixed σ_{min} = 124 MPa (18 ksi)	441 (64)	344 (50)	50,184
Out-of-Phase	LATMF	427-1038 (800-1900)	0.6	1	Fixed σ_{min} = 72.4 MPa (10.5 ksi)	648 (94)	396 (58)	4,140
Out-of-Phase	LATMF	427-1038 (800-1900)	0.4	1	Fixed σ_{min} = 72.4 MPa (10.5 ksi)	427 (62)	286 (42)	15,432
Out-of-Phase	LATMF	427-1093 (800-2000)	0.4	0.5	Fixed σ_{min} = 62 MPa (9 ksi)	420 (61)	272 (40)	9,298
Out-of-Phase	LATMF	427-1038 (800-1900)	0.6	4	—	648 (94)	138 (20)	6,149
Out-of-Phase	LATMF	427-1038 (800-1900)	0.4	4	—	427 (62)	76 (11)	63,243
Out-of-Phase	LATMF	427-1038 (800-1900)	0.6	1	—	648 (94)	165 (24)	5,575
Out-of-Phase	LATMF	427-1038 (800-1900)	0.4	1	—	427 (62)	83 (12)	32,855
Out-of-Phase	LATMF	427-1038 (800-1900)	0.6	1	30-sec hold at T_{max}	648 (94)	200 (29)	4,278
Out-of-Phase	LATMF	427-1038 (800-1900)	0.4	1	30-sec hold at T_{max}	434 (63)	93 (14)	11,388
Out-of-Phase	LATMF	427-1038 (800-1900)	0.6	1	2-min hold at T_{max}	648 (94)	193 (28)	3,064
Out-of-Phase	LATMF	427-1038 (800-1900)	0.4	1	2-min hold at T_{max}	427 (62)	131 (19)	7,834
Out-of-Phase	LATMF	427-1038 (800-1900)	0.6	1	Inert Environment ($<10^{-5}$ ppm O_2)	648 (94)	186 (27)	5,853

TABLE 9. PWA 1480/286 TMF Test Results (Continued)

Cycle Type	*Control Mode*	*ΔT,°C(°F)*	*Δε-%**	*Frequency cpm*	*Special Conditions*	*Δσ at $N_f/2$, MPa (ksi)*	*σ_{mean} at $N_f/2$, MPa (ksi)*	*N_f*
Out-of-Phase	LATMF	427-1038 (800-1900)	0.6	1	30-sec hold T_{max}, Inert Environment ($<10^{-5}$ ppm O_2)	648 (94)	203 (30)	4,744
Out-of-Phase	LATMF	427-1038 (800-1900)	0.6	1	120-sec hold T_{max}, Inert Environment ($<10^{-5}$ ppm O_2)	648 (94)	203 (30)	4,545
Shutdown	LATMF	38-1093 (100-2000)	0.6	0.3	—	688 (100)	227 (33)	2,965
Shutdown	LATMF	38-1093 (100-2000)	0.4	0.3	Fixed σ_{min} = 0 MPa (0 ksi)	475 (69)	238 (35)	7,515
Shutdown	LATMF	38-1093 (100-2000)	0.3	0.3	Fixed σ_{min} = 0 MPa (0 ksi)	358 (52)	179 (26)	12,711
Out-of-Phase	LATMF	427-1038 (800-1900)	0.6	0.2	—	648 (94)	193 (28)	4,275
Out-of-Phase	LATMF	427-1038 (800-1900)	0.4	0.2	—	421 (61)	121 (17.5)	12,441
Out-of-Phase	LATMF	427-1093 (800-2000)	0.6	0.5	Inert Environment ($<10^{-5}$ ppm O_2)	610 (89)	240 (35)	4,458
In-Phase	LATMF	427-1038 (800-1900)	0.8	1	Inert Environment ($<10^{-5}$ ppm O_2)	814 (118)	241 (35)	3,324

* All tests $\bar{\varepsilon}_m = 0$, except tests with a fixed minimum stress.

R20505/1

TABLE 10. Uncoated PWA 1480 TMF Test Results

Cycle Type	*Control Mode*	*ΔT,°C(°F)*	*Δε-%**	*Frequency cpm*	*Special Conditions*	*Δσ at $N_f/2$, MPa (ksi)*	*σ_{mean} at $N_f/2$, MPa (ksi)*	*N_f*
Out-of-Phase	SCTMF	427-927 (800-1700)	0.8	1	—	841 (122)	207 (30)	11,913
Out-of-Phase	SCTMF	427-927 (800-1700)	0.6	1	—	670 (97)	148 (21)	33,004
Out-of-Phase	SCTMF	427-1038 (800-1900)	0.6	1	—	655 (95)	234 (34)	8,593
Out-of-Phase	SCTMF	427-1038 (800-1900)	0.4	1	—	441 (64)	165 (24)	27,978
Out-of-Phase	SCTMF	427-1093 (800-2000)	0.6	0.5	—	620 (90)	248 (36)	5,343
Out-of-Phase	SCTMF	427-1093 (800-2000)	0.4	0.5	—	420 (61)	176 (26)	20,536
Out-of-Phase	SCTMF	427-1038 (800-1900)	0.6	1	Fixed σ_{min} = 75.8 MPa (11.0 ksi)	655 (95)	403 (59)	5,175
Out-of-Phase	SCTMF	427-1038 (800-1900)	0.4	1	Fixed σ_{min} = 72.4 MPa (10.5 ksi)	424 (62)	285 (41)	25,035
Out-of-Phase	SCTMF	427-1093 (800-2000)	0.6	0.5	Fixed σ_{min} = 62 MPa (9 ksi)	717 (104)	420 (61)	2,494
Quadrilateral	SCTMF	427-1093 (800-2000)	1.05	0.5	—	950 (138)	117 (17)	2,235
Out-of-Phase	SCTMF	427-1093 (800-2000)	0.4	0.5	Fixed σ_{min} = 62 MPa (9 ksi)	503 (73)	314 (46)	+13,632 DNF
Quadrilateral	SCTMF	427-1093 (800-2000)	0.7	0.5	—	565 (82)	55 (8)	18,037

* All tests $\bar{\varepsilon}_m = 0$, except tests with a fixed minimum stress.

R20505/1

TABLE 11. PWA 1480/275 TMF Test Results

Cycle Type	*Control Mode*	*ΔT,°C(°F)*	*Δε-%**	*Frequency cpm*	*Special Conditions*	*Δσ at $N_f/2$, MPa (ksi)*	*σ_{mean} at $N_f/2$, MPa (ksi)*	*N_f*
Out-of-Phase	SCTMF	427-927 (800-1700)	0.8	1	—	848 (123)	179 (26)	1,530
Out-of-Phase	SCTMF	427-927 (800-1700)	0.6	1	—	614 (89)	121 (18)	6,236
Out-of-Phase	SCTMF	427-1038 (800-1900)	0.8	1	--	841 (122)	310 (45)	718
Out-of-Phase	SCTMF	427-1038 (800-1900)	0.6	1	–	641 (93)	231 (34)	4,426
Out-of-Phase	SCTMF	427-1093 (800-2000)	0.8	0.5	—	861 (125)	348 (51)	480
Out-of-Phase	TMF	427-1093 (800-2000)	0.6	0.5	—	627 (91)	245 (36)	1,826
In-Phase	SCTMF	427-1038 (800-1900)	0.8	1	—	*855 (124)*	*−310 (−45)*	7,305
Out-of-Phase	SCTMF	427-1038 (800-1900)	0.8	1	Fixed σ_{min} = 72.4 MPa (10.5 ksi)	907 (132)	526 (76)	784
Out-of-Phase	SCTMF	427-1093 (800-2000)	0.8	0.5	Fixed σ_{min} = 62 MPa (9 ksi)	903 (131)	514 (75)	407
Out-of-Phase	SCTMF	427-1093 (800-2000)	0.6	0.5	Fixed σ_{min} = 62 MPa (9 ksi)	676 (98)	400 (58)	2,759
Quadrilateral	SCTMF	427-1093 (800-2000)	1.05	0.5	—	951 (138)	138 (20)	3,531
Quadrilateral	SCTMF	427-103 (800-2000)	0.7	0.5	—	593 (86)	69 (10)	+8,823*+
Quadrilateral	SCTMF	427-1093 (800-2000)	1.05	0.5	Fixed σ_{min} = −275 MPa (−40 ksi)	951 (138)	200 (29)	3,574
Quadrilateral	SCTMF	427-1093 (800-2000)	0.7	0.5	Fixed σ_{min} = −172 MPa (−25 ksi)	579 (84)	177 (17)	16,367

* All tests $\bar{\varepsilon}_m = 0$, except tests with a fixed minimum stress.
**DNF = Did Not Fail

R20505/1

TABLE 12. PWA 1480/286 TMF Test Results

Cycle Type	*Control Mode*	*ΔT,°C(°F)*	*Δε-%**	*Frequency cpm*	*Special Conditions*	*Δσ at $N_f/2$, MPa (ksi)*	*σ_{mean} at $N_f/2$, MPa (ksi)*	*N_f*
Out-of-Phase	SCTMF	427-927 (800-1700)	0.8	1	—	869 (126)	179 (26)	3,931
Out-of-Phase	SCTMF	427-927 (800-1700)	0.6	1	—	648 (94)	93 (14)	27,399
Out-of-Phase	SCTMF	427-1038 (800-1900)	0.8	1	—	834 (121)	286 (42)	2,324
Out-of-Phase	SCTMF	427-1038 (800-1900)	0.6	1	—	614 (89)	197 (29)	4,729
Out-of-Phase	SCTMF	427-1093 (800-2000)	0.8	0.5	—	861 (125)	383 (56)	1,423
Out-of-Phase	SCTMF	427-1093 (800-2000)	0.6	0.5	—	586 (85)	231 (34)	3,208
In-Phase	SCTMF	427-1038 (800-1900)	0.8	1	—	826 (120)	−303 (−44)	11,546
Out-of-Phase	SCTMF	427-1038 (800-1900)	0.8	1	Fixed σ_{min} = 72.4 MPa (10.5 ksi)	789 (115)	467 (68)	1,365
Out-of-Phase	SCTMF	427-1093 (800-2000)	0.8	0.5	Fixed σ_{min} = 62 MPa (9 ksi)	909 (132)	516 (75)	1,282
Out-of-Phase	SCTMF	427-1093 (800-2000)	0.6	0.5	Fixed σ_{min} = 62 MPa (9 ksi)	668 (97)	399 (58)	2,260
Quadrilateral	SCTMF	427-1093 (800-2000)	1.05	0.5		943 (137)	121 (18)	3,678
Quadrilateral	SCTMF	427-1093 (800-2000)	0.7	0.5		620 (90)	69 (10)	11,950
Quadrilateral	SCTMF	427-1093 (800-2000)	1.05	0.5	Fixed σ_{min} = −276 MPa (−40 ksi)	896 (130)	172 (25)	3,577
Quadrilateral	SCTMF	427-1093 (800-2000)	0.7	0.5	Fixed σ_{min} = −172 MPa (−25 ksi)	614 (89)	134 (20)	5,942

Note:
All tests $\bar{\varepsilon}_m = 0_1$ except tests with a fixed minimum stress.

R20606/1

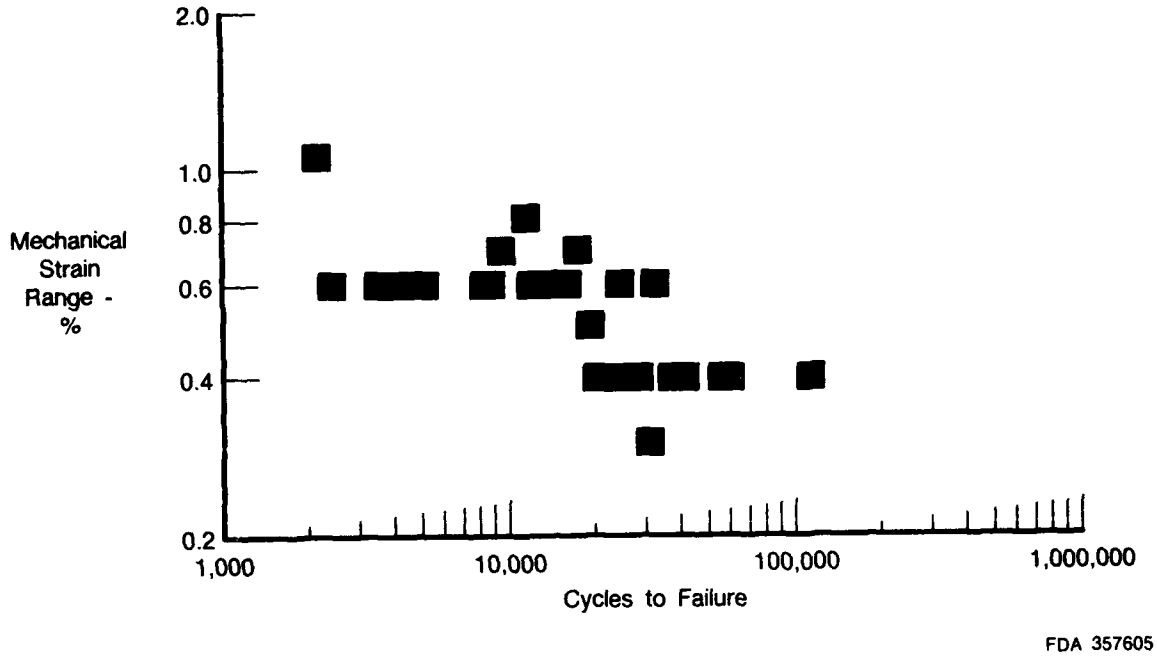

Figure 35. Mechanical Strain Range Versus Fatigue Life for All Uncoated PWA 1480 TMF Tests

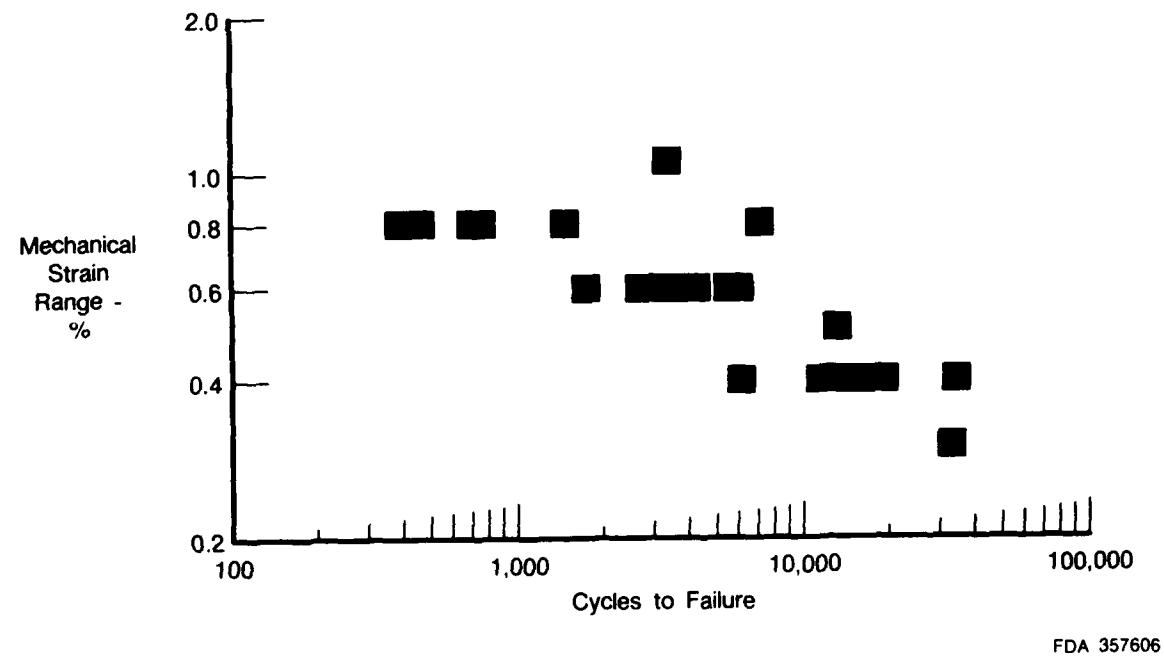

Figure 36. Mechanical Strain Range Versus Fatigue Life for All PWA 275 Coated PWA 1480 TMF Tests

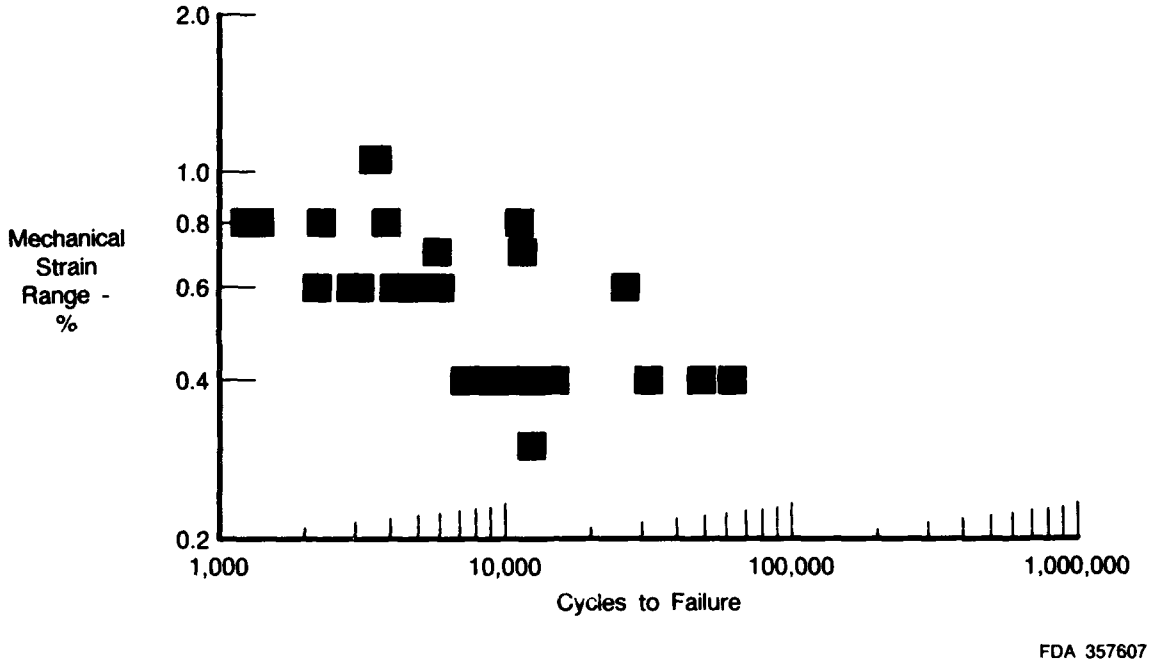

Figure 37. Mechanical Strain Range Versus Fatigue Life for All PWA 286 Coated PWA 1480 TMF Tests

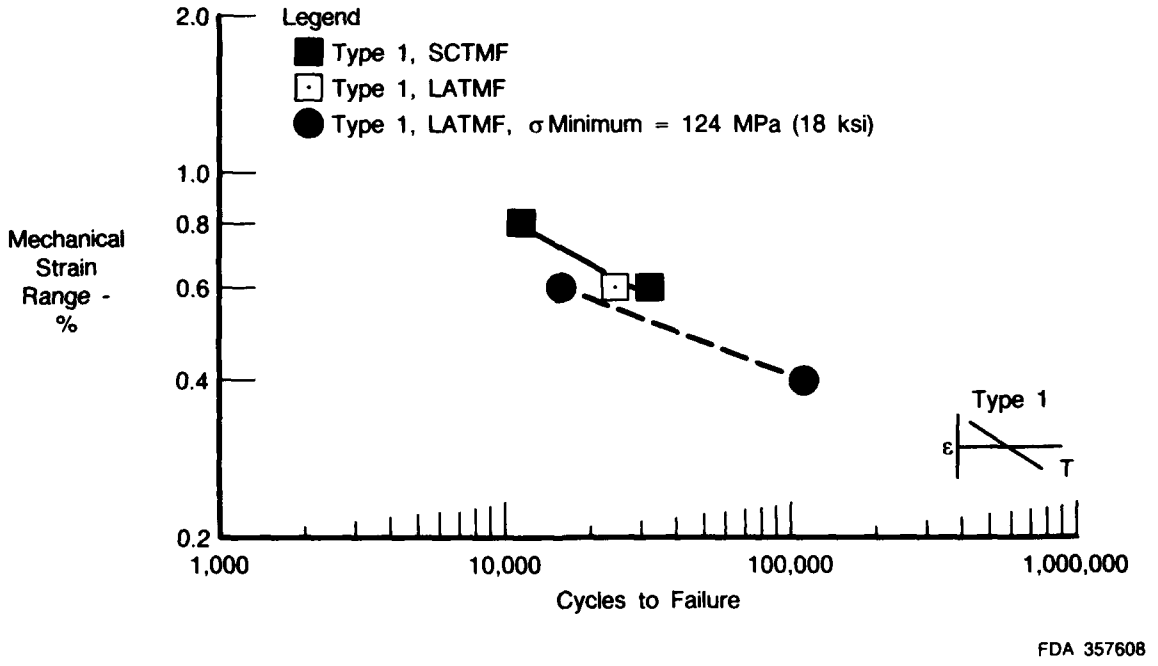

Figure 38. Controlled Minimum Stress Effects on Uncoated PWA 1480 (Out-of-Phase TMF Cycle, 1 cpm, 427-927°C (800-1700°F))

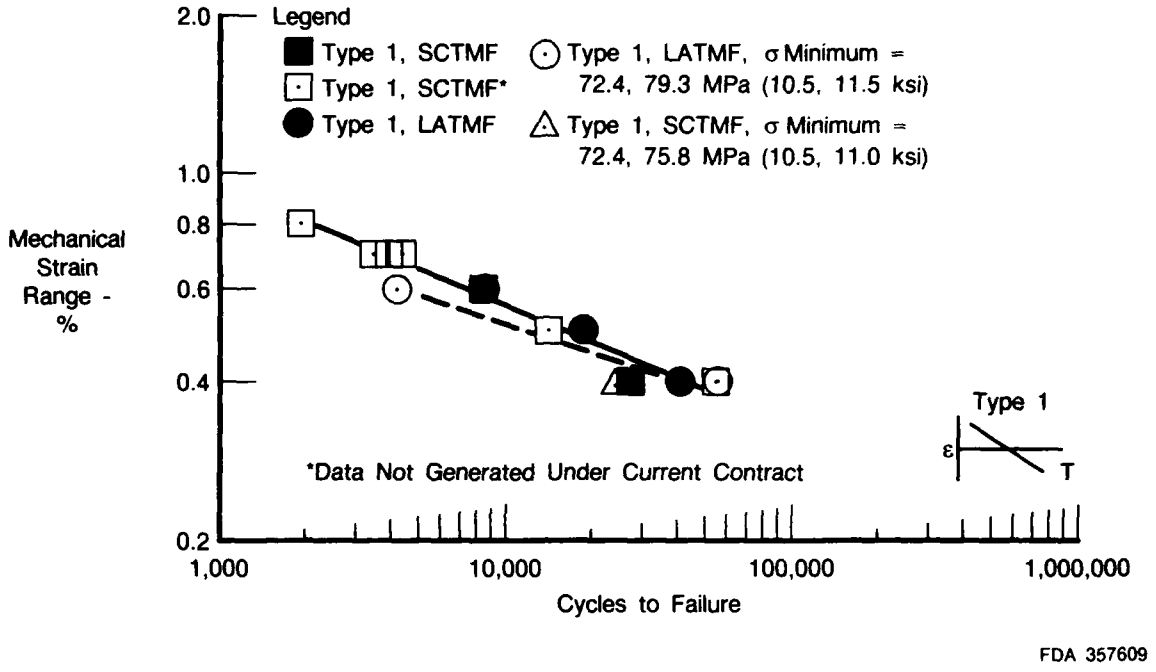

Figure 39. Controlled Minimum Stress Effects on Uncoated PWA 1480 (Out-of-Phase TMF Cycle, 1 cpm, 427-1038°C (800-1900°F))

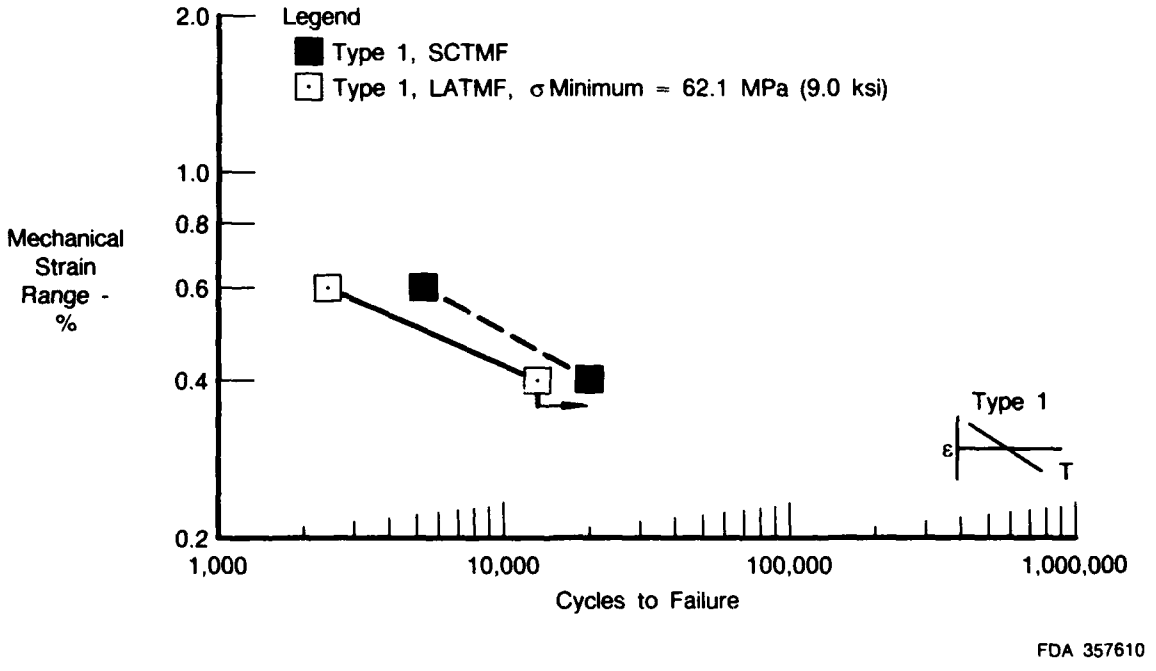

Figure 40. Controlled Minimum Stress Effects on Uncoated PWA 1480 (Out-of-Phase TMF Cycle, 0.5 cpm, 427-1093°C (800-2000°F))

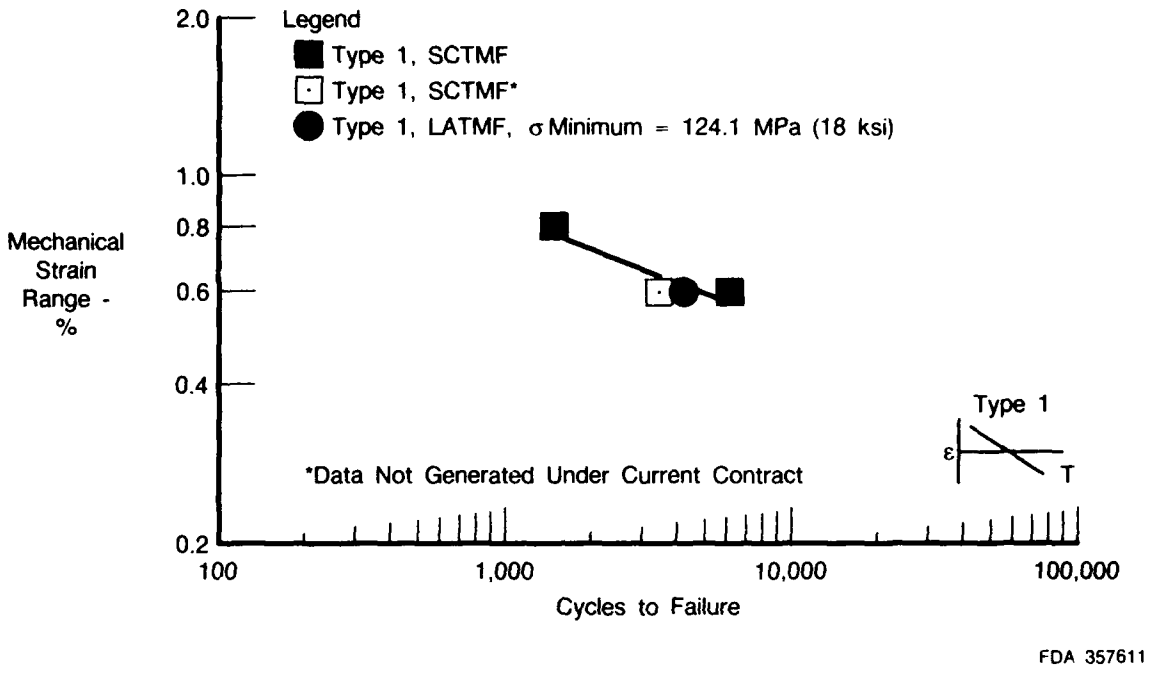

Figure 41. Controlled Minimum Stress Effects on PWA 275 Coated PWA 1480 (Out-of-Phase TMF Cycle, 1 cpm, 427-927°C (800-1700°F))

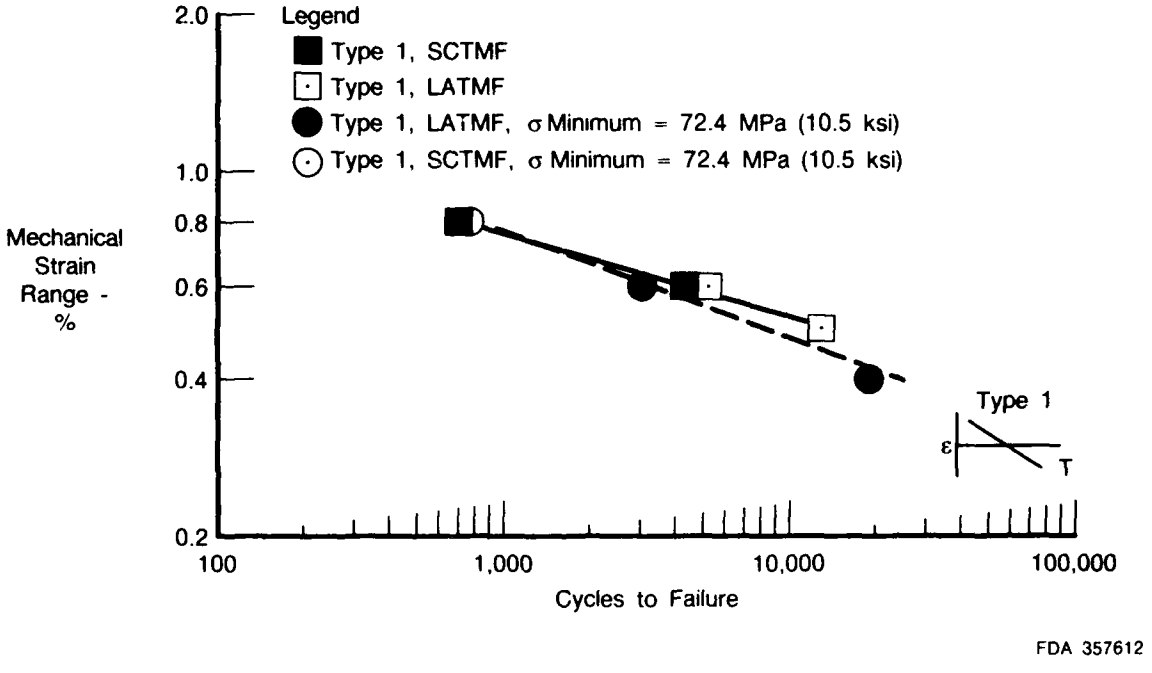

Figure 42. Controlled Minimum Stress Effects on PWA 275 Coated PWA 1480 (Out-of-Phase TMF Cycle, 1 cpm, 427-1038°C (800-1900°F))

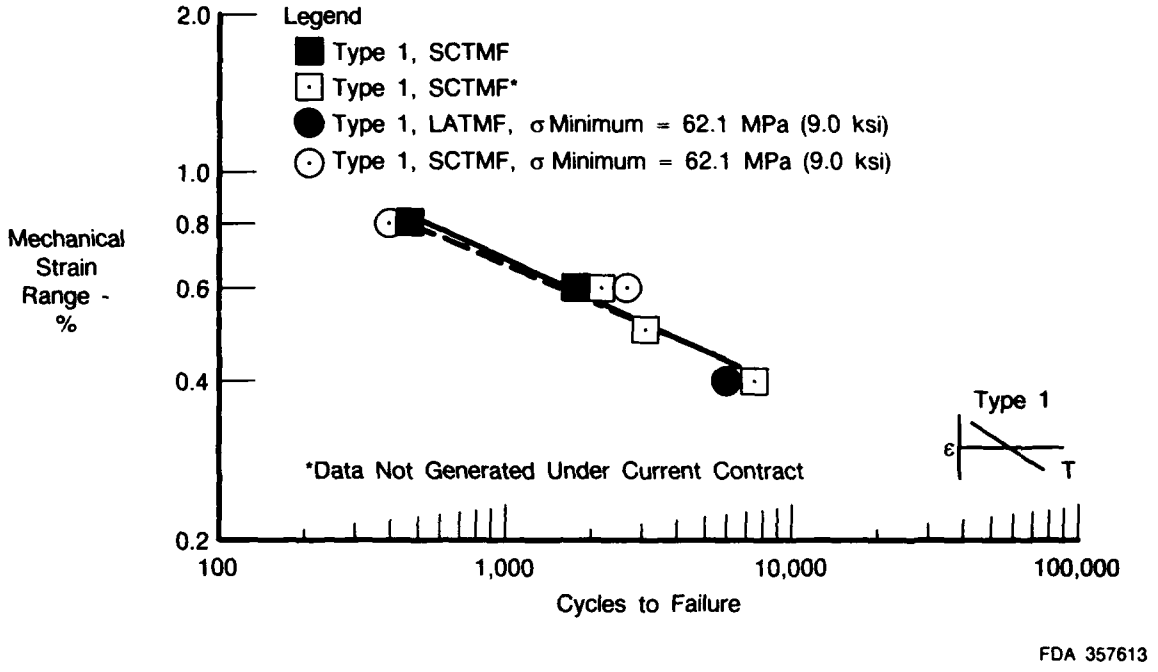

Figure 43. Controlled Minimum Stress Effects on PWA 275 Coated PWA 1480 (Out-of-Phase TMF Cycle, 0.5 cpm, 427-1093°C (800-2000°F))

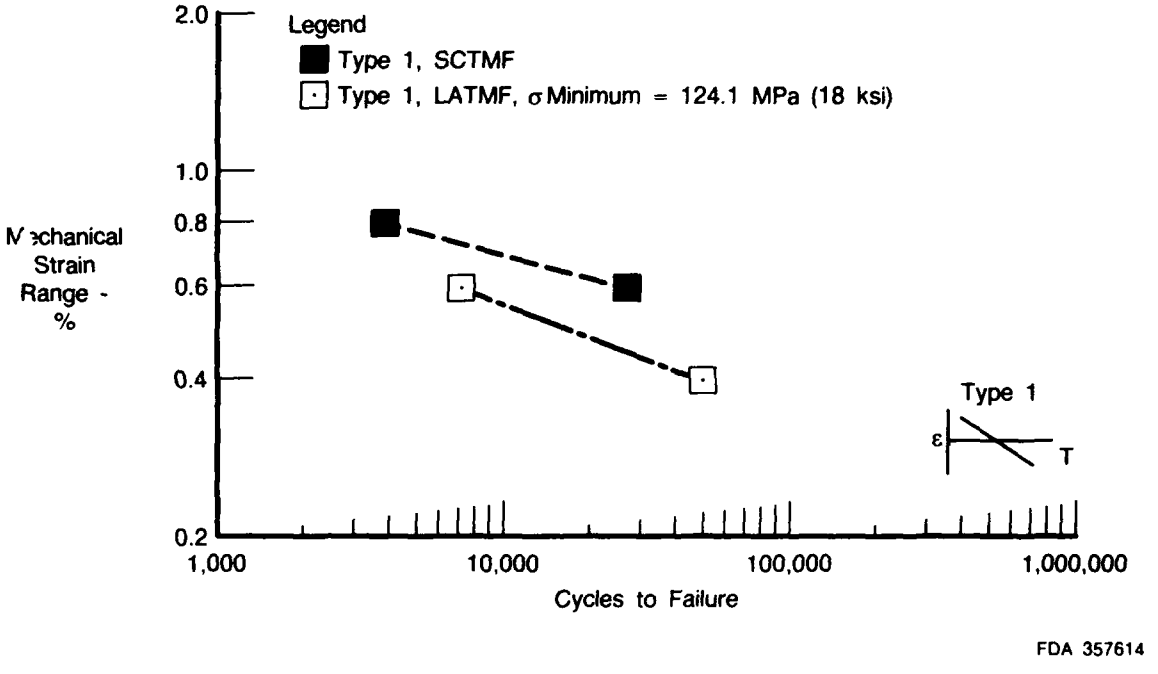

Figure 44. Controlled Minimum Stress Effects on PWA 286 Coated PWA 1480 (Out-of-Phase TMF Cycle, 1 cpm, 427-927°C (800-1700°F))

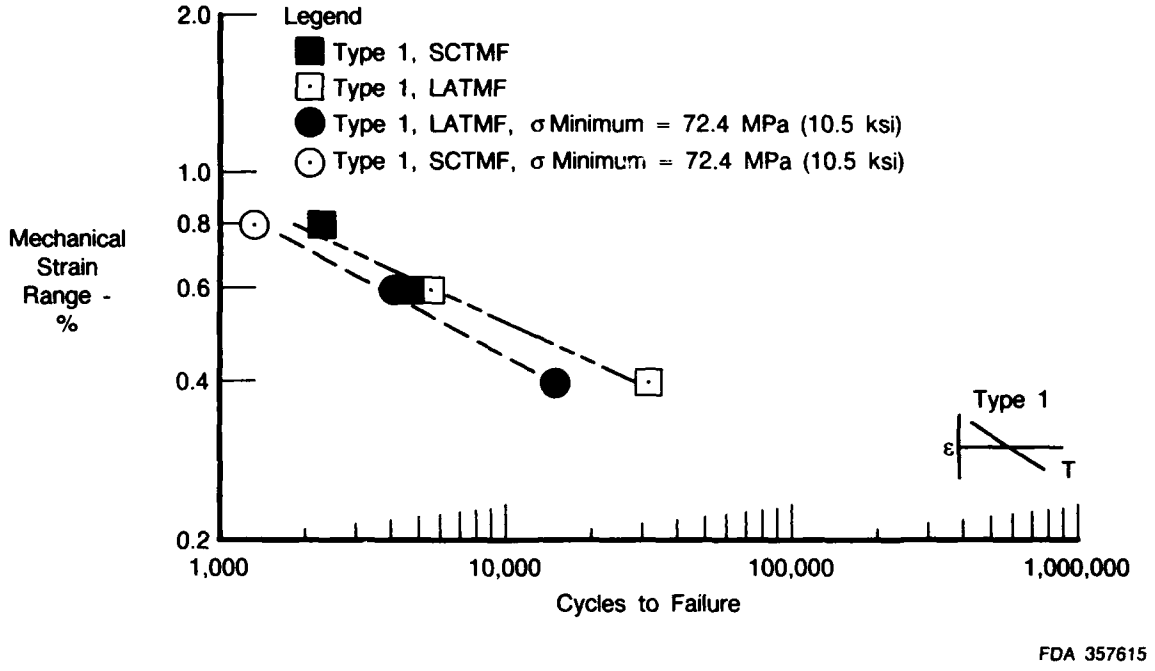

Figure 45. Controlled Minimum Stress Effects on PWA 286 Coated PWA 1480 (Out-of-Phase TMF Cycle, 1 cpm, 427-1038°C (800-1900°F))

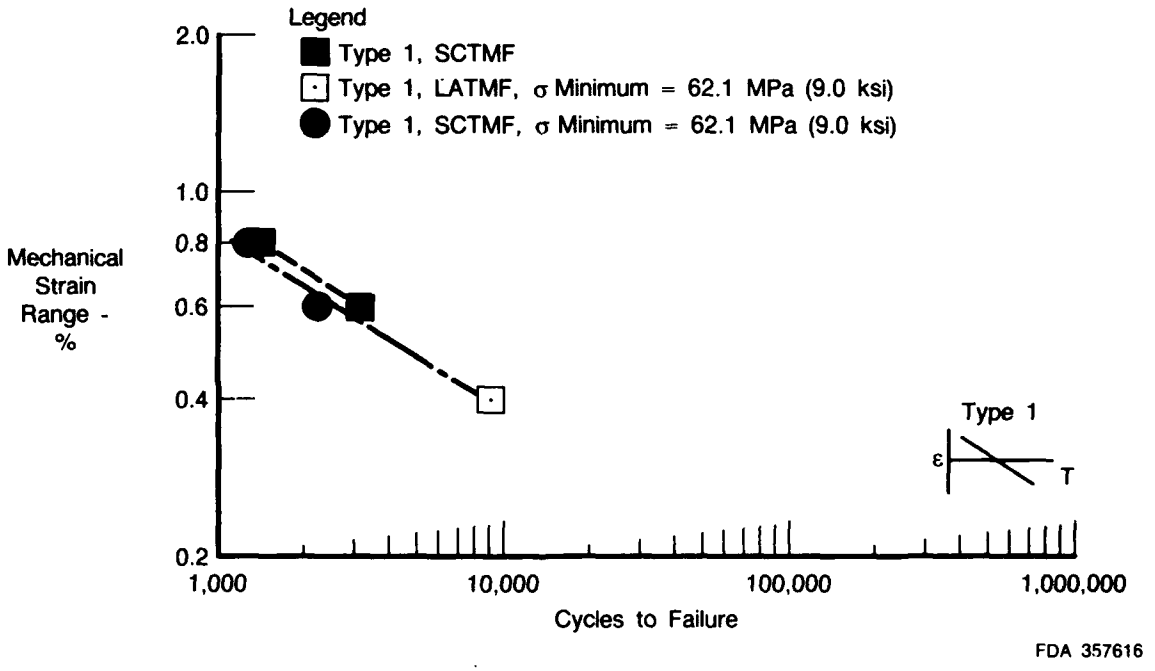

Figure 46. Controlled Minimum Stress Effects on PWA 286 Coated PWA 1480 (Out-of-Phase TMF Cycle, 0.5 cpm, 427-1093°C (800-2000°F))

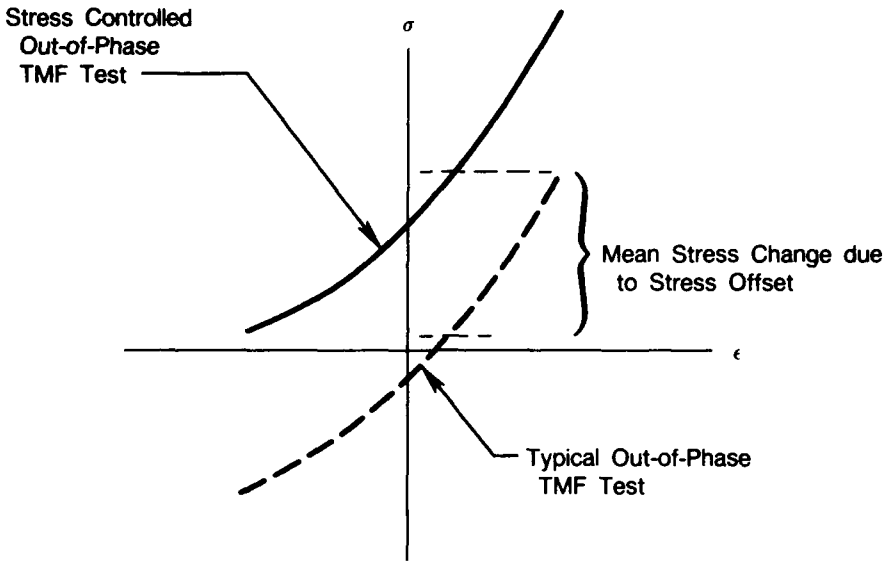

FDA 335050

Figure 47. Effects of Mean Stress on TMF Mechanical Behavior

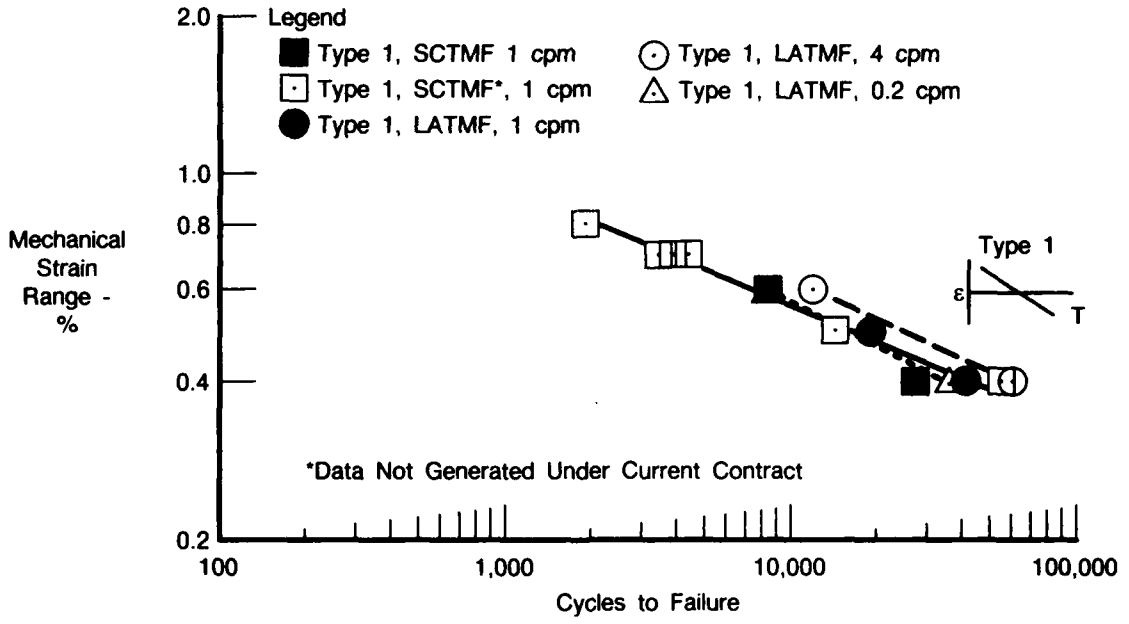

FDA 357617

Figure 48. Cyclic Frequency Effects on TMF for Uncoated PWA 1480 (Out-of-Phase Cycle, 427-1093°C (800-1900°F))

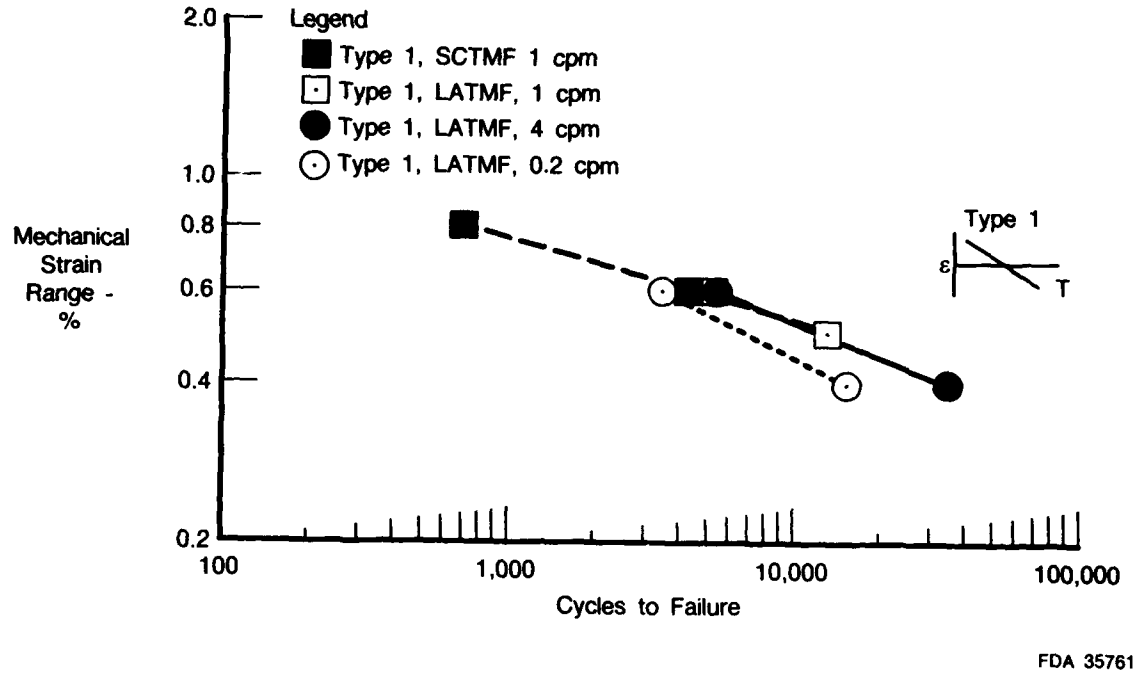

Figure 49. Cyclic Frequency Effects on TMF for PWA 275 Coated PWA 1480 (Out-of-Phase Cycle, 427-1038°C (800-1900°F))

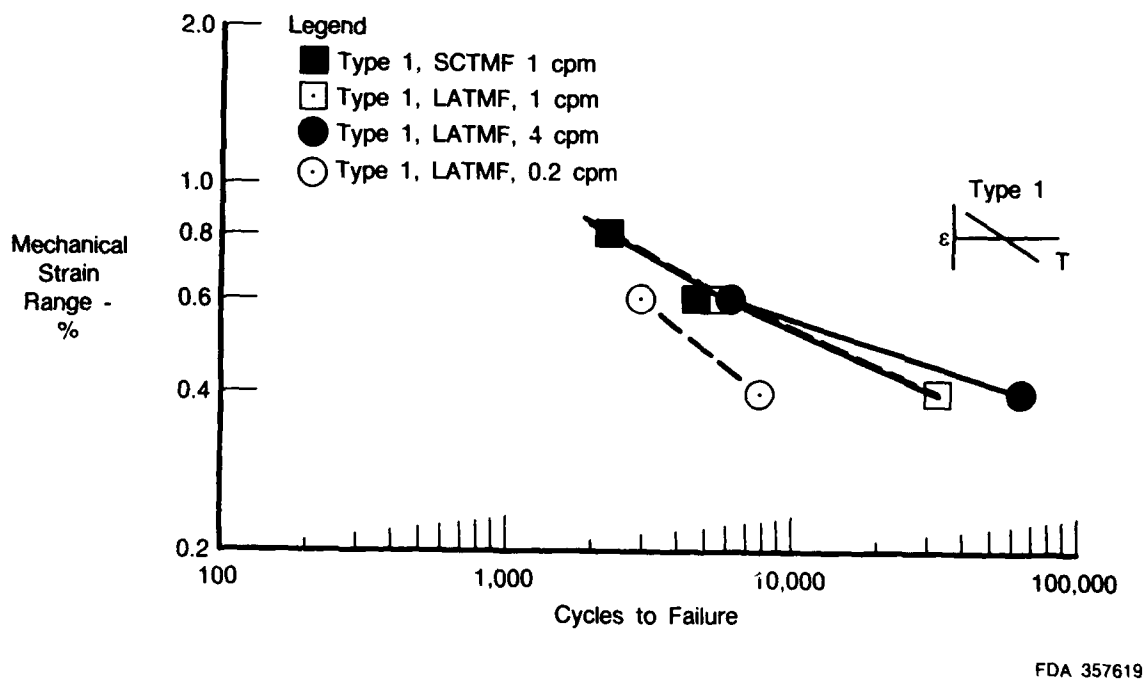

Figure 50. Cyclic Frequency Effects on TMF for PWA 286 Coated PWA 1480 (Out-of-Phase Cycle, 427-1038°C (800-1900°F))

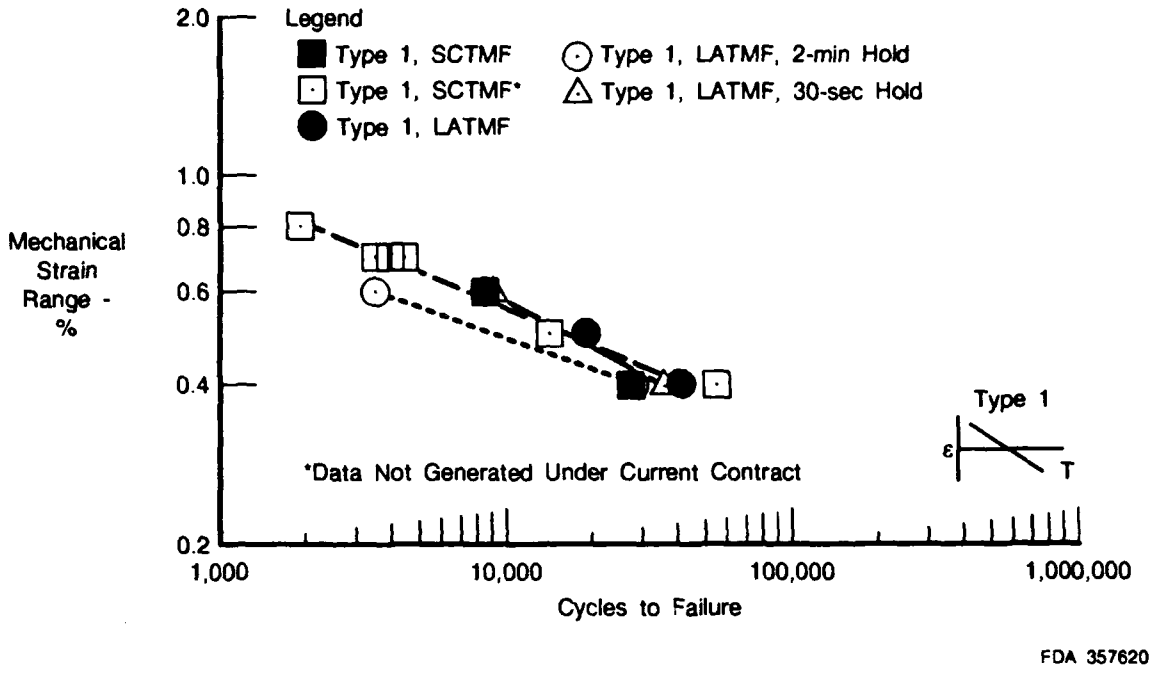

Figure 51. Hold Time Effects on TMF for Uncoated PWA 1480 (Type 1 Cycle, 1 cpm, 427-1038°C (800-1900°F))

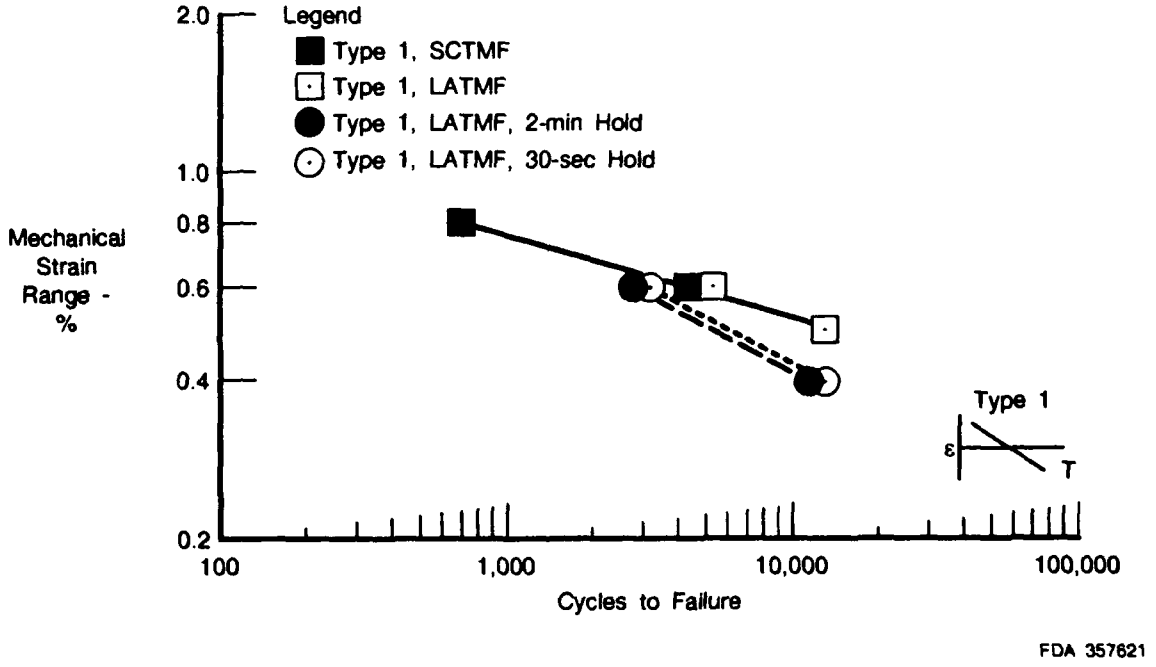

Figure 52. Hold Time Effects on TMF for PWA 275 Coated PWA 1480 (Type 1 Cycle, 1 cpm, 427-1038°C (800-1900°F))

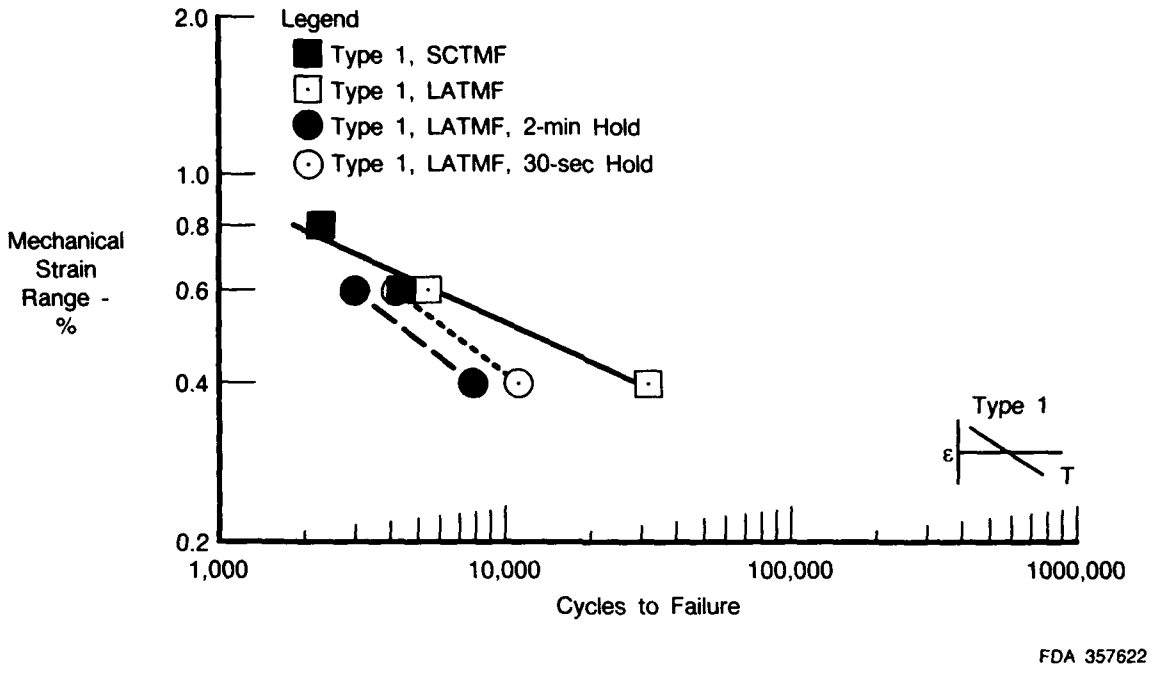

Figure 53. Hold Time Effects on TMF for PWA 286 Coated PWA 1480 (Type 1 Cycle, 1 cpm, 427-1038°C (800-1900°F))

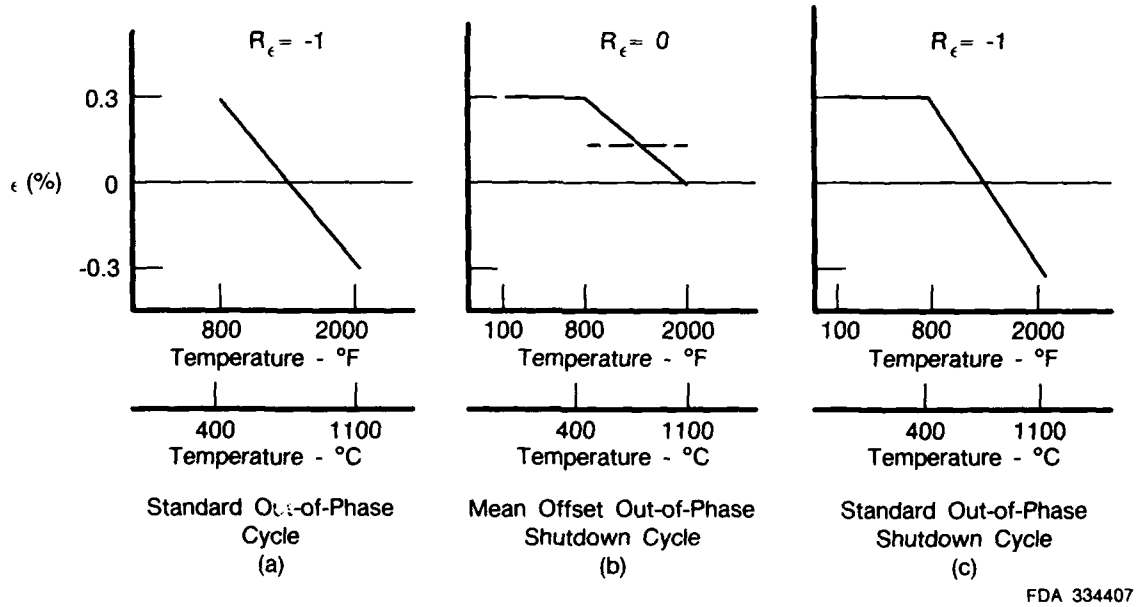

Figure 54. Typical Out-of-Phase and Shutdown TMF Cycles

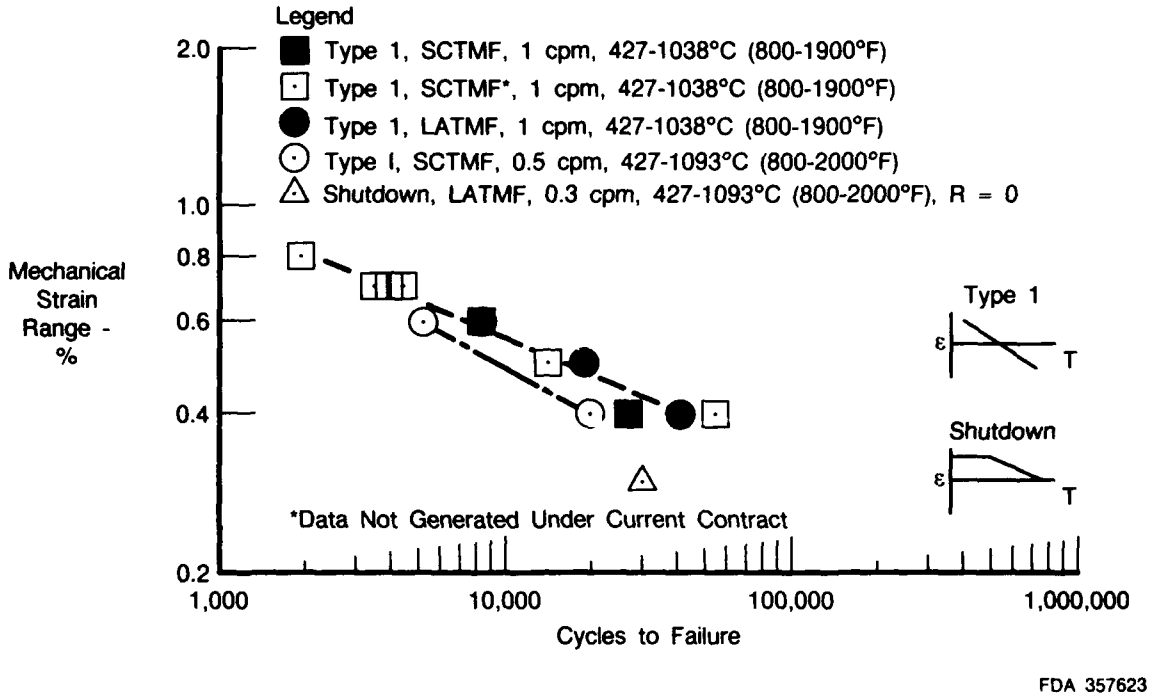

Figure 55. Shutdown Cycle Effect on TMF Testing of Uncoated PWA 1480

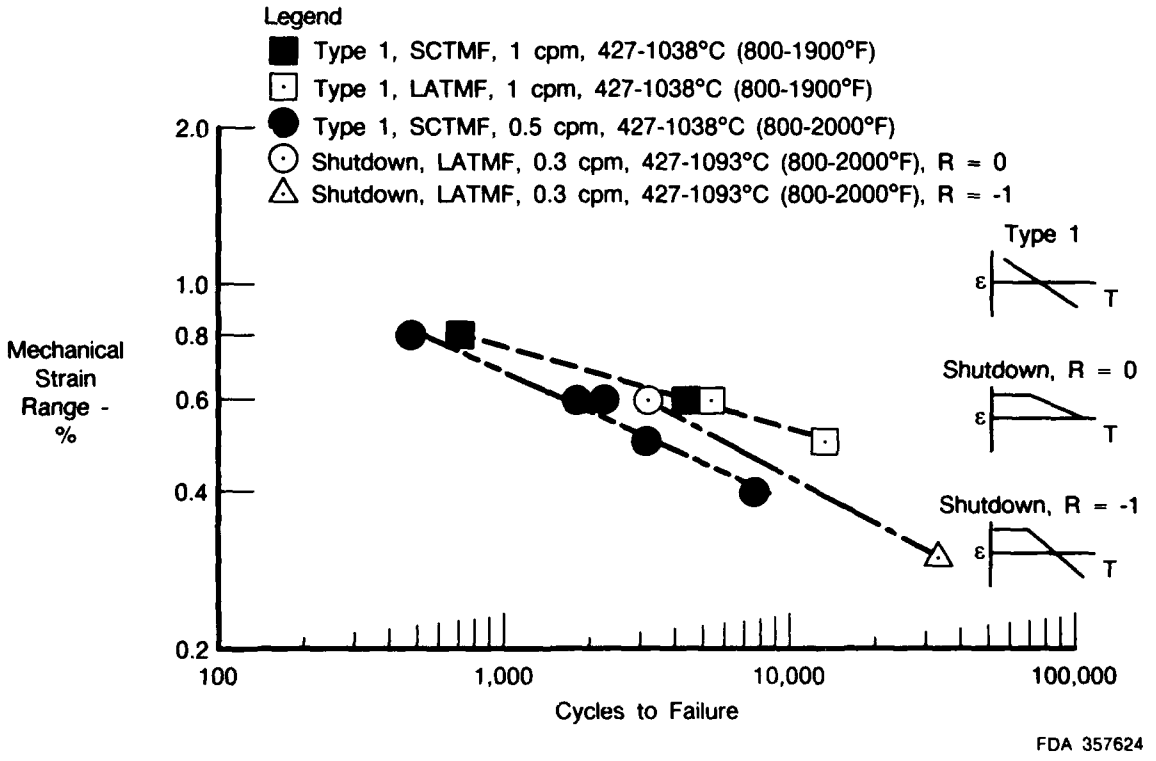

Figure 56. Shutdown Cycle Effect on TMF Testing of PWA 275 Coated PWA 1480

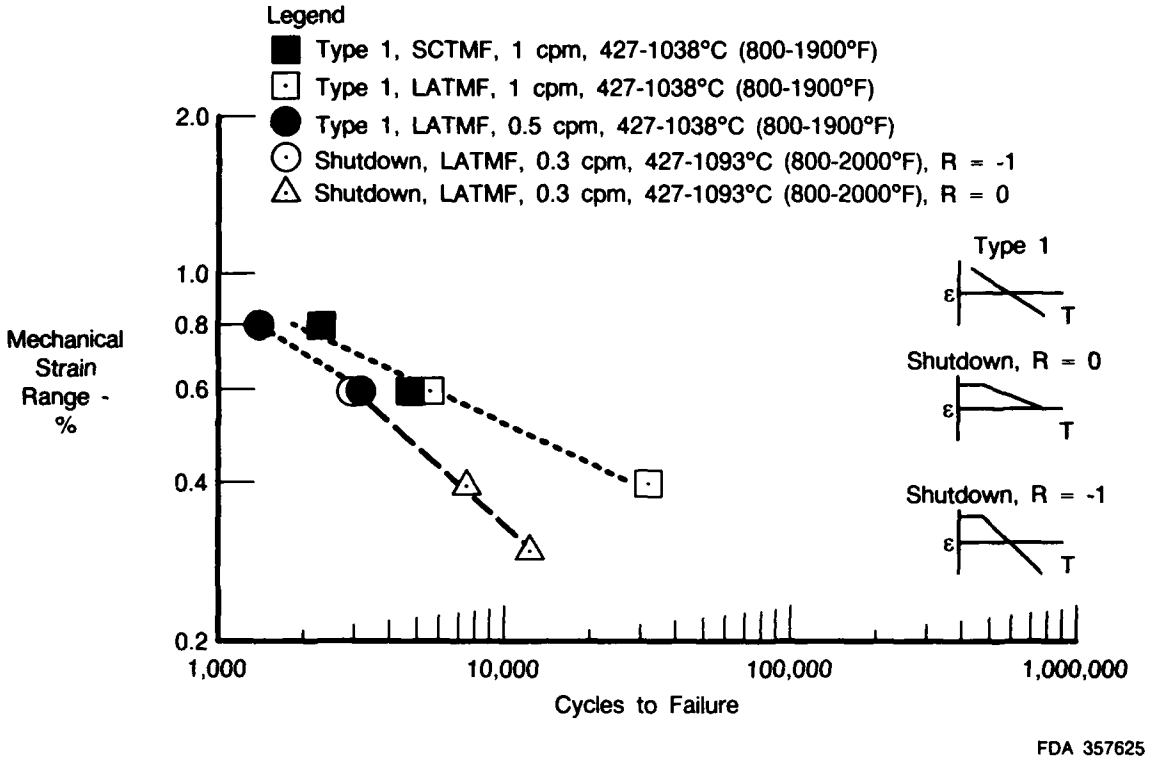

Figure 57. Shutdown Cycle Effect on TMF Testing of PWA 286 Coated PWA 1480

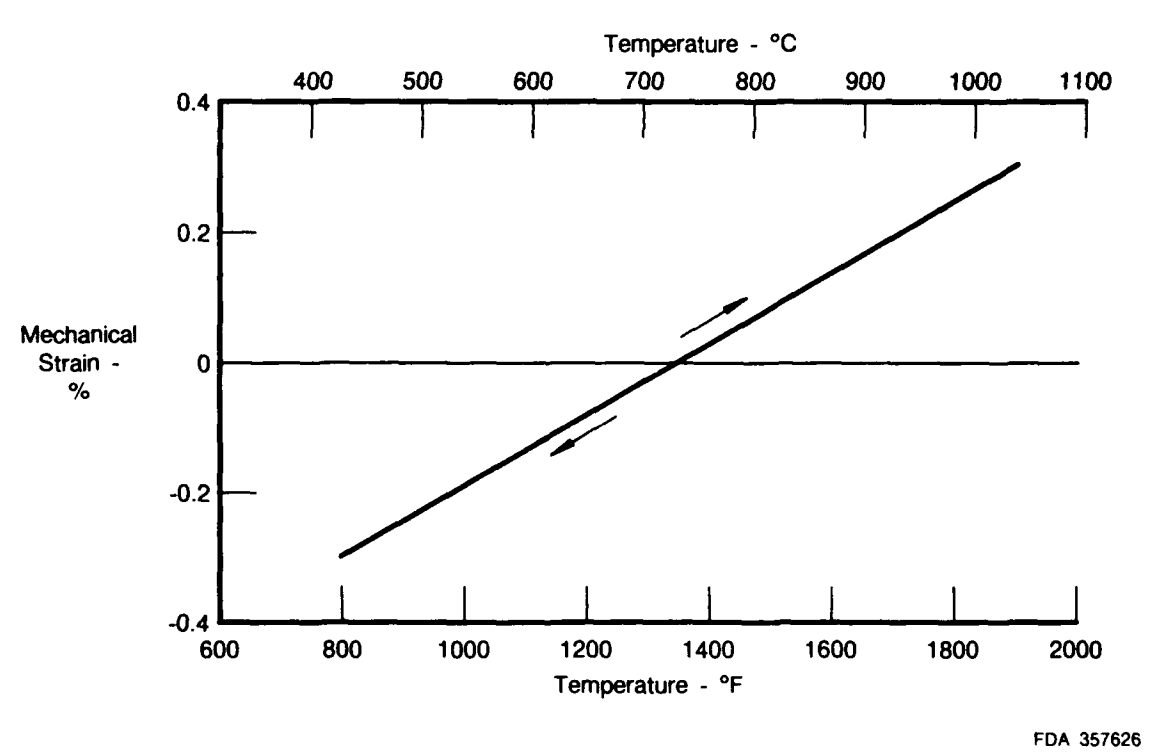

Figure 58. Typical In-Phase Cycle (Type 2 Cycle)

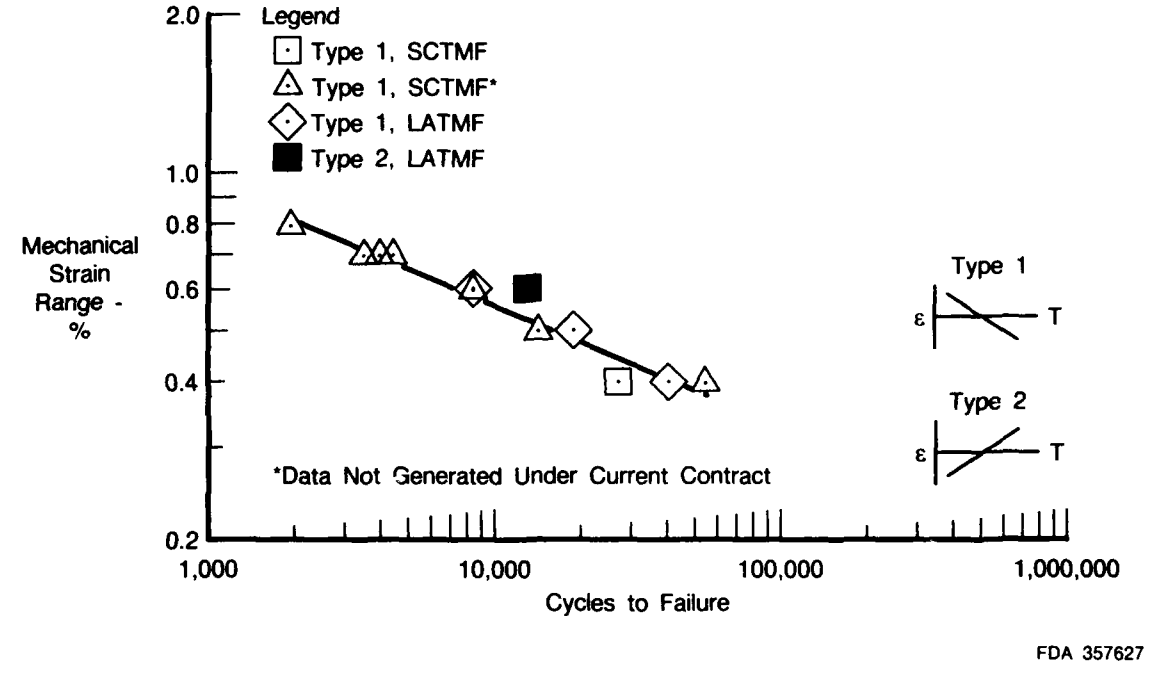

Figure 59. In-Phase Versus Out-of-Phase Cycles for Uncoated PWA 1480 (1 cpm (427-1038°C (800-1900°F))

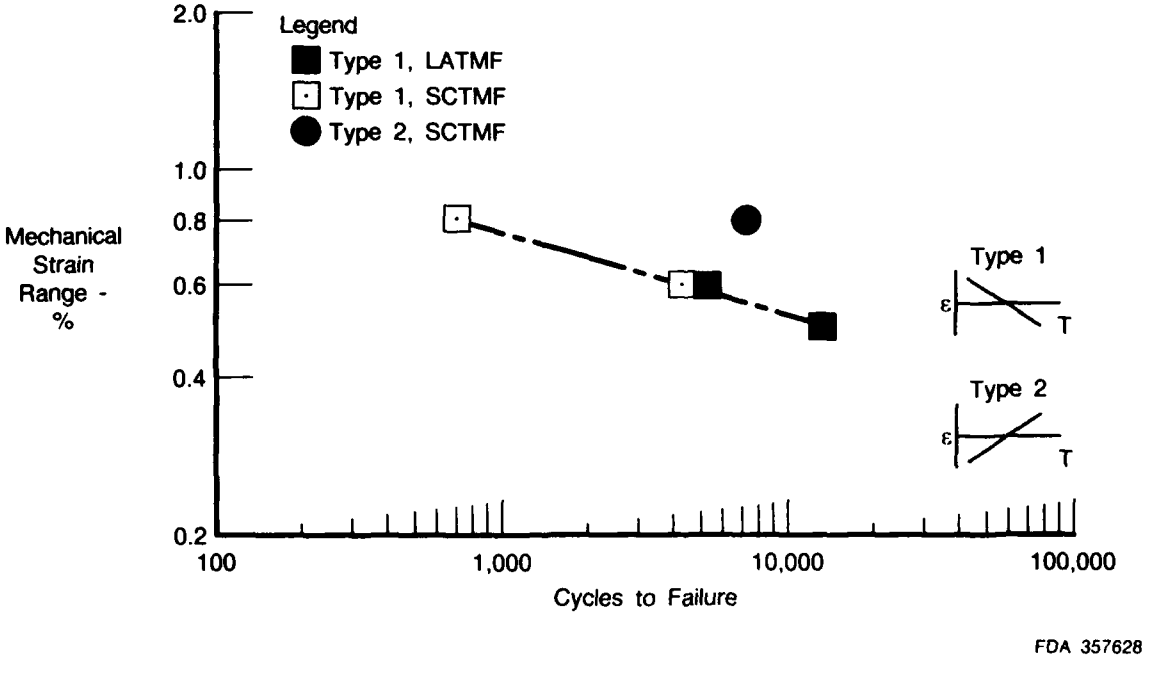

Figure 60. In-Phase Versus Out-of-Phase Cycles for PWA 275 Coated PWA 1480 (1.0 cpm, 427-1038°C (800-1900°F))

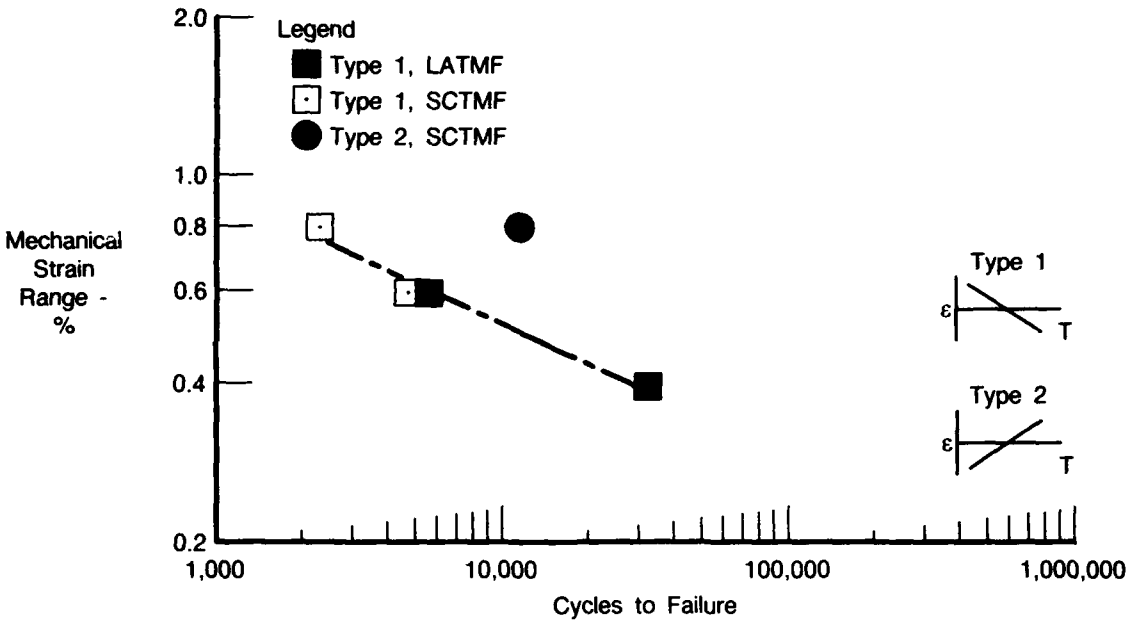

Figure 61. In-Phase Versus Out-of-Phase Cycles for PWA 286 Coated PWA 1480 (1.0 cpm (427-1038°C (800-1900°F))

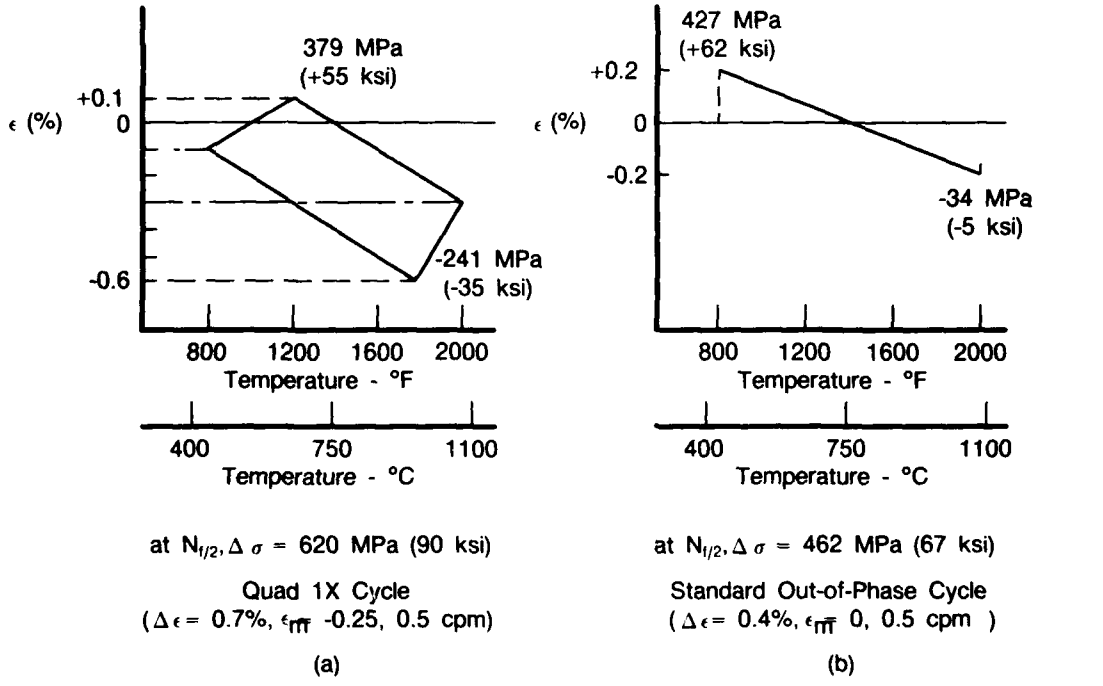

Figure 62. Quadrilateral and Out-of-Phase TMF Cycle Descriptions

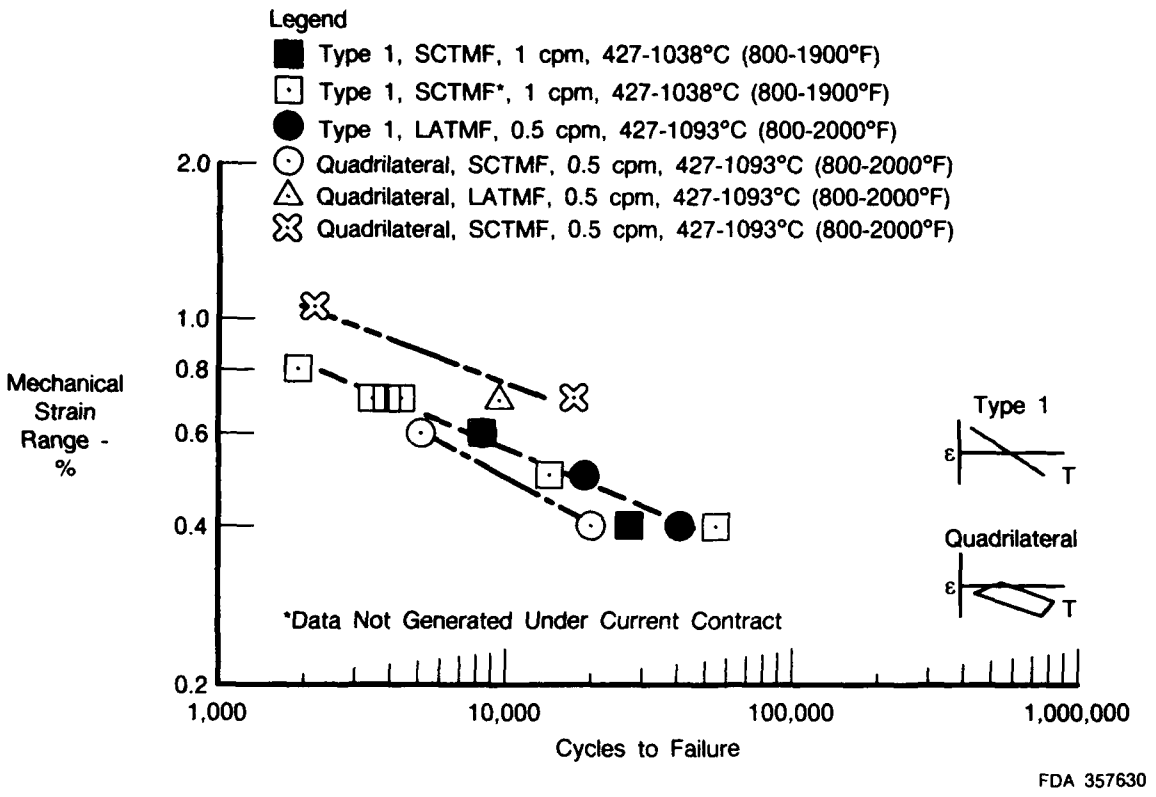

Figure 63. Quadrilateral Cycle Comparison for TMF Testing of Uncoated PWA 1480, (0.5 cpm, 427-1093°C (800-2000°F))

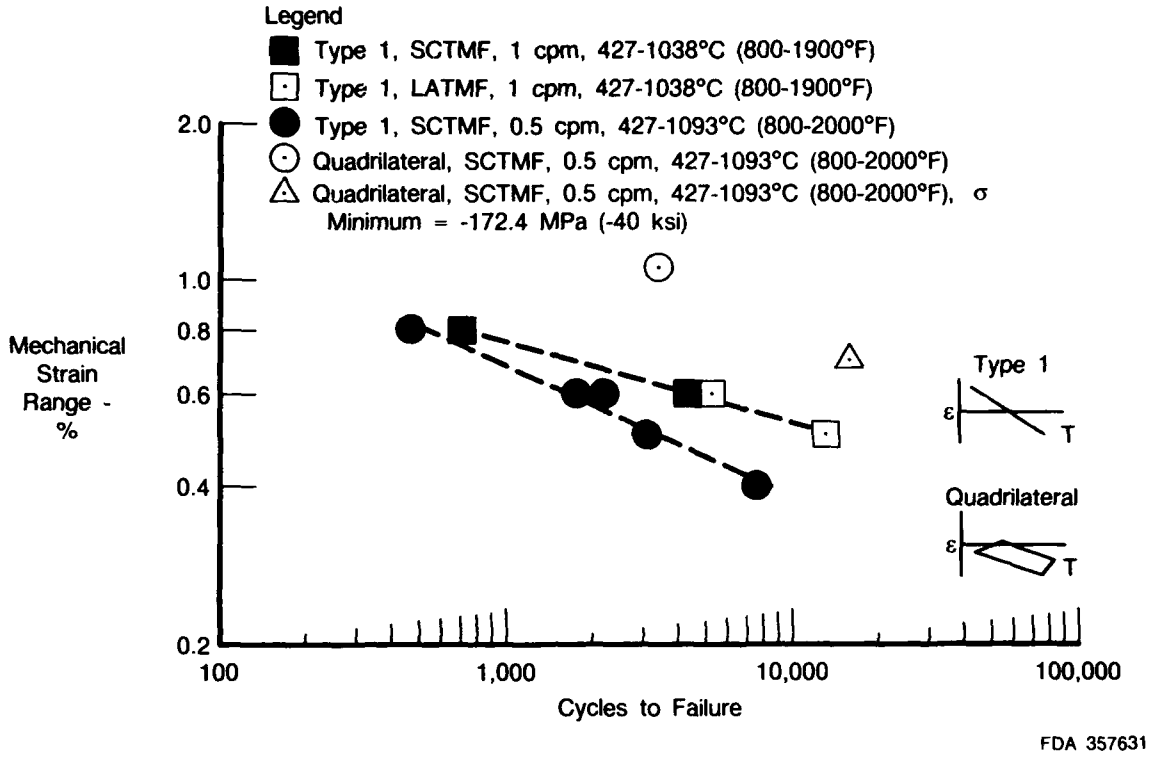

Figure 64. Quadrilateral Cycle Comparison for TMF Testing of PWA 275 Coated PWA 1480, (0.5 cpm, 427-1093°C (800-2000°F))

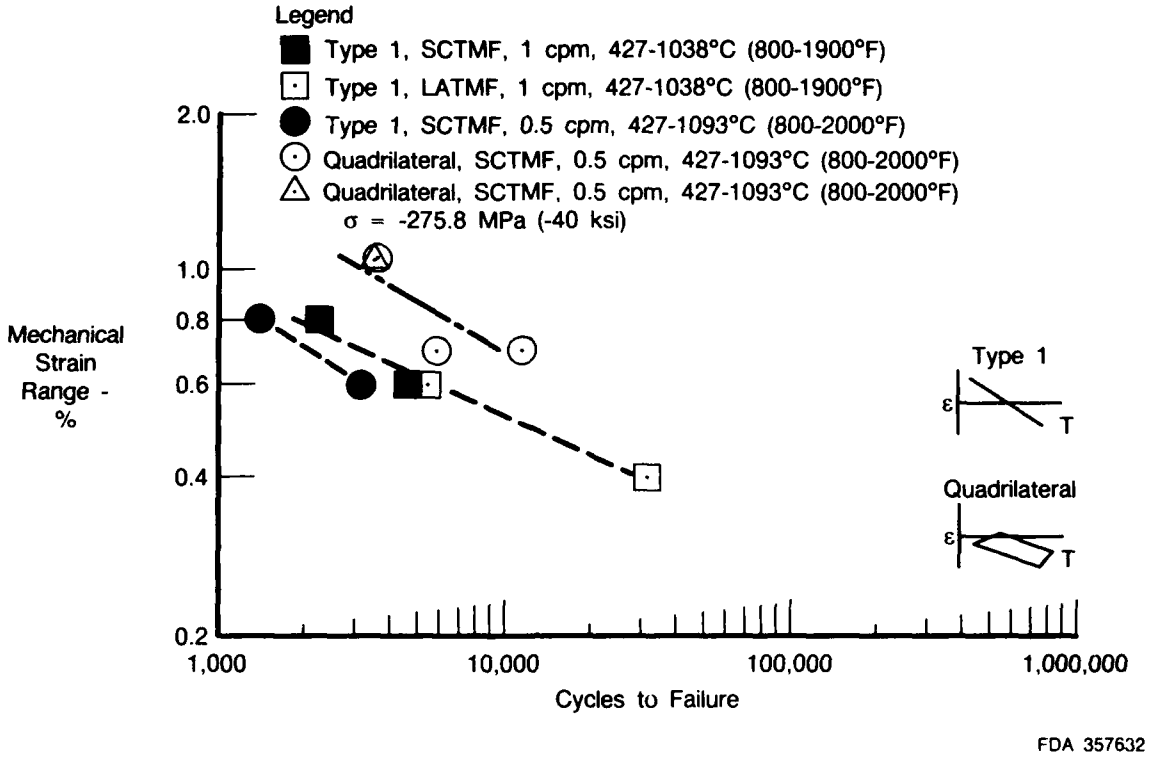

Figure 65. Quadrilateral Cycle Comparison for TMF Testing of PWA 286 Coated PWA 1480, (0.5 cpm, 427-1093°C (800-2000°F))

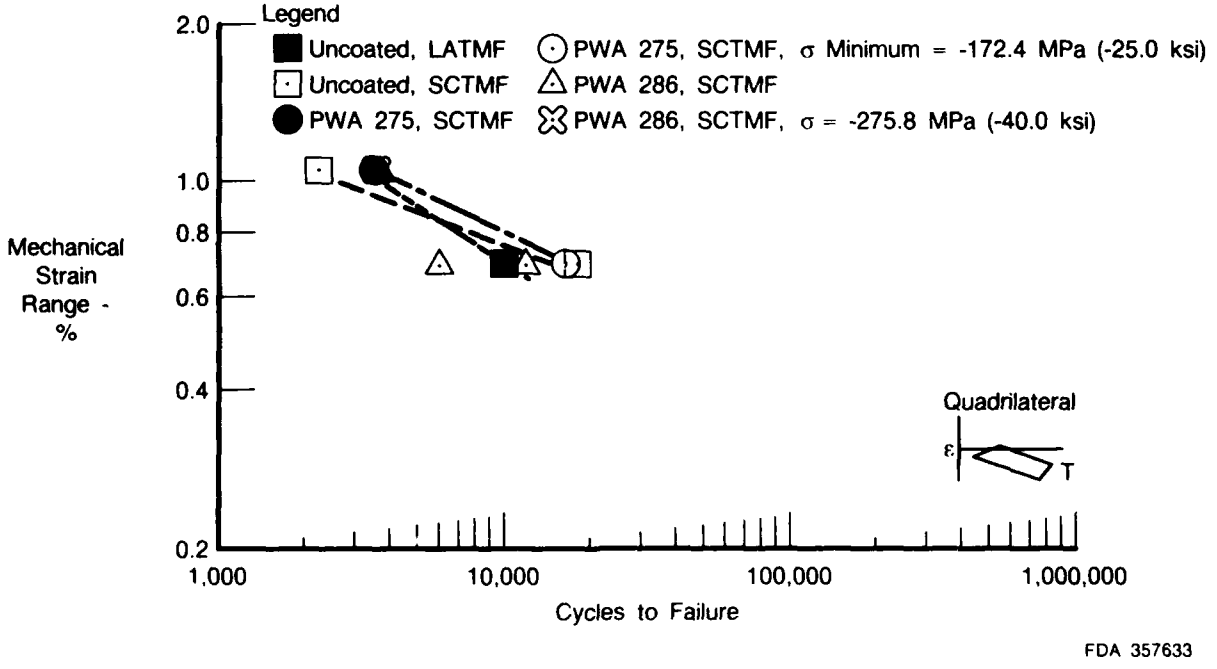

Figure 66. Quadrilateral Cycle Comparison of All Coating Systems on Coated PWA 1480, (0.5 cpm, 427-1093°C (800-2000°F))

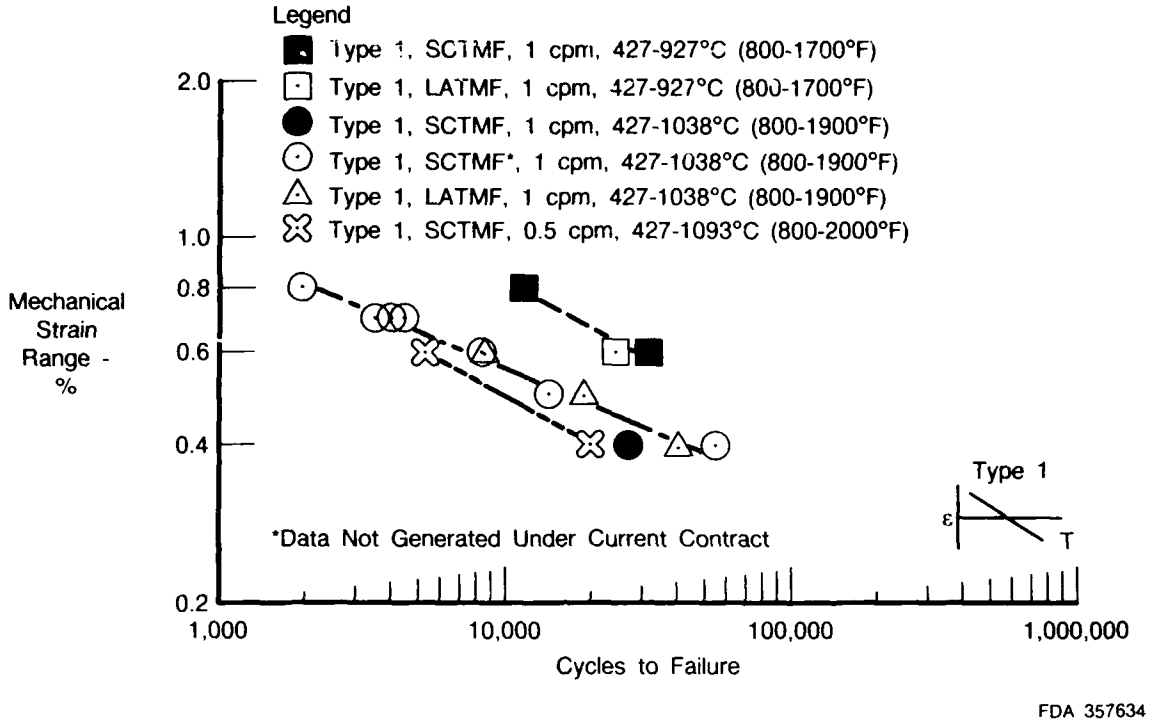

Figure 67. Effect of Maximum Temperature on the TMF Behavior of Uncoated PWA 1480 (Type 1 Cycle, 1 cpm)

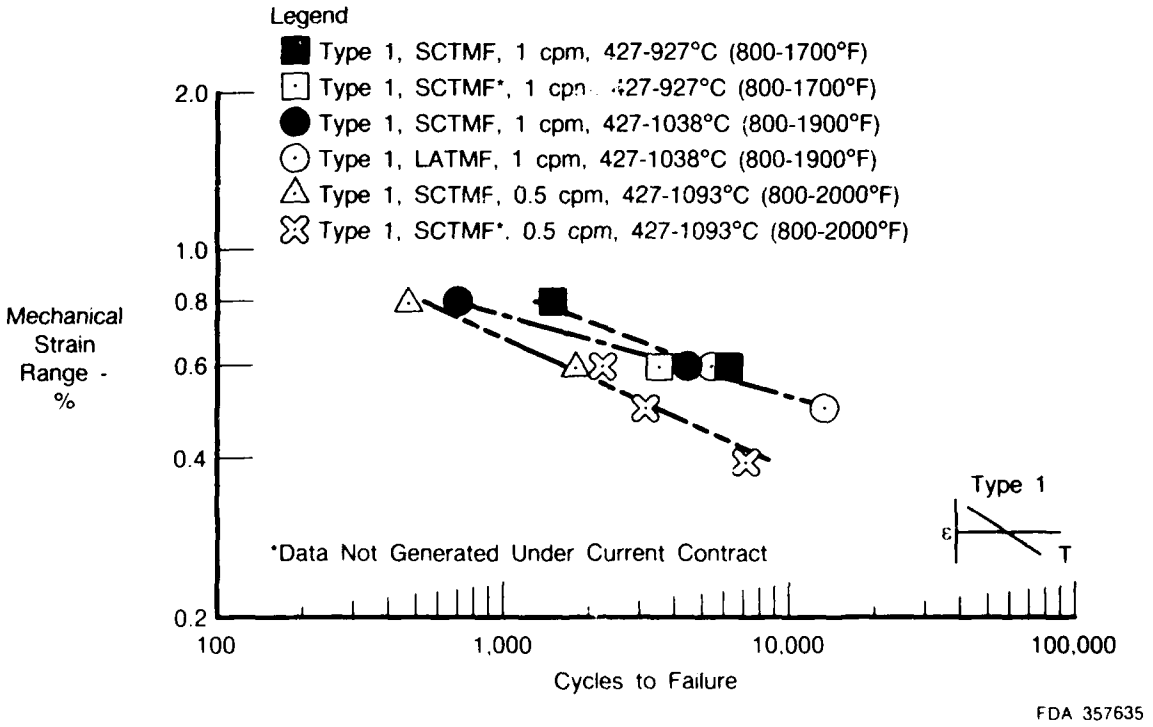

Figure 68. Effect of Maximum Temperature on the Behavior of PWA 275 Coated PWA 1480 (Type 1 Cycle, 1 cpm)

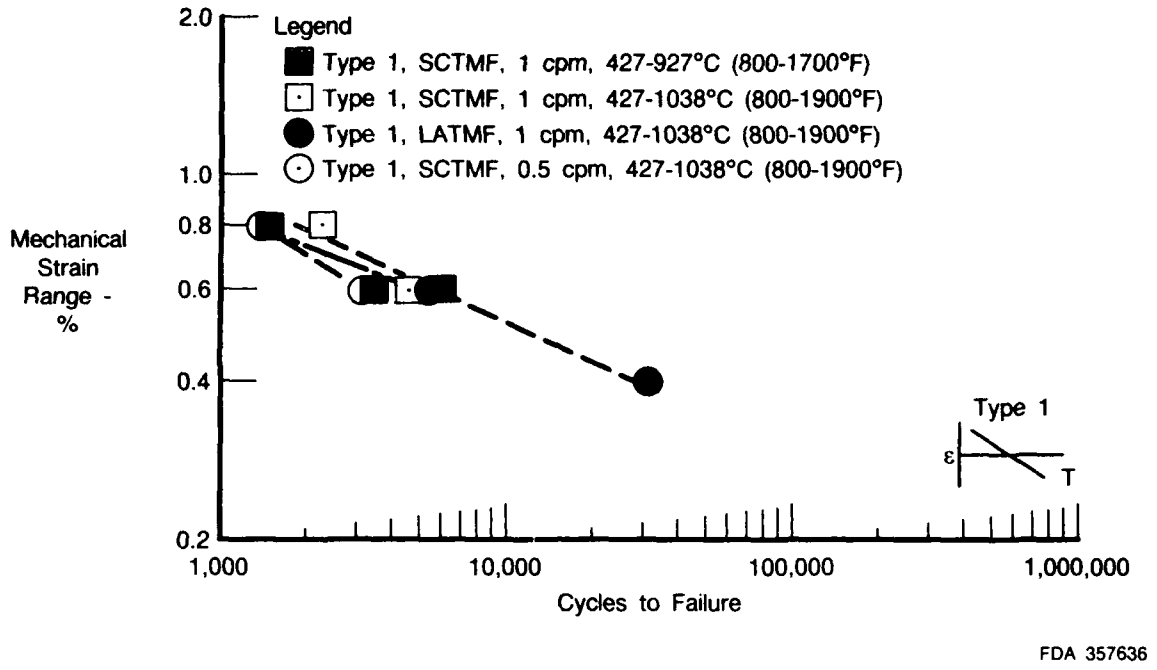

Figure 69. Effect of Maximum Temperature on the Behavior of PWA 286 Coated PWA 1480 (Type 1 Cycle, 1 cpm)

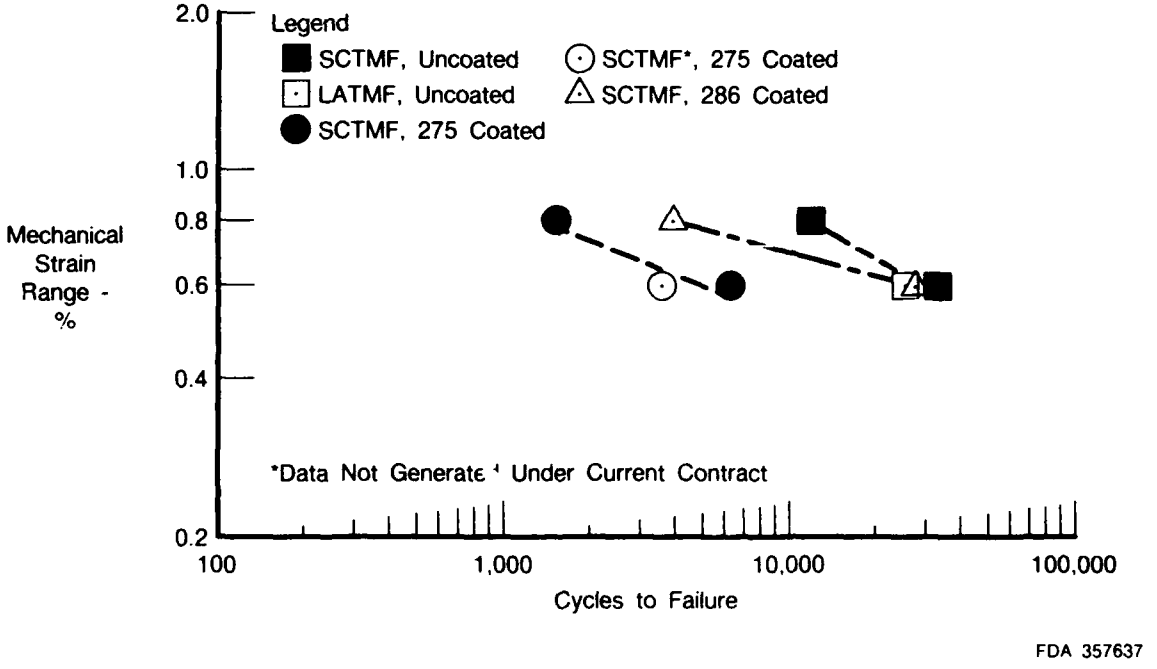

Figure 70. Coating Effects on TMF Testing of PWA 1480 (Type 1 Cycle, 1 cpm, 427-927°C (800-1700°F))

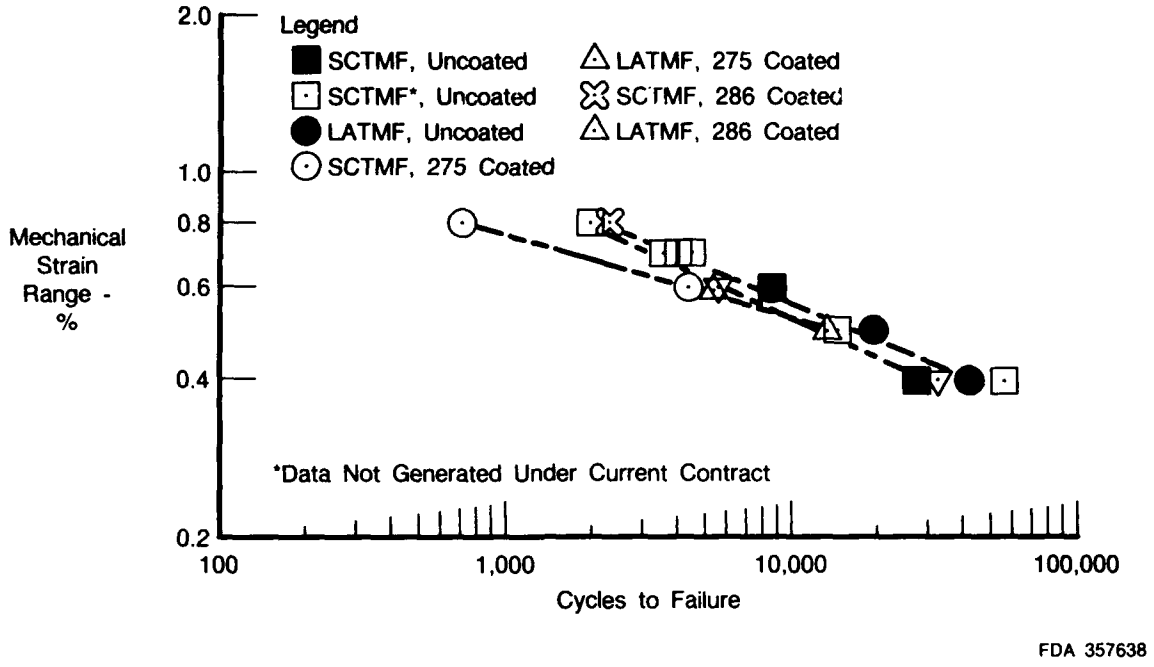

Figure 71. Coating Effects on TMF Testing of PWA 1480 (Type 1 Cycle, 1 cpm, 427-1037°C (800-1900°F))

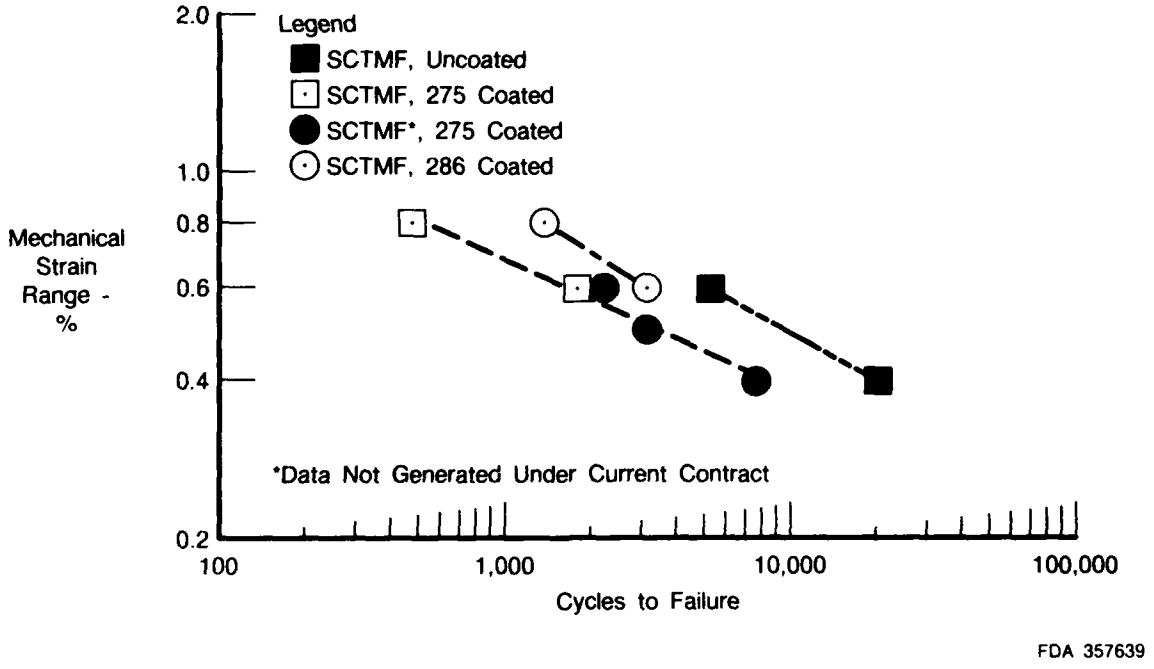

Figure 72. Coating Effects on TMF Testing of PWA 1480 (Type 1 Cycle, .5 cpm, 427-1093°C (800-2000°F))

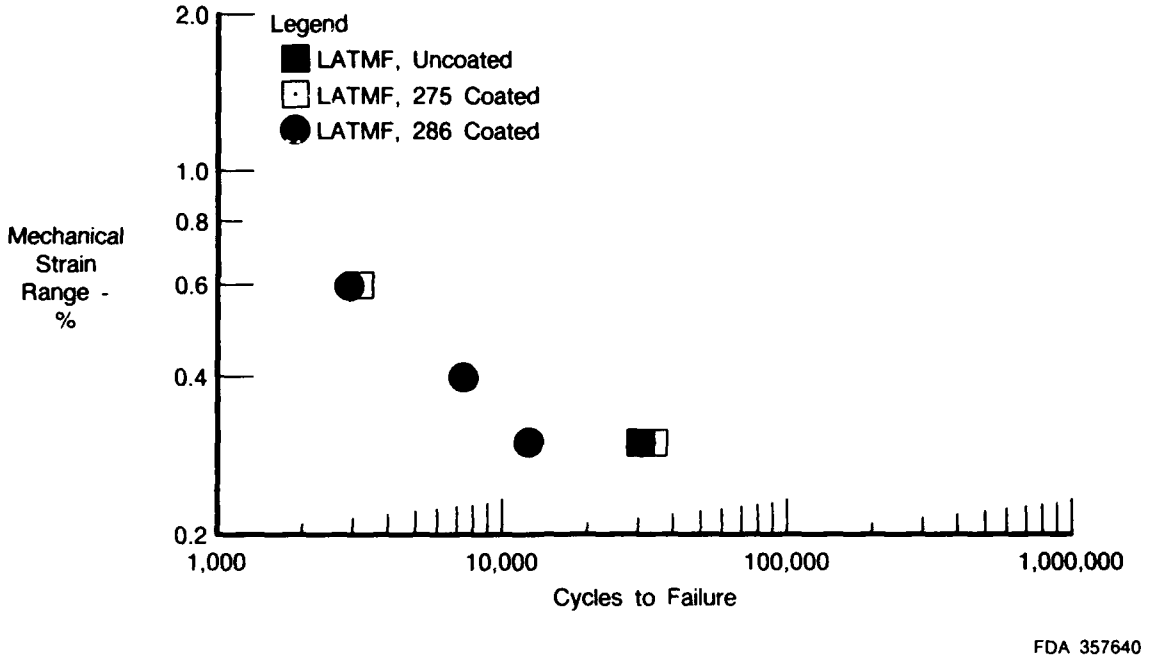

Figure 73. Coating Effects on TMF Testing of PWA 1480 (Shutdown Cycles, 427-1093°C (800-2000°F), 0.3 cpm)

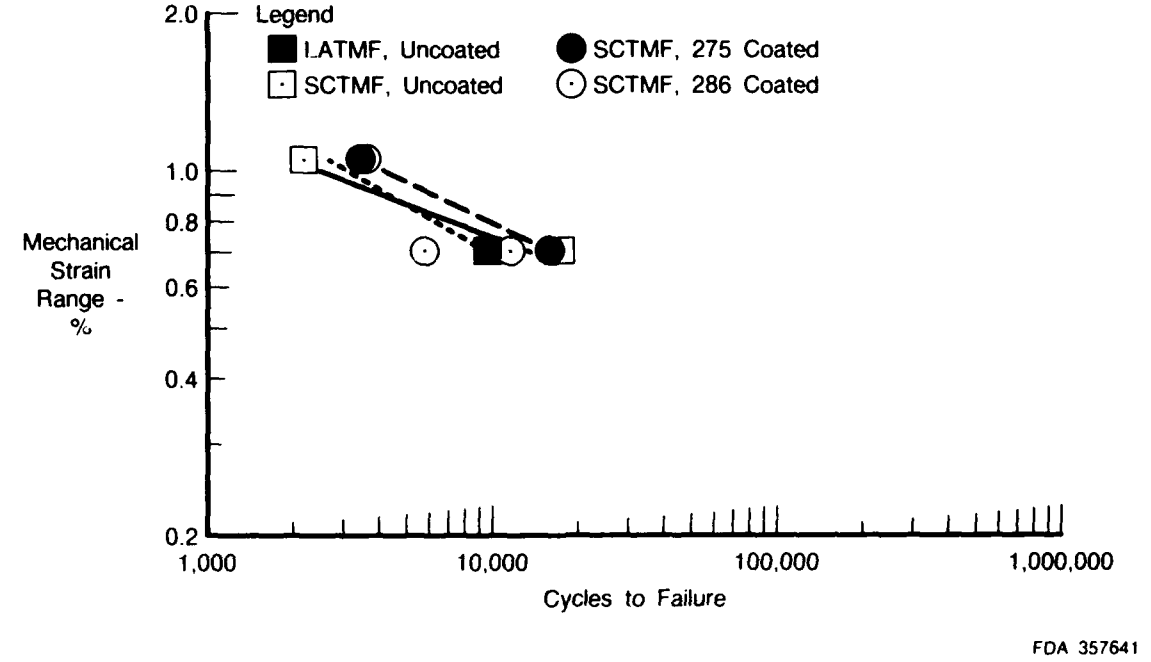

Figure 74. Coating Effects on TMF Testing of PWA 1480 (Quadrilateral Cycles, 427-1093°C (800-2000°F), 0.5 cpm)

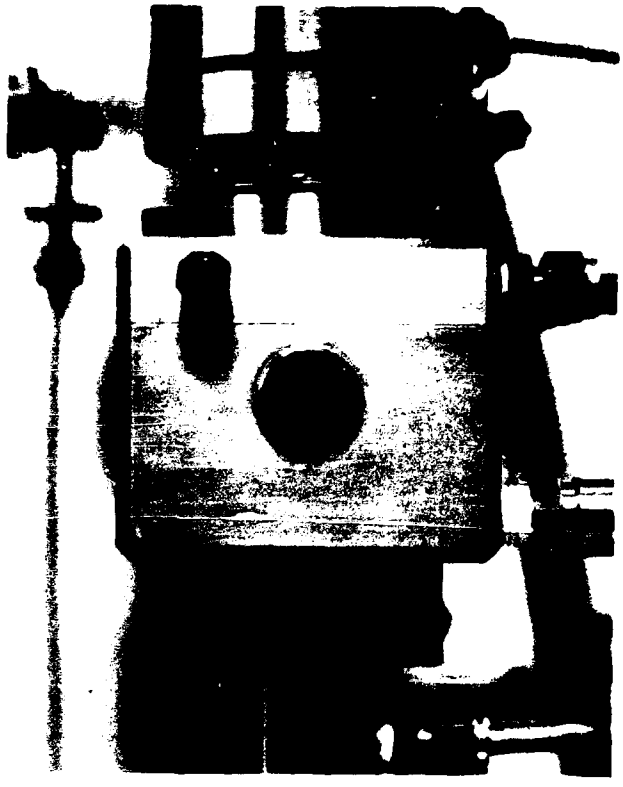

FE 249453

Figure 75. TMF Test in Progress in Argon Chamber

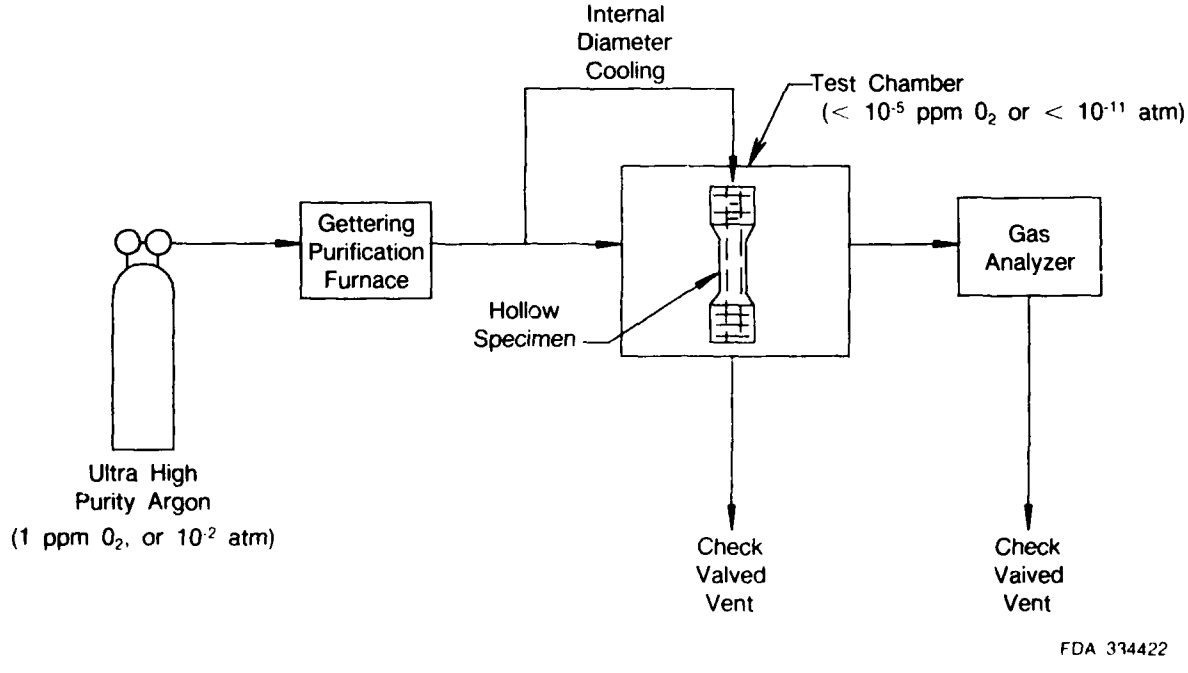

FDA 334422

Figure 76. Schematic of Inert Environment Gas Purification System

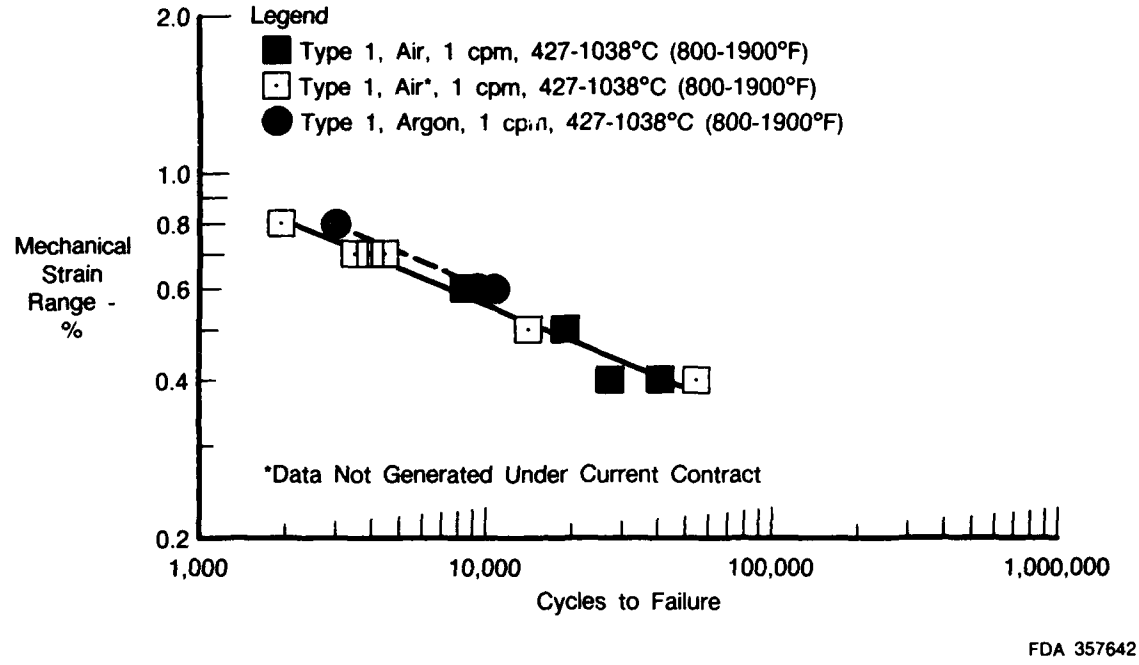

Figure 77. Inert Environment TMF Test Results for Uncoated PWA 1480 (Various Cycles)

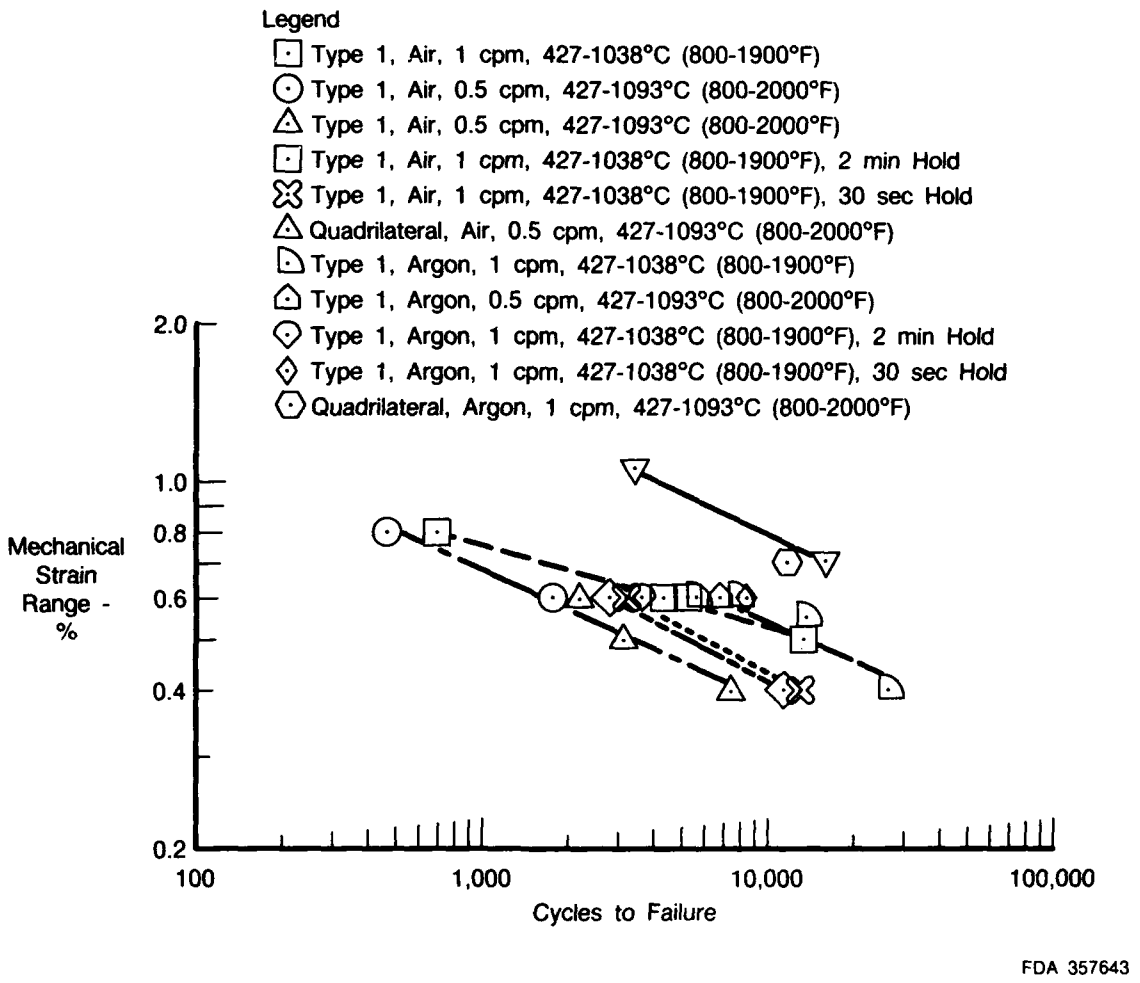

Figure 78. Inert Environment TMF Test Results for PWA 275 Coated PWA 1480 (Various Cycles)

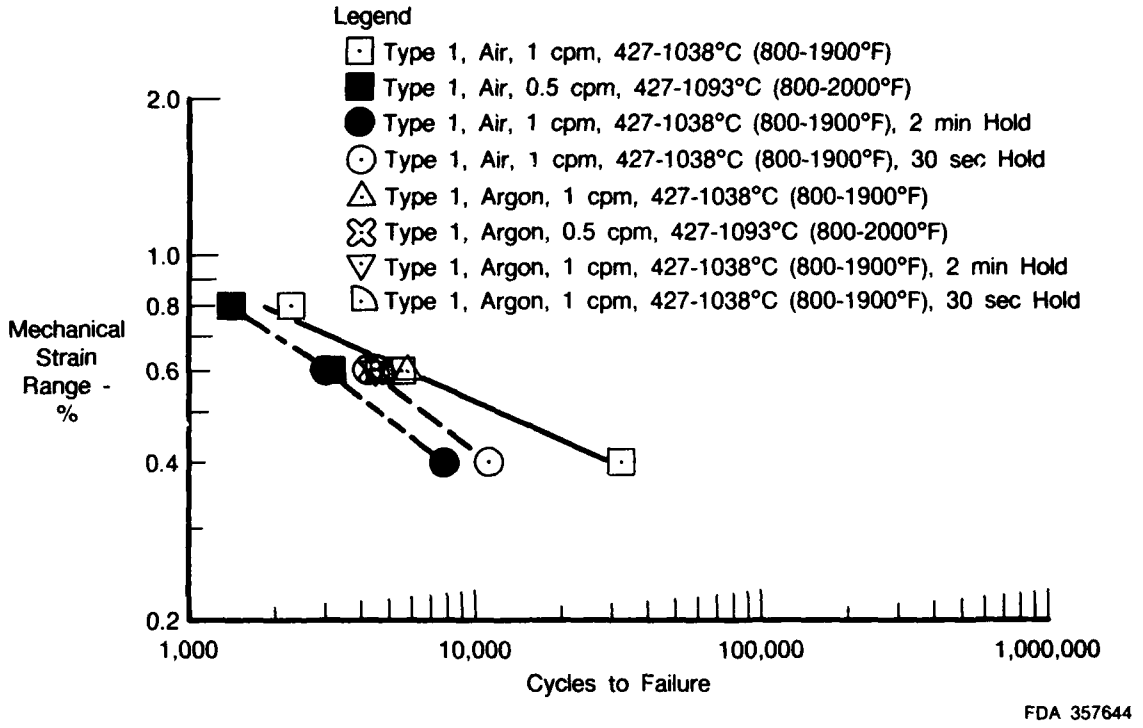

Figure 79. Inert Environment TMF Test Results for PWA 286 Coated PWA 1480 (Various Cycles)

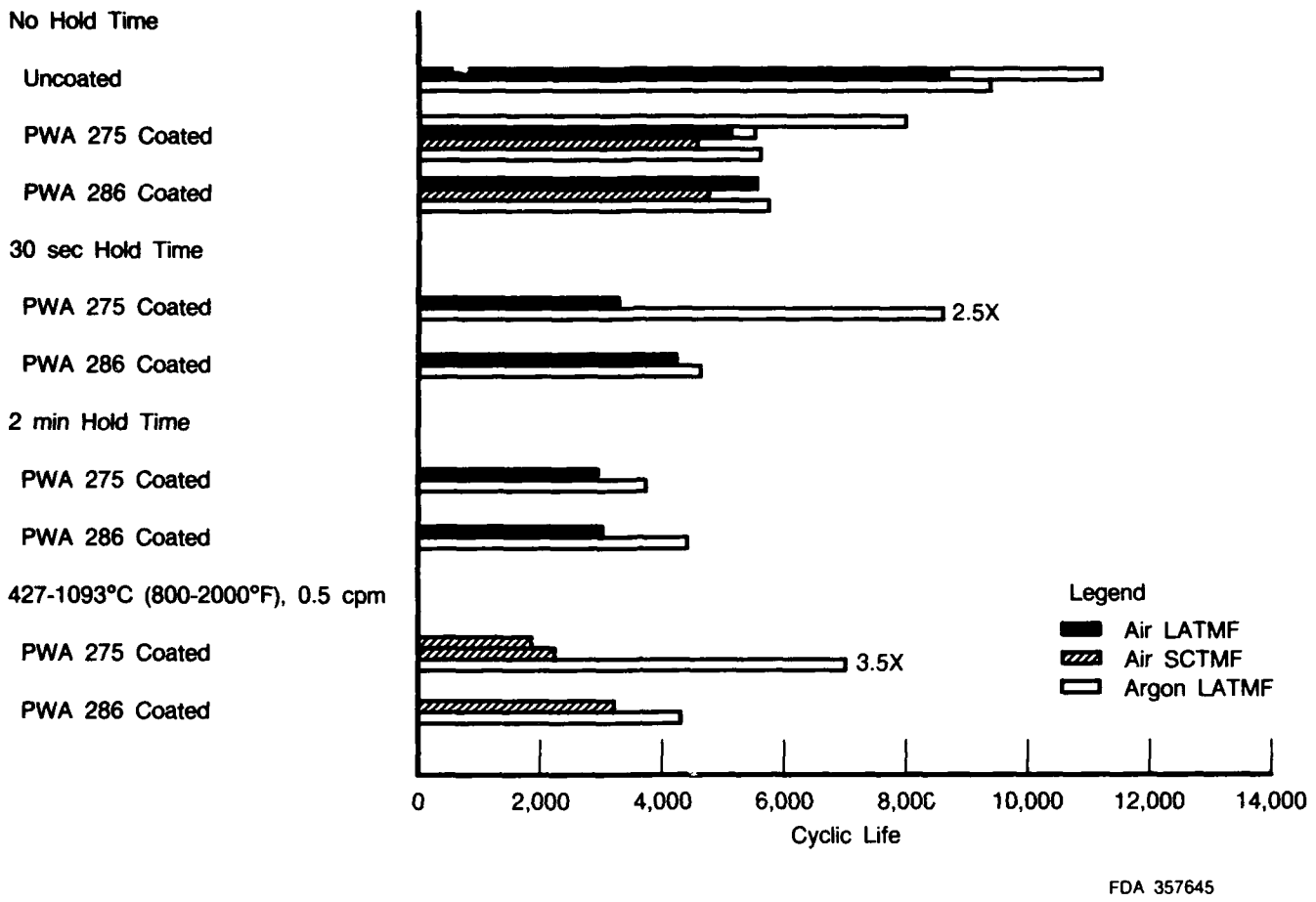

Figure 80. Inert Environment Testing of PWA 1480 (Type 1, 0.6 Strain Range, 800-1900°F, and 1 cpm) (Unless so indicated)

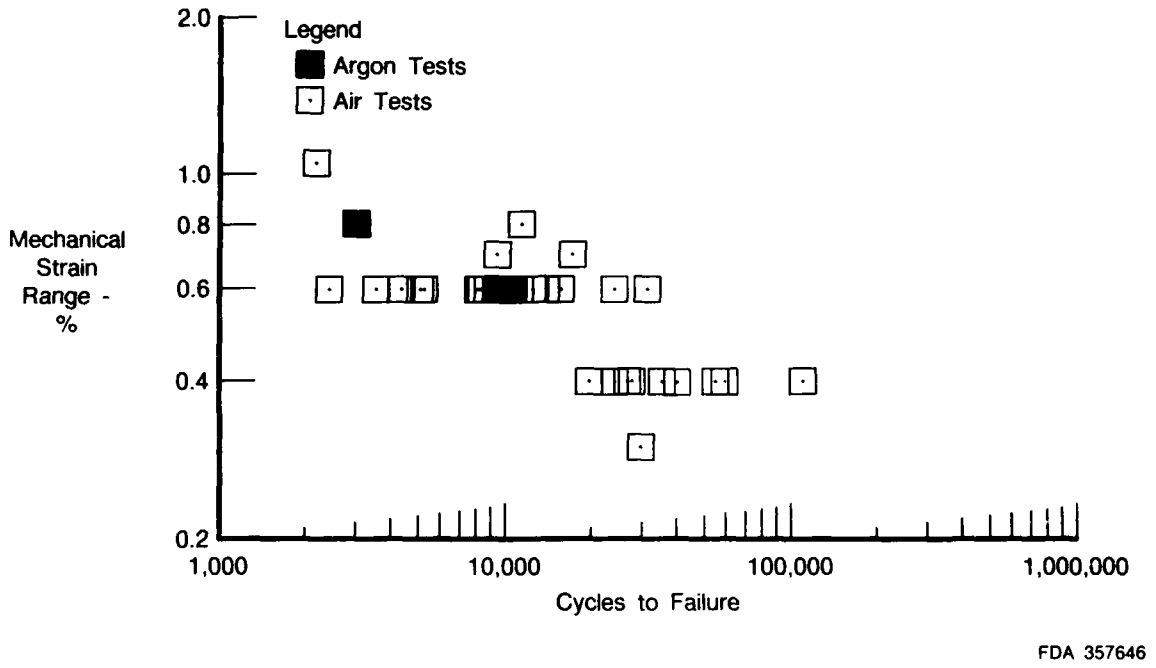

Figure 81. Inert Environment Testing Within the Scatter of All TMF Tests for Uncoated PWA 1480

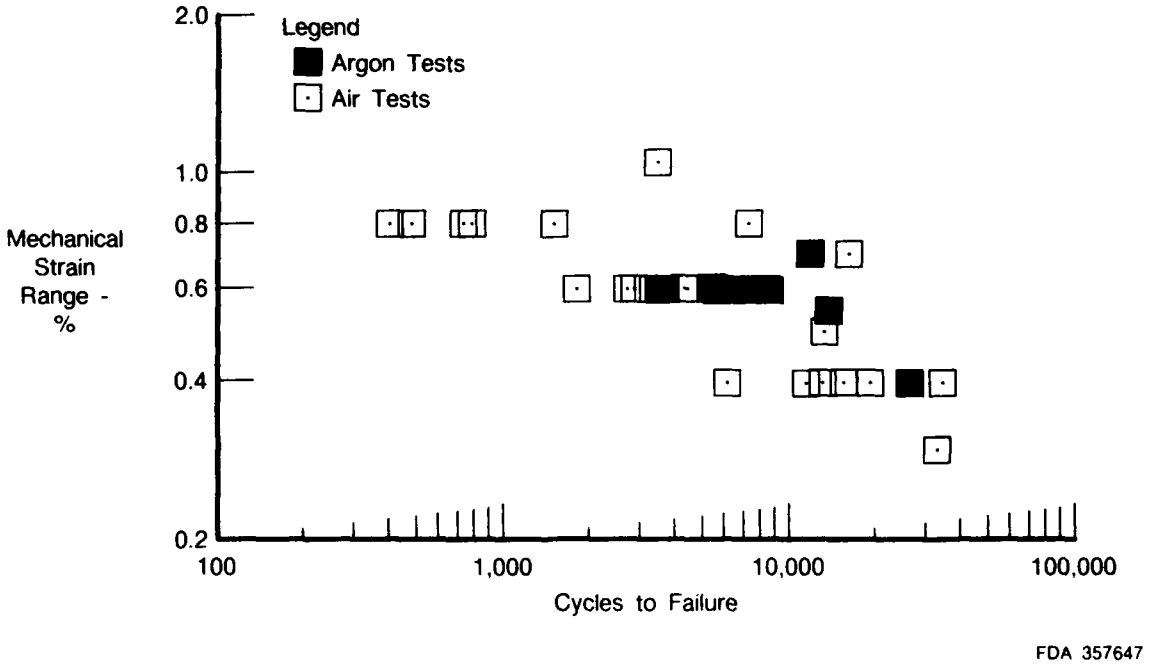

Figure 82. Inert Environment Testing Within the Scatter of All TMF Tests for PWA 275 Coated PWA 1480

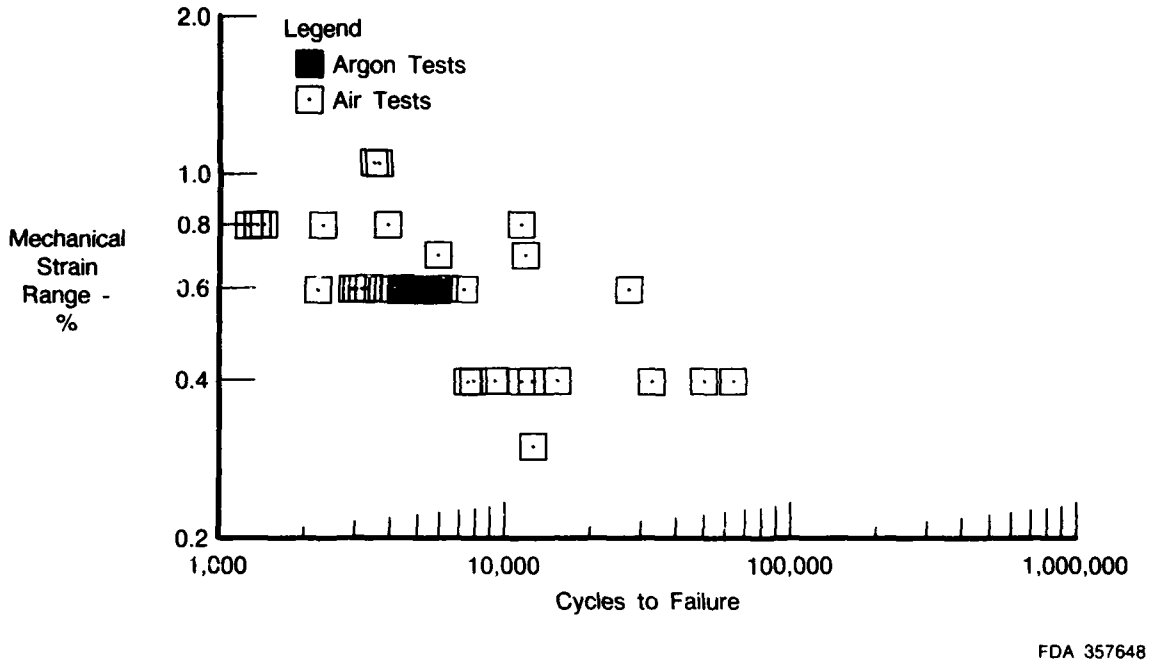

Figure 83. Inert Environment Testing Within the Scatter of All TMF Tests for PWA 286 Coated PWA 1480

2.4 METALLURGICAL EVALUATION

Failed TMF specimens from Task III were examined to identify failure modes for selected TMF tests. This analysis was performed to determine metallurgical differences due to cycle type and environment, and their effect on TMF behavior.

2.4.1 Oxidation

A discussion of general oxidation behavior of superalloys is relevant to the results presented in this section. Oxidation degradation of a superalloy may be considered as a two-stage process: an initiation stage followed by a propagation state (Figure 84). Note these terms are not necessarily interchangeable with similar stages in the fatigue cracking process. In the initiation stage, relatively protective oxidation products (i.e. Al- and Cr-rich oxides) form and spall off fairly regularly from the alloy surface, resulting in the slow, uniform development of an alloy-depleted zone. In this state, the loss of cross-sectional area in a TMF test specimen is negligible. The onset of the propagation stage occurs when the alloy becomes sufficiently depleted in Al and Cr that mounds of NiO form. When this happens, the rate of material consumption increases significantly, and the loss of cross-sectional area in the test specimen becomes significant.

In general, there is no significant metallographic difference caused by the effects of frequency, strain range, maximum temperature, and hold time, except for increased oxidation due to higher temperatures and longer exposure time at high temperature. The uncoated samples initiated in either the ID or the OD. There was no systematic trend in the initiation. The coated samples initiated on the OD, being dependent on the mechanical behavior of the coating.

An example of this behavior can be seen in a comparison of failed specimens from uncoated PWA 1480 TMF tests conducted using an out-of-phase cycle (Δ T = 427°C (800°F) to 1038°C (1900°F), $\Delta \varepsilon$ = 0.6%) at two cyclic frequencies, 0.2 cpm and 4 cpm. Due to the increased time at elevated temperature (75 hours versus 6 hours at T $\leq$ 982°C ($\leq$ 1800°F)), the Al-depleted zone is larger in the 0.2 cpm specimen, (Figure 85). Also, a pitting attack has started in this specimen. There was, however, no evidence of oxidation-initiated cracking in either specimen. Cycles to failure were within 30 percent (8481 for the 0.2 cpm versus 12,250 for the 4 cpm). Although the number of cycles to f re was higher for the 4-cpm test compared to 1-cpm and 0.2-cpm test results, the frequency effect appears to be minimal and may be within experimental scatter. It is apparent that oxidation attack was still in the initiation stage in both specimens.

2.4.2 Long Exposure Time Effects

The effect of oxidation on the uncoated alloy is the formation of a thin Al-depleted zone, which etches white against the unaffected structure of the superalloy. The depth of this zone increases with maximum temperature and testing time. A low strain range test has a thicker denuded zone at failure simply because of the longer testing time. Similarly, a sample with an isothermal hold at the maximum temperature has a thicker denuded zone because of the increased time at temperature. However, the increased oxidation does not have a fundamental effect on crack initiation or crack growth. The cracks have formed before most of the oxidation has occurred. Hence, oxidation does not reduce fatigue life except in long exposure time tests where the loss of cross section can become significant.

The long exposure time effects of oxidation are related to the initiation-propagation effects of oxidation. The long exposure time effect in TMF testing can be thought of as the propagation stage of superalloy oxidation. Initially, the alloy depleted zone, due to the regular formation and spallation of Al- and Cr-rich oxides, develops slowly and uniformly, and the loss of cross section is very slow. The loss of cross section due to oxidation and alloy depletion is negligible during this initiation state of oxidation. In order to reach the propagation stage of superalloy oxidation in

TMF, testing times on the order of 1000 hours at a maximum temperature of 1037°C (1900°F) and approximately 400 hours at 1093°C (2000°F) maximum temperature are required. If the total exposure time ($\frac{N}{cpm}$ + Nx (hold time) was less than these values, there was not enough oxidation to affect test results. For tests with long exposure times, an examination for the loss of material was made of the cross section near the fracture surface to determine if oxidation had an effect on the fatigue life.

2.4.3 Fracture Modes of Air Tests

The TMF behavior of the coated samples was determined by the OD coating, not by ID recrystallization or oxidation. None of the tests were run long enough or at sufficiently high temperatures to significantly degrade the coating by oxidation or interdiffusion.

Secondary cracks for uncoated and coated PWA 1480 out-of-phase tests (427-1038°C (800-1900°F)) are shown in Figures 86, 87, and 88. The uncoated PWA 1480, tested at 0.4 percent strain range and 1 cpm, showed heavy oxidation on the ID due to the testing time. There is a thick aluminum depleted zone on the ID and a thinner denuded zone on the OD (Figure 89), possibly due to rough ID machining. Internal oxidation formed in the denuded zone, which appear as angular slivers in Figure 86. The secondary crack initiated in the ID from a NiO mound. The alumina scale is continuous behind the blunted crack tip. The aluminide (PWA 275) coated material, tested at 0.8 percent strain range and 1 cpm, had negligible coating oxidation or interdiffusion because of the short testing time (Figure 87). There is a slight Al-depleted zone in the superalloy. A continuous alumina scale has formed behind the crack tip. Again, the crack tip is blunted. Initiation of the crack was caused by mechanical coating damage. The crack propagated from the coating into the substrate. The overlay (PWA 286) coated alloy, tested at 0.6 percent strain range and 1 cpm, also had negligible coating oxidation or interdiffusion (Figure 88). This sample exhibited many secondary cracks which initiated mechanically through the coating and propagated into the substrate. A very slight continuous alumina scale formed on the substrate material.

In general, the air tests exhibited "typical" TMF behavior, i.e., all failed in the gage section, and the fracture surfaces were characterized by well defined thumbnail initiation sites and Stage II cracks extending through a significant percentage of the wall thickness. Longitudinal microstructures showed secondary cracks, and the crack surfaces and uncoated ID were oxidized.

2.4.4 Inert Environment Effects

In an attempt to determine if there is a fundamental effect due to oxidation (as opposed to the growth effects due to reduction in cross-sectional area discussed above) on TMF life, a number of LATMF tests were performed in a inert (argon) atmosphere. The environment contained less than 1 ppm oxygen. Cycles to failure were similar to lives observed under identical conditions but in laboratory air (Figure 80).

Secondary cracks for uncoated and aluminide coated PWA 1480 are shown in Figures 90 and 91. The secondary crack for the uncoated material exhibits a noncontinuous alumina scale and a thick alloy depleted zone. The aluminide coated material shows no discernable coating oxidation. A non-continuous alumina scale formed along the crack surface, with a thick Al-depleted zone.

High magnification photos of the failure surface of the aluminide coated sample are presented in Figure 92. The distribution and depth of secondary cracks (Figure 93a) are similar to those observed in air tests. Although the partial pressure of oxygen was lowered to less than 0.3 Pa ($+13 \times 10^{-6}$ atm), enough of the species remains to form oxides in the Ni-Cr-Al system.

Hence, some oxidation is present on the fracture and secondary crack surfaces. Uncoated PWA 1480 specimens formed a less continuous alumina scale in the reduced partial pressure oxygen tests than those tested similarly in air (Figures 92b and 93). It is further observed in Figure 92b that the Al_2O_3 subscale on the primary fracture surface and the secondary crack surface is similar. The "inert" environment tested specimens also indicate a deeper Al-depleted zone under the non-continuous alumina scale. The increased depth of the Al-depleted zone is further emphasized by the secondary crack shown in Figure 92b. The tendency of localized non-continuous alumina to increase the depth of the alloy depleted zone may create localized notch factors capable of crack initiation. More importantly, the secondary crack in Figure 92b indicates that oxidation is occurring behind the crack tip. The crack tip shows only a thin Al-depleted zone, which indicates that oxidation occurs after the crack formed, and that the oxidation has minimal effect on the mechanism of crack propagation.

A preliminary conclusion drawn from these results is that environmental effects on TMF failure under these conditions are minimal. However, the opposite may be true, that a partial pressure of oxygen lower than 10^{-1} Pa (10^{-6} atm) is sufficiently high to produce an environmental effect on TMF crack initiation. To investigate these possibilities, later tests performed in argon, included extended hold periods at an elevated temperature, reproducing test conditions that, when the test was conducted in air, produced a significant effect on TMF life, apparently attributable to an environmental effect.

2.4.5 Purified Inert Environment Effects

Modifications to the inert environment chamber succeeded in reducing the oxygen partial pressure to less than 10^{-11} atm (<0.00001 ppm oxygen).

Metallurgical evaluation of uncoated internal diameter surfaces for similar ambient air and inert environment out-of-phase TMF tests (427-1038°C (800-1900°F), 1 cpm, no hold time) show significantly reduced oxidation in argon (Figure 94). The ambient air test shows surface oxidation indicated by the rough texture and thick irregular alloy depleted zone (Figure 94a). The inert environment test sample surface shows a much thinner oxide scale and depletion zone (Figure 94b) regardless of the longer testing time.

Standard ambient air out-of-phase TMF tests (427-1093°C (800-1900°F), with no hold time) of aluminide coated (PWA 274) PWA 1480 show numerous secondary cracks over the entire gage length (Figure 95a). Sectioning of the failed specimen shows the cracks to be oxidized and often multiple path (Figure 95b). A similarly tested inert environment specimen indicates very little secondary cracking (quantity) in the gage section (Figure 96a). The sample failure actually occurred out of gage despite the two large secondary cracks shown in Figure 96a. A sectioned view of one of these large secondary cracks is shown in Figure 96b. The crack width is very similar to the air crack shown in Figure 96b. The large secondary cracks shown are not generally typical of the argon tests and the width of these cracks may be a result of final overstress. Apparently, the surface discoloration, shown in the overview of the specimen, is superficial, since no oxidation of the coating is observed in the photomicrograph. However, the secondary crack does shown an Al-depleted zone and noncontinuous alumina subscale, indicating that the substrate material was oxidized despite the reduced oxygen pressure (Figure 96b). Such effects are expected, since the affinity of aluminum for oxygen is very high and equilibrium partial pressures for alumina formation are of the order 10^{-30} atmospheres.

2.4.6 Fracture Modes for Inert Environment Tests

A typical secondary crack is shown in Figure 97 for the inert environment tested sample. There is no coating oxidation, either on the specimen surface or the surfaces of the TMF crack. However, a thin depletion zone with alumina subscale is evident on the crack surfaces in the

substrate alloy. Presumably, from these features, oxidation processes were not involved in the formation of the coating crack, but environmental reaction is still affecting crack behavior in the substrate superalloy.

In addition to the standard out-of-phase TMF cycle comparisons, a hold time at maximum cyclic temperature was incorporated into this cycle to further investigate the effects of oxidation and creep. Results of this test comparison on aluminide coated (PWA 275) PWA 1480 showed a 2.5 × life benefit in argon over a similar air test. Comparisons of the two environments show that the air test sample has a greater number of larger secondary cracks than the argon sample (Figure 98). Again, the argon environment displays the tighter, less-oxidized, secondary cracks.

Secondary crack tip appearance comparisons were also made between the argon and air tested samples. Results indicate a difference between crack tip morphology. Secondary cracks for the air-tested specimen shows extreme oxidation along the crack surfaces with a blunt crack tip (Figure 99). No indication of an unoxidized leading crack tip is observed. The square crack tips shown may indicate that propagation has essentially stopped in these secondary cracks and continued surface oxidation produced the square appearance. Therefore, only the rapidly propagating cracks (those that produce failure) would exhibit sharp crack tips. The inert environment test sample shows the tight secondary cracks and very little crack surface oxidation, as compared to the air test (Figure 100). Argon secondary crack width is approximately a quarter of that seen in air. Argon crack tips appear much sharper than the air test "squared" crack tips. In addition, the argon tested crack tips show depleted regions ahead of the opened crack, which suggest that aluminum depletion and oxidation may be occurring ahead of the crack tip to weaken the material and, subsequently, the crack tip moves forward into these weakened areas. Reducing the amount of oxidation would then be assumed to retard the crack propagation.

The fracture surfaces of the aluminide coated (PWA 275) PWA 1480 tested with the 30-second hold time (427-1093°C (800-1900°F), out-of-phase, 1.0 cpm) in the inert environment exhibited very little Stage II crack propagation resulting in fracture faces containing mainly overstress shear planes. The air tested fracture surface was characterized by multiple thumbnail fatigue origins covering 10-15 percent of the specimen cross-sectional area (Figure 101). This is typical of ambient air out-of-phase 427-1093°C (800-1900°F) cycles for uncoated and coated PWA 1480. In contrast, the argon fracture faces when identically tested were characterized by Stage II fatigue origins comprising less than 3.0 percent of the specimen cross sectional area (Figure 102). This dramatic reduction of Stage II crack propagation may be a result of the sharper argon cracks having a greater total stress intensity than the blunted air cracks. In addition, the air environment crack formed in groups further reducing the effective stress intensity. The argon tested secondary cracks were typically singular and had much sharper crack tips. The higher stress intensity could create the earlier overstress from shorter life limiting cracks.

2.4.7 TMF Temperature Range Comparisons for Coated PWA 1480

Typical fracture behavior of the aluminide coated (PWA 275) and overlay coated (PWA 286) PWA 1480 systems are necessary to understand the effect of maximum temperature on coating degradation. Standard out-of-phase TMF cycles were examined for these coated systems at 427-927°C (800-1700°F) and 427-1093°C (800-2000°F), representing two temperature range extremes for comparison. The following fracture behavior comparisons were made on strain-controlled TMF specimens tested at a fully reversed 0.6% strain range.

The aluminide coated (PWA 275) PWA 1480 specimen tested at 427-927°C (800-1700°F) showed sharp coating cracks that extend circumferentially around the specimen gage section (Figure 103a). This coating failure mode would indicate poor coating ductility at the 427°C (800°F) high tensile strain portion of the cycle. The fracture face (Figure 103c) shows complete

coating failure (one continuous fatigue thumb nail around the perimeter) in which coating cracks propagated directly into the substrate. Figure 103b shows the very sharp planar fracture face resulting from the sharp coating crack. Failure life indicates an approximate 5X-life degradation due to the PWA 275 coating as compared to uncoated PWA 1480 (Figure 70) under identical test conditions. This debit is associated with early coating failure, and subsequent propagation into the substrate. Overlay coated (PWA 286) PWA 1480 tested at the same temperature range exhibited no significant life debit in comparison to uncoated PWA 1480 (Figure 70). The surface condition of the overlay coating shows a mild rumpled appearance with sharp, short cracks initiating from the "valleys" (Figure 104a). The specimen fracture face shows a jagged appearance indicating multiple coating crack fatigue origins (Figures 104b and 104c). The short cracks in the overlay coating (PWA 286) are random in nature, which is in sharp contract to the ordered fully circumferential cracks exhibited in the aluminide coating (PWA 275). The shorter overlay cracks appear to degrade PWA 1480 less severely since a linking of initiation origins was required for the final specimen failure.

The aluminide coated (PWA 275) PWA 1480 specimen tested at the high temperature range (out-of-phase, 0.6 percent $\Delta\varepsilon$, 0.5 cpm, 427-1093°C (800-2000°F)) shows many distressed coating areas (Figure 105a). These distressed areas feature many coating cracks that have filled with oxide producing local discoloration. The specimen overview shows general gage section discoloration with the white spots being the areas of coating distress (Figure 105b). Again coating failure appears planar. The initiation area is bracketed on the fracture face view (Figure 105c). Failure life indicates an approximate 3X-life degradation due to the PWA 275 coating as compared to uncoated PWA 1480 (Figure 72) under identical test conditions. This debit is less than the debit associated with the lower temperature range test of 427-927°C (800-1700°F), where a 5X-degradation occurred. The reduced debit of the higher temperature range may be associated with the coating not cracking continuously around the gage section as with the lower temperature range test. Overlay coated (PWA 286) PWA 1480 tested similarly exhibited no significant life debit (less than 2X) in comparison to uncoated PWA 1480 (Figure 72). The surface condition of the overlay coating shows an extremely rumpled appearance with many visible cracks initiating from the "valleys" (Figure 106a). The specimen fracture face shows a jagged appearance indicating multiple coating crack fatigue origins (Figure 106b and 106c). The appearance of the fracture face is very similar to the PWA 286 coated 427-927°C (800-1700°F) test with the exception of the much greater oxidation produced from the increased maximum temperature 1093°C (2000°F). Coating rumpling is also much more severe (compare Figures 104a and 106a).

2.4.8 Substrate Failure Modes

Fracture behavior of single crystal PWA 1480 exhibits marked differences according to TMF cycle type. Typical fatigue crack initiation and propagation of [001] PWA 1480 under isothermal conditions at elevated temperature, occurs normal to the direction of the loading axis (i.e., typical Stage II fracture behavior). Crack propagation continues normal to the loading axis until significant reduction in specimen area results in final tensile overstress. Tensile overstress commonly occurs on high shear-stress (111) octahedral planes (Figure 107).

In-phase (Type 2 cycle) TMF testing in which maximum tensile loading and maximum cyclic temperature coincide, would be expected to fracture in a similar manner to isothermal elevated temperature testing. However, test results on in-phase TMF indicate crack initiation and propagation occur on the (111) octahedral plane with overstress fracture normal to the loading direction (Figure 108). The (111) crack propagation plane is represented in Figure 109 relative to the secondary orientations.

The out-of-phase (Type 1 cycle) TMF testing shows Stage II crack propagation behavior normal to the loading direction (similar to elevated temperature isothermal results) with

overstress fracture on (111) octahedral planes (Figure 110). Often multiple overstress planes are observed corresponding geometrically to the crystallographic octahedral planes. Examples of these overstress planes are presented in Figures 111 and 112. Figures 113, 114, and 115 show the typical fracture behavior for out-of-phase cycles. The flat surface perpendicular to the loading axis in Figure 113 is characteristic of Stage II crack growth, which typically covers a large percent of the fracture surface. Unstable crack growth occurs when the critical stress intensity is reached. This is characterized by crack propagation along octahedral planes until the final overstress (Figure 114). The origin site in this specimen had the typical thumbnail initiation along the ID (Figures 114 and 115).

A comparison of the typical surface behavior during test for out-of-phase and quadrilateral cycles is shown in Figure 116. The out-of-phase tests for uncoated and coated PWA 1480 show very little oxidation compared to the quadrilateral cycles. The surfaces of the Type 1 cycle tests are smooth with only a small amount of oxidation in the uncoated samples and negligible oxidation in the coated samples. The quadrilateral cycles exhibit extreme surface oxidation in the uncoated sample with significant loss of cross section. The coated sample tested with the quadrilateral cycle exhibited less oxidation than the uncoated sample, but the coating spalled off during the test causing the specimen to have no oxidation protection. In addition, very little cracking is apparent in the out-of-phase cycles. Cracks become apparent just prior to failure. Most of the life of the out-of-phase cycle is spend in initiation. The surface of the quadrilateral cycle samples were so badly damaged that observing cracks is very difficult. Crack growth measurements in TMF samples is therefore prohibitive.

The standard quadrilateral cycle has been extremely aggravating to both uncoated and coated PWA 1480. The typical fracture surface (Figures 117, 118, and 119) for the quadrilateral cycle generally displays well defined thumbnails along the OD and Stage II crack propagation. Quadrilateral cycles with low strain ranges show crack growth perpendicular to the loading axis with typical Stage II crack propagation (Figure 120). Quadrilateral cycles with high strain ranges exhibit crack propagation along octahedral shear planes (Figure 121). The lower strain ranges usually have crack growth along the octahedral planes during later stages of testing when the crack growth becomes rapid. This crack propagation along octahedral shear planes occurs when the stresses exceed the critical shear stress. The cycles with high strain ranges have stresses which exceed the critical shear stress much sooner than cycles with low strain ranges.

The uncoated alloy tested with the low strain range quadrilateral cycle appeared to go through an alternating series of first surface oxidation and subsequent spallation on the OD (Figure 116d). Large amounts of dark oxide adhered to the ID. There was less oxide on the OD but this was because the oxide spalled and did not adhere to the surface as did the oxide on the ID. The short spike in Figure 120 is a common feature of quadrilateral cycle samples of uncoated PWA 1480 and may be a mechanism of crack initiation.

The aluminide coating (PWA 275) was so degraded by the quadrilateral cycle, that at approximately 8000 cycles the coating had completely spalled off, essentially leaving an uncoated sample as shown in Figure 122. The coating turned white at 600 cycles and began cracking and spalling at 1200 cycles. A photo micrograph of the OD is shown in Figure 123. The coating degradation begins with the beta grain boundaries pulling apart. Beta grains can fall out due to oxidation of grain boundaries on both sides, or perhaps simply be consumed by the oxidation spreading laterally from the grain boundaries. No secondary cracks were observed in the center gage section where the coating spalled off (Figure 124). This may be because of the noticeable loss of substrate cross section due to bulk substrate oxidation. If a crack was initiated, it would have spalled off with the oxides.

The overlay coated (PWA 286) PWA 1480 specimen tested with the same quadrilateral cycle as the aluminide coated and uncoated samples did not spall the coating off the substrate.

The overlay coating surface show an extremely rumpled appearance with many visible cracks initiating from the "valleys" (Figure 125a). The specimen fracture face shows a jagged appearance indicating multiple coating crack fatigue origins (Figures 125b and 125c). A photo micrograph of specimen secondary cracks shows that preferential oxidation of the coating beta-NiAl phase contributed to crack propagation by initiating in the coating and moving into the substrate (Figure 126). The micrograph shows black oxide holes (Figure 126, dotted area) that have precisely the same shape as adjacent islands of beta-NiAl. This preferential oxidation of beta-NiAl produces "valleys" in the coating (Figure 126, white arrows). The PWA 286 overlay coating contains small additions of Si and Hf. The Hf stringers in the overlay keep the coating adherent in many areas. With this adherence, the coating cracks continue into the substrate producing specimen failure. The PWA 275 aluminide coating does not contain these adherent stringers. Therefore, the quarilateral cycle spalls the aluminide coating without propagating life limiting cracks into the substrate. This coating spallation was not seen in engine parts but it is a factor in the life of tested specimens.

The temperature cycles for the out-of-phase and quadrilateral cycle are identical. The significant oxidation reaction with environment takes place at temperatures of 982°C (1800°F) and above. A possible effect on oxidation behavior must, therefore, involve the high temperature portions of these cycles. In the out-of-phase cycle, the stress is decreasing from approximately +27 MPa (+4 ksi) to −62 MPa (−9 ksi) as the temperature increases from 982 to 1093°C (1800 to 2000°F). In the same temperature interval of the quadrilateral cycle, stress increases from −276 MPa (−40 ksi) to +7 MPa (+1 ksi). The increasing stress and increasing temperature, combined with a greater stress change, could conceivably aggravate oxidation by pulling apart both surface scale and grain boundaries in the coating, thus facilitating access of oxygen to the coating material.

2.4.9 Environment Effect

The oxidation process is summarized below. First, the coatings generally are not oxidized in the duration of the out-of-phase TMF tests, even in air. There is a tendency for fewer cracks in the inert environment tests for which there is no explanation. Second, the transient effects of oxidation are the most poorly understood part of the overall effects of oxidation, i.e., the initial stages of reaction with unoxidized metal. It is generally believed that everything oxidizes in situ, because there is no time for diffusion, and that the stable scale develops by exchange reactions. The exchange reaction in the PWA 1480 system occurs by the formation of transient NiO and its conversion to alumina by:

$$3\ NiO + 2\ Al == > Al_2O_3 + 3\ Ni$$

The aluminum comes from aluminum dissolved in the metal, and nickel goes back into solution. The reaction proceeds to the right because the free energy of formation of Al_2O_3 is much more negative than the free energy of formation of NiO. Because the kinetics of Ni formation are very rapid, this reaction contributes to the formation of a continuous, protective scale when the alloy is oxidized in air, thus becoming a barrier to further oxidation and alloy depletion.

The "inert" environment is sufficient to prevent NiO formation. Generally, one must be three orders of magnitude away from equilibrium to have a driving force strong enough to cause oxidation. Hence, a continuous, protective scale cannot form by the above reaction. Lacking a continuous surface scale, oxygen can diffuse inward to form the discontinuous Al_2O_3 subscale that is seen on the surface of the TMF cracks in the "inert" environment. The green color is probably a mixture of Cr_2O_3 and $NiCR_2O_4$ spinel. The chromia and the spinel kinetically form faster than Al_2O_3.

The cycles tested in this program were not the types of tests that produce significant damage by oxidation. In addition, the purified "inert" environment produced oxide formation

that, although less than in air, had a similar effect on the TMF life of the cycles tested. It was, therefore, not possible to differentiate a consistent environment or time/temperature damage effect to include in the life prediction model. Accordingly, an environment term for the TMF life prediction model was discontinued.

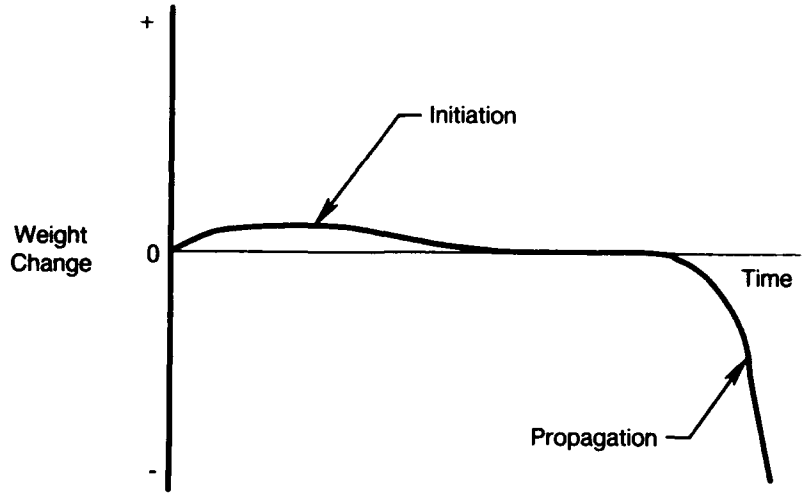

Figure 84. Oxidation Behavior of Nickel-Base Superalloys Showing Initiation and Propagation Stages

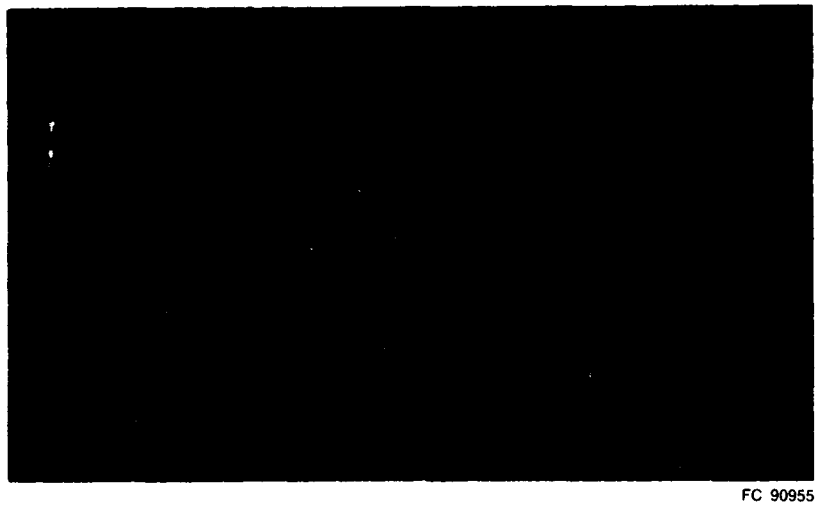

FC 90955

Type 1 Test, ΔT = 427-1038°C (800-1900°F), 0.2 cpm, OD

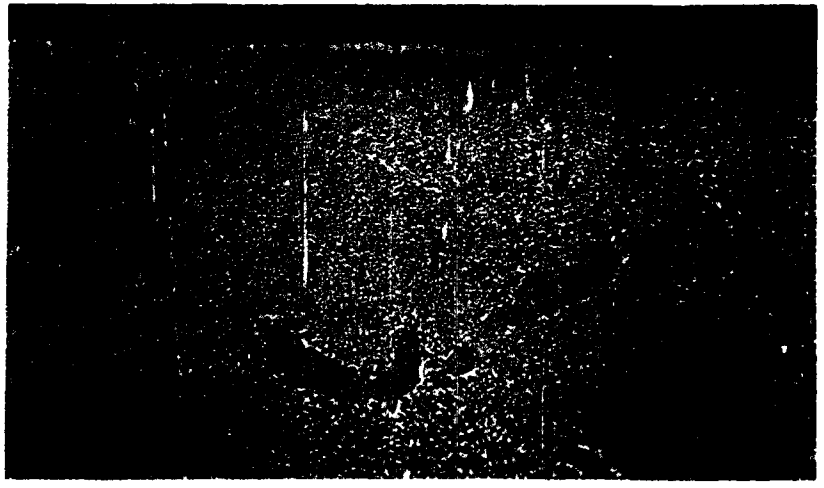

FC 90954

Type 1 Test, ΔT = 427-1038°C (800-1900°F), 0.2 cpm, ID

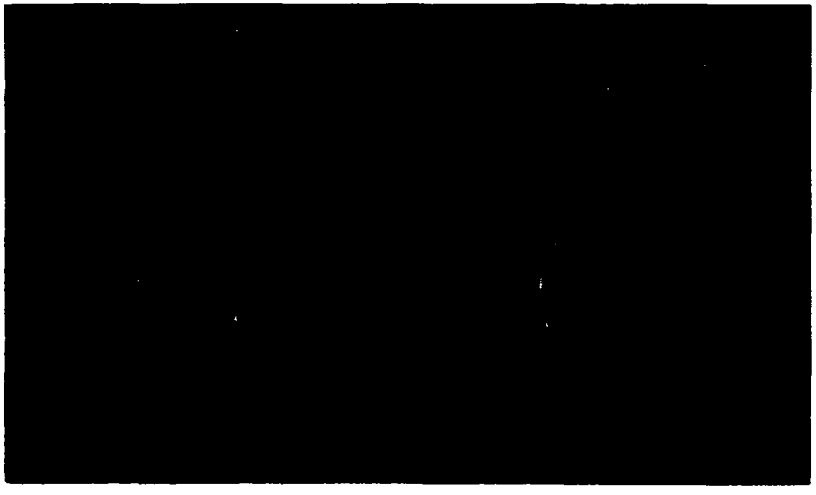

FC 90956-H

Type 1 Test, ΔT = 427-1038°C (800-1900°F), 4 cpm, OD

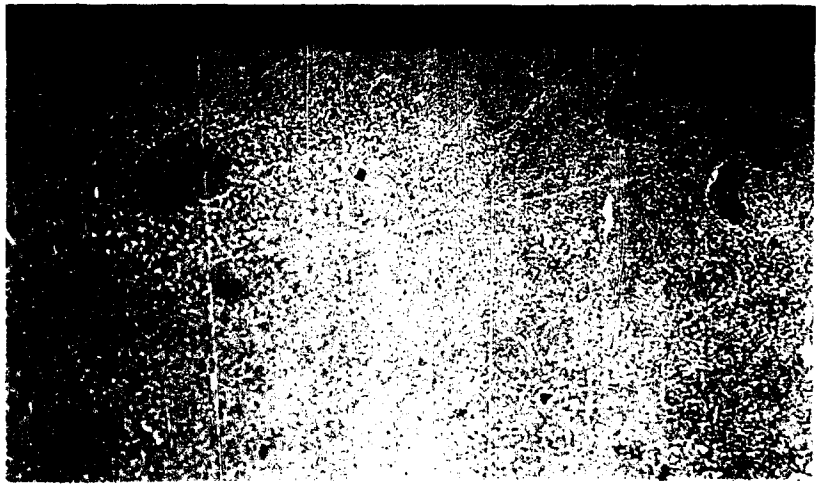

FC 90953-H

Type 1 Test, ΔT = 427-1038°C (800-1900°F), 4 cpm, ID

FD 299489

Figure 85. Test Frequency Effect on Microstructure of Uncoated PWA 1480

Mag: 500X

FD 357696

Figure 86. Secondary Crack for Uncoated PWA 1480 Initiated on ID (Type 1 Cycle, $\Delta\varepsilon$ = 0.4%, ΔT = 427-1038°C (800-1900°F), 1 cpm, N_f = 41906)

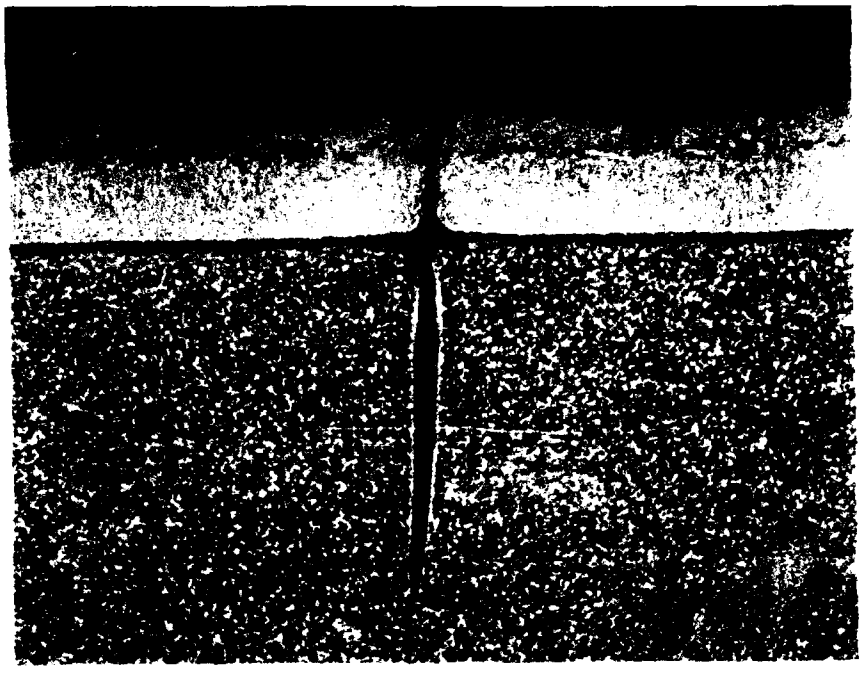

Mag: 500X

FDA 357697

Figure 87. Secondary Crack for PWA 275 Coated PWA 1480 Initiated on OD (Type 1 Cycle, $\Delta\varepsilon$ = 0.8%, ΔT = 427-1038°C (800-1900°F), 1 cpm, N_f = 718)

Mag: 500X

FD 357698

Figure 88. Secondary Crack for PWA 286 Coated PWA 1480 Initiated on OD (Type 1 Cycle, $\Delta\varepsilon$ = 0.6%, ΔT = 427-1038°C (800-1900°F), 1 cpm, N_f = 4729)

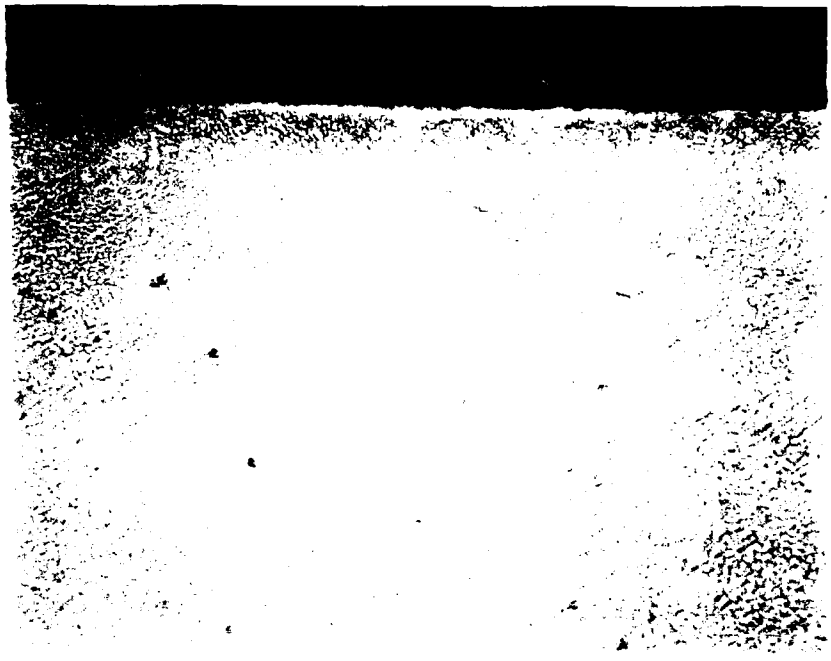

500X

FD 317544

Figure 89. Typical Surface Oxidation of Uncoated PWA 1480 Tested In Air Type 1, ΔT = 427-1038°C (800-1900°F), $\Delta\varepsilon$ = 0.4%, 1 cpm N_f = 41906)

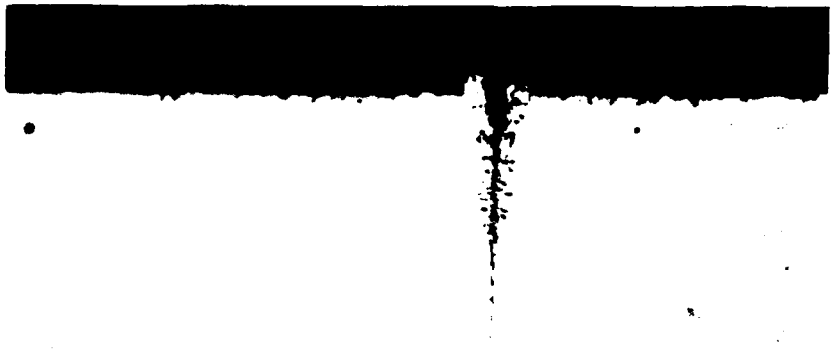

Mag: 500X FDA 357699

Figure 90. Secondary Crack for Uncoated PWA 1480 Tested in Argon Environment (Type 1 Cycle, $\Delta\varepsilon$ = 0.6%, ΔT = 427-1038°C (800-1900°F), 1 cpm, N_f = 9658)

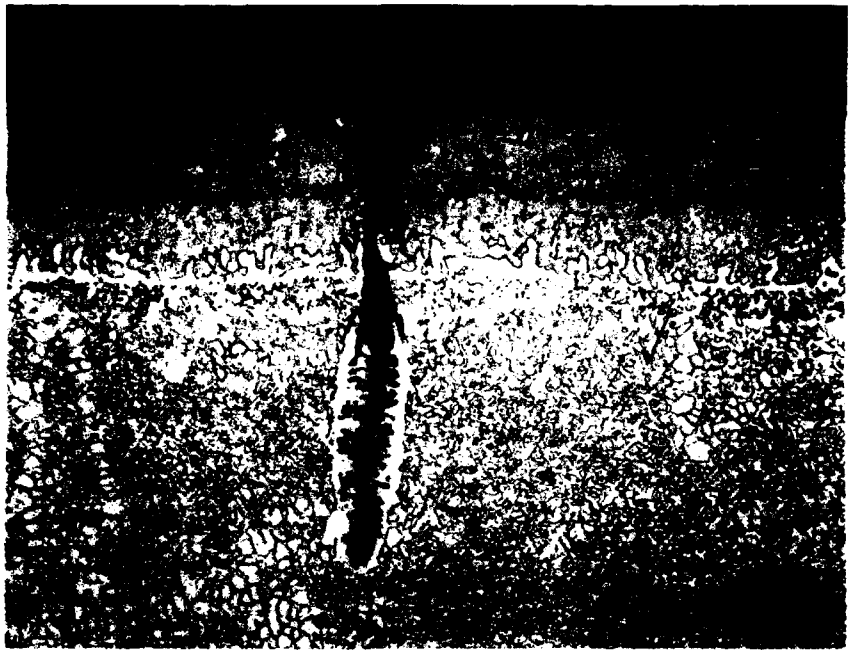

Mag: 500X

FDA 357700

Figure 91. Secondary Crack for PWA 275 Coated PWA 1480 Tested in Argon Environment (Type 1 Cycle, $\Delta\varepsilon$ = 0.4%, ΔT = 427-1038°C (800-1900°F), 1 cpm, N_f = 26809)

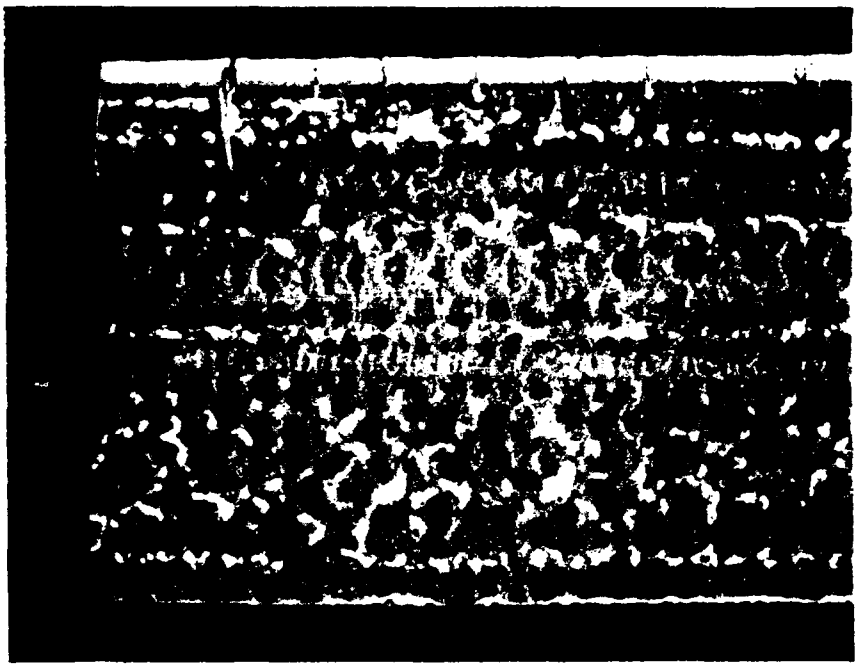

a. Longitudinal Cross-Section of Failed PWA 1480/275 Tubular LATMF Specimen Tested in Argon Showing Fracture Surface and Multiple Secondary Cracks

150μm

b. Close-Up of Upper Left-Hand Corner Showing Similar Oxidation on Fracture Surface and a Large Secondary Crack

30 μm

FD 312681

Figure 92. Metallography of a PWA 275 Coated PWA 1480 LATMF Specimen Tested in Argon (Type 1, ΔT 800-1900°F, Δε 0.6%, 1 cpm, N_f 5,720)

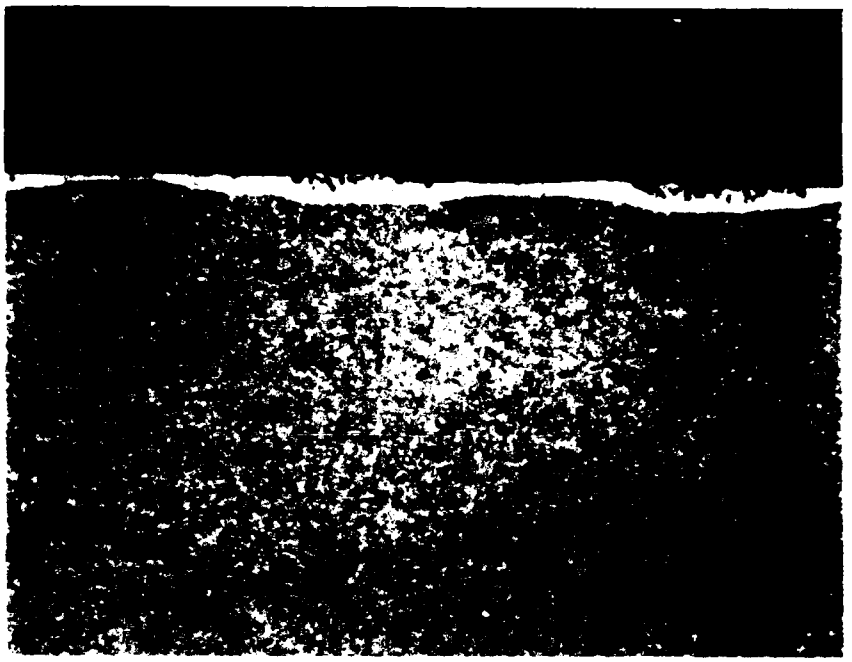

500X

FD 317545

Figure 93. Surface Oxidation of Uncoated PWA 1480 Tested in Reduced Partial Pressure Oxygen Environment (< 1.0 ppm) (Type 1, ΔT = 427-1038°C (800-1900°F), $\Delta\varepsilon$ = 0.8%, 1 cpm, N_f = 3069)

(a) Mag: 1000X

(b) Mag: 1000X

FD 338173

Figure 94. Comparison of Uncoated Internal Diameter Surfaces In Ambient Air and Inert Environment. Test Cycle Was 427-1038°C (800-1900°F) Out-of-Phase TMF, 1 cpm, With No Hold Time For Both Examples (a) Ambient Air Test Showing Extreme Surface Oxidation Indicated By the Rough Texture and Thick Al Depleted Zone (b) Inert Environment Test Showing No Significant Amounts of Oxidation or Depleted Zone

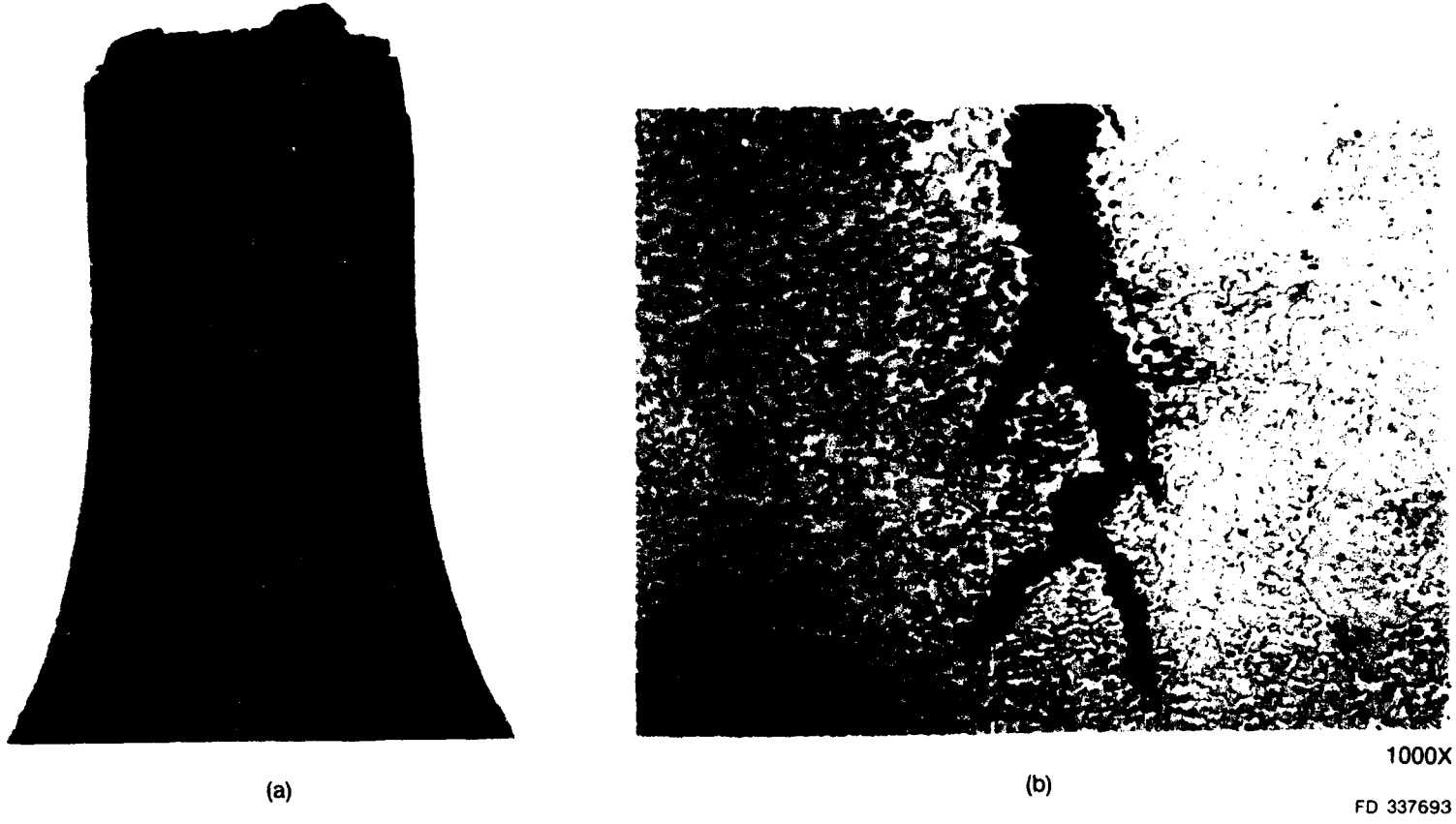

Figure 95. Ambient Air Out-of-Phase TMF Test on PWA 275 Coated PWA 1480 (Type 1, 1 cpm, ΔT = 427-1038°C (800-1900°F), $\Delta\varepsilon$ = 0.6%, N_f = 3180)

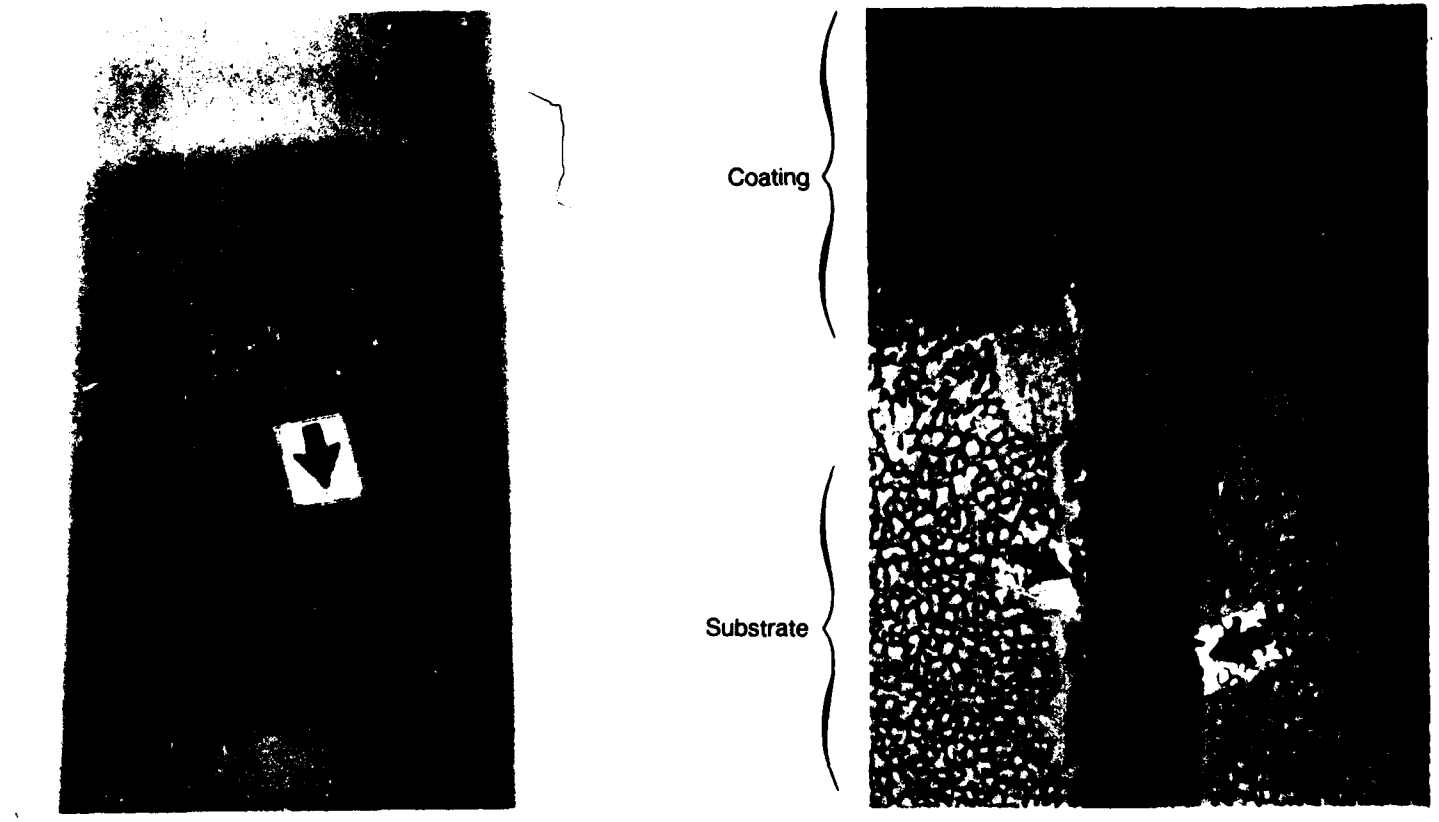

a) Specimen Gage Section Showing Superficial Discoloration and Two Large Secondary Cracks. (Specimen Failure Occurred Out of Gage).
b) Sectioned Photomicrograph of Secondary Crack Shown in View (a). Coating Shows no Discernable Oxidation, However Secondary Crack is Oxidized in the Substrate Material (Noncontinuous Aluminide Subscale, Arrows).

FD 324973

Figure 96. Increased Purity Inert Environment Out-of-Phase TMF on PWA 275 Coated PWA 1480 (Type 1, 1 cpm, ΔT = 427-1038°C (800-1900°F), $\Delta\varepsilon$ = 0.6%, N_f = 8000-Contamination) (a) Specimen Gage Section Showing Superficial Discoloration and Two Large Secondary Cracks (Specimen Failure Occurred Out of Gage) (b) Sectioned Photomicrograph of Secondary Crack Shown in View (a). Coating Shows No Discernable Oxidation; However, Secondary Crack Is Oxidized in the Substrate Material (Noncontinuous Alumina Subscale — Arrows)

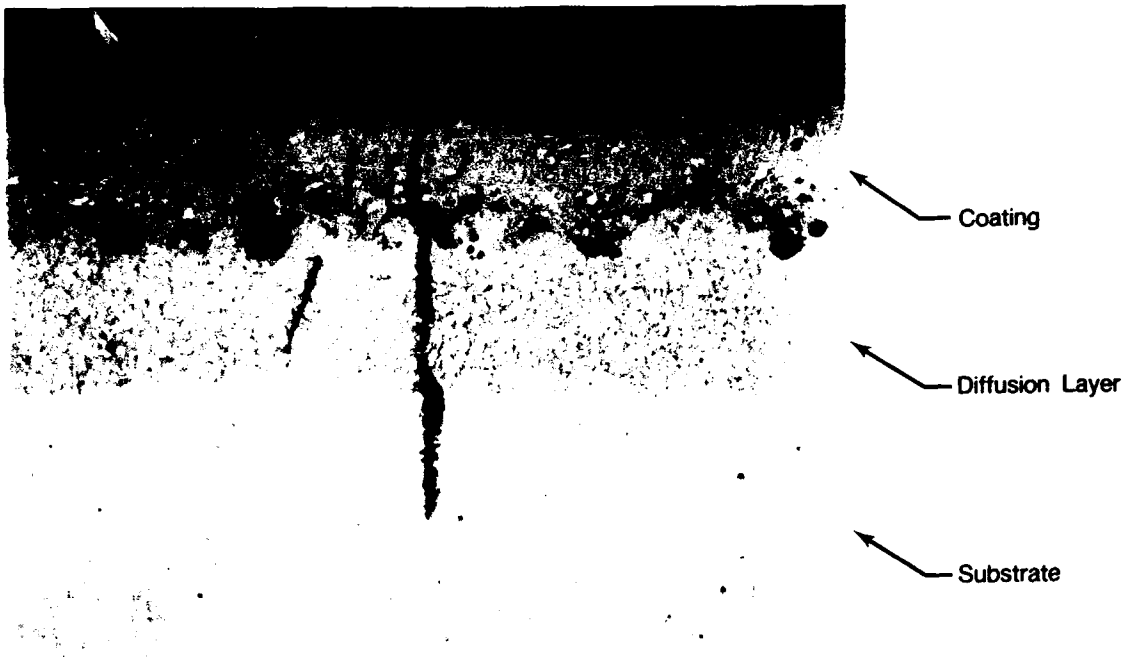

Figure 97. Typical Secondary Crack of PWA 275 Coated PWA 1480 in Out-of-Phase Test in Inert Environment (Type 1, 1 cpm). Characterized by Very Tight Crack Propagation into the Substrate

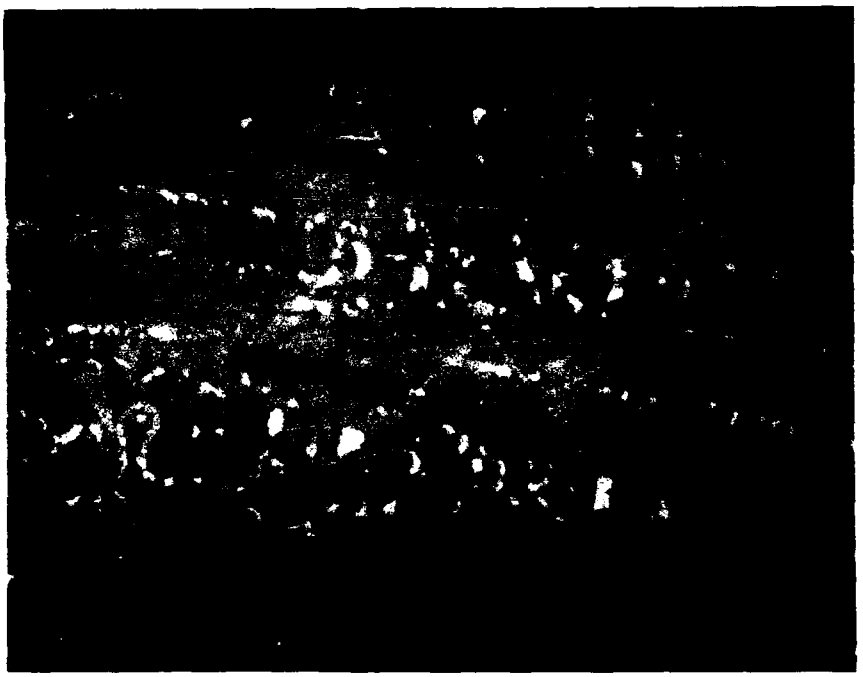

Mag: 50X

(b)

FD 338177

Figure 98. Comparison of PWA 275 Coated PWA 1480 Secondary Cracks in Ambient Air and Inert Environment (Cycle Type: Out-of-Phase, 427-1038°C (800-1900°F), 1 cpm, With 30 Second Hold at T_{max}) (a) Ambient Air Test Showing Many Large Secondary Cracks (b) Inert Environment Test Showing Smaller, Tighter Secondary Cracks. Note the Orientation of the Eutectic Gamma Prime Strings Indicate the Crystal Axis Could Be Off by Approximately 10°

1000X

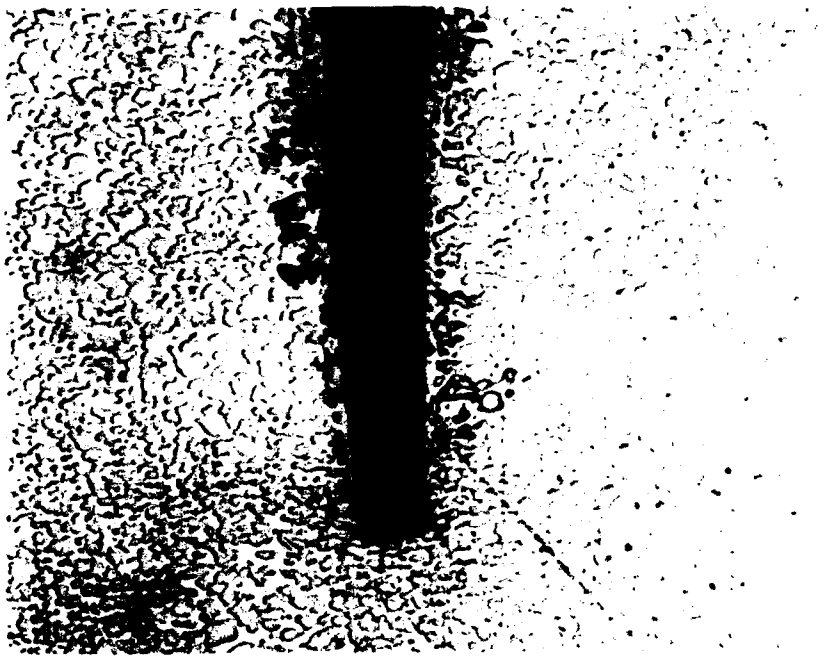

1000X

FD 337696

Figure 99. Secondary Cracks of Ambient Air Tested PWA 275 Coated PWA 1480 (Cycle Type: Out-of-Phase, 427-1038°C (800-1900°F), 1 cpm, With 30-Second Hold at T_{max}). Note Extreme Width of Cracks With Heavy Denuded Zone Along Crack Sides. Both Photographs Have Same Magnification

Figure 100. Secondary Cracks of Inert Environment Tested PWA 275 Coated PWA 1480 (Cycle Type: Out-of-Phase, 427-1038°C (800-1900°F), 1 cpm, With 30-Second Hold at T_{max}). Crack Widths Are Approximately ¼ the Width of the Similar Ambient Air Test (Figure 99). Higher Magnification (Views b and c) Are of Crack Shown on Left Side of View (a)

FD 338175

Figure 101. Fracture Face of PWA 275 Coated PWA 1480 Specimen Tested in Ambient Air (Cycle Type: Out-of-Phase, 427-1038°C (800-1900°F), 1 cpm, With 30-Second Hold at T_{max}). Fracture Face Shows Multiple Thumbnail Origins Covering 10-15% of Specimen Cross-Sectional Area

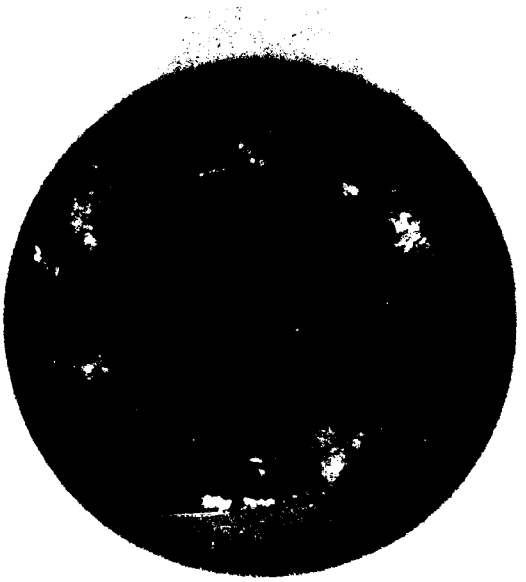

FD 338174

Figure 102. Fracture Face of PWA 275 Coated PWA 1480 Specimen Tested in an Inert Environment (Cycle Type: Out-of-Phase, 427-1038°C (800-1900°F), 1 cpm, With 30-Second Hold at T_{max}). Fracture Face Shows Extremely Limited Stage II Crack Propagation (Less Than 3% of Specimen Cross-Sectional Area)

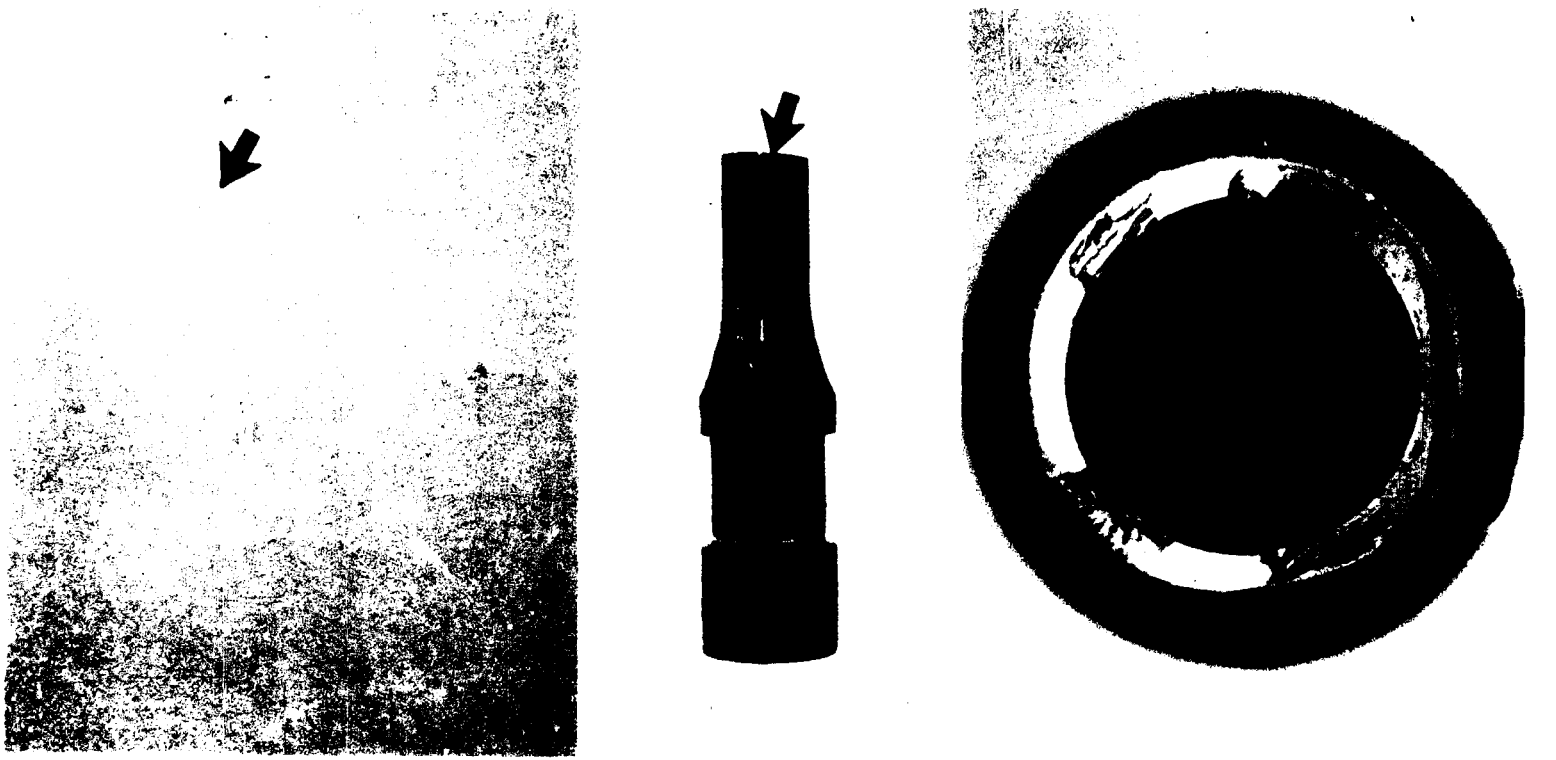

a) Surface Condition Showing Sharp Coating Cracks Which Extend Completely Around the Specimen Gage Section (Circumferentially) (Arrow).
b) Specimen Overview Showing Sharp Planner Fracture Face Resulting From Sharp Coating Cracks (View a).
c) Specimen Fracture Face Showing Circumferential Coating Crack Initiation and Subsequent Propagation Into Substrate (Bracket).

FD 324966

Figure 103. Fracture Morphology of PWA 275 Coated PWA 1480 (Out-of-Phase Cycle, $\Delta\varepsilon$ = 0.6%, 1 cpm, 427-927°C (800-1700°F))

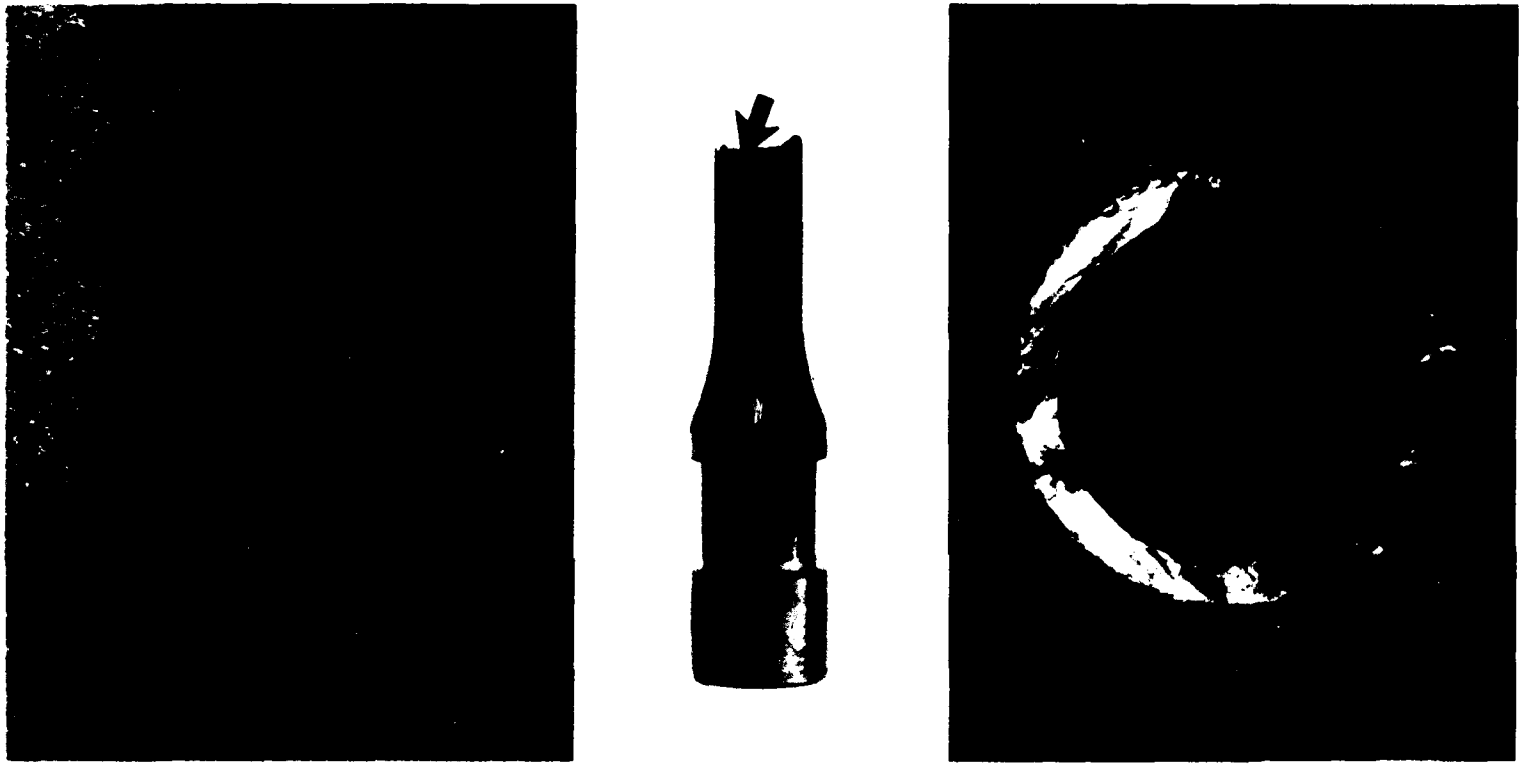

a) Surface Condition Showing a Mild Rumpled Appearance With Sharp Short Cracks Initiating From the Pores.
b) Specimen Overview Showing Jagged Appearance of Fracture Face Indicating Multiple Coating Crack Link Up (Arrow).
c) Specimen Fracture Face Showing Several Fatigue Origins With Jagged Origin Link Up.

FD 324967

Figure 104. Fracture Morphology of PWA 286 Coated PWA 1480 (Out-of-Phase Cycle, $\Delta\varepsilon$ = 0.6%, 1 cpm, 427-927°C (800-1700°F))

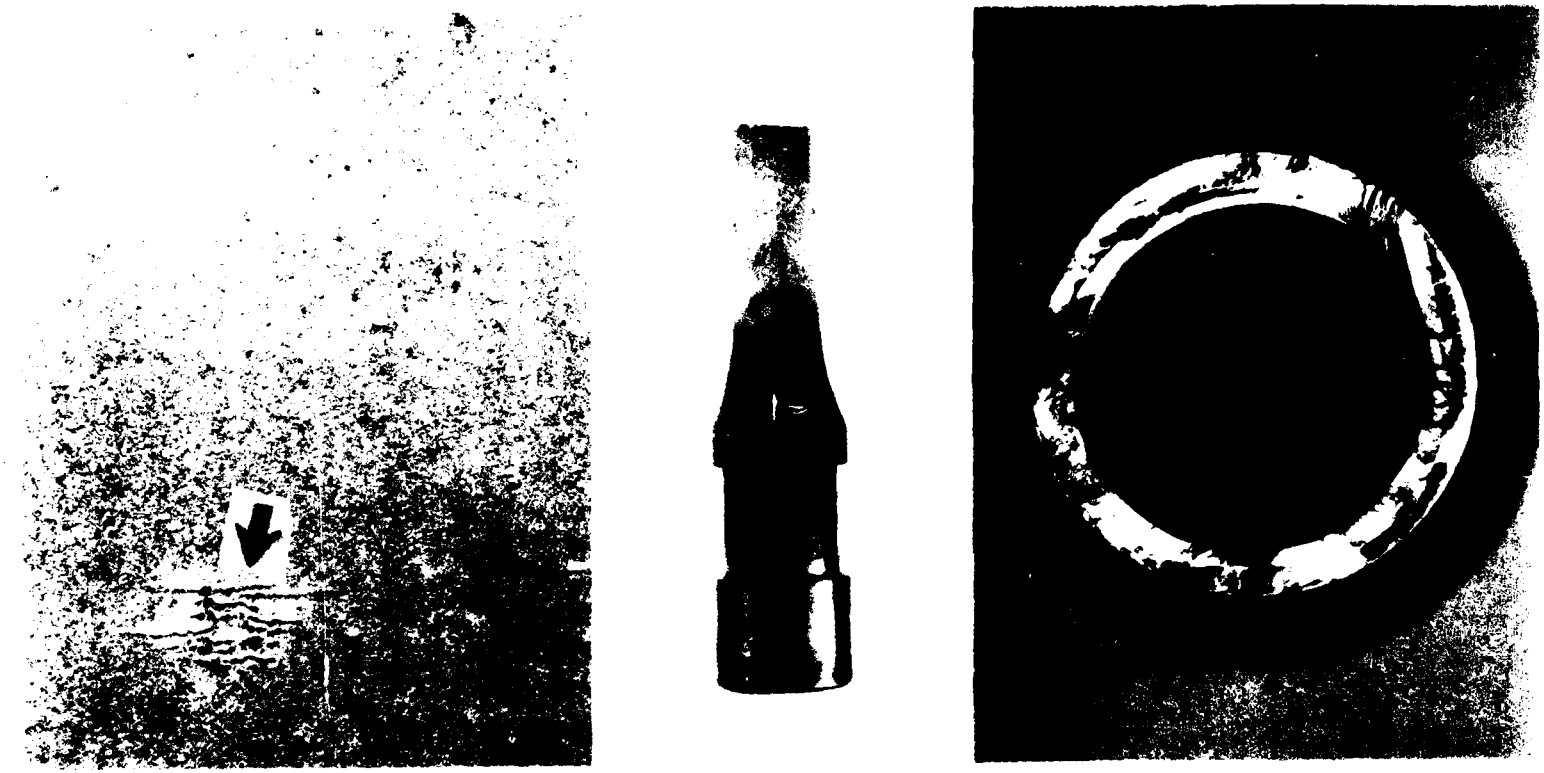

a) Surface Condition Showing Distressed Coating Area Where Cracks Have Filled With Oxide (Arrow).
b) Specimen Overview Showing Gage Section Discoloration Brought On By Coating Crack Oxides, as Shown in View (a).
c) Specimen Fracture Face Showing Large Origin With Depletion Zone.

FD 324968

Figure 105. Fracture Morphology of PWA 275 Coated PWA 1480 (Out-of-Phase Cycle, $\Delta\varepsilon$ = 0.6%, 0.5 cpm, 427-1093°C (800-2000°F))

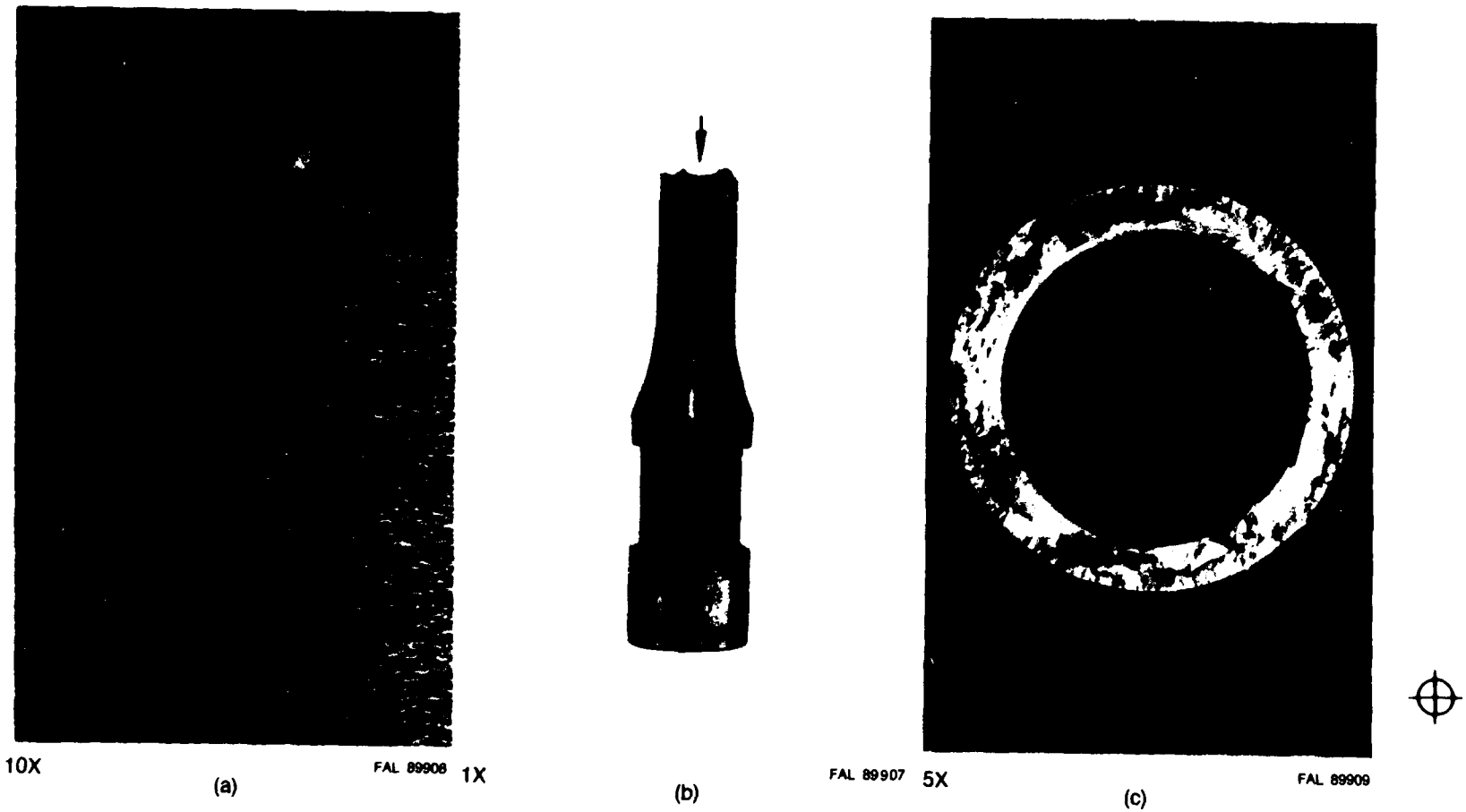

a) Surface Condition Showing Extreme Coating Rumpling with Associated Cracking.
b) Specimen Overview Showing Jagged Appearance of Fracture Face Indicating Multiple Coating Crack Link Up (Arrow).
c) Specimen Fracture Face Showing Numerous Fatigue Origins with Jagged Origin Link Up.

FD 324969

Figure 106. Fracture Morphology of PWA 286 Coated PWA 1480 (Out-of-Phase Cycle, $\Delta\varepsilon$ = 0.6%, 0.5 cpm, 427-1093°C (800-2000°F))

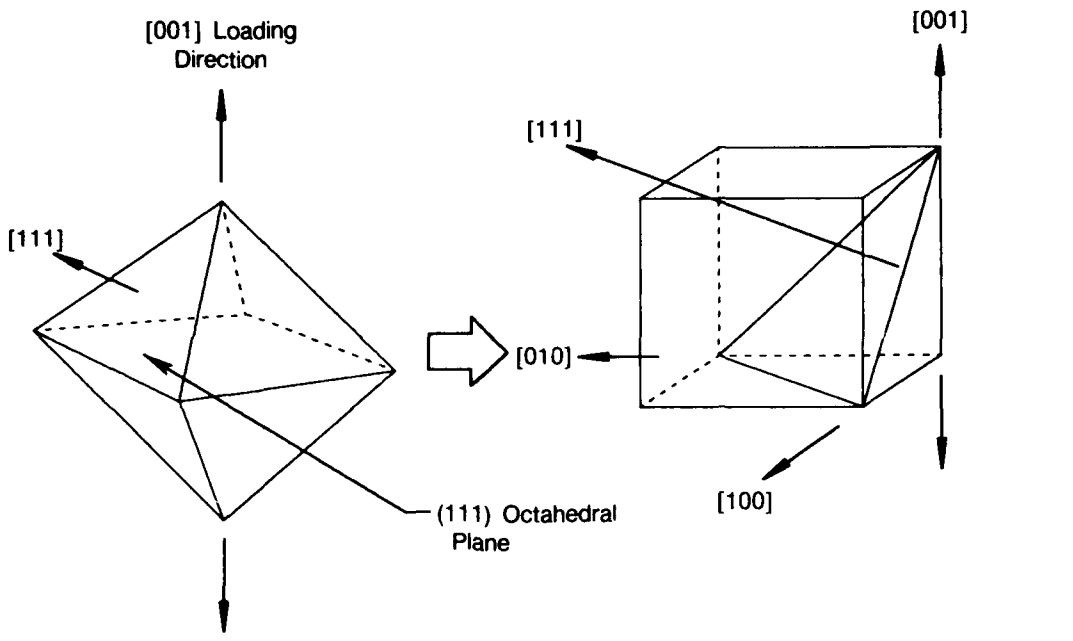

Figure 107. (111) Octahedron With Corresponding Crystallographic Orientations in Single Crystal PWA 1480

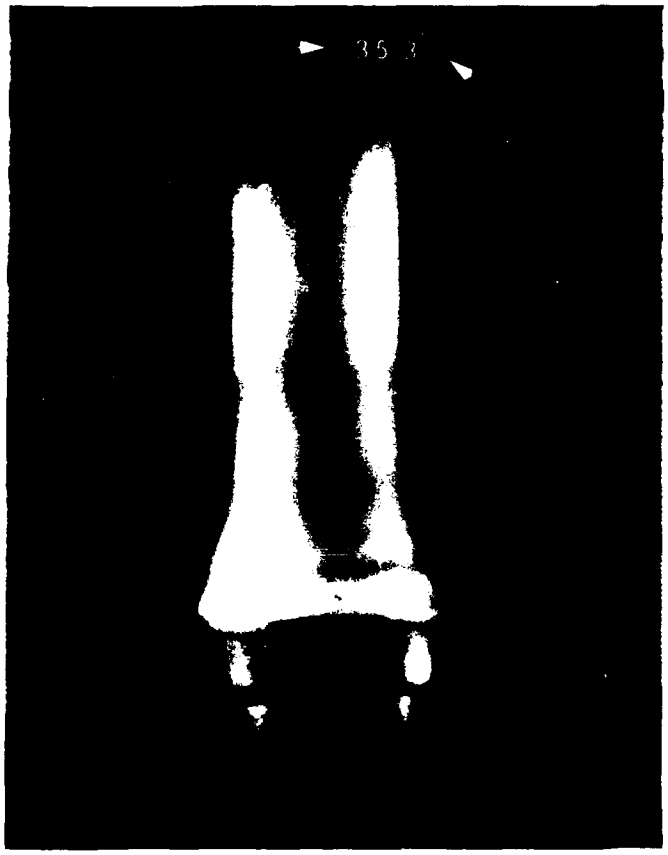

FAL87978 2X

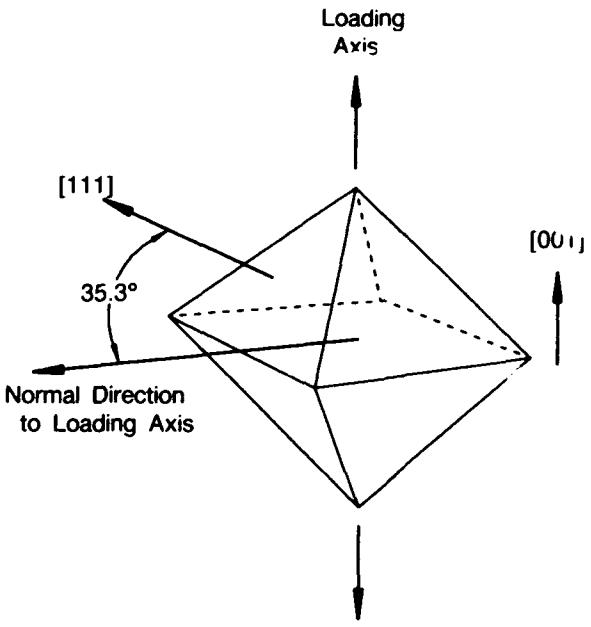

FD 317548

Figure 108. (111) Octahedral Propagation Observed in PWA 275 Coated PWA 1480 In-Phase TMF Test (427-1038°C/800-1900°F)

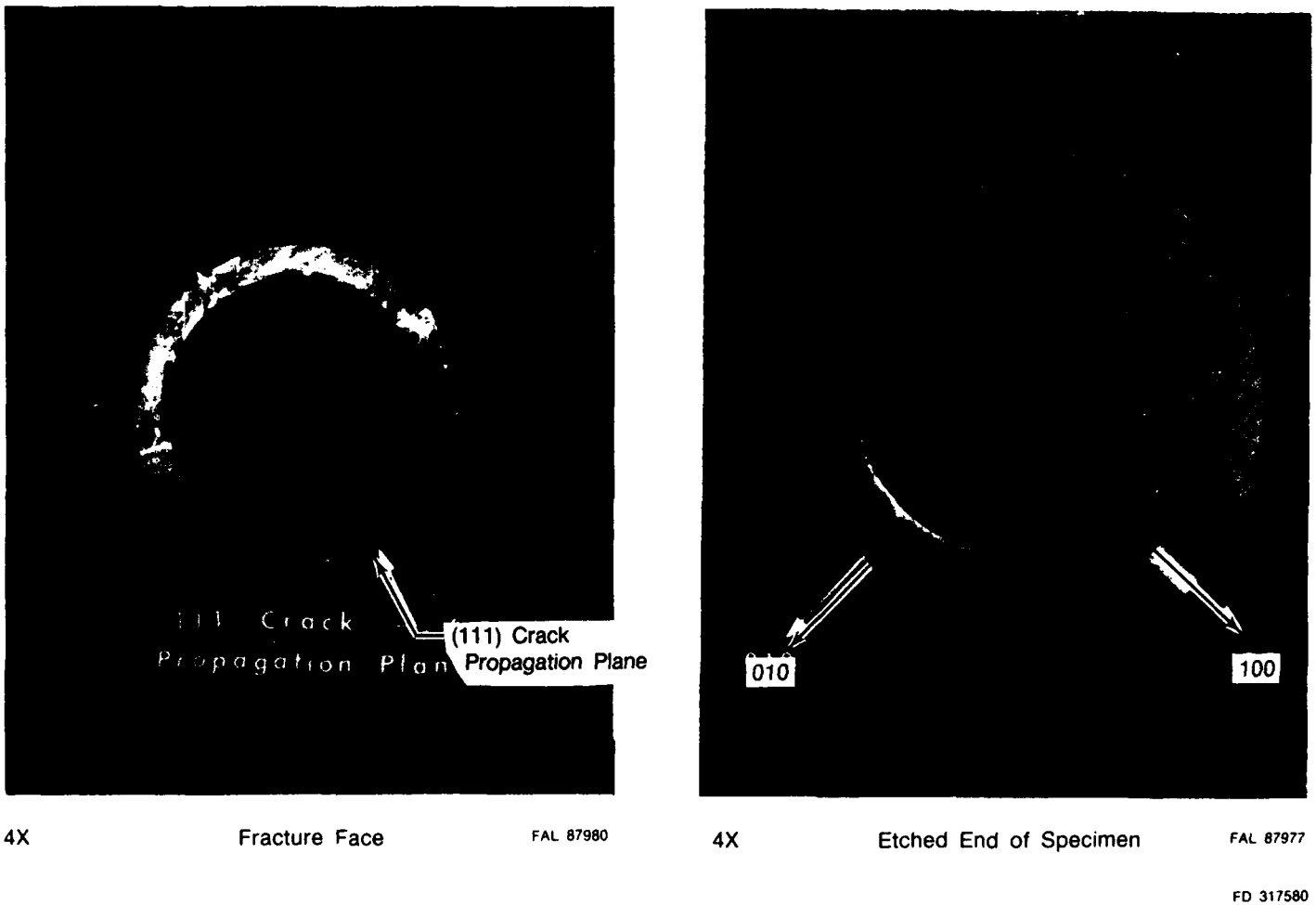

Figure 109. (111) Crack Propagation Plane Relative to Secondary Orientations Determined From Dendrite Arms (Photographs are Oriented With Respect to One Another)

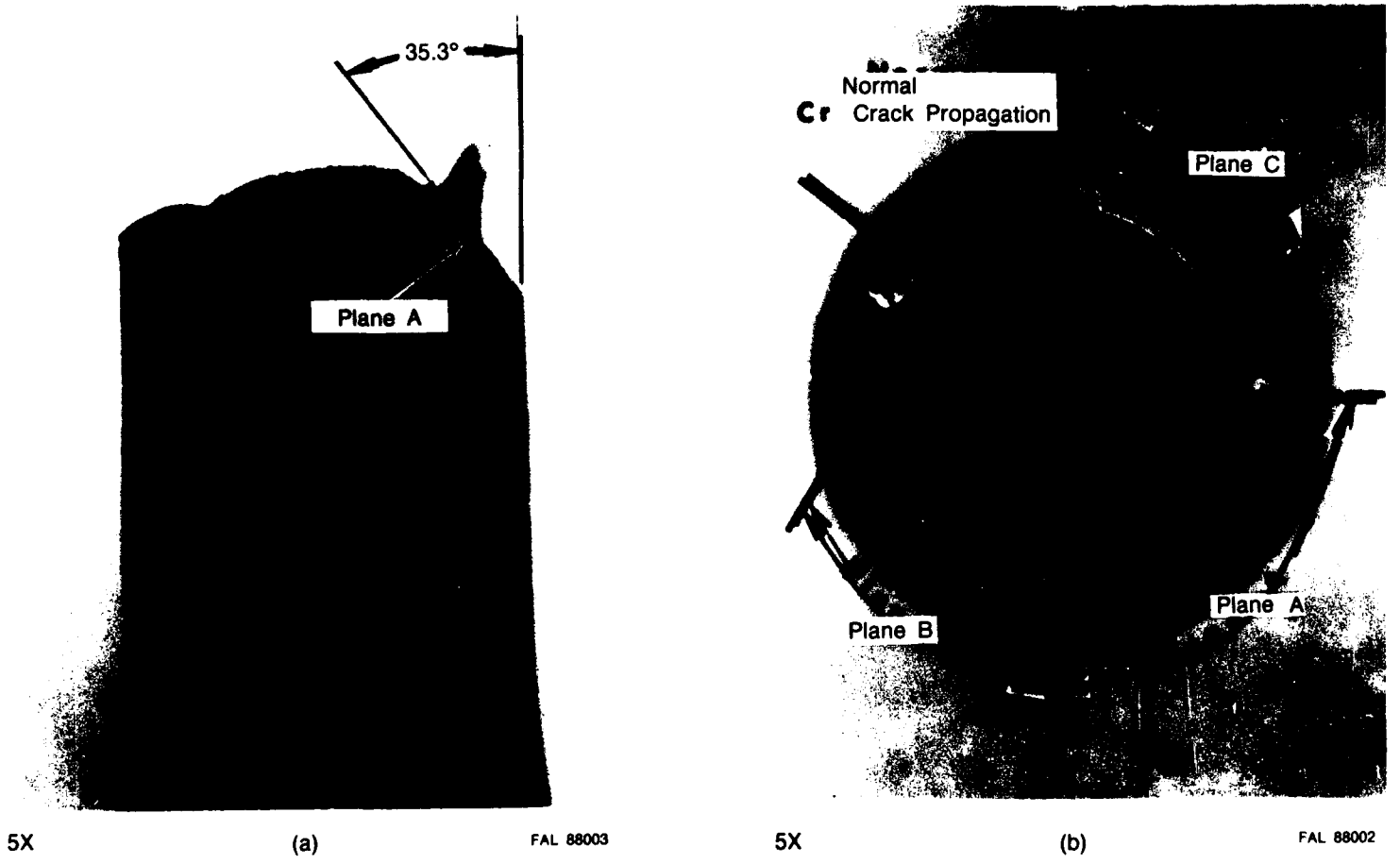

Figure 110. (111) Octahedral Overstress Planes Observed in PWA 1480 Out-of-Phase TMF Test (427-1038°C/800-1900°F)

10X FAL 88004

FD 317582

Figure 111. (111) Octahedral Overstress — Plane A

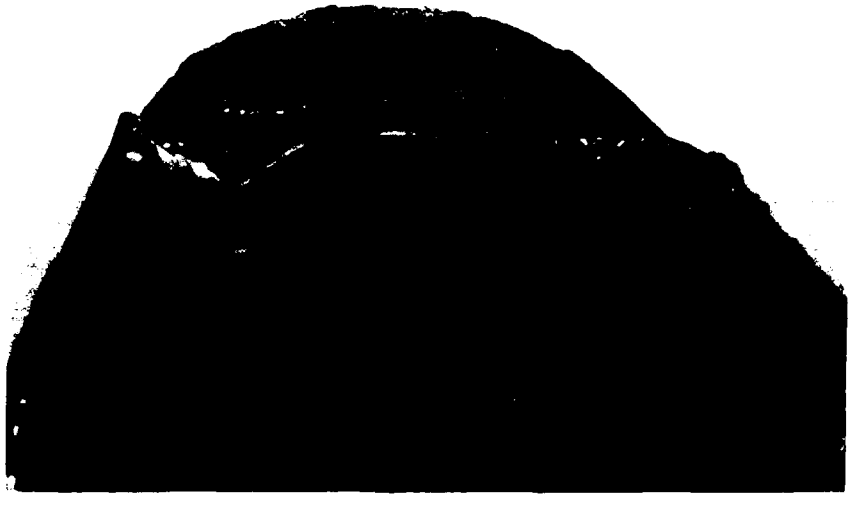

10X FAL 88005

FD 317583

Figure 112. (111) Octahedral Overstress — Plane B

Mag: 7X

FD 357701

Figure 113. Typical Fracture Surface Side View for Type 1 Cycle, Uncoated PWA 1480 ($\Delta\varepsilon$ = 0.5%, 1 cpm, 427-1038°C (800-1900°F), S/N 2)

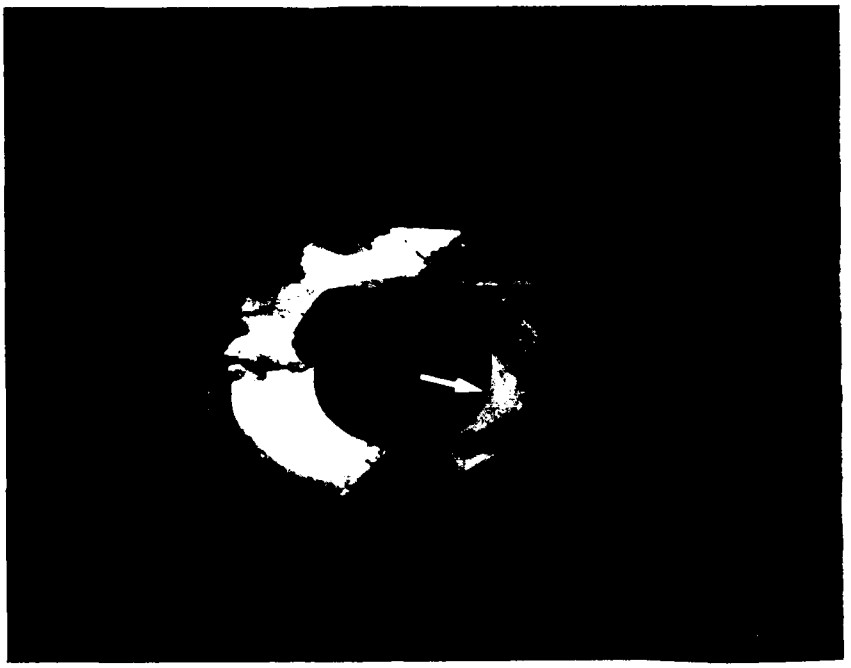

Mag: 6X

FD 357702

Figure 114. Typical Fracture Surface for Type 1 Cycle, Uncoated PWA 1480 ($\Delta\varepsilon$ = 0.5%, 1 cpm, 427-1038°C (800-1900°F), S/N 2), White Arrow Indicates Origin

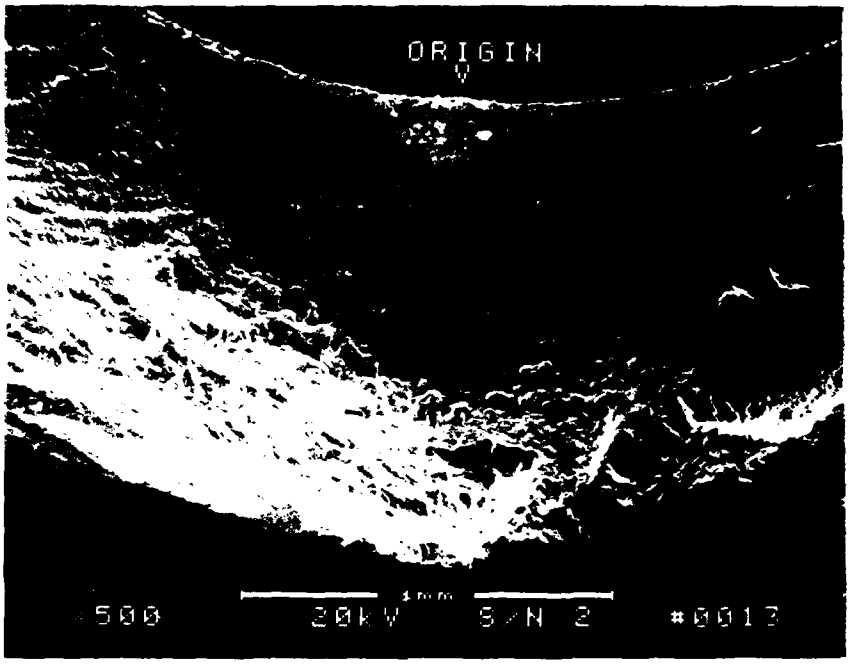

FD 357703

Figure 115. SEM of Fracture Origin Showing Thumbnail for Type 1 Cycle, Uncoated PWA 1480 ($\Delta\varepsilon$ = 0.5%, 1 cpm, 427-1038°C (800-1900°F), S/N 2)

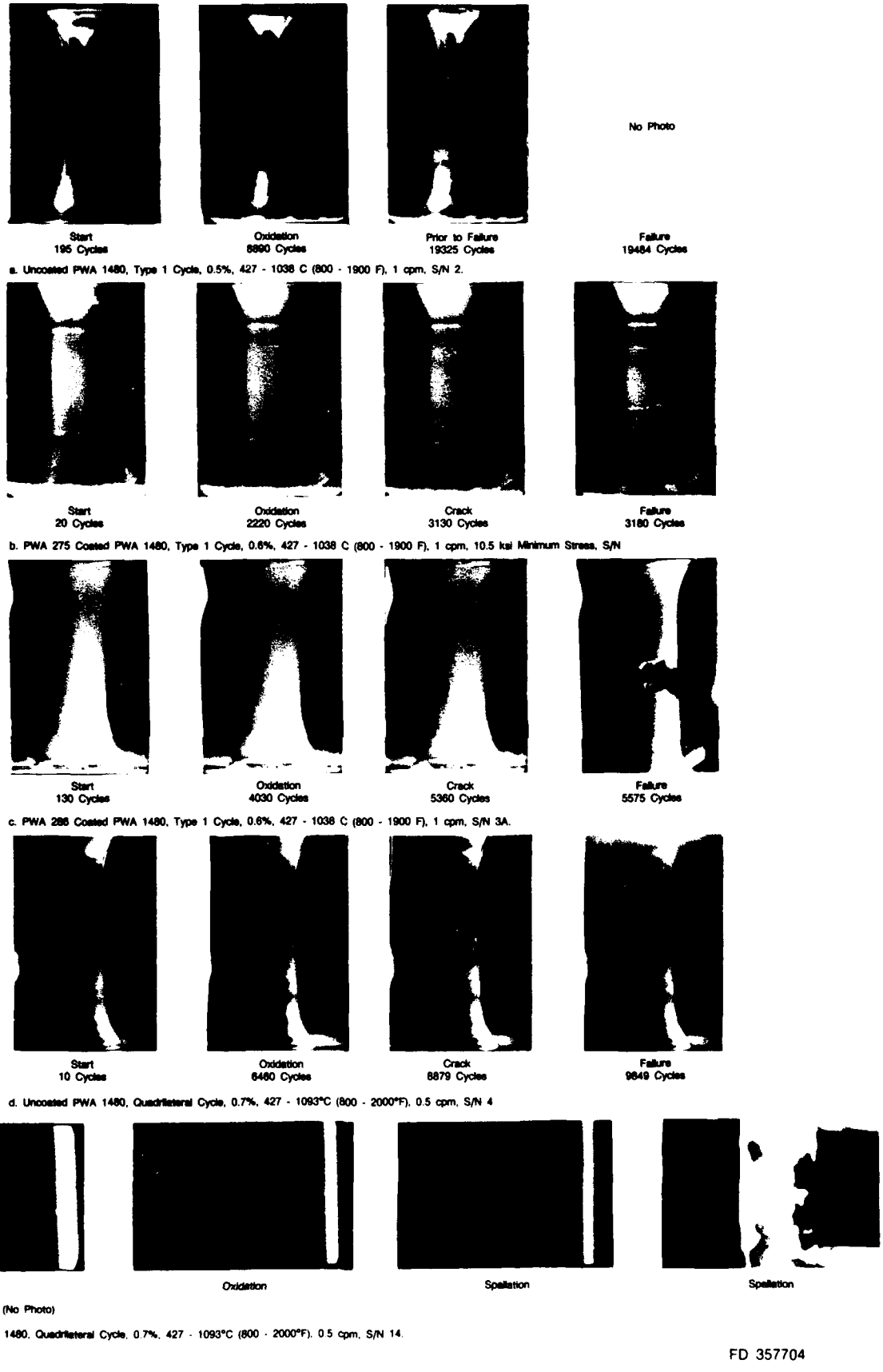

Figure 116. In-test Surface Conditions for Type 1 and Quadrilateral TMF Cycles

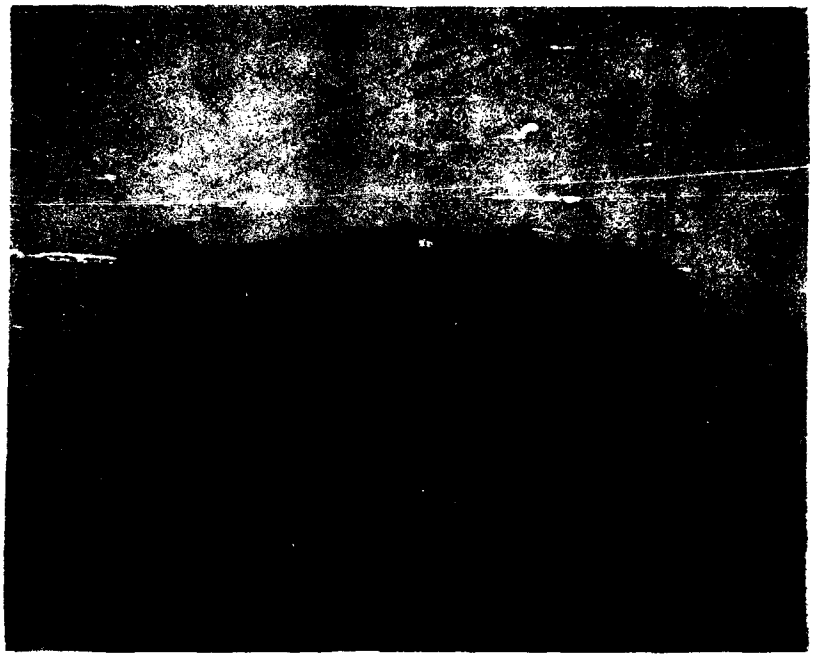

Mag: 7X

FD 357705

Figure 117. Typical Fracture Surface Side View for Quadrilateral Cycle PWA 286 Coated PWA 1480, ($\Delta\varepsilon$ = 0.7%, 1 cpm, 427-1093°C (800-2000°F), S/N 31)

Mag: 6X

FD 357706

Figure 118. Typical Fracture Surface for Quadrilateral Cycle PWA 286 Coated PWA 1480, ($\Delta\varepsilon$ = 0.7%, 1 cpm, 427-1093°C (800-2000°F), S/N 31)

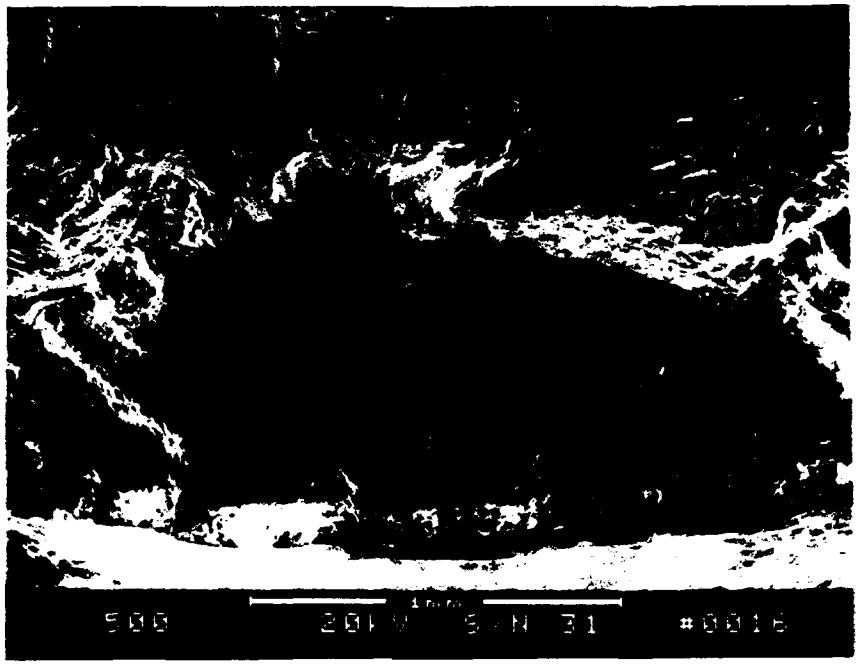

FD 357707

Figure 119. Typical Fracture Surface Showing Thumbnail Initiation for Quadrilateral Cycle, PWA 286 Coated PWA 1480 ($\Delta\varepsilon$ = 0.7%, 0.5 cpm, 427-1093°C (800-1900°F), S/N 31)

FD 357708

Figure 120. Typical Scale/Metal Interface for Uncoated PWA 1480, (Quadrilateral Cycle, $\Delta\varepsilon$ = 0.7%, ΔT = 427-1093°C (800-2000°F), 0.5 cpm)

Figure 121. Secondary Crack Along Octahedral Plane for Uncoated PWA 1480, (Quadrilateral Cycle, $\Delta\varepsilon$ = 1.05%, ΔT = 427-1093°C (800-2000°F), 0.5 cpm)

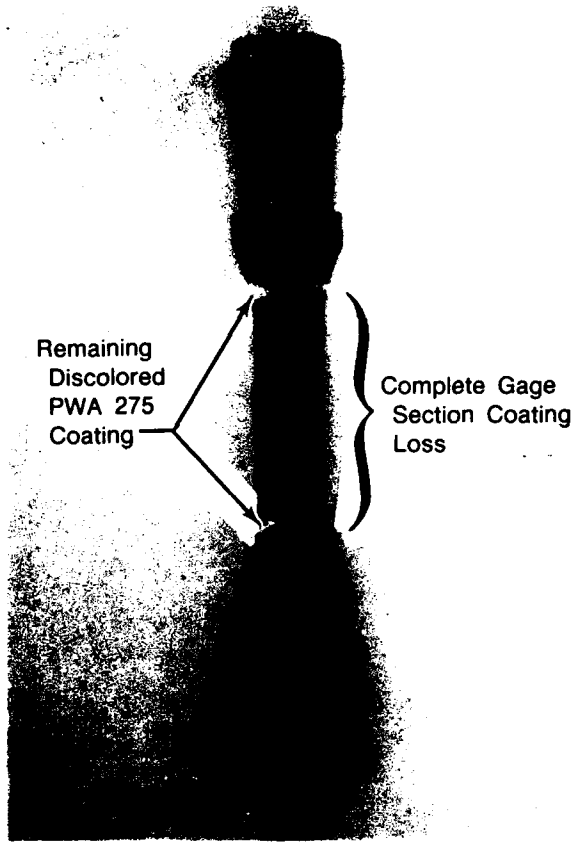

FD 324970

Figure 122. Complete Aluminide Coating (PWA 275) Loss Experienced on Quadrilateral Cycle (PWA 1480, $\Delta\varepsilon$ = 0.7%, 0.5 cpm, 427-1093°C (800-2000°F))

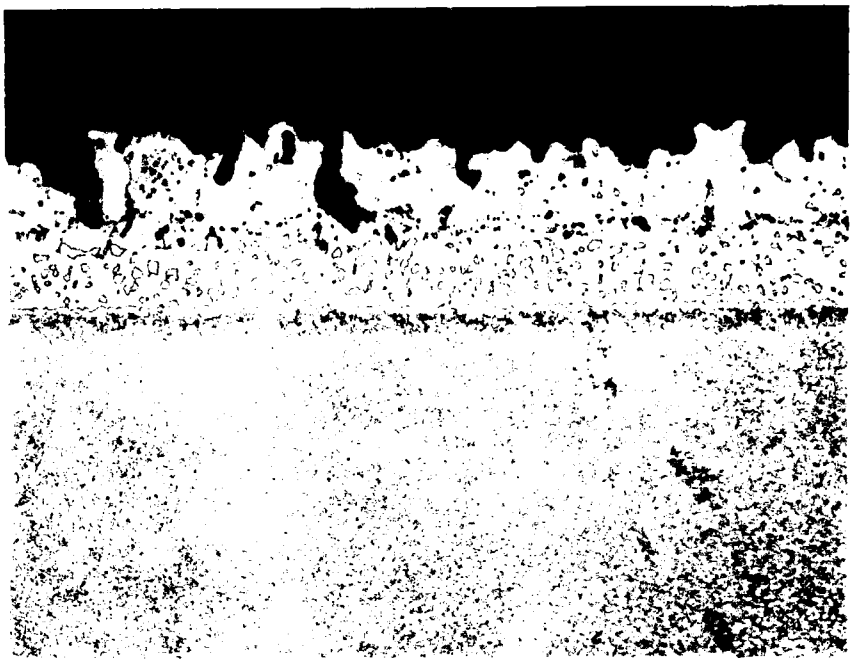

Mag: 500X

FD 357710

Figure 123. Initiation of Coating Degradation in PWA 275 Coated PWA 1480 (Quadrilateral Cycle, $\Delta\varepsilon$ = 0.7%, ΔT = 427-1093°C (800-2000°F),0.5 cpm, S/N 11)

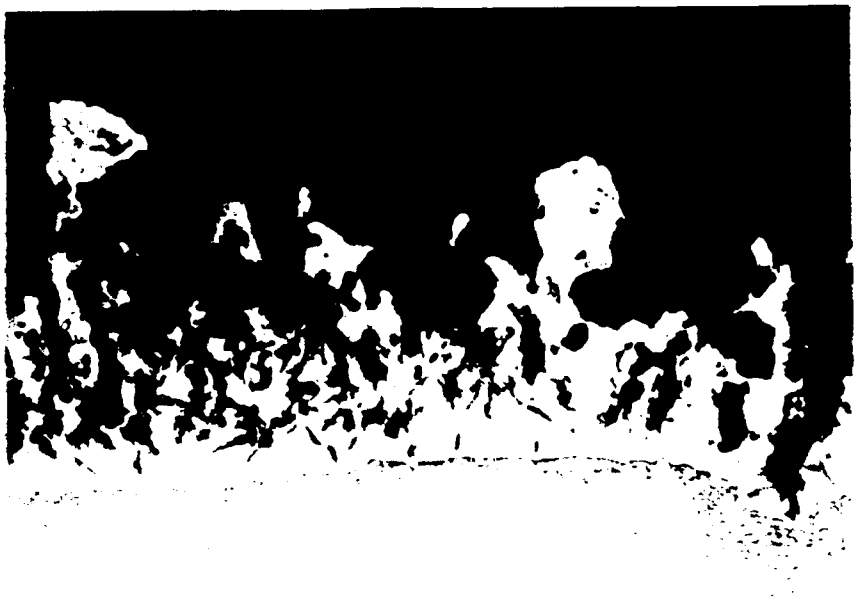

Mag: 500X

FD 357711

Figure 124. Severe Bulk Substrate Damage Following Coating Spallation in PWA 275 Coated PWA 1480 (Quadrilateral Cycle, $\Delta\varepsilon$ = 0.7%, ΔT = 427-1093°C (800-2000°F),0.5 cpm, S/N 11)

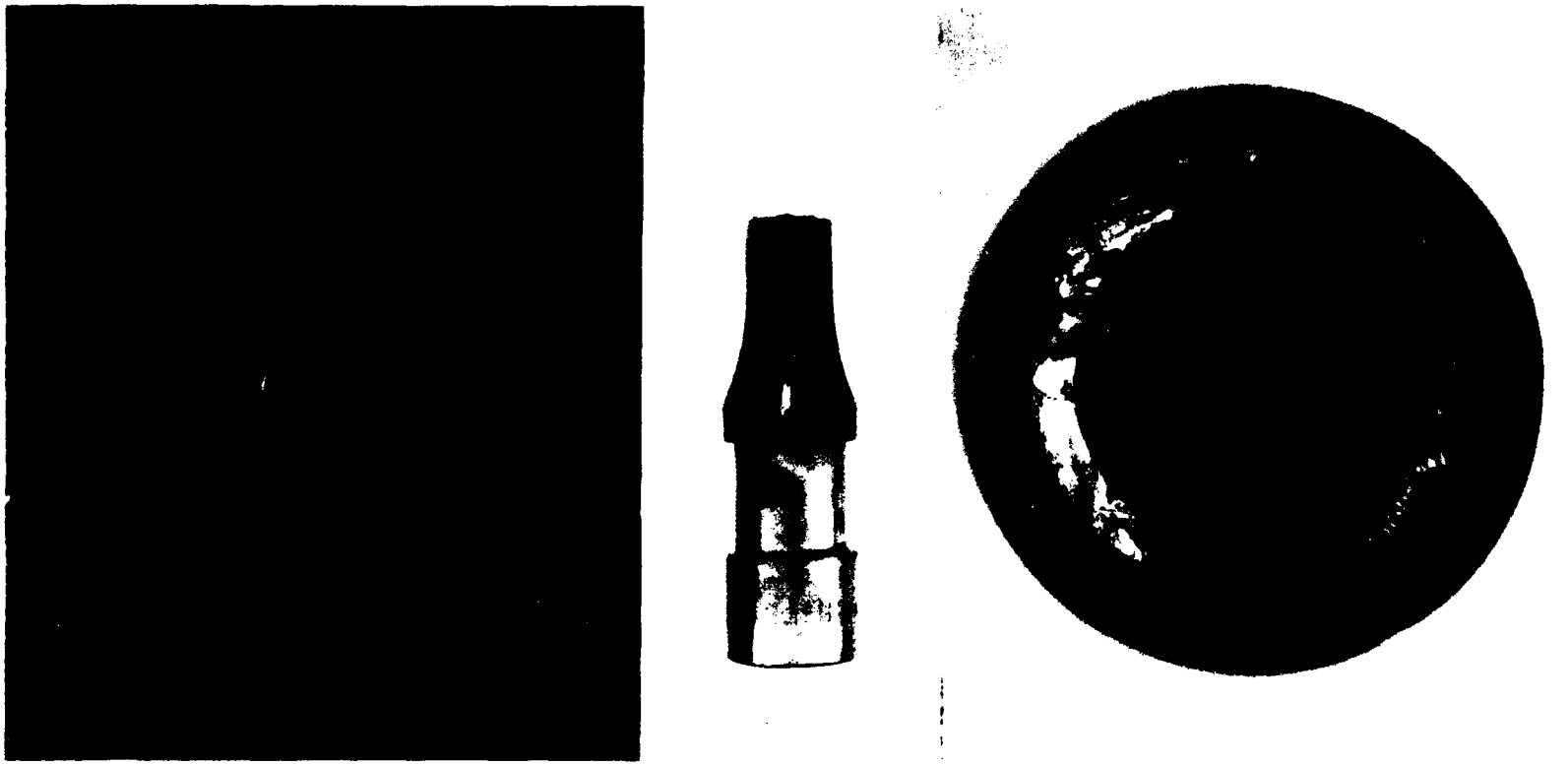

a) Surface Condition Showing an Extreme Rumpled Appearance With Short Cracks Initiating From the Valleys.
b) Specimen Overview Showing Jagged Appearance of Fracture Face Indicating Multiple Coating Crack Link Up. (Arrow).
c) Specimen Fracture Face Showing Numerous Fatigue Origins With Jagged Origin Link Up.

FD 324971

Figure 125. Fracture Morphology of Overlay Coated (PWA 286) PWA 1480, Quadrilateral Cycle, (S/N 31, $\Delta\varepsilon$ = 0.7%, 0.5 cpm, 427-1093°C (800-2000°F))

FC 99819

- Black Arrows —Showing Coating Cracks Propagating Into the Substrate
- White Arrows —Showing "Valleys" Produced by Oxides
- Dotted Area —Showing Black Oxide Holes Whose Shape Precisely Matches That of the Adjacent Islands of Beta-NiAl.

FD 324972

Figure 126. Preferential Oxidation of the Beta-NiAl Phase in the PWA 286 Overlay Coating Which Contributes to Crack Propagation Into the Substrate Quadrilateral Cycle, (S/N 31, $\Delta\varepsilon$ = 0.7%, 0.5 cpm, 427-1093°C (800-2000°F))

2.5 MODEL DEVELOPMENT

Development of the life prediction model focused on the two-bar model for determining coating/substrate stress/temperature behavior, the hysteretic energy model for determining cyclic mechanical damage and the Arrhenius relationship for determination of cyclic environmental damage. The development of the Arrhenius relationship was discontinued after no significant effect on life was observed in the inert environment.

A FORTRAN code has been developed with organization based on subroutines, so that the overall package is modular and, therefore, straightforward to append or edit. The main program enters conditions for a given cycle type, as shown in the table headings in Figure 127. Cycle description input is based on cycle strain/temperature endpoints, as shown in the examples in Figure 128. In the case of the quadrilateral cycle, strain/temperature endpoints are entered A through D in the order that the endpoints occur sequentially with time. The out-of-phase cycle has only two endpoints and are entered in strain/temperature endpoint columns A and B endpoint columns C and D remain empty. Additional columns in the input file (Figure 127) include hold time, hold temperature, hold strain, minimum stress offset, and cycle ramp rate (frequency). Stress range and mean stress columns are included for additional modeling accuracy, if the data are available.

Prior to cyclic damage calculations the input data are processed to accurately define the particular cycle type. An incremented description of the cycle, based on the strain/temperature endpoints, is calculated which is then used to determine hysteretic damage. Since the cycle definition is based on bulk mechanical strain and temperature endpoints, the cycle definition output is identical for uncoated and coated systems for any given cycle type. The life degradation exhibited in coated systems is assessed in the two-bar model. A flowchart showing the general programming structure is presented in Figure 129. The flowchart indicates how the cycle definition programming will be used to determine hysteretic damage as well as two-bar model calculations.

The model was developed to calculate the mechanical damage of the substrate and coating separately and combine them to produce an optimum prediction damage parameter. The uncoated system uses one of the three interrelated methods to calculate a substrate mechanical damage parameter. The three methods are the "Incremented Inelastic Strain" technique, the "Plastic Strain Balancing" technique, and the "Simplified Constitutive" technique. The coated system uses the "Two-Bar" model to determine the coating mechanical damage parameter. These techniques will be discussed in detail later in this section. An optimum combined damage parameter, using both the substrate and coating damage parameters, correlates the data and provides the life prediction model.

To include the effect of orientation of the single crystal, results from previous research under contract F33615-82-C-5109 (Reference 4) was very useful. We found that the octahedral normal stress normalized by the elastic modulus correlates low cycle fatigue data of differing crystallographic orientations (Figure 130). We proposed that a similar factor be used to correlate TMF data of differing crystallographic orientations. TMF data of [111] orientation with various coatings similar to those used in the current program was obtained from the NASA HOST program (contract NAS3-23939).

2.5.1 Modeling Approach

The thermal cycle component of TMF complicates the problem of determining stress-strain behavior and subsequently predicting lives, especially for coated systems. The development of a life prediction model therefore involves some special considerations. The addition of temperature as a variable can make models involving a large number of numerically or otherwise determined constants very difficult to apply in situations with varying temperature. Also, the high cost of

fatigue testing, especially TMF testing, precludes use of models requiring extensive data bases or purely empirical approaches. Finally, approaches which require difficult, expensive, or impractical analytical computation of life-related parameters are further complicated when varying temperature must be considered.

Two general attributes were considered highly desirable in guiding selection of a life model for development:

1. Simple physical basis: which captures effects of fundamental life-controlling variables such as strain range and mean stress.

2. Simple to apply: able to relate life to parameters typically calculated for turbine airfoils such as strain range or strain endpoints, and mean or peak stress.

In addition, it was considered desirable to avoid integral dependence of the life prediction model upon complex constitutive models. It was intended that the life model be capable of application using parameters estimated from simple constitutive models, albeit with potentially lower accuracy. Some of these parameters included total strain, stress range, and mean stress.

Finally, we expected significant contribution of environmental effects and considered it desirable to begin with an approach which would separately address deformation and environmental damage.

The model selected for development was the tensile hysteretic energy model, as proposed by Ostergren (Reference 5), with modifications to simplify estimation of the very small inelastic strain ranges typical of turbine airfoils (Reference 1). This approach was consistent with the desired attributes previously described. Results are described in the following sections. Specific details of Ostergren's model are described in Section 2.5.3.

2.5.2 Two-Bar Model

To separate stresses into the loads carried by the coating and the substrate for damage calculations, a two-bar model was developed. A FORTRAN code has been written that will determine approximate coating stress-strain behavior for a given TMF cycle type. The TMF life debit exhibited in coated systems is associated with coating cracks (coating failure) propagating into the substrate, thereby, producing ultimate failure.

Coating fatigue and failure in a thermal mechanical cycle is a result of both thermal and mechanical strains. Strains are produced in the coating through the thermal expansion mismatch between coating and substrate (Figure 131). In addition, coating strains are applied mechanically to the coating/substrate system as required by the particular cycle type (Figure 132). The coating and diffusion layer represent less than 15 percent of the total gage cross-sectional area. Therefore, due to the minimal load carrying area and the generally reduced mechanical properties of the coating (compared to the substrate), strains induced in the coating approximately follow the strain of the substrate. Strain versus temperature profiles can then be calculated for the substrate alone and applied to the known mechanical properties of the coating to determine relative coating degradation.

The program determines coating behavior in a given TMF cycle using known coating and substrate mechanical properties. This programming effort uses existing TMF cycle definition software which defines the particular TMF cycle at 56°C (100°F) increments. With the cycle well-defined at 56°C (100°F) increments for substrate mechanical strain, the effective incremental coating strain can be calculated by the addition of thermal mismatch strain by the equation:

$$\varepsilon_{(coating)} = \varepsilon_{(substrate)} + \varepsilon_{(thermal\ mismatch)}$$

for each 56°C (100°F) increment. However, since the substrate and coating strain are equal by definition, the coating mismatch strain converts to stress through its modulus. The stresses in the coating throughout the cycle can be calculated using monotonic coating properties by:

$$\sigma_c = \varepsilon_c E_c$$

at each 56°C (100°F) increment, where the subscript "c" refers to coating properties. Coating behavior is assumed to be perfectly elastic/perfectly plastic in nature. Therefore, if the calculated stress exceeds the yield strength of the coating (at a particular temperature), the resulting stress is limited to that yield stress. This shedding of load by the coating is common at the higher temperature extremes of typical TMF cycles. The perfectly inelastic strain behavior is a valid assumption, since the coatings are extremely ductile at these temperatures (temperatures greater than the ductile-to-brittle transition). The aluminide coating ductile-to-brittle transition occurs at 649°C (1200°F), as shown in Figure 133 with virtually unlimited strain to crack properties above this temperature. The overlay coating does not exhibit this extreme change in ductility. However, strain-to-crack values are above the strains typically experienced by the coating on PWA 1480 material.

The actual FORTRAN programming for the Two Bar Model determines the hysteretic energy of the coating. Starting at the mean temperature of the cycle, and increasing the temperature by 56°C (100°F) increments, the strain for the coating is the sum of the mechanical substrate strain and the thermal mismatch strain. The thermal mismatch is determined using the mean thermal expansion coefficients for the coating and the substrate at the midpoint temperature of the increment. (The instantaneous thermal expansion coefficients were used during some of the iterations but caused the coating hysteresis loops to behave erratically. Therefore, the mean thermal expansion coefficients were used.) The coating stress is determined from the coating strain using elastic-perfectly plastic assumptions. Hold time and frequency effects are not included in this extremely simplified constitutive analysis of the coating. The tensile and compressive areas of the coating hysteresis loop are calculated using the Trapezoidal Rule.

Examples of the aluminide coating (PWA 275) mechanical behavior in a standard out-of-phase and a quadrilateral TMF cycle are shown in Figures 134 and 135, respectively. Similarly, examples of the overlay coating (PWA 286) mechanical behavior in a standard out-of-phase and a quadrilateral TMF cycle are shown in Figures 136 and 137, respectively. The symbols represent the 56°C (100°F) increments where coating stresses were calculated. The strains shown are total mechanical strains applied to the substrate/coating system. The thermal mismatch strains are used only to determine coating stress values. Stress relaxation due to yielding can be seen in the compressive portion of the cycles, where high temperature exposure of the coating creates loss of load carrying capability. The coating stress-strain hysteresis loop stabilizes quickly due to this extreme inelastic behavior. The quadrilateral cycle exhibits much larger inelastic behavior in the coating than the standard out-of-phase cycle. In the test, the quadrilateral cycle was particularly degrading to the aluminide coating (PWA 275) with the coating completely spalling from the substrate (Figure 122). In contrast, the standard out-of-phase cycle produced no adverse coating behavior. The excessive amount of inelastic coating deformation occurring in the quadrilateral cycle explains the extreme coating degradation seen in testing.

Similarly, the quadrilateral cycle caused severe rumpling and cracking of the overlay (PWA 286) coating (Figure 125). The computer generated hysteresis loop for the quadrilateral cycle for this coating has a loop in the tensile portion of the curve. This is due to the elastic modulus of PWA 286. As the high temperature modulus approaches 704°C (1300°F) the slope of the modulus versus temperature curve (Figure 24) does not change drastically as it does for PWA 275. If the curves were folded back on themselves at 704°C (1300°F), the PWA 275 curve would diverge and the PWA 286 curve would form a loop. The loop in the PWA 286 generated

stress-strain curve forms a negative hysteresis loop, thus reducing the damage seen by the coating, as was seen in actual tests. The compressive portion of the hysteresis loop for PWA 286 was also smaller compared to the PWA 275 quadrilateral cycle. In actual testing, the PWA 286 coated PWA 1480 did not spall off but demonstrated severe rumpling. This suggests that the overlay coated material was not subjected to as severe a quadrilateral cycle as did the PWA 275 coated PWA 1480.

The computer generated hysteresis loops for standard out-of-phase cycles of 0.8 percent strain range and various maximum temperatures are shown in Figures 138 and 139 for PWA 275 and PWA 286, respectively. For both of the coatings, as the maximum temperature increased, the size of the hysteresis loop decreased. This is because the coatings drastically lose load carrying capacity at high temperatures (Figure 27). Similar hysteresis loops were generated for the out-of-phase cycle for 427-1038°C (800-1900°F) at various strain ranges for each coating (Figures 140 and 141). As expected, an increase in the strain range resulted in an increase in the size of the hysteresis loop.

2.5.3 Hysteretic Energy

Comparisons of TMF hysteresis loops to those generated under completely reversed isothermal LCF reveals that the TMF cycling results in significant mean stress being developed in the material (Reference 3). Figure 142, 143 and 144 show inelastic strain versus cyclic life for uncoated, aluminide (PWA 275) coated, and overlay (PWA 286) coated PWA 1480, respectively. It is evident that inelastic strain alone cannot characterize TMF behavior.

One measure of cycle damage that contains both of these terms is hysteretic (or plastic strain) energy. The cyclic hysteretic energy (References 5, 6, and 7), ΔW, developed in the fatigue loading of a material may be expressed by the relationship:

$$\Delta W = \int \sigma d\varepsilon,$$

and it is postulated that only the tensile portion contributes to damage in the material (Figure 145). The damage parameter may then be approximated by the equation

$$\Delta W \approx (\sigma_t)(\Delta\varepsilon_i) = \left(\sigma_m + \frac{\Delta\sigma}{2}\right)(\Delta\varepsilon_i),$$

where σ_t is the maximum tensile stress and σ_m is the mean stress. ΔW is then assumed to be related to N_f cycles to crack initiation, by

$$N_f = A\ (\Delta W)^B$$

where A and B are regressed constants, which results in the equation

$$N_f = A\left[\left(\sigma_m + \frac{\Delta\sigma}{2}\right)(\Delta\varepsilon_i)\right]^B$$

Accurate measurement of hysteretic damage is the basis of the model under development. Several methods were developed to more accurately determine hysteretic damage for all TMF cycle types. These methods direct more attention to the strain and temperature extremes; specifically, maximum tensile and compressive strains and the associated temperatures. In addition, closer attention was directed to the order of strain and temperature events, as they occur sequentially with time (strain/temperature history).

2.5.4 Incremented Inelastic Strain Technique

The "Incremented Inelastic Strain" (IIS) technique is a variation on the original life prediction method, where damage was calculated at the mean temperature. This improved method determines the inelastic strain for each leg of the cycle and then totals the inelastic strain for the cycle. This is similar to accumulating the damage of the cycle using the Palmgren/Miner rule (References 8, 9). A diagram illustrating this method is shown in Figure 146. The cycle is divided into its component legs between strain/temperature endpoints. For each 56°C (100°F) temperature increment in a leg, a stress range is determined based on the elastic modulus and the total strain range. The stress range is used to determine an inelastic strain from regressed cyclic stress-strain data. The new elastic strain range is the difference between the total strain range and the inelastic strain. Using the new elastic strain, a stress range is calculated again, and the loop is repeated. By using the Half Interval Search to perform the iterations, convergence for cycles with large strain ranges is guaranteed. The inelastic strain for each temperature increment is averaged for the leg. The inelastic strain for the entire cycle is the sum of the inelastic strains for the legs. It is important to note that a cycle must return to its initial temperature and strain. Therefore, out-of-phase and in-phase cycles have two legs, and quadrilateral and shutdown cycles have four legs.

To determine the hysteretic damage, ΔW, the inelastic strain of the cycle is multiplied by the tensile stress. The tensile stress is determined by either the Simplified Constitutive technique or from observed test data. This incremented technique does not determine the tensile stress.

The results for the coated and uncoated data using this technique for inelastic strain and the observed test data for tensile stress are shown in Figures 147, 148 and 149. Similar results were obtained using the Simplified Constitutive technique to determine the tensile stress and are shown in Figures 150, 151 and 152. The hysteretic energy shown is for the substrate only and does not include any coating damage terms. The data sets were regressed using the following model:

$$\log_{10} (N_f) = A + B \log_{10} (\Delta W)$$

where

N_f = cycles to failure
A, B = regression constants
ΔW = substrate hysteretic energy

The results of the regression are given in Table 13. This technique correlates the uncoated PWA 1480 to within $\pm 2X$ limits. A larger amount of scatter exists for the coated material. In particular, the aluminide coated material shows the data with a maximum temperature of 927°C (1700°F) and quadrilateral cycles separated distinctly from the mean line. Both effects appear to be coating related and should be accounted for by the Two Bar Model.

2.5.5 Plastic Strain Balancing Technique

The second method of determining inelastic strain, termed the "Plastic Strain Balancing" (PSB) technique, balances compressive and tensile inelastic strains to develop a stabilized hysteresis loop for a given cycle type. This computer generated hysteresis loop is then used for calculating hysteretic damage for the cycle type. The steps for this balancing method, are shown in Figure 153.

The FORTRAN programming for the "Plastic Strain Balancing" technique uses three subroutines to determine the hysteretic energy. The first subroutine estimates the limits of the

maximum and minimum stress and approximates the stress at 56°C (100°F) increments around the cycle using elastic behavior. The second subroutine uses the maximum stress limits to calculate the plastic strain and the stress at each temperature increment. The tensile and compressive inelastic strains are summed independently. It is assumed that for a stabilized cycle the total tensile plastic strain equals the total compressive plastic strain. Using the Half Interval Search to perform the interation, the maximum stress is adjusted until the tensile and compressive plastic strains balance.

The hysteretic energy is calculated in the third subroutine. The averaged tensile plastic strain is used for the inelastic strain. The tensile stress used in the calculation is either the observed test stress or the tensile stress calculated from the above iteration. This method is dependent upon the size of the temperature increment because the same tensile stress is used at each temperature regardless of the temperature increment size. Therefore, if a smaller increment size is used, a larger plastic strain results. This means that this method does not actually estimate the cyclic inelastic strain for the TMF cycle, but calculates a parameter that is dependent upon the inelastic strain. The hysteretic energy term determined using this method is, therefore, somewhat arbitrary. However, the term still correlates the data if used consistently.

The results for this method for uncoated and coated PWA 1480 are shown in Figures 154, 155 and 156. The observed test stress was used as the tensile stress in the hysteretic energy calculation. The results for coated and uncoated PWA 1480 using this technique for both the inelastic strain and the tensile stress are shown in Figures 157, 158 and 159. The data sets were regressed using the same model as the Incremented Inelastic Strain method. The results of this regression analysis are given in Table 14. The Plastic Strain Balancing technique, in general, does not correlate the data as well as the Incremented Inelastic Strain technique.

2.5.6 Simplified Constitutive Technique

The "Simplified Constitutive" technique was developed in BASICA and converted to FORTRAN. This simplified constitutive exercise determines the stabilized hysteresis loop using elastic-perfectly plastic assumptions and stress relaxation data. A diagram of this method is shown in Figure 160.

The BASICA program interactively asks for the strain-temperature endpoints of the cycle, hold times, frequency, offset stress and output selection. If selected as output, the movement of the hysteresis loop to the steady state condition can be observed graphically on the screen. In both the BASICA program and the FORTRAN program, the simplified constitutive technique uses the following method to determine the stabilized hysteresis loop. The stress-strain points of the hysteresis loop are determined at temperature increments of 5.6°C (10°F) from the strain calculated between the temperature increments and the modulus interpolated at the mean temperature of the increment. To incorporate the effect of yielding, the yield stress is substituted for the stress when the stress exceeds the yield, according to the elastic-perfectly plastic assumption. To determine the stress relaxation between 871°C (1600°F) and 1093°C (2000°F), the time in seconds is calculated using a sinusoidal temperature-time equation or, if appropriate, a hold time. The stress relaxation is divided into two regions: (1) an exponential regression approximating the primary creep behavior at high initial stresses and (2) a straight line regression corresponding to the secondary creep behavior at lower stresses. If the cycle becomes locked into the same loop due to repeated yielding (which causes the same numbers to be calculated repetitively), then a hysteretic area balance is performed on the loop to allow the stresses to approach the steady state values. The hysteretic area balance calculates and compares the tensile and compressive areas of the hysteresis loop and determines a stress step to add to each stress endpoint in the loop. This is repeated until the stresses stabilize. If the cycle does not require a hysteretic area balance, then the stress relaxation is accelerated artificially to reduce the computing time. This hysterech area balance is based on the same theory as the Plastic Strain Balancing technique.

It was noted that during the hysteretic area balance that the stress calculated at the minimum strain corresponded to the minimum stress measured during the tests. Due to predicted yielding, the minimum stress calculated by the program occurs at a strain other than the minimum strain. This predicted minimum stress was much less than the measured minimum stress. It was proposed that the yielding is minimal when the steady-state hysteresis loop is reached, i.e. the measured minimum load is above the yield stress. Therefore, the compressive hysteretic area is reduced by truncating the compressive stresses to the stress at the minimum strain.

It is obvious that there are other mechanisms involved in predicting the stabilized hysteresis loop for TMF cycles, but these have been compensated for by the use of the acceleration terms for stress relaxation and the hysteretic area balance. These other mechanisms are outside the scope of this study. The corrective techniques used to compensate for these other mechanisms give reasonable results. The predicted tensile stresses versus the actual tensile stresses for uncoated PWA 1480, aluminide (PWA 275) coated PWA 1480, and overlay (PWA 286) coated PWA 1480 are shown in Figures 161, 162 and 163 respectively. The correlation coefficient about a straight line for uncoated PWA 1480, aluminide (PWA 275) coated PWA 1480, and overlay (PWA 286) coated PWA 1480 are 0.95, 0.97 and 0.98, respectively, showing very good correlation for predicting the tensile stress. The predicted tensile stresses versus the actual tensile stresses for (111) crystallographic orientation of PWA 1480 are shown in Figure 164.

The primary purpose of this simplified constitutive method is to accurately predict the tensile stress. The tensile stress will then be used to determine the hysteretic energy using the inelastic strain from the "Incremented Inelastic Strain" method. In addition to the tensile stress, an inelastic strain parameter and a hysteretic damage parameter were determined from the stabilized hysteresis loops. Preliminary analysis of these damage parameters indicated that this method of determining the inelastic strain, and consequently hysteretic damage, is not adequate (Figure 165). The inelastic strain term estimated using this method is apparently subject to cumulative errors resulting from the very small temperature increment calculations.

2.5.7 Octahedral Normal Stress Factor

Single crystal materials have anisotropic behavior and properties. Accordingly, in jet engines turbine blades, principal strains are predominantly in the axial (radial) direction, but some transverse loads can occur. Therefore, the life prediction model requires a method of incorporating the effect of crystal orientation. In previous research (References 4, 10), it was found that a normalized octahedral normal stress factor correlated low cycle fatigue data of differing crystallographic orientations. The octahedral normal stress theoretically characterizes crack propagation and the octahedral shear stress characterizes crack initiation. Although the focus of this investigation has been on crack initiation, it is believed that a significant percentage of the life of the part is spent in crack propagation. In addition, the use of the octahedral shear stress did not correlate data of differing crystallographic orientations as well as the octahedral normal stress.

It is proposed that a similar factor be used to correlate TMF data of differing crystallographic orientations. For the LCF data, the octahedral normal stress is normalized by the dynamic modulus at the test temperature. The dynamic modulus varies with temperature during the TMF cycle. Therefore, the modulus for a single temperature would not be appropriate for the TMF regime. A modulus parameter which includes variation with temperature is the secant modulus.

$$E_{sec} = \frac{\Delta\sigma}{\Delta\varepsilon}$$

where $\Delta\sigma$ = stress range
$\Delta\varepsilon$ = mechanical strain range

The secant modulus includes temperature effects due to the stress range. The stress range characterizes the modulus/temperature behavior over the entire TMF cycle because it is calculated using the modulus at every 56°C (100°F) of the cycle.

Thermal mechanical fatigue data for the [111] orientation was obtained from the NASA HOST program being conducted in East Hartford (Reference 11). The octahedral normal stress factor, as used by the life prediction model, is given in the equation below.

$$\text{Octahedral Normal Stress Factor} = \frac{\Delta\sigma_{[111]}}{E_{sec}}$$

where $\Delta\sigma_{[111]}$ = octahedral normal stress

$$= \begin{cases} 0.333\Delta\sigma, \text{ for } [001] \text{ orientation} \\ 0.970\Delta\sigma, \text{ for } [111] \text{ orientation} \end{cases}$$

2.5.8 Optimum Life Prediction Model

The selection of the optimum life prediction model depends on the inelastic strain and tensile stress calculation for the substrate and the best combination of the coating damage parameter with the substrate damage parameter. The best substrate damage calculation is the Incremented Inelastic Strain (IIS) Method using the tensile stress from the observed test data or the Simplified Constitutive (SC) Method. The IIS method was selected because it best reduced the variability in the model for the TMF data. This constitutes two methods to determine the damage associated with the substrate. The Two-Bar portion of the program provides the damage associated with the coating.

The fatigue life of the quadrilateral cycles does not vary significantly for coated and uncoated material (Figure 166) and falls within ±2X limits of the substrate damage parameter versus life regression. The coated material behaves similarly to the uncoated material. Because of the large strain ranges associated with the quadrilateral cycles, the substrate damage parameter is large compared to out-of-phase cycles. This causes the life to appear longer for the quadrilateral cycle than for out-of-phase cycles at the same damage level. The difference between the quadrilateral cycles and the out-of-phase cycles is the coating behavior. Because of the large compressive stresses associated with the quadrilateral cycles, the coating becomes severely damaged and no longer protects the substrate. It is necessary to simulate this coating degradation in the determination of the coating damage. It was noted that the coating hysteresis loops for the quadrilateral cycle have a very large compressive area. The compressive area of the hysteresis loop is negligible compared to the tensile area for all other cycles except the quadrilateral cycle. This suggests that the compressive hysteretic area is significant to the coating behavior. It was proposed that the coating hysteretic damage be the difference between the tensile and compressive hysteretic areas. This causes the quadrilateral cycles to have a negative coating damage value. To prevent this negative coating damage value from exceeding the substrate damage, resulting in negative total damage, the magnitude of the negative coating damage is limited. The limit is based upon the differences between the coated material's substrate damage and the uncoated material's substrate damage.

The model selected to combine the substrate damage and the coating damage to form an effective hysteretic damage for the coated system is:

$$N_f = A' \left[(\Delta\sigma_{[111]} / E_{SEC}) (dW_{sub} + (A_C / A_S) (S_C) (dW_{COAT}) \right]^B$$

$$= A'(dW_{EFF})^B$$

where

N_f	=	cycles to failure,
A', B	=	regression constants,
$\Delta\sigma_{[111]}$	=	octahedral normal stress,
E_{SEC}	=	secant modulus,
dW_{SUB}	=	substrate hysteretic energy (damage),
A_C, A_S	=	coating and substrate cross sectional areas,
S_C	=	scale factor based on coating,
dW_{COAT}	=	coating hysteretic energy (damage), and
dW_{EFF}	=	effective hysteretic energy

The octahedral normal stress is used to correlate data of different crystallographic orientations. Two orientations are presented in the data, [001] and [111]. The following is used to determine the octahedral normal stress,

$$\Delta\sigma_{[111]} = \begin{cases} 0.333\Delta\sigma, \text{ for } [001] \text{ orientation} \\ 0.970\Delta\sigma, \text{ for } [111] \text{ orientation} \end{cases}$$

The octahedral normal stress is normalized by the elastic modulus for LCF data (performed under contract number F33615-82-C-5109). For TMF data, the elastic modulus must be modified to account for the temperature cycling, by using the secant modulus,

$$E_{SEC} = \Delta\sigma/\Delta\varepsilon$$

where $\Delta\varepsilon$ = mechanical strain range.

To combine the substrate and coating hysteretic energy, the ratio of the coating area to the substrate area is used to initially scale the magnitude of the coating damage relative to the substrate damage. Further investigation revealed that the area ratio would require an additional scale factor. It was noted that the aluminide (PWA 275) coated data had behavior that was weighted more toward the coating behavior. The overlay (PWA 286) coated data appeared to be weighted toward substrate behavior. Therefore, by trial and error, the scale factor was determined,

$$S_C = \begin{cases} 1.5, \text{ for aluminide coating} \\ 0.1, \text{ for overlay coating} \end{cases}$$

The scale factor for the aluminide coating is limited to being less than 1.6 because it can cause negative coating damage values to exceed the substrate damage value.

The effective hysteretic energy versus cycles to failure for coated and uncoated PWA 1480 are shown in Figures 167 through 170, using the observed tensile stress for the substrate damage. Figures 171 through 174 show similar results using the Simplified Constitutive Method for the

tensile stress. For both cases, the data generally fall within the ±2X limits. The predicted life versus actual life using the model with observed tensile stresses is shown in Figures 175 through 178, and with the constitutive stress in Figures 179 through 182. Again, the data generally fall within the ±2X limits. When the data are combined for all coatings and orientations (Figures 183 and 184), the correlation of the data are better than 0.80 (r^2) indicating that the model accounts for much of the scatter associated with different cycle types, maximum temperatures, frequency and hold times, coatings, and orientations. An environmental term is not included because no significant life benefit was seen for the inert environment testing. The results of the regressions of all of the final life prediction model data are presented in Table 15.

TABLE 13. Regression Results for the Incremented Inelastic Strain Technique

Substrate/Coating	*Intercept A MPa (ksi)*	*Slope B*	*Correlation Coefficient*
Observed Test Tensile Stress:			
PWA 1480/Uncoated	4.31371 (3.76492)	−0.65447	0.8317
PWA 1480/PWA 275	3.93635 (3.44249)	−0.58897	0.5824
PWA 1480/PWA 286	4.04370 (3.59066)	−0.54029	0.7906
Simplified Constitutive Stress:			
PWA 1480/Uncoated	4.29688 (3.74998)	−0.65222	0.8328
PWA 1480/PWA 275	3.91631 (3.42871)	−0.58150	0.5678
PWA 1480/PWA 286	4.04106 (3.59002)	−0.53790	0.7814

R20606/1

TABLE 14. Regression Results for the Plastic Strain Balancing Technique

Substrate/Coating	*Intercept A MPa (ksi)*	*Slope B*	*Correlation Coefficient*
Observed Test Tensile Stress:			
PWA 1480/Uncoated	3.78019 (3.52827)	−0.30043	0.6572
PWA 1480/PWA 275	3.31294 (3.03395)	−0.33272	0.6529
PWA 1480/PWA 286	3.56113 (3.35284)	−0.24840	0.6015
Plastic Strain Balancing Stress:			
PWA 1480/Uncoated	3.79007 (3.54305)	−0.29459	0.6335
PWA 1480/PWA 275	3.31610 (3.03969)	−0.32964	0.6329
PWA 1480/PWA 286	3.56877 (3.36253)	−0.24596	0.5810

R20606/1

TABLE 15. Regression Results for the Final Life Prediction Model $Log_{10}(N_f) = A + B\ Log_{10}(DW_{EFF})$

Substrate/Coating	*Intercept A MPa (ksi)*	*Slope B*	*Correlation Coefficient*
Observed Test Tensile Stress:			
PWA 1480 (001)/Uncoated	2.67899 (2.18525)	−0.58882	0.8684
PWA 1480 (001)/PWA 275	2.32018 (1.79898)	−0.62157	0.8010
PWA 1480 (001)/PWA 286	2.72571 (2.32193)	−0.48154	0.7871
PWA 1480 (111)/Uncoated	2.22275 (1.77419)	−0.53494	0.8926
PWA 1480 (111)/PWA 275	2.52783 (2.12655)	−0.47856	Only 3 Points
PWA 1480 (111)/PWA 286	3.84313 (2.51147)	−0.39553	0.8626
PWA 1480 (111)/All Data	2.24070 (1.69347)	−0.65261	0.8960
All Data	2.41011 (1.88603)	−0.62501	0.8154
Simplified Constitutive Tensile Stress:			
PWA 1480 (001)/Uncoated	2.67872 (2.18967)	−0.58323	0.8638
PWA 1480 (001)/PWA 275	2.32280 (1.79612)	−0.62811	0.7522
PWA 1480 (001)/PWA 286	2.73269 (2.33155)	−0.47839	0.7762
PWA 1480 (111)/Uncoated	2.18948 (1.74044)	−0.53551	0.9000
PWA 1480 (111)/PWA 275	2.33140 (1.85267)	−0.57092	Only 3 Points
PWA 1480 (111)/PWA 286	2.83491 (2.50820)	−0.38963	0.8893
PWA 1480 (111)/All Data	2.18690 (1.64324)	−0.64836	0.9062
All Data	2.40306 (1.87758)	−0.62667	0.8052

R20505/1

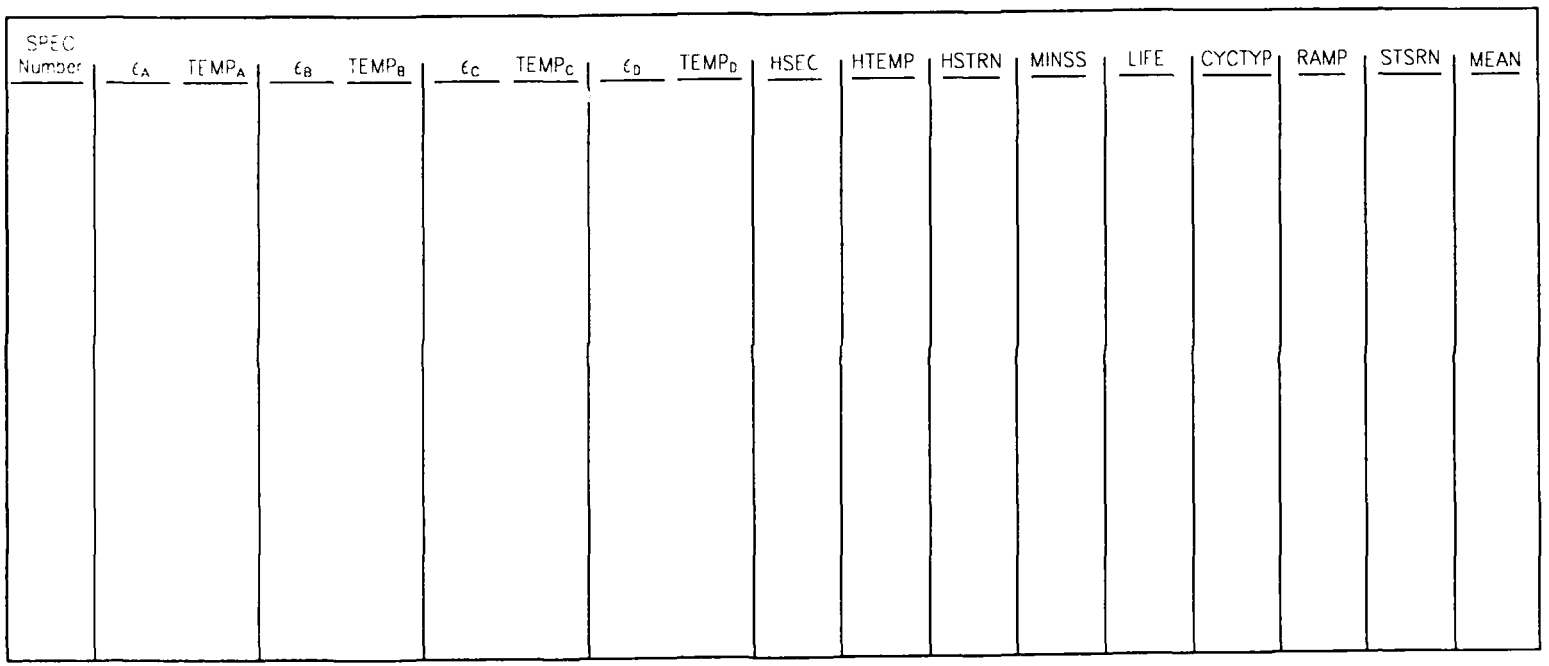

Figure 127. TMF Life Prediction Data Input File

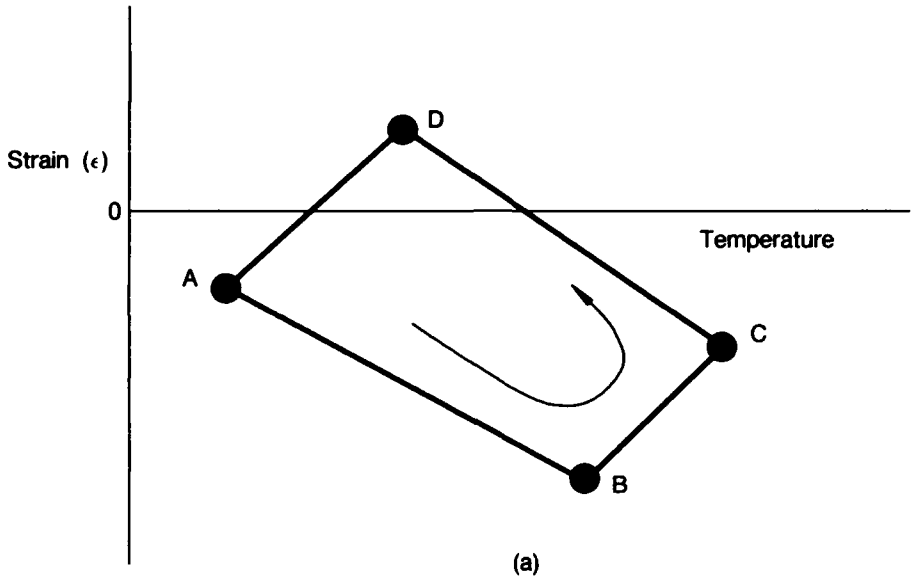

(a)
Quadrilateral Cycle Type

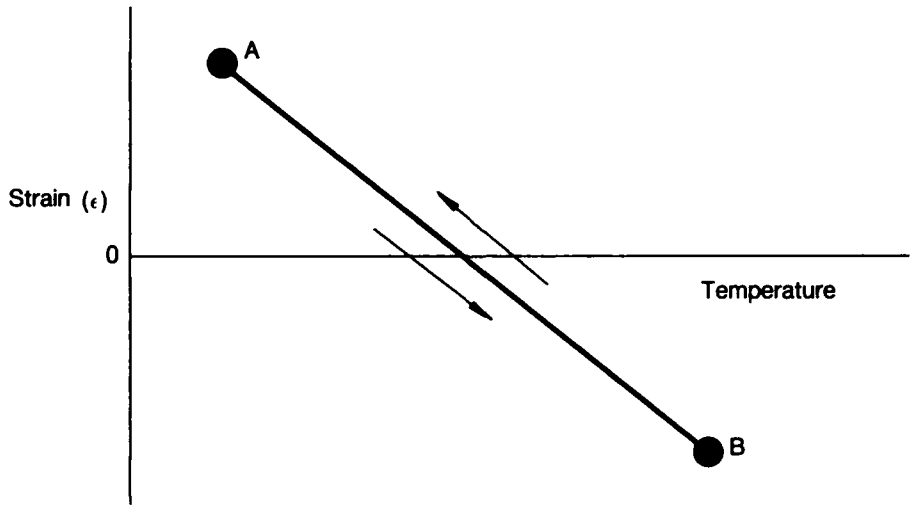

(b)
Out of Phase Cycle Type

FDA 324965

Figure 128. Computer Cycle Type Formats

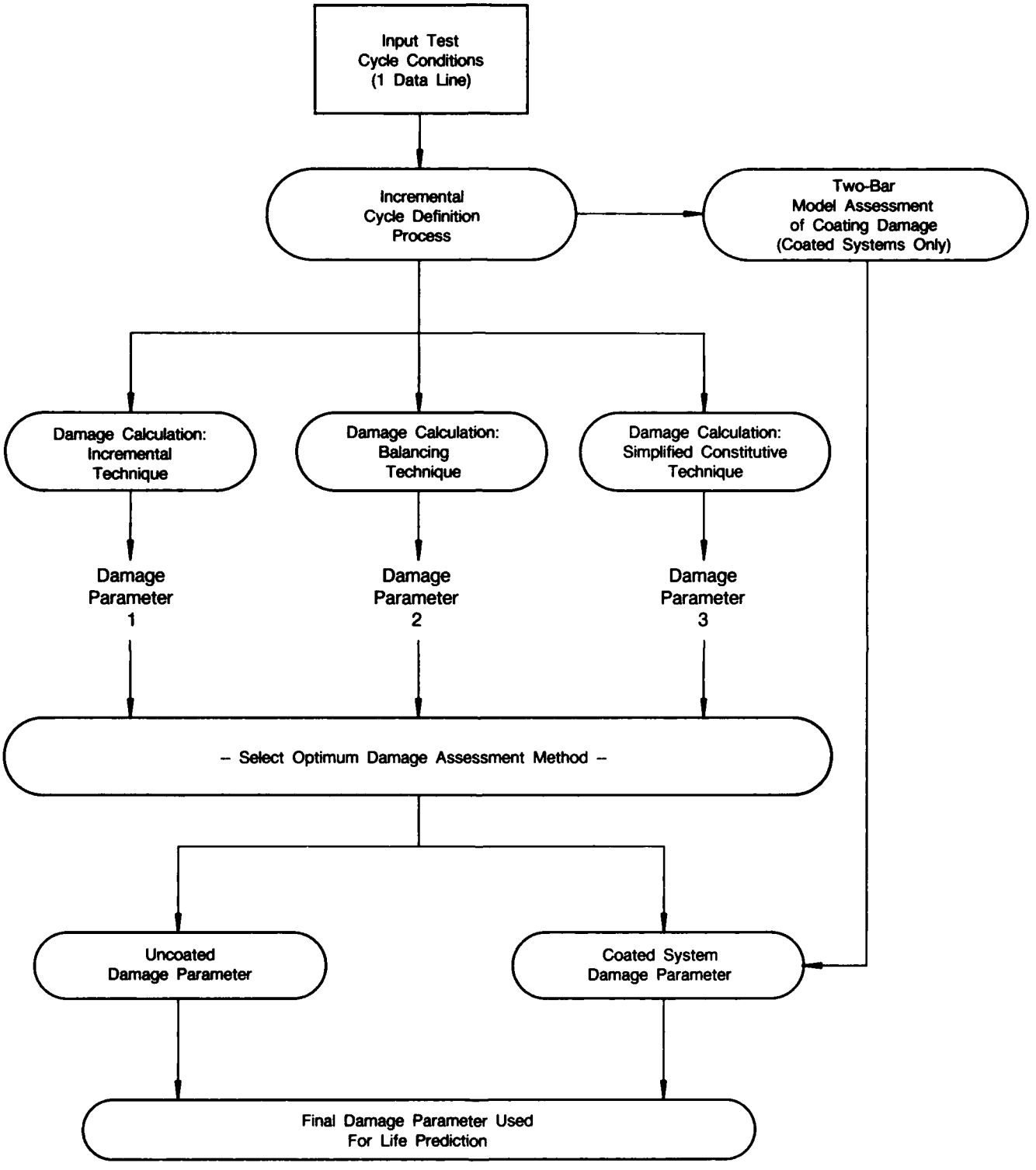

Figure 129. Program Structure

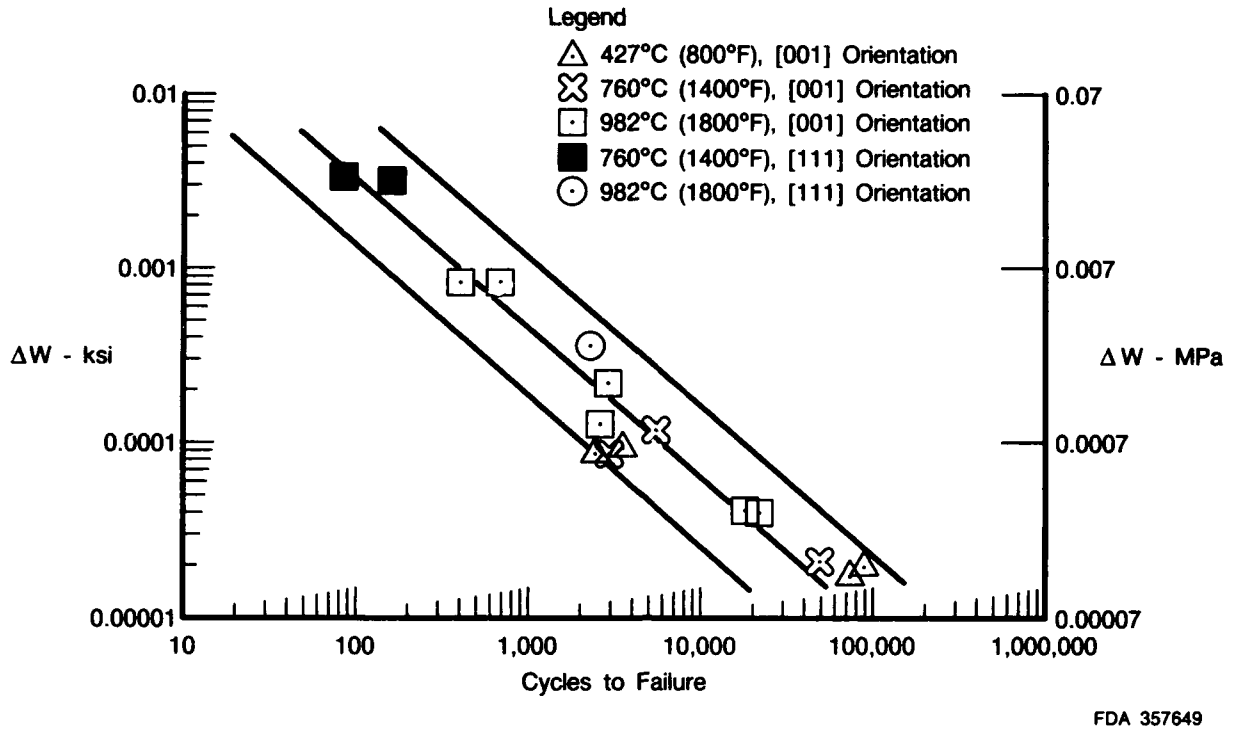

Figure 130. Hysteretic Energy with Octahedral Normal Stress Factor Versus Cycles to Failure for PWA 1480, Strain Control LCF, ΔE = 0.5-1.5%, 427°C (800°F), 760°C (1400°F), and 982°C (1800°F) from F33165-82-C-5109

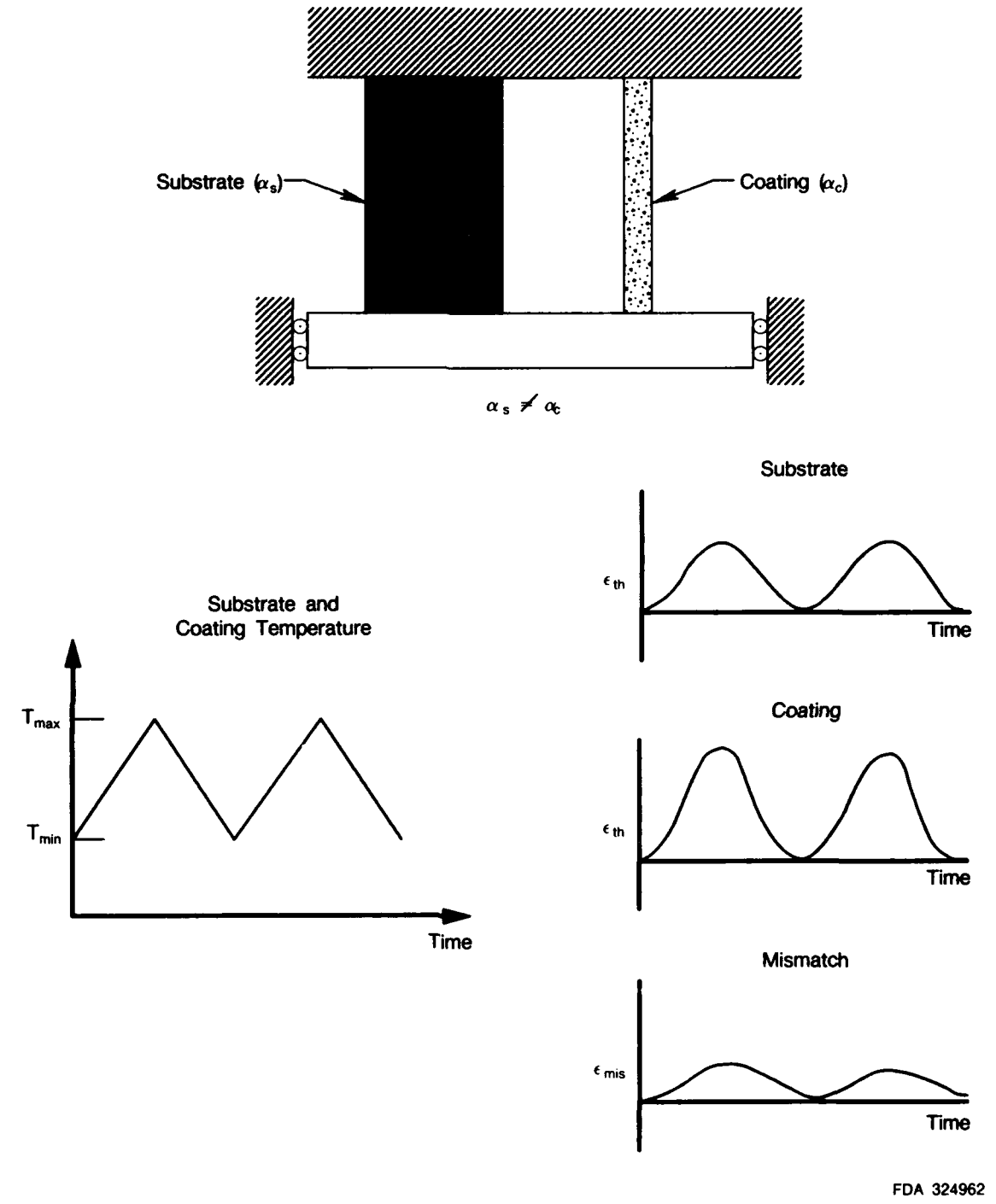

Figure 131. Thermal Strains Produced in the Coating as a Result of Thermal Expansion Mismatch

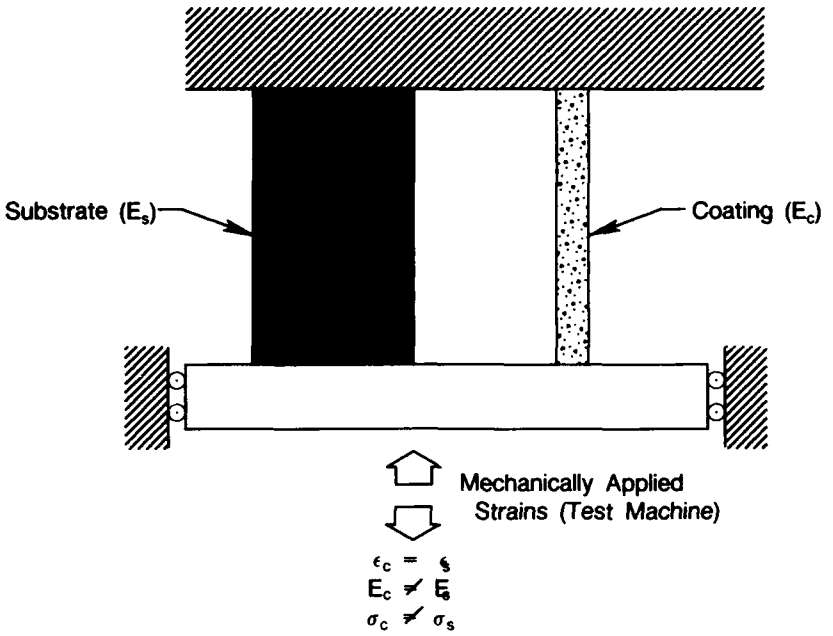

FDA 324963

Figure 132. Mechanically Applied Strain on the Coating/Substrate System

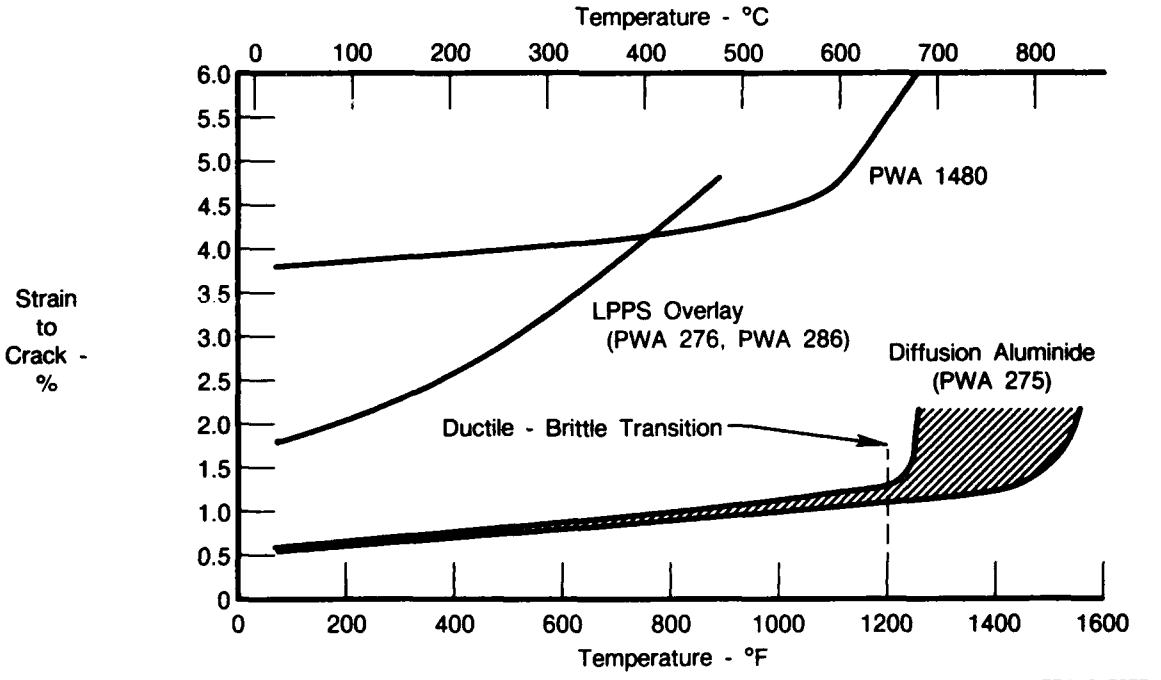

FDA 317577

Figure 133. Ductility Versus Temperature for Aluminide and Overlay Coatings (Data Not Generated Under this Contract)

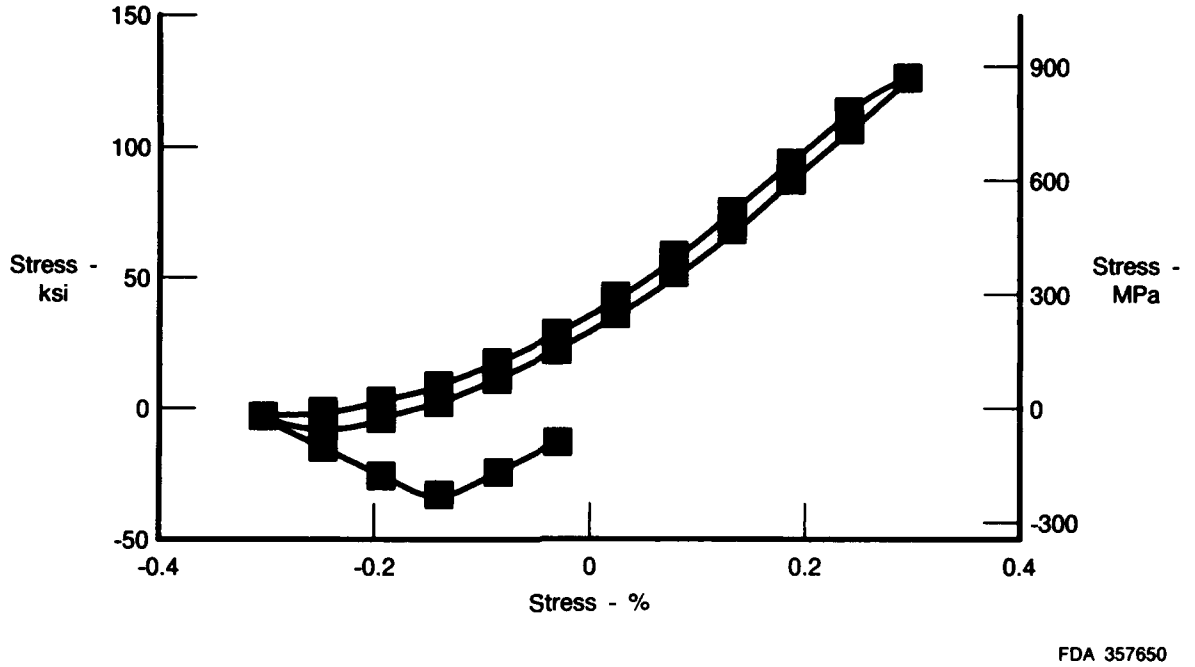

Figure 134. Stress Versus Strain Plot of PWA 275 Coating on PWA 1480 Substrate (Out-of-Phase Cycle, 427-1038°C (800-1900°F), Δε = 0.6%)

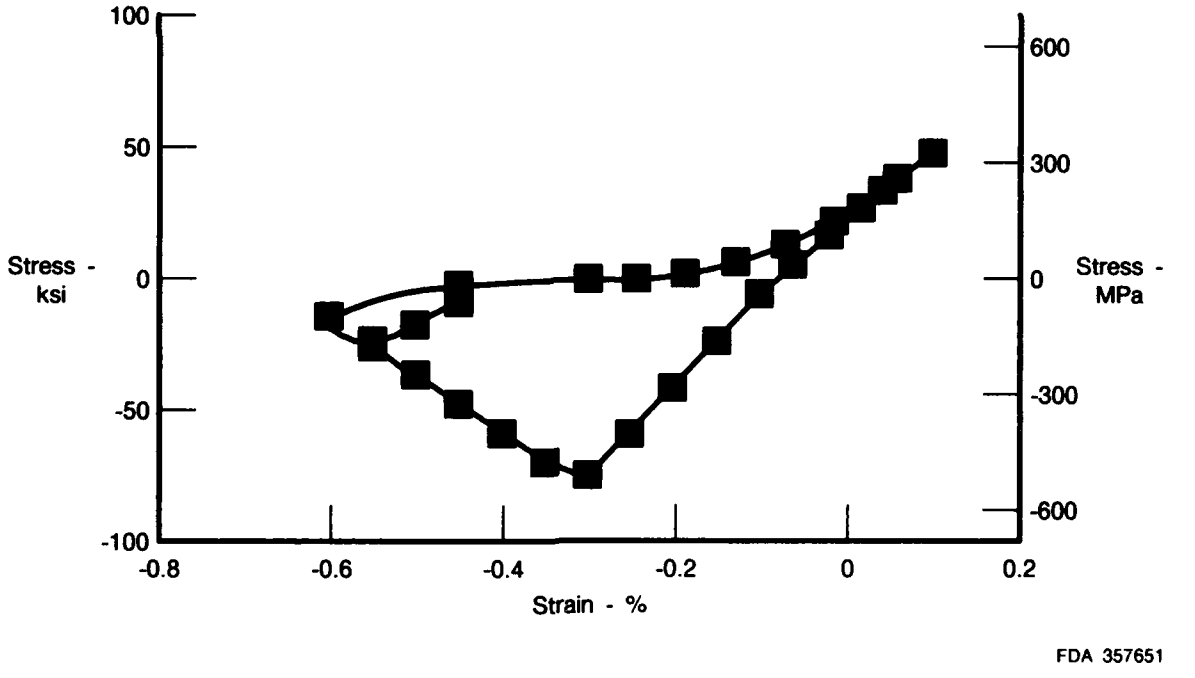

Figure 135. Stress Versus Strain Plot of PWA 275 Coating on PWA 1480 Substrate (Quadrilateral Cycle, 427-1093°C (800-2000°F), Δε = 0.7%)

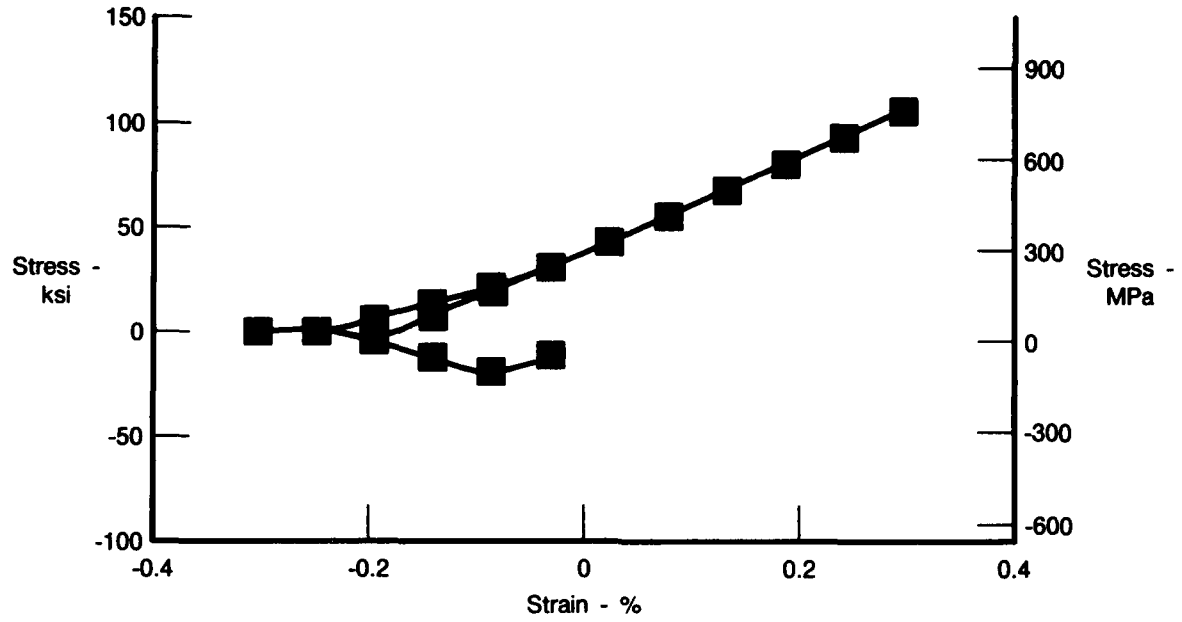

Figure 136. Stress Versus Strain Plot of PWA 286 Coating on PWA 1480 Substrate (Out-of-Phase Cycle, 427-1038°C (800-1900°F), Δε = 0.6%)

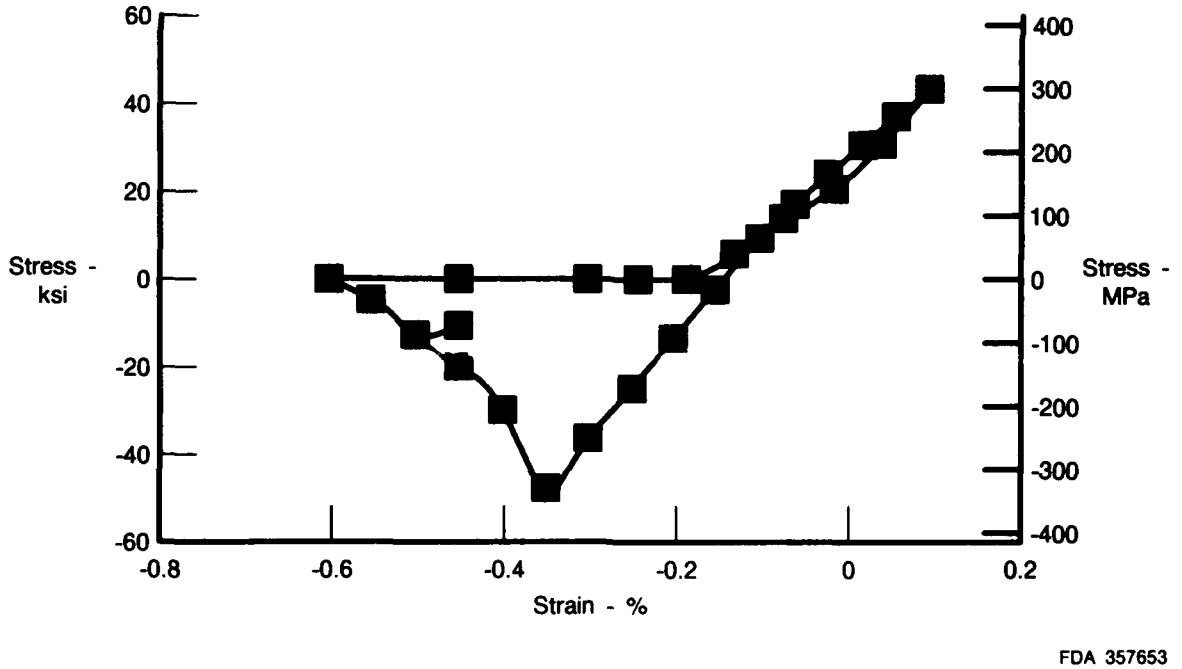

Figure 137. Stress Versus Strain Plot of PWA 286 Coating on PWA 1480 Substrate (Quadrilateral Cycle, 427-1093°C (800-2000°F), Δε = 0.7%)

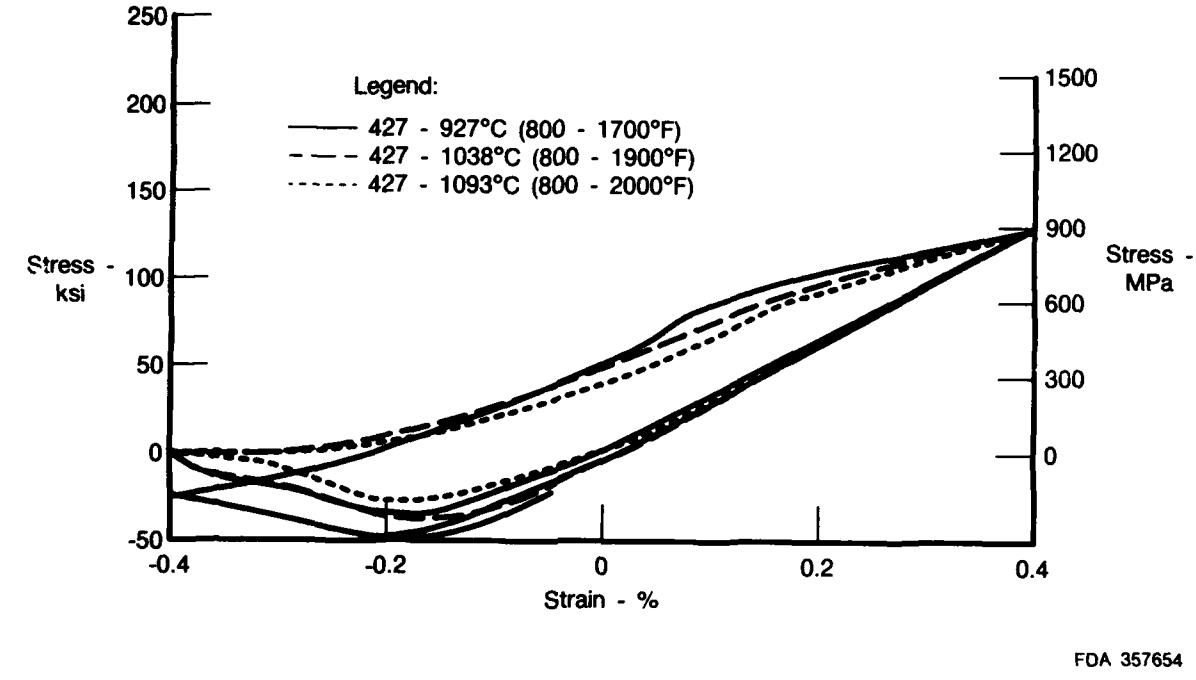

Figure 138. Coating Hysteresis Loops for PWA 275 Coating, Out-of-Phase Cycles, 0.8% Strain Range and Various Temperatures

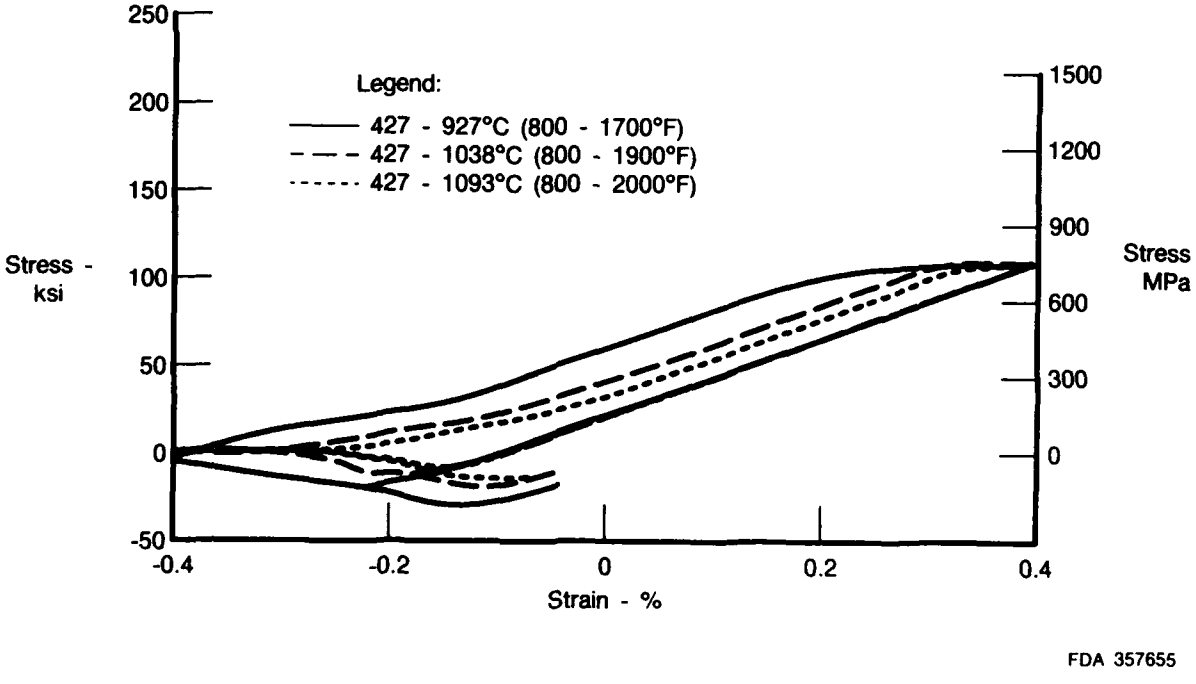

Figure 139. Coating Hysteresis Loops for PWA 286 Coating, Out-of-Phase Cycles, 0.8% Strain Range and Various Temperatures

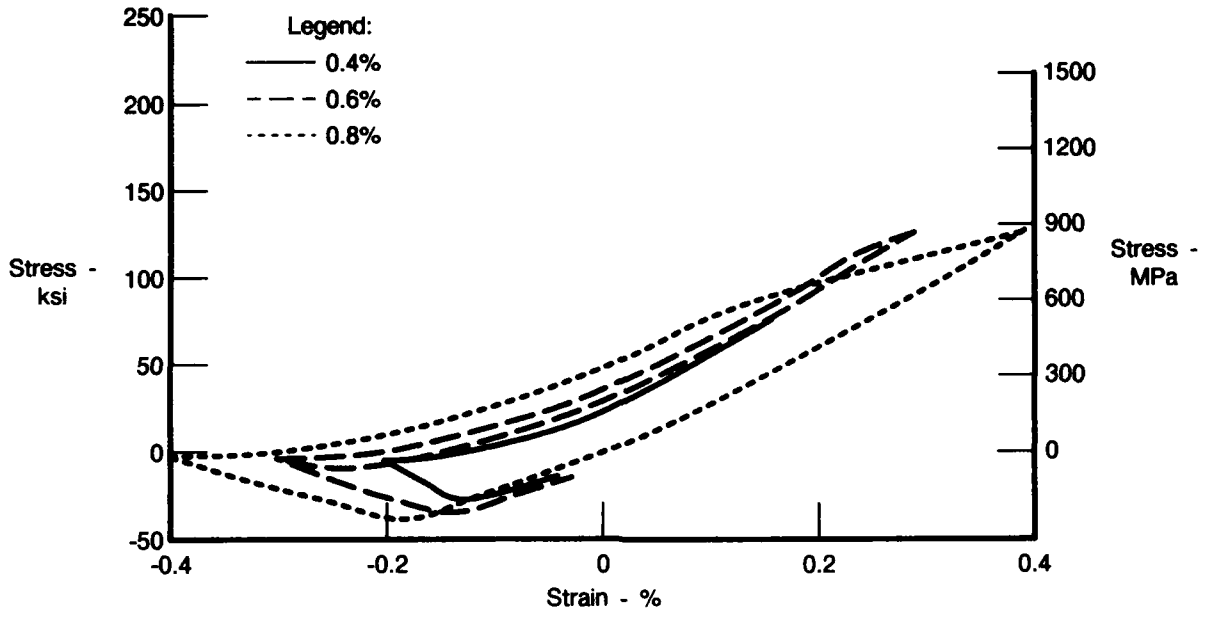

Figure 140. Coating Hysteresis Loops for PWA 275 Coating, Out-of-Phase Cycles, 427-1037°C (800-1900°F) Temperature Range and Various Strain Ranges

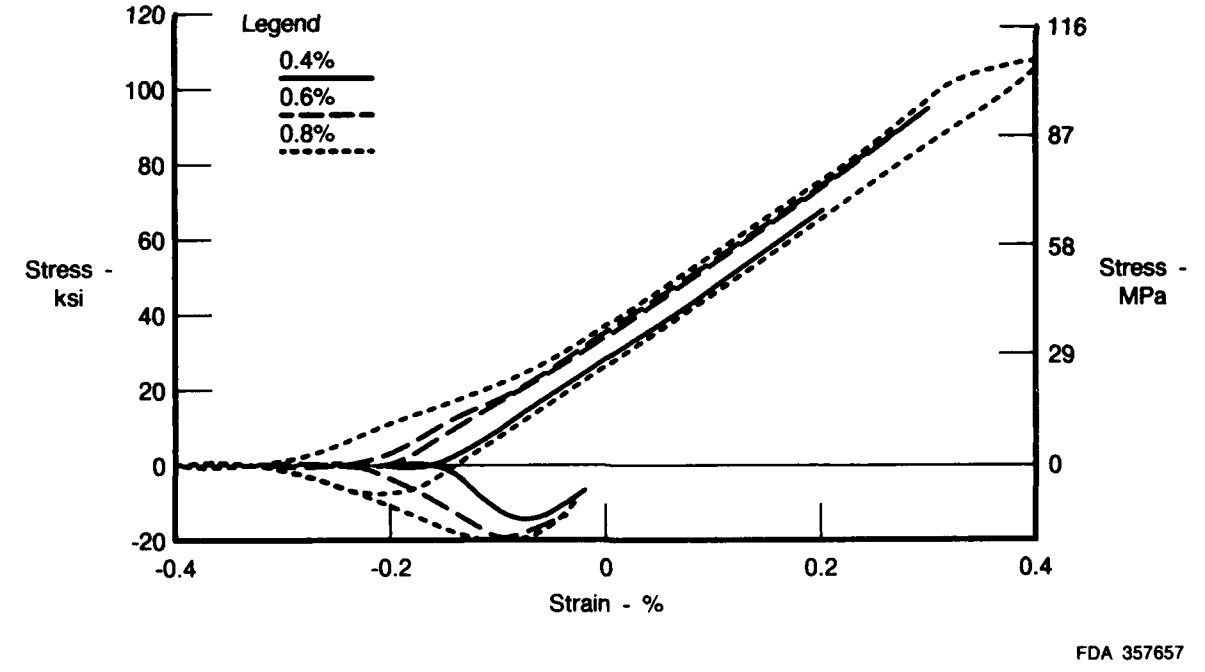

Figure 141. Coating Hysteresis Loops for PWA 286 Coating, Out-of-Phase Cycles, 427-1038°C (800-1900°F) Temperature Range and Various Strain Ranges

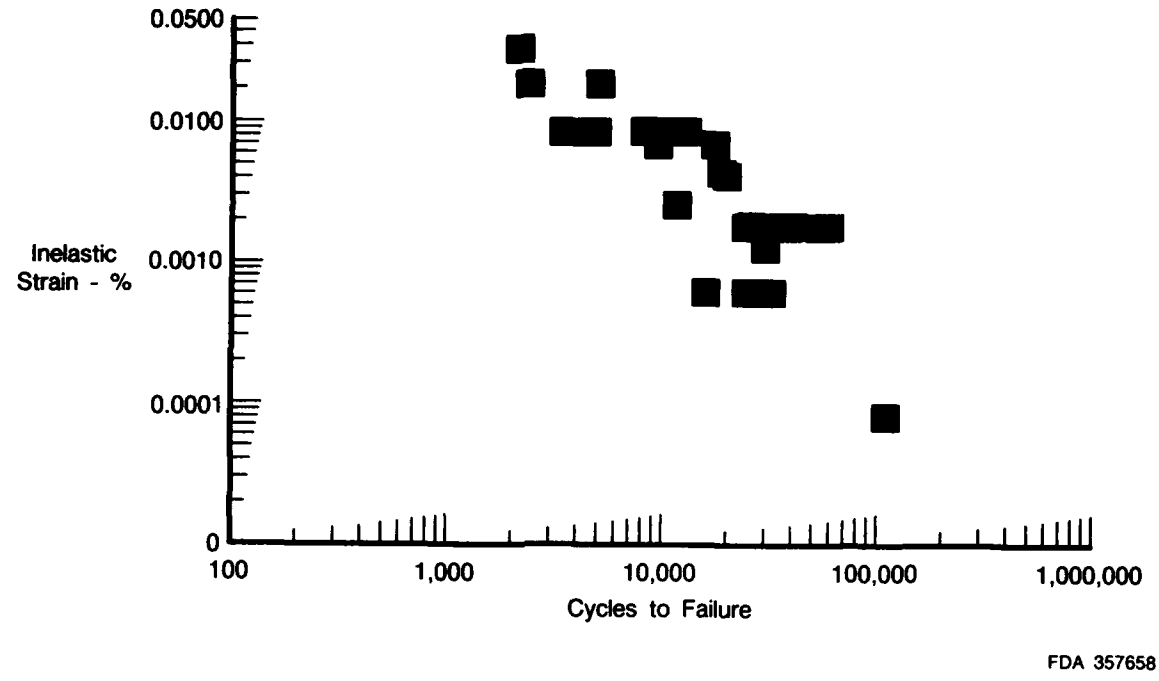

Figure 142. Inelastic Strain Versus Cycles to Failure for Uncoated PWA 1480, All TMF Data (Incremented Inelastic Strain Method)

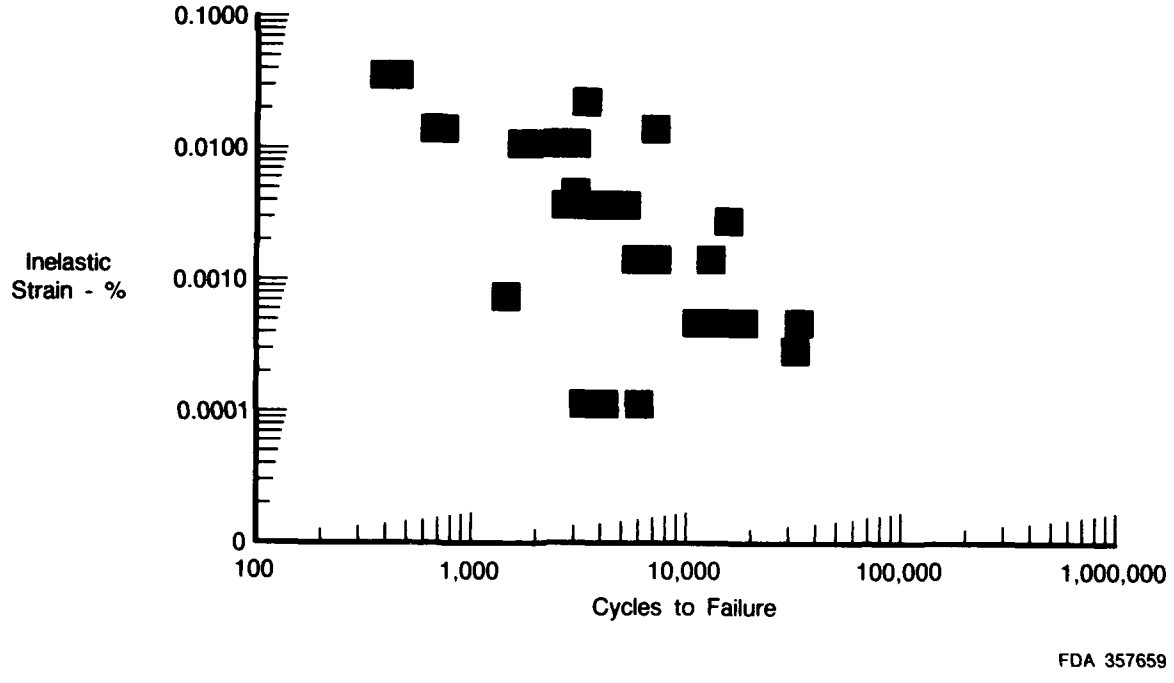

Figure 143. Inelastic Strain Versus Cycles to Failure for PWA 275 Coated PWA 1480, All TMF Data (Incremented Inelastic Strain Method)

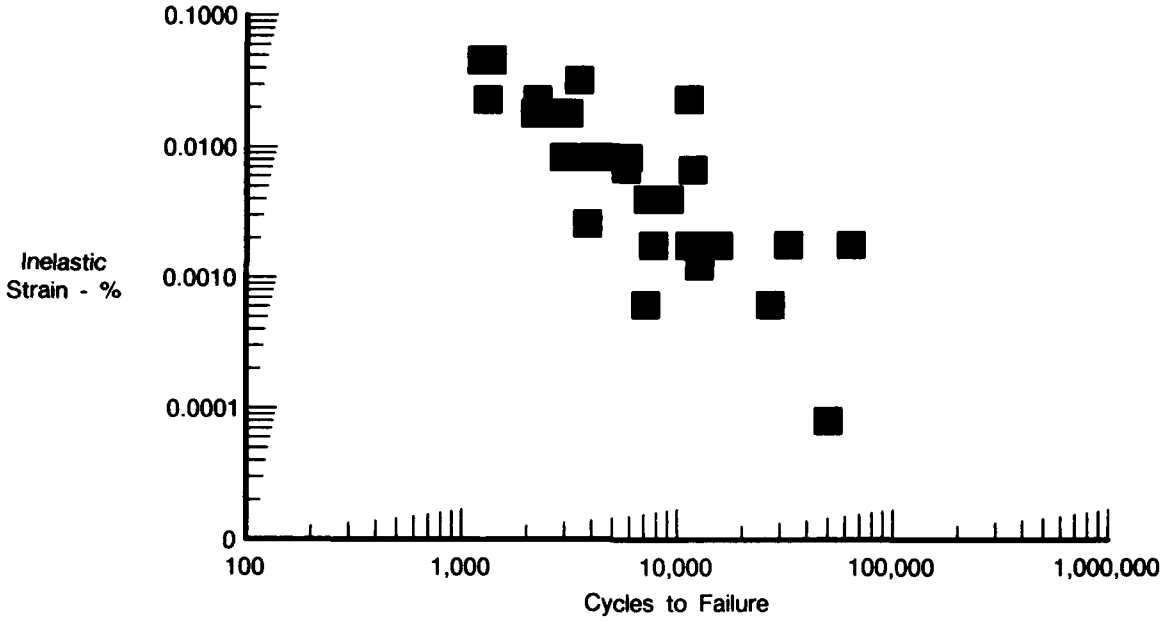

Figure 144. Inelastic Strain Versus Cycles to Failure for PWA 286 Coated PWA 1480, All TMF Data

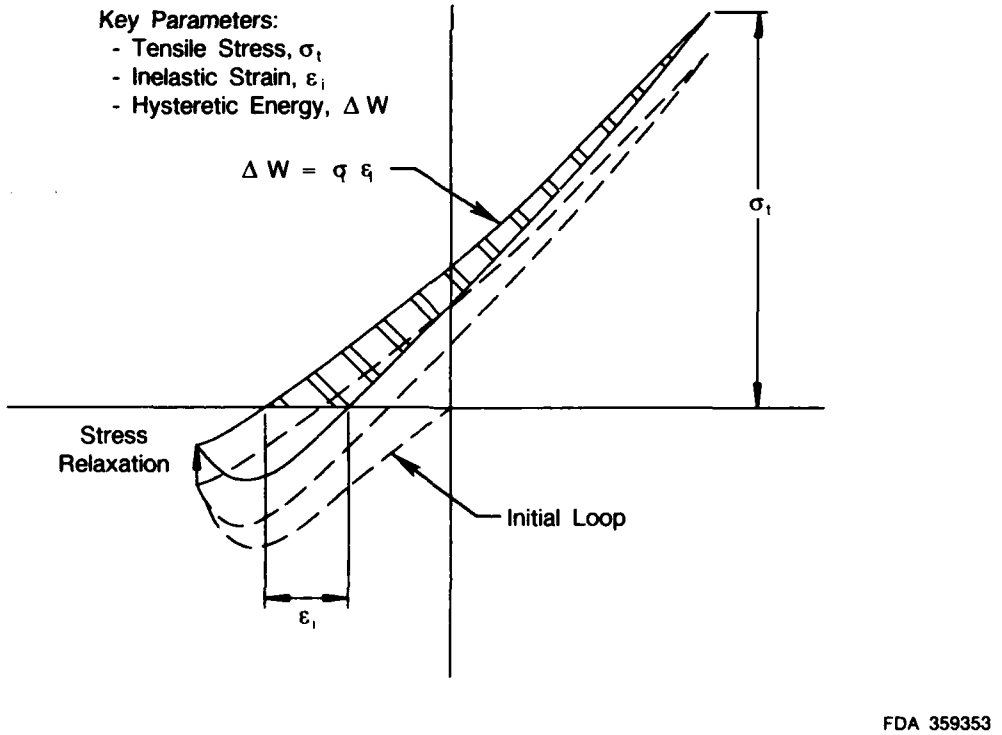

Figure 145. Hysteretic Energy Approach

For A Given 100°F Temperature Increment . . .

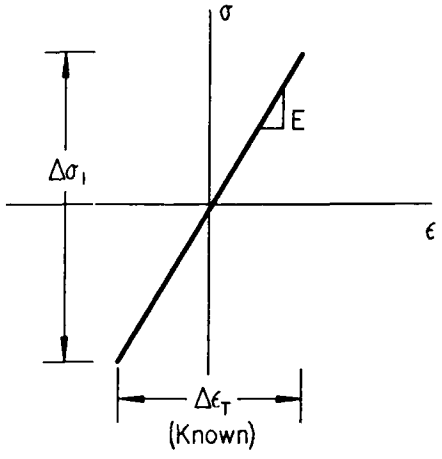

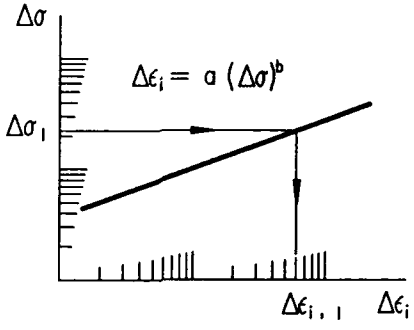

Determine $\Delta\epsilon_i$ For $\Delta\sigma_1$

Input: $\Delta\epsilon$, ΔT, Cycle Type
Yields: $\Delta\epsilon_i$

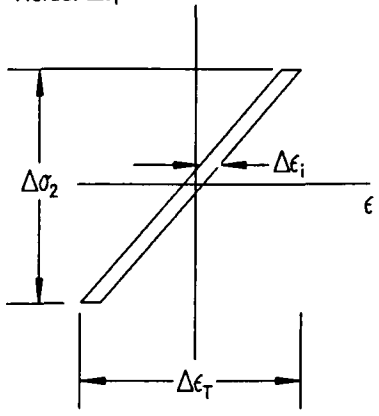

$\Delta\epsilon_e = \Delta\epsilon_T - \Delta\epsilon_i$
Then Recalculate $\Delta\sigma$, $\Delta\epsilon_i$
$\Delta\sigma_2 = \Delta\epsilon_e$ XE
$\Delta\epsilon_i = a\ (\Delta\sigma_2)^b$
E, a and b Are Known at a Given Temperature.
Inelastic and Elastic Strain Equations Are Iterated Until $\Delta\sigma$ Converges and Then $\Delta\epsilon_i$ is Calculated for the Temperature Increment

This is Repeated for All the Temperature Increments of the Leg

The Final Inelastic Strain is Averaged Over the Leg - Each Leg Is Then Totaled

$$\Delta\epsilon_{i,\ Final} = \frac{\sum_{k=1}^{n} \Delta\epsilon_k}{n}$$

Where n = Number of Temperature Increments

ϵ_k = Inelastic Strain at Temperature K

The Hysteretic Energy, ΔW_L, is Then Calculated by Using σ_t from:

(1) Testing
(2) Simple Elastic Calculation
(3) Inelastic Strain Balancing
(4) Constitutive Hysteresis Loop Constituative

FDA 350741

Figure 146. Inelastic Strain Calculation (Incremented Inelastic Strain Method)

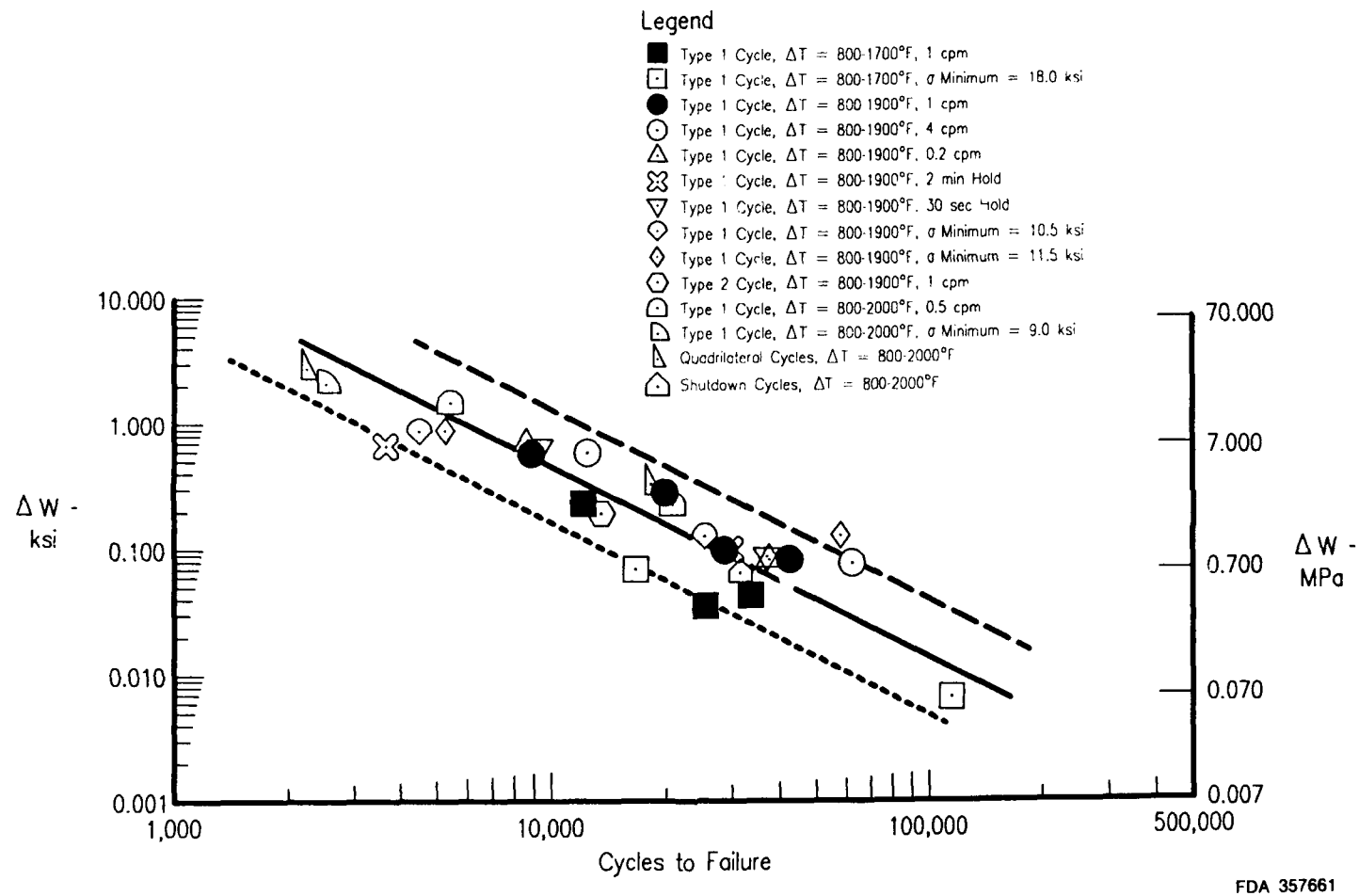

Figure 147. Substrate Hysteretic Energy Damage Function Versus Cycles to Failure, Uncoated PWA 1480, Incremented Inelastic Strain Method, Observed Tensile Stress from Test Data

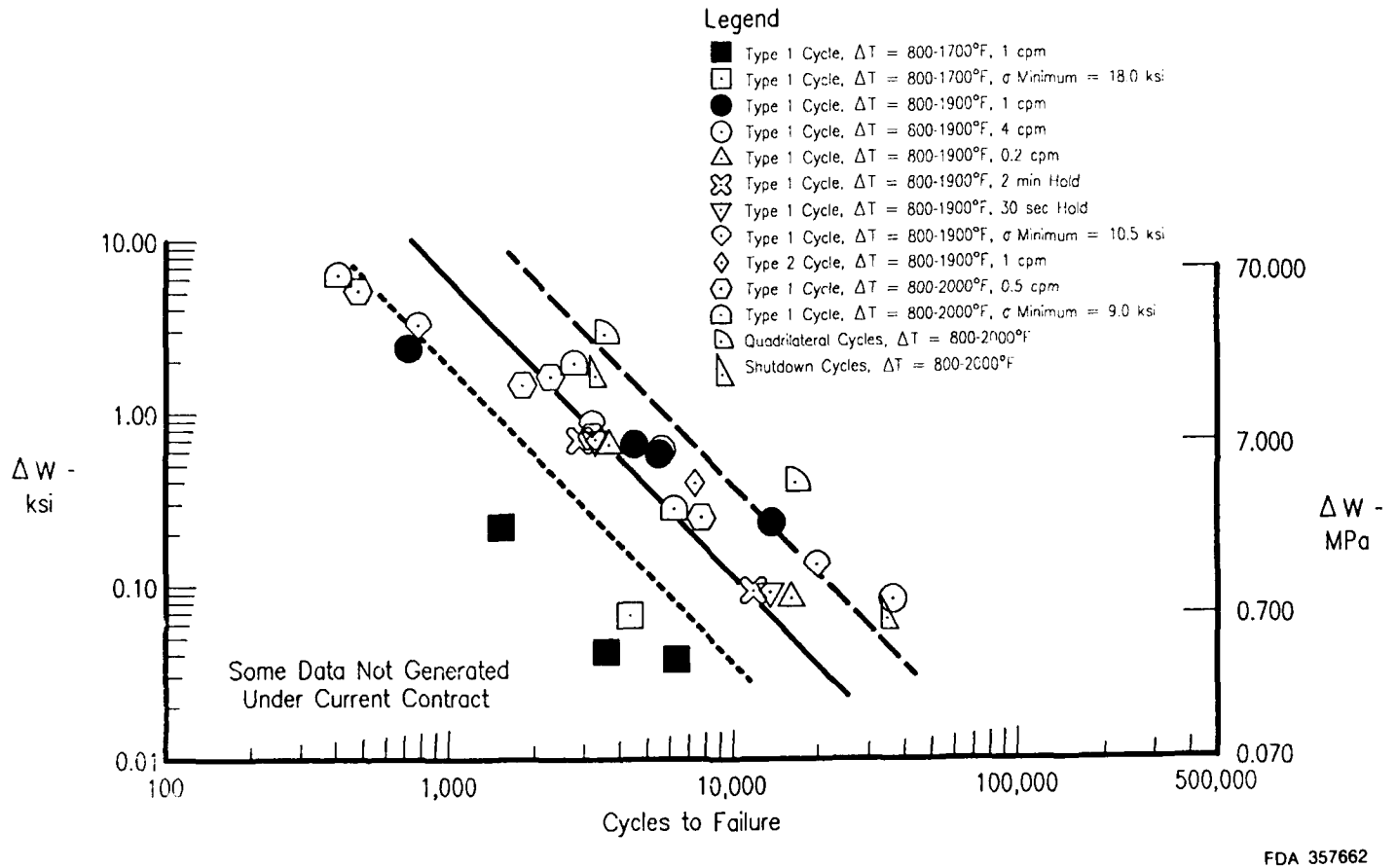

Figure 148. Substrate Hysteretic Energy Damage Function Versus Cycles to Failure, Aluminide Coated (PWA 275) PWA 1480, Incremented Inelastic Strain Method, Observed Tensile Stress from Test Data

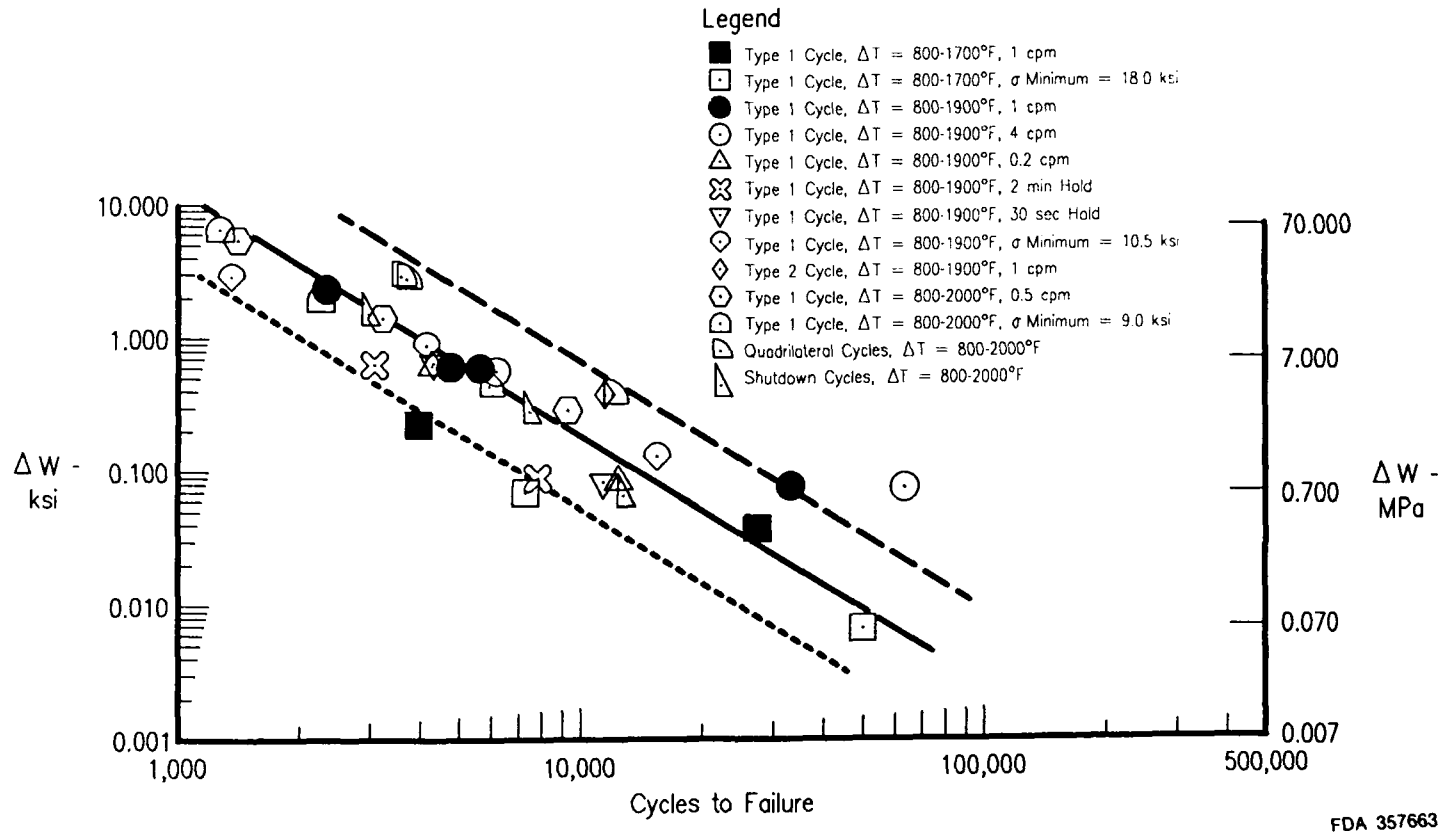

Figure 149. Substrate Hysteretic Energy Damage Function Versus Cycles to Failure, Overlay Coated (PWA 286) PWA 1480, Incremented Inelastic Strain Method, Observed Tensile Stress from Test Data

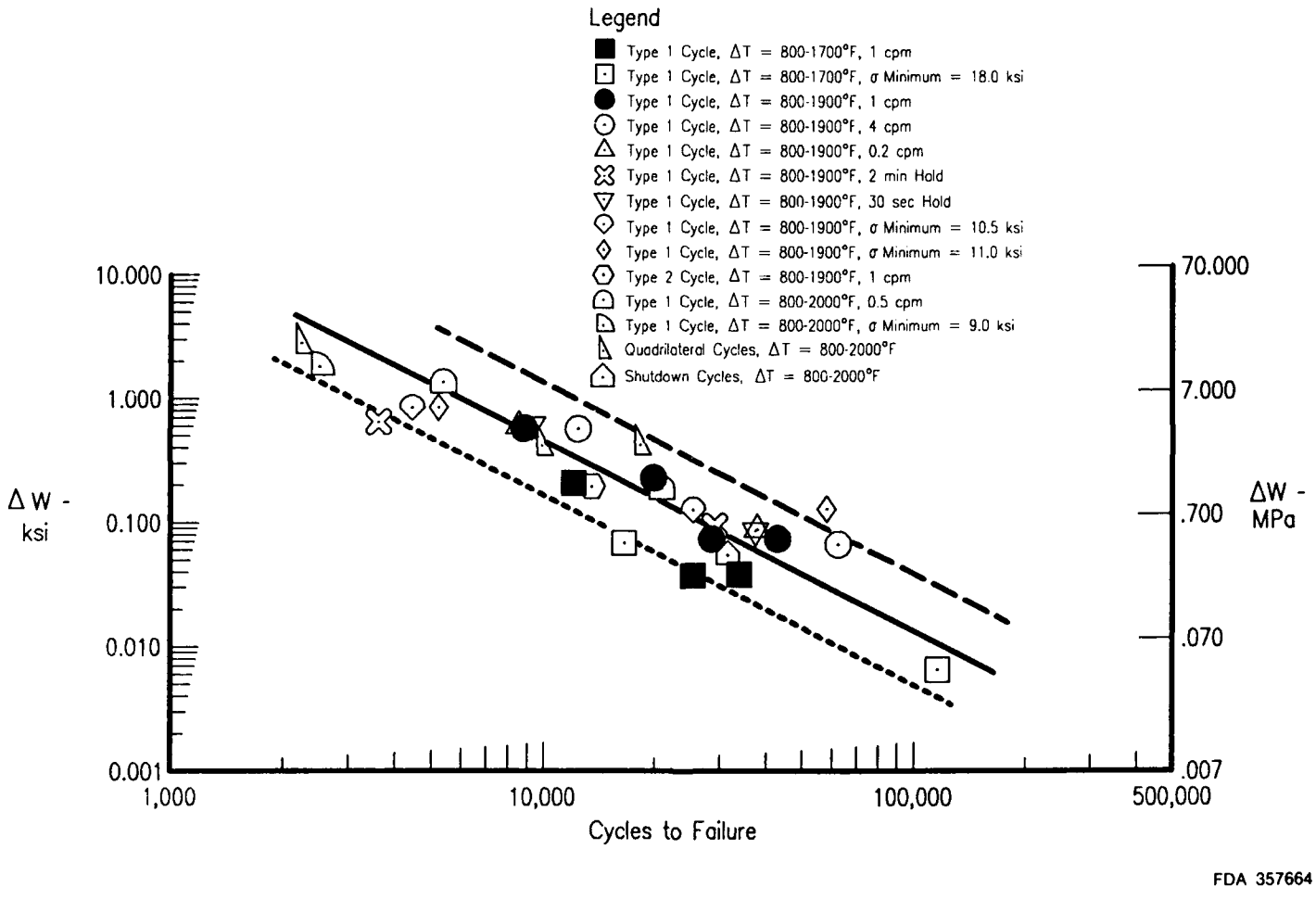

Figure 150. Substrate Hysteretic Energy Damage Function Versus Cycles to Failure, Uncoated PWA 1480, Incremented Inelastic Strain Method Simplified Constitutive Tensile Stress

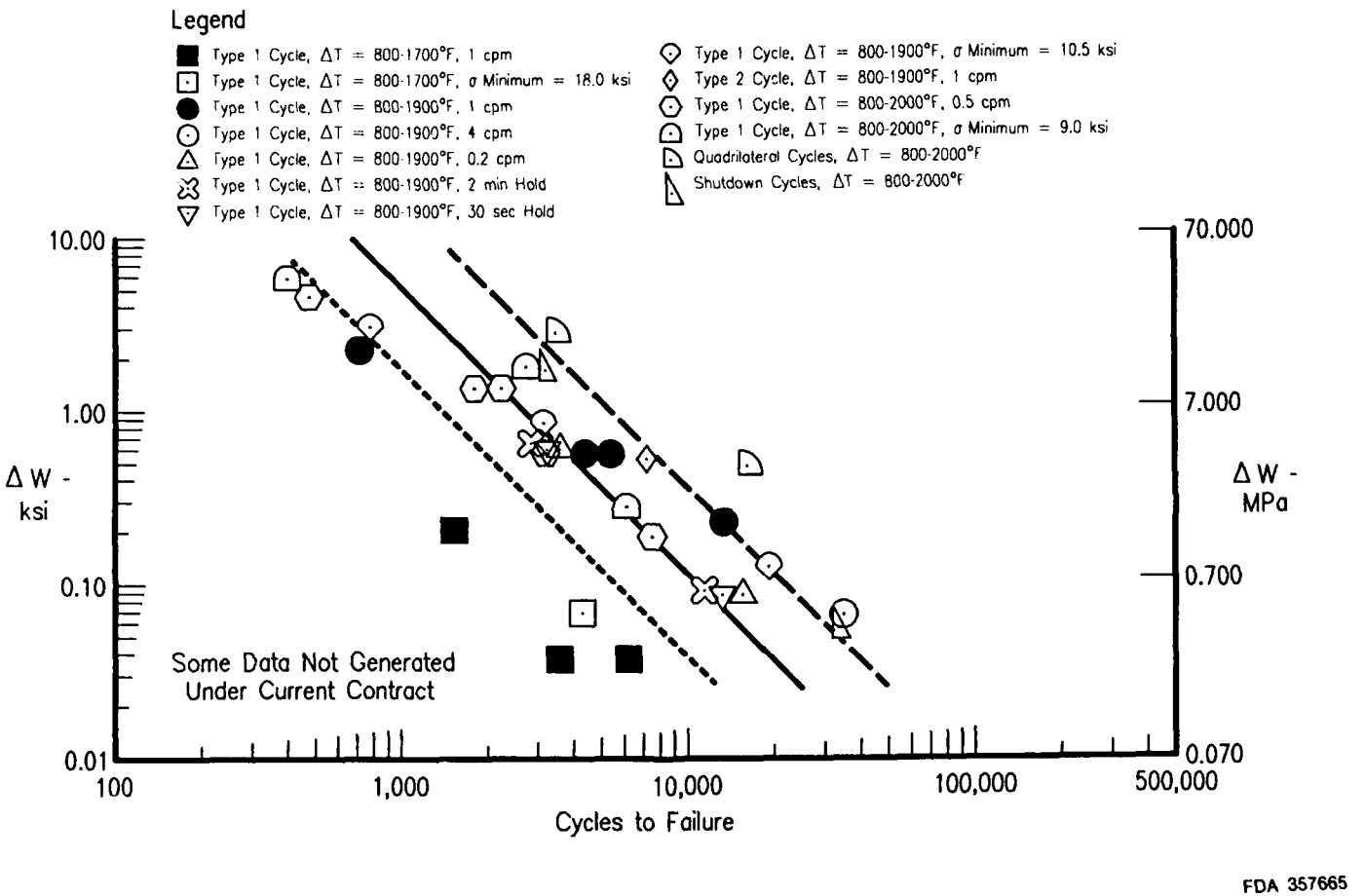

Figure 151. Substrate Hysteretic Energy Damage Function Versus Cycles to Failure, Aluminide Coated (PWA 275) PWA 1480, Incremented Inelastic Strain Method, Simplified Constitutive Tensile Stress

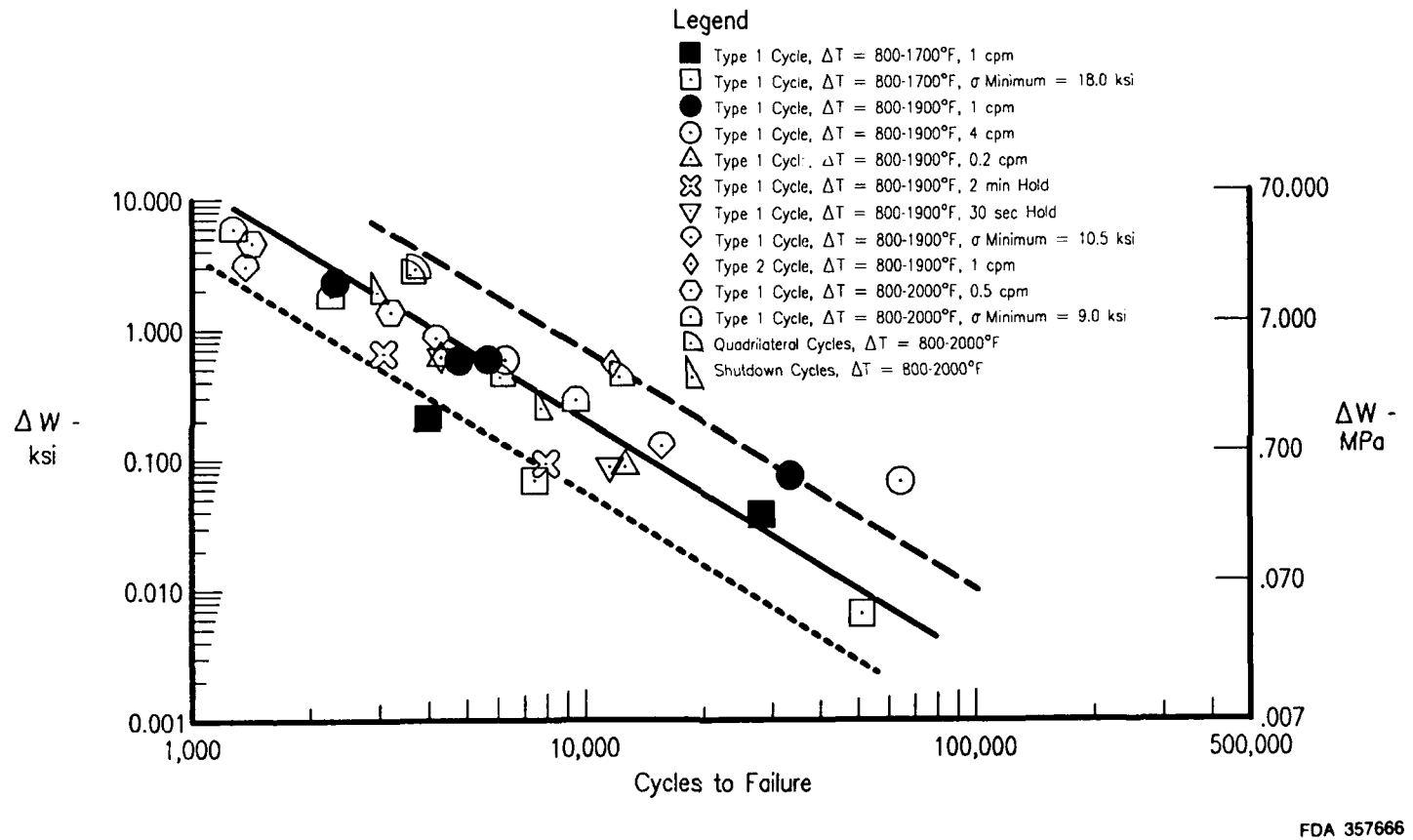

Figure 152. Substrate Hysteretic Energy Damage Function Versus Cycles to Failure, Overlay Coated (PWA 286) PWA 1480, Incremented Inelastic Strain Method, Simplified Constitutive Tensile Stress

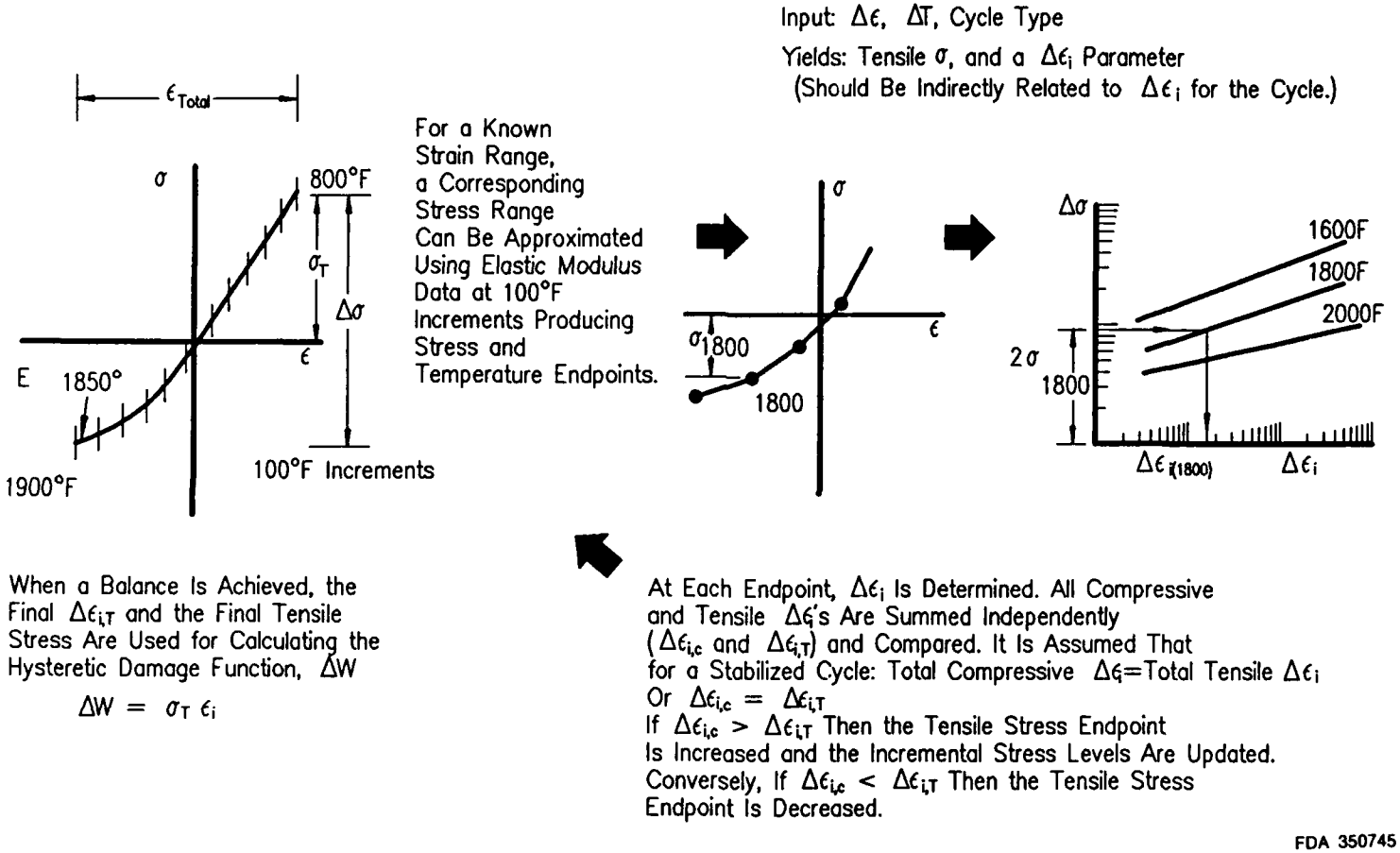

Figure 153. Damage Parameter, ΔW, Calculation (Plastic Strain Balancing Method)

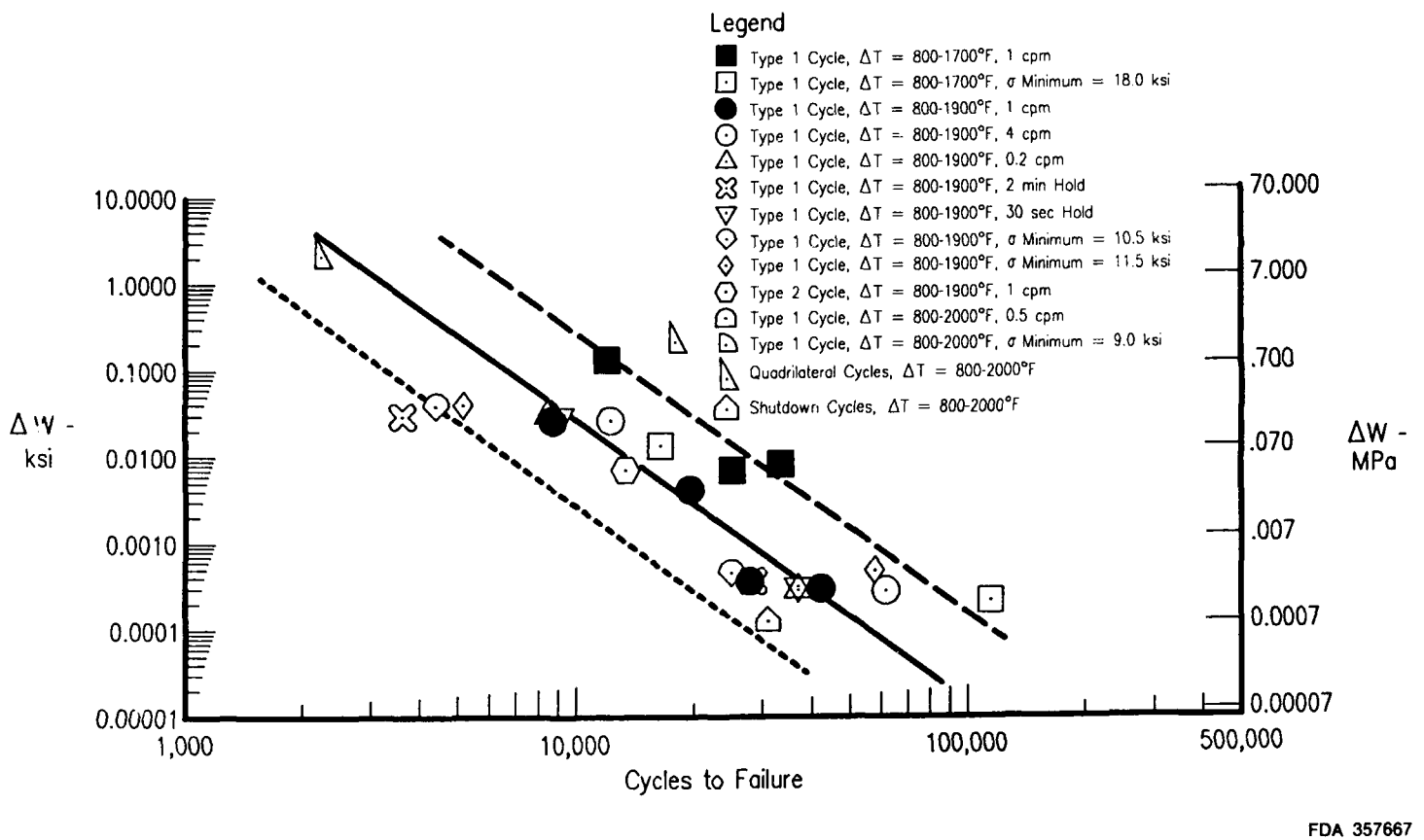

Figure 154. Substrate Hysteretic Energy Damage Function Versus Cycles to Failure, Uncoated PWA 1480, Plastic Strain Balancing Method, Observed Tensile Stress from Test Data

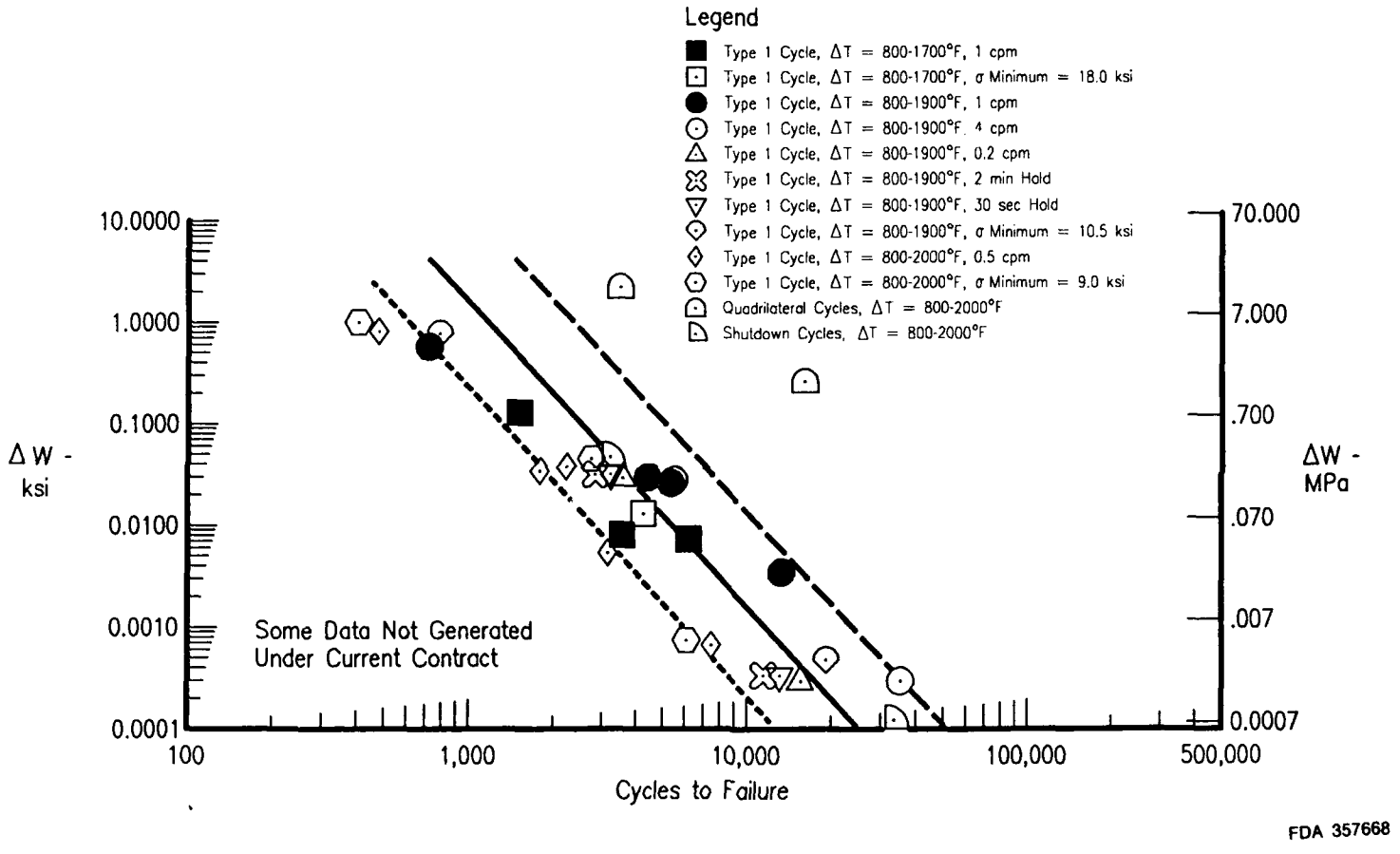

Figure 155. Substrate Hysteretic Energy Damage Function Versus Cycles to Failure, Aluminide Coated (PWA 275) PWA 1480, Plastic Strain Balancing Method, Observed Tensile Stress from Test Data

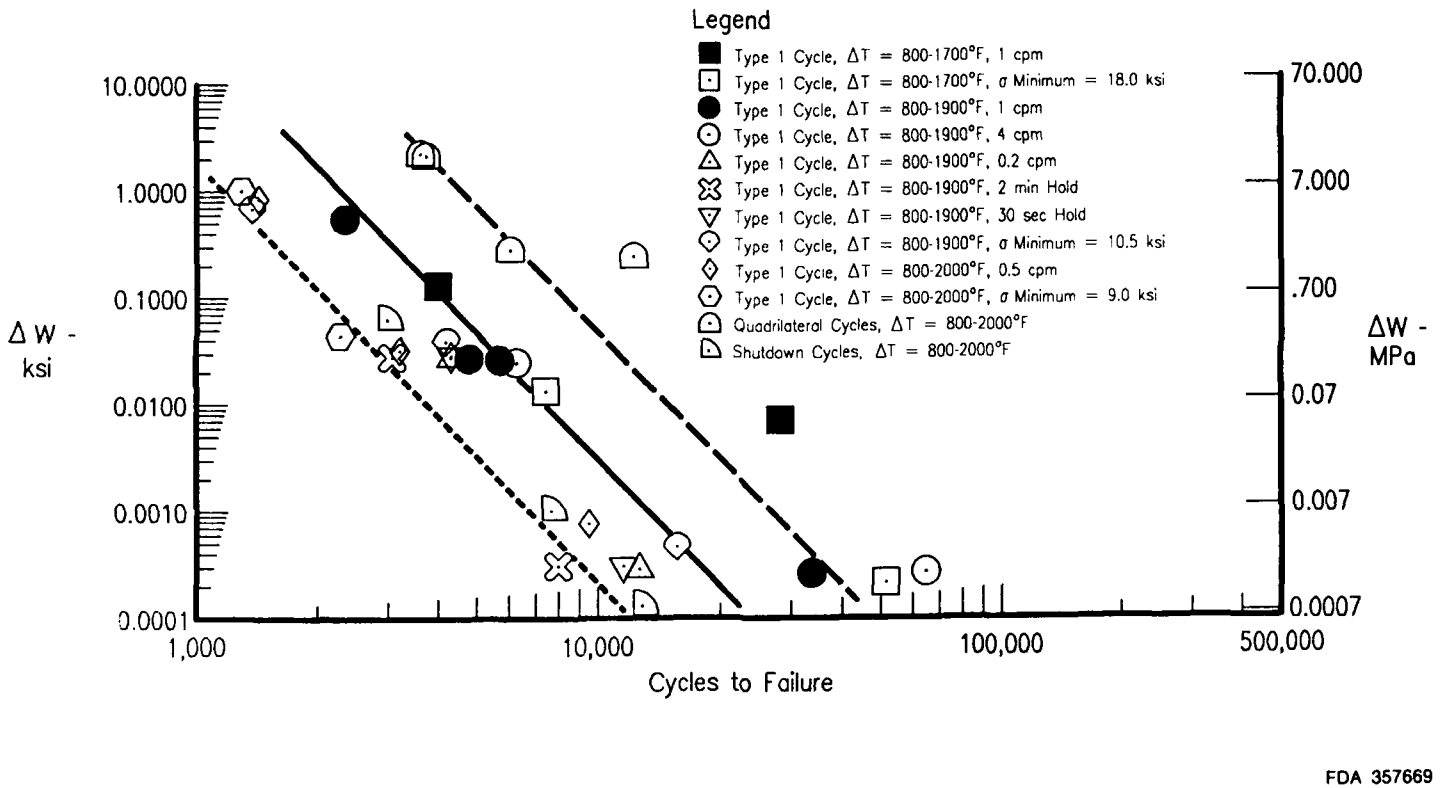

Figure 156. Substrate Hysteretic Energy Damage Function Versus Cycles to Failure, Overlay Coated (PWA 286) PWA 1480, Plastic Strain Balancing Method, Observed Tensile Stress from Test Data

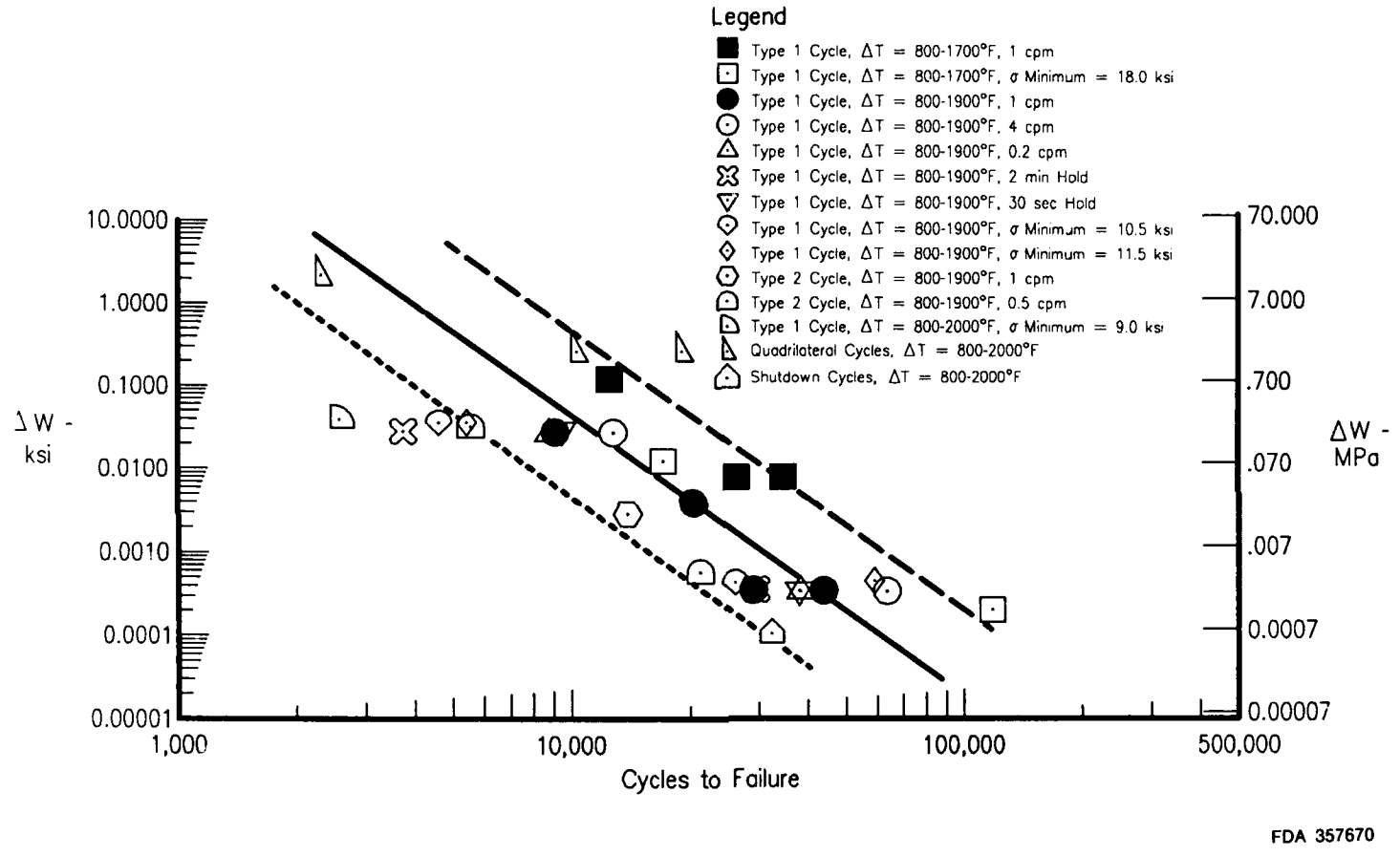

Figure 157. Substrate Hysteretic Energy Damage Function Versus Cycles to Failure, Uncoated PWA 1480, Plastic Strain Balancing Method for Stress and Strain

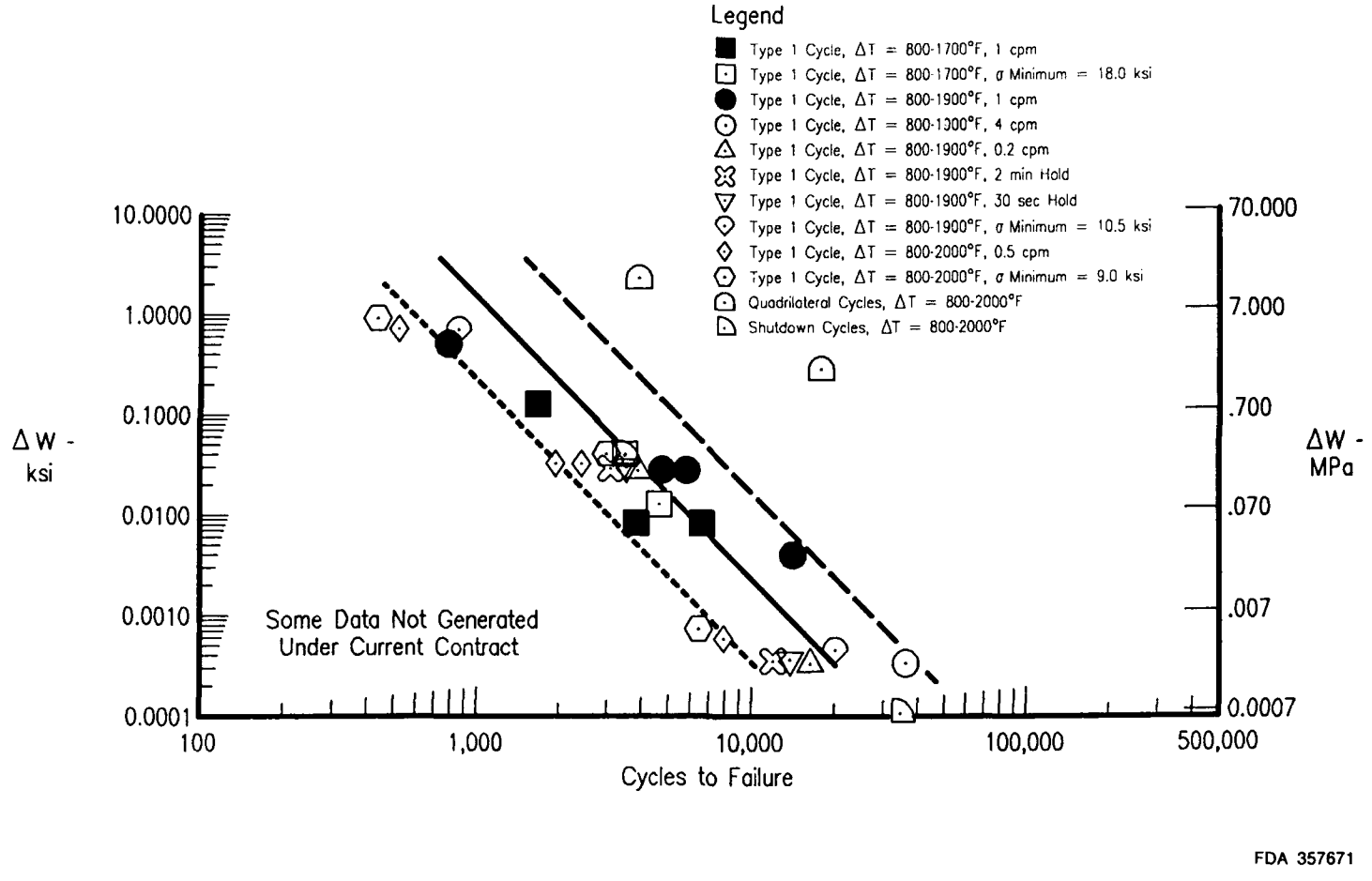

Figure 158. Substrate Hysteretic Energy Damage Function Versus Cycles to Failure, Aluminide Coated (PWA 275) PWA 1480, Plastic Strain Balancing Method for Stress and Strain

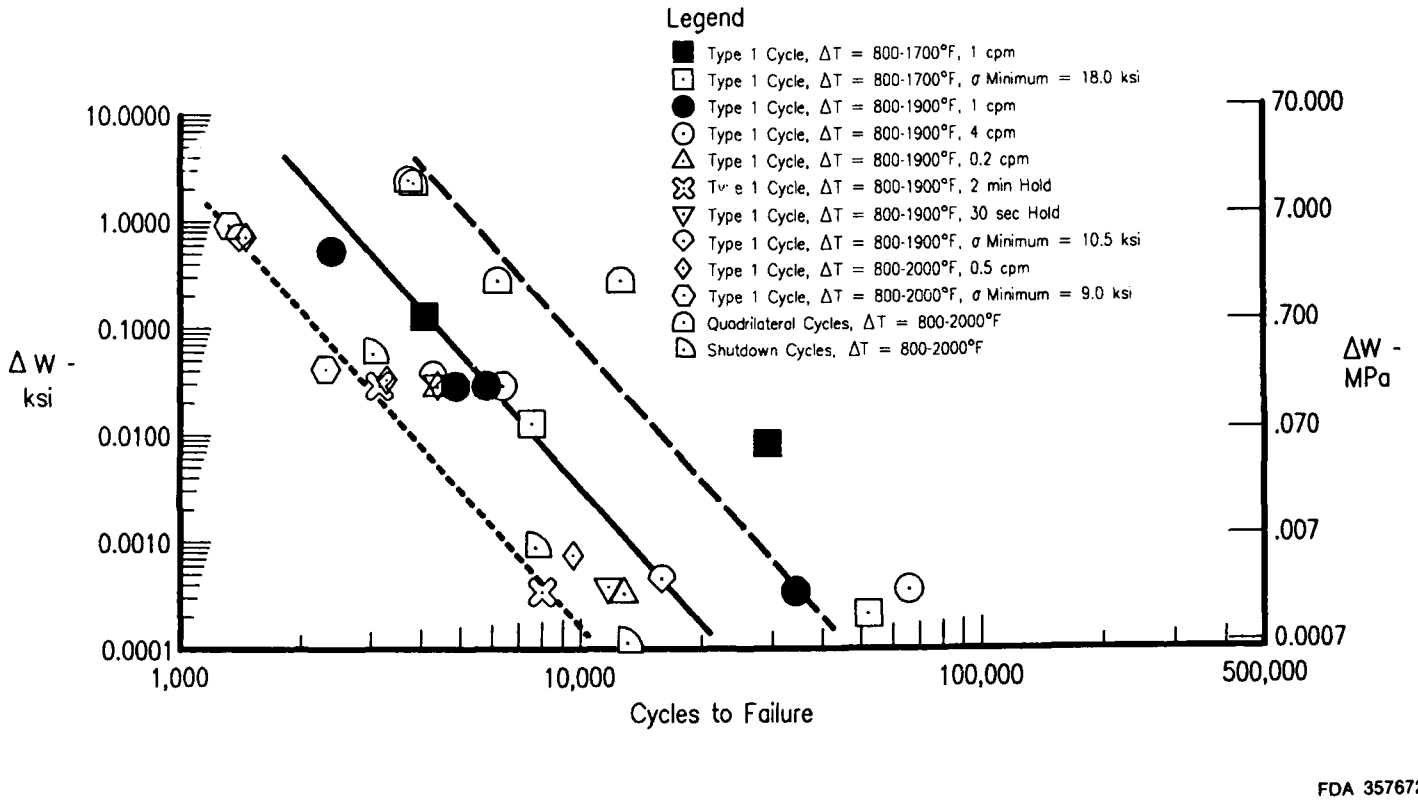

Figure 159. Substrate Hysteretic Energy Damage Function Versus Cycles to Failure, Overlay Coated (PWA 286) PWA 1480, Plastic Strain Balancing Method for Stress and Strain

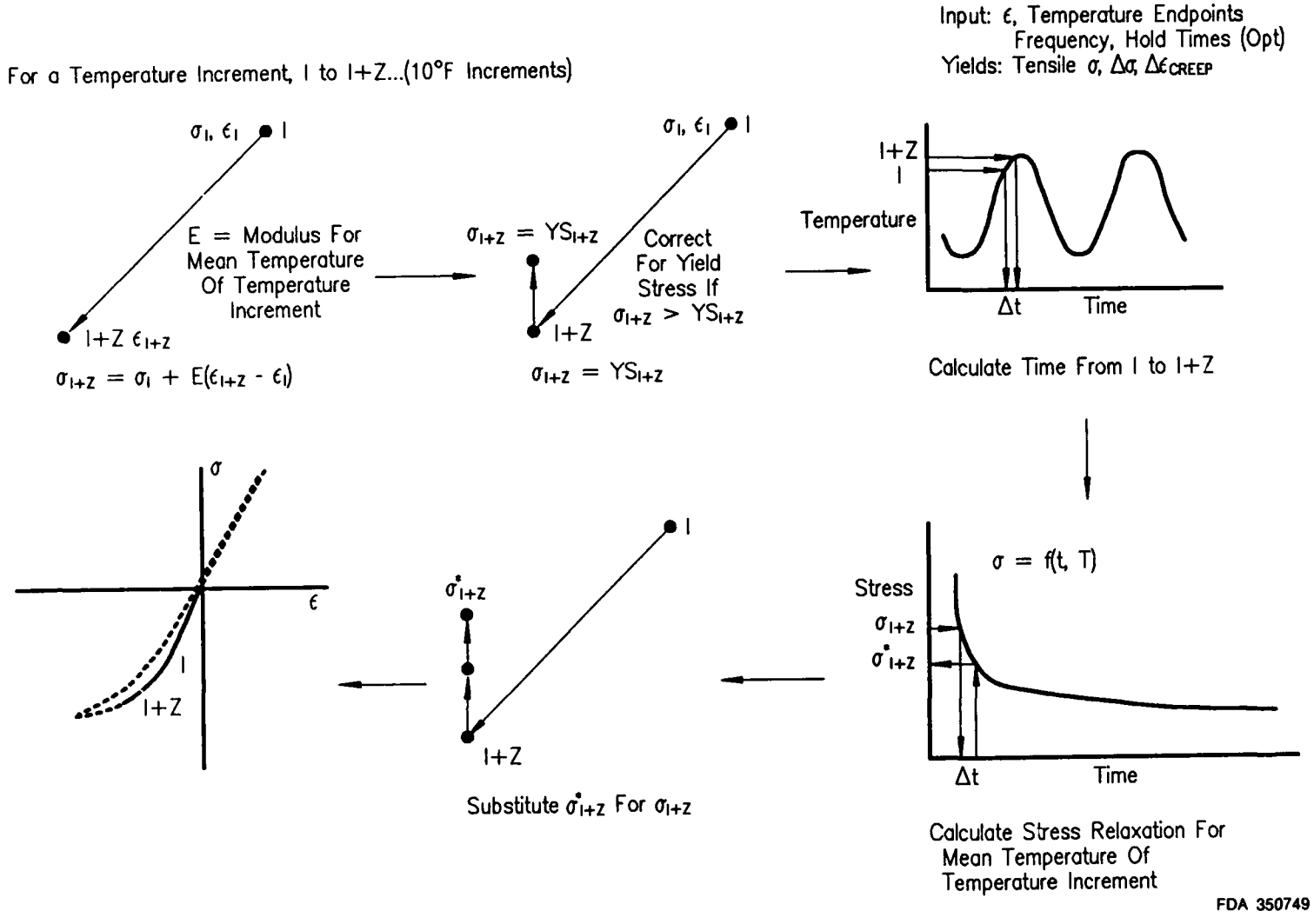

Figure 160. Hysteresis Loop Calculation (Simplified Constitutive Method)

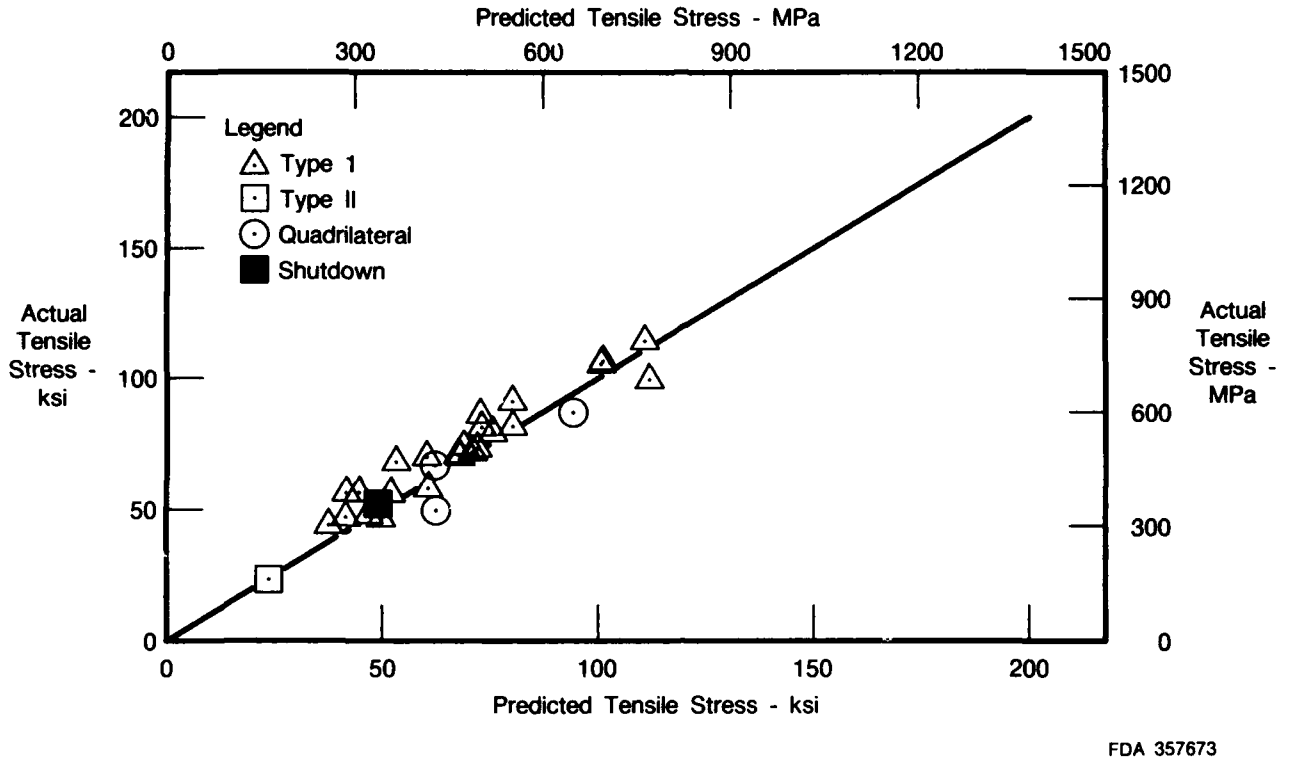

Figure 161. Actual Tensile Stress Versus Predicted Tensile Stress — Uncoated PWA 1480, [001] Orientation (Simplified Constitutive Method)

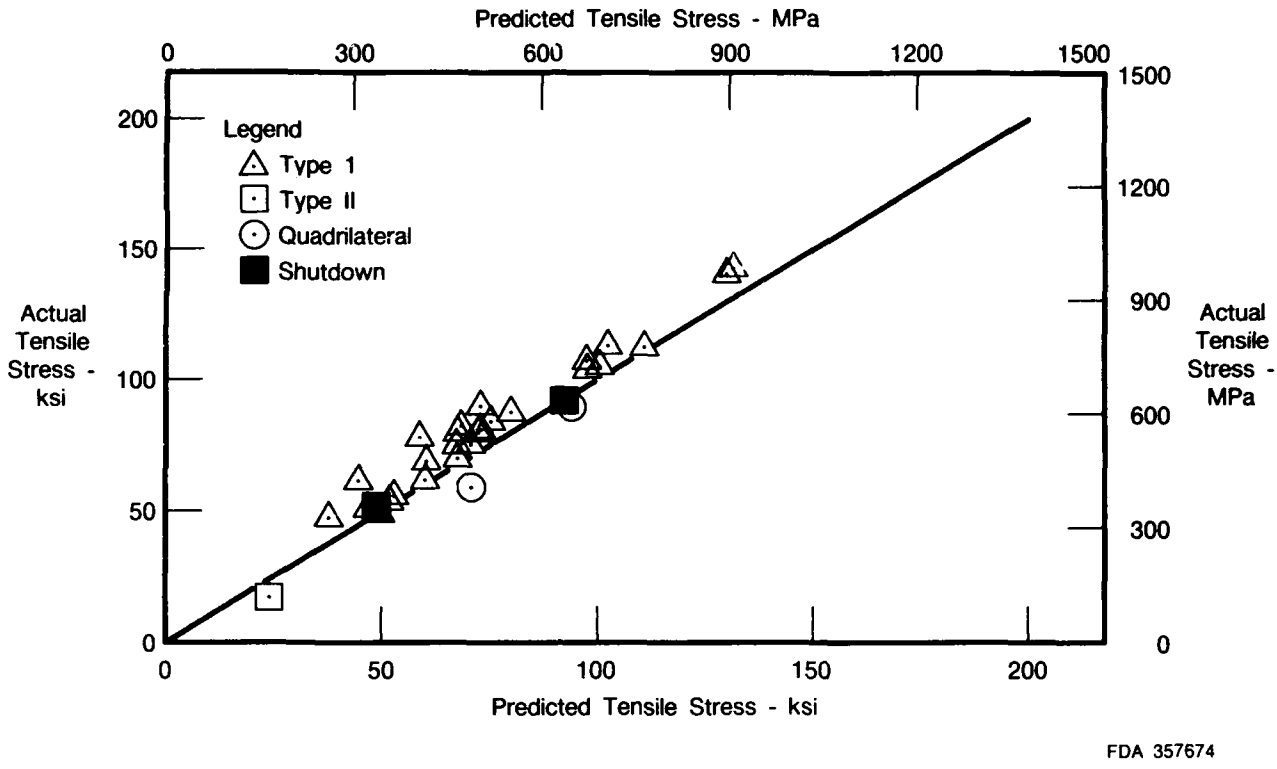

Figure 162. Actual Tensile Stress Versus Predicted Tensile Stress — PWA 275 Coated PWA 1480, [001] Orientation (Simplified Constitutive Method)

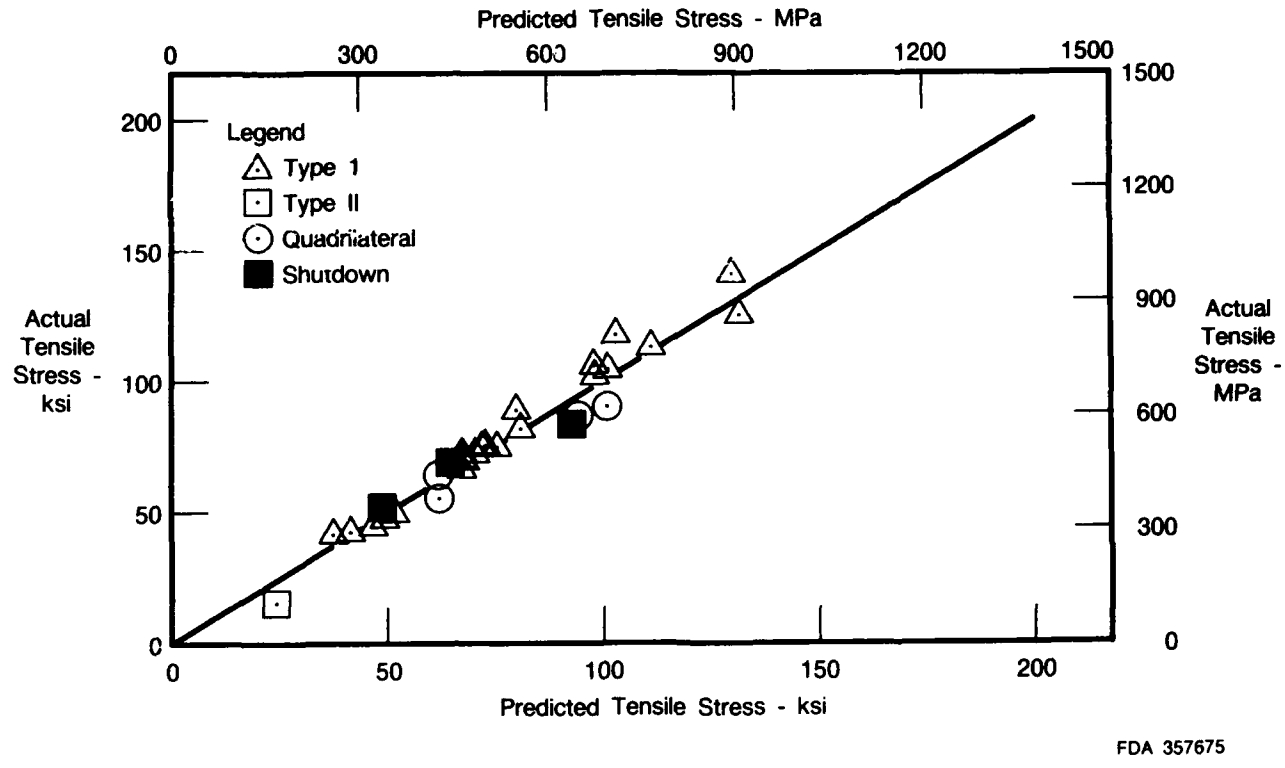

Figure 163. Actual Tensile Stress Versus Predicted Tensile Stress — PWA 286 Coated PWA 1480 [001] Orientation (Simplified Constitutive Method)

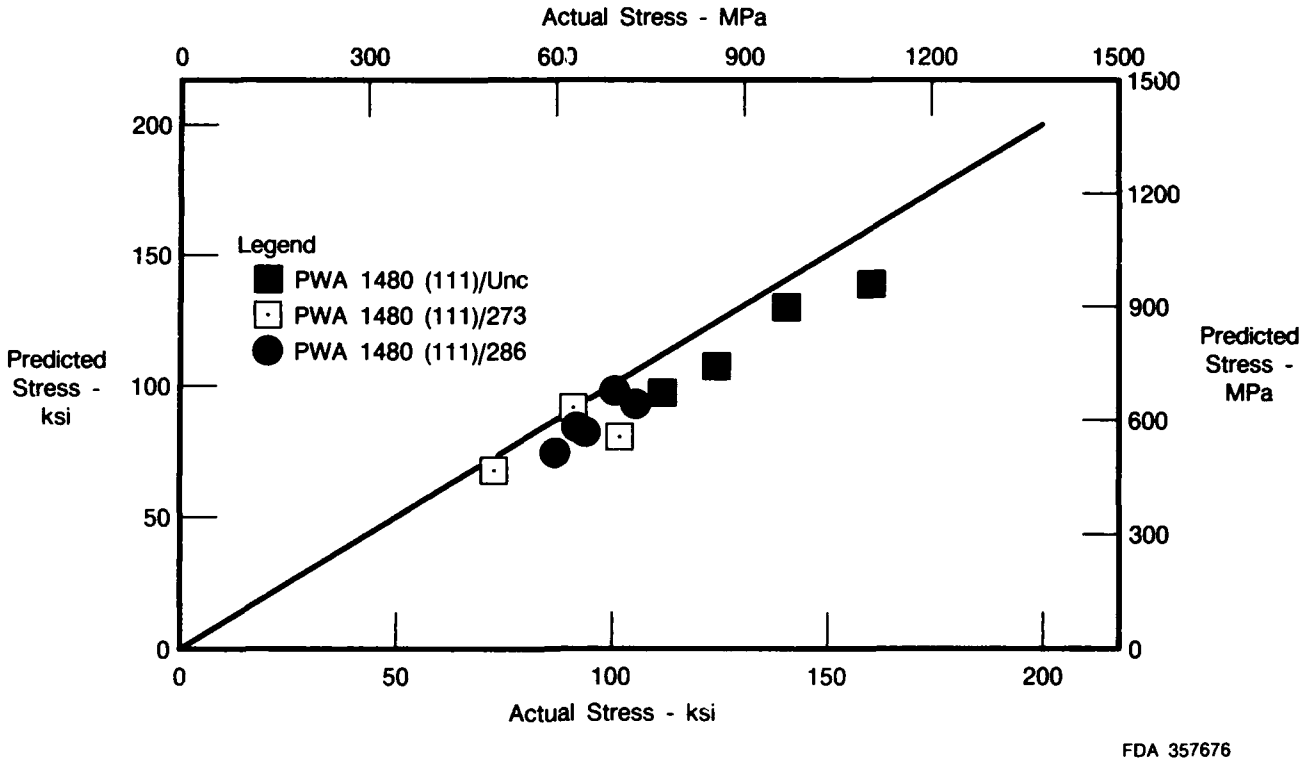

Figure 164. Actual Tensile Siress Versus Predicted Tensile Stress — PWA 1480 [111] Orientation, Simplified Constitutive Method (Data not Generated Under Current Contract)

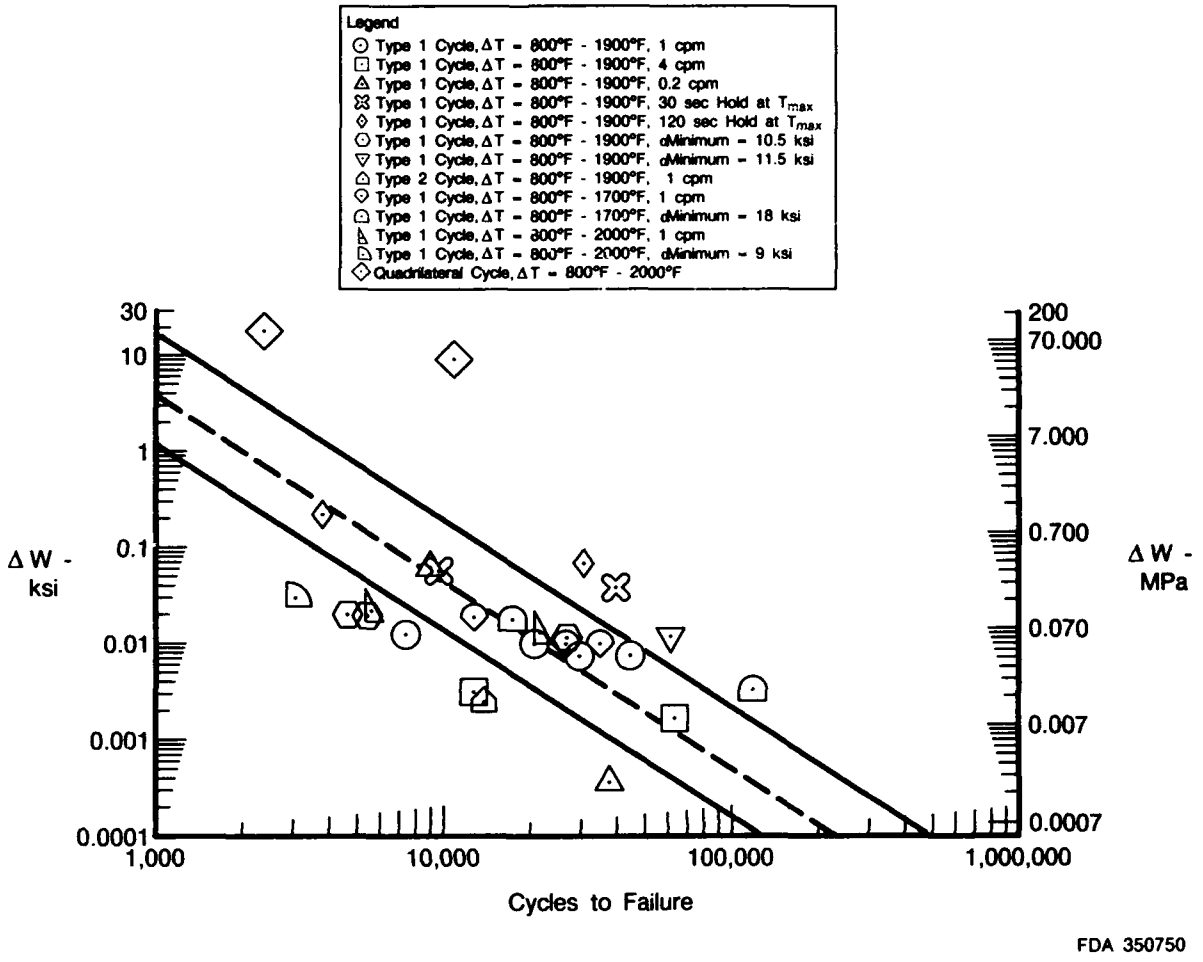

Figure 165. Life Versus Damage Parameter ΔW, for Uncoated PWA 1480 (Simplified Constitutive Method)

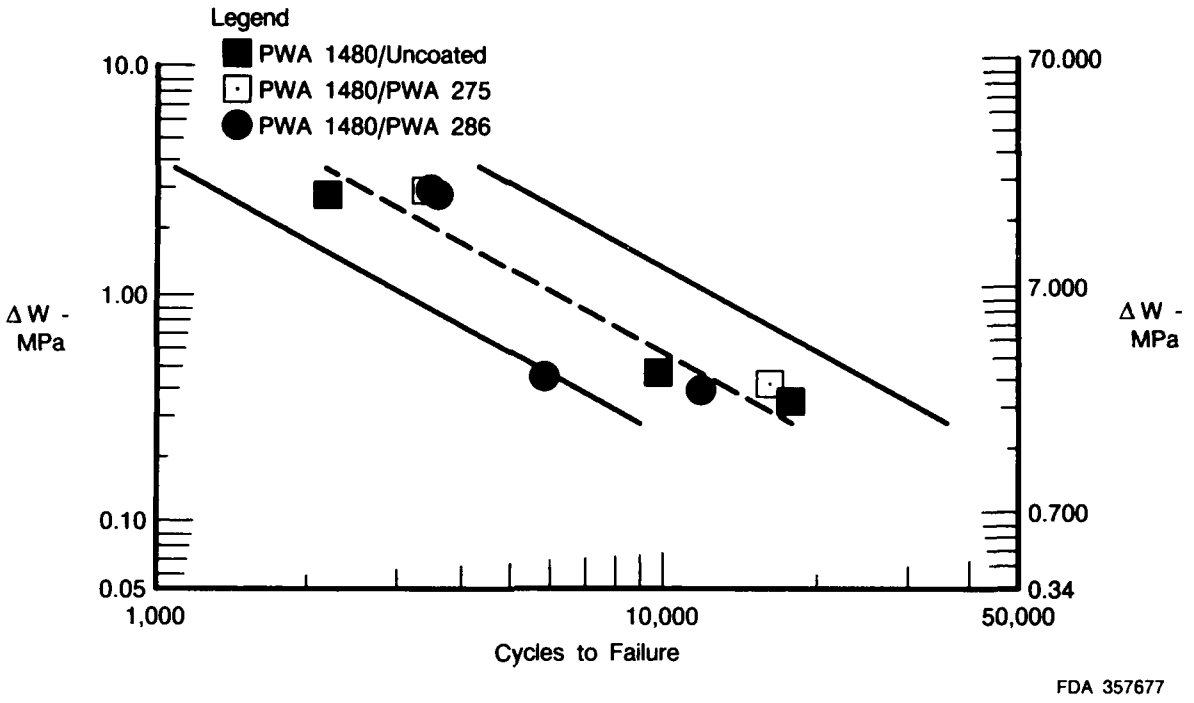

Figure 166. Hysteretic Energy Damage Function Versus Cycles to Failure for Quadrilateral Cycles, Substrate dW Only (Observed Test Tensile Stress and Incremented Inelastic Strain Method)

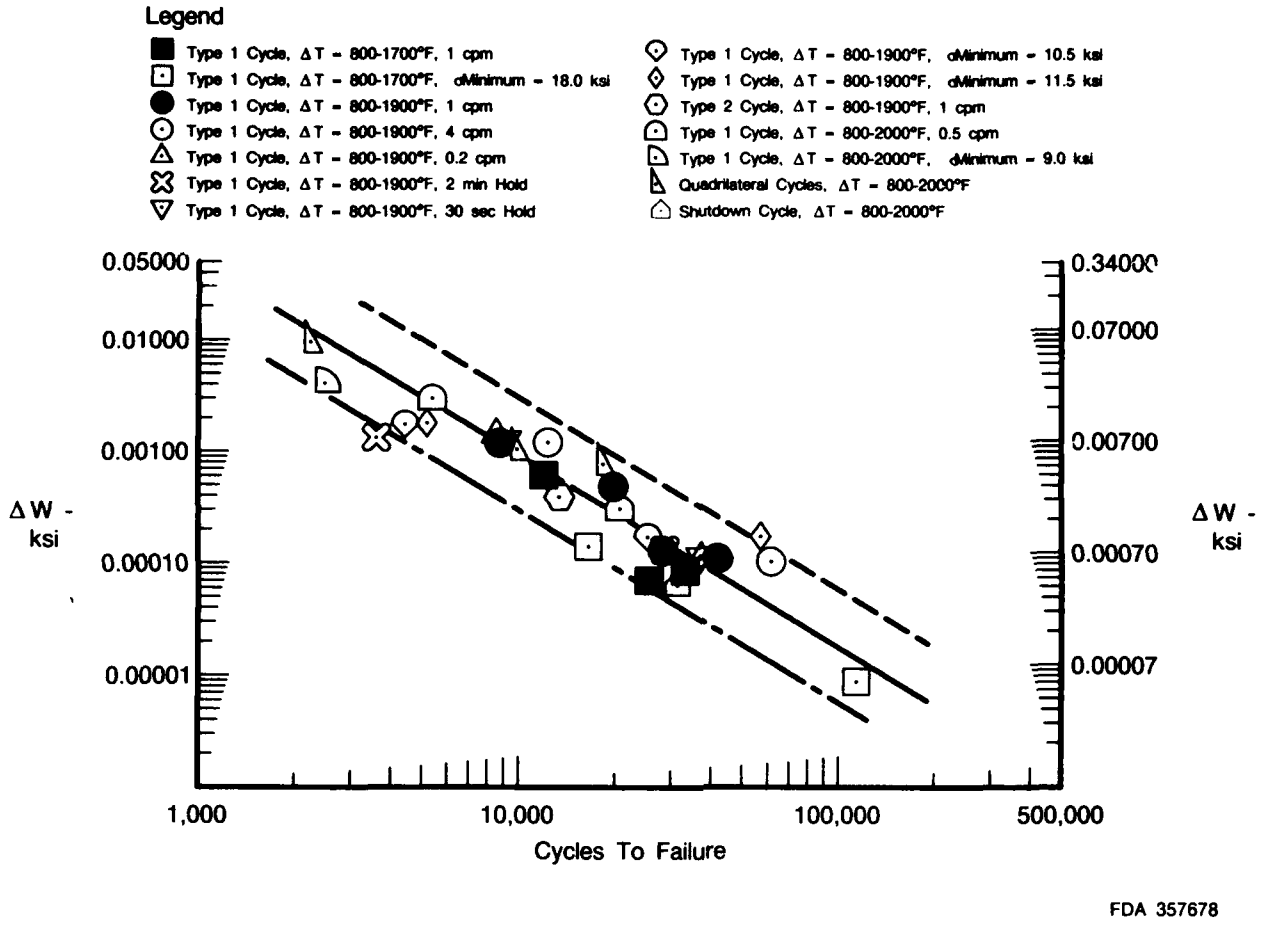

Figure 167. Effective Hysteretic Energy Damage Function Versus Cycles to Failure for Uncoated PWA 1480 [001], Observed Tensile Stress

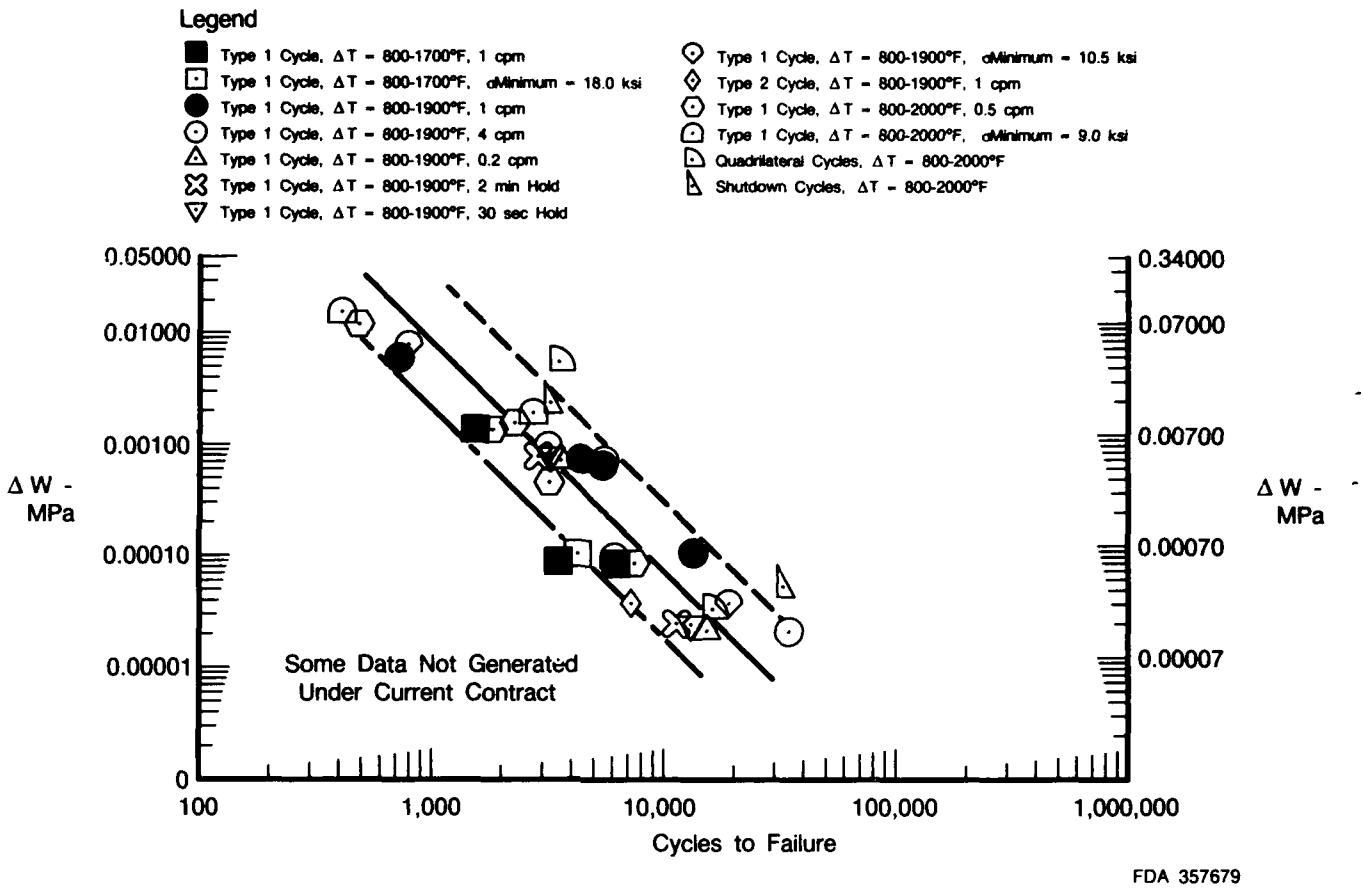

Figure 168. Effective Hysteretic Energy Damage Function Versus Cycles to Failure for Aluminide Coated (PWA 275) PWA 1480 [001], Observed Tensile Stress

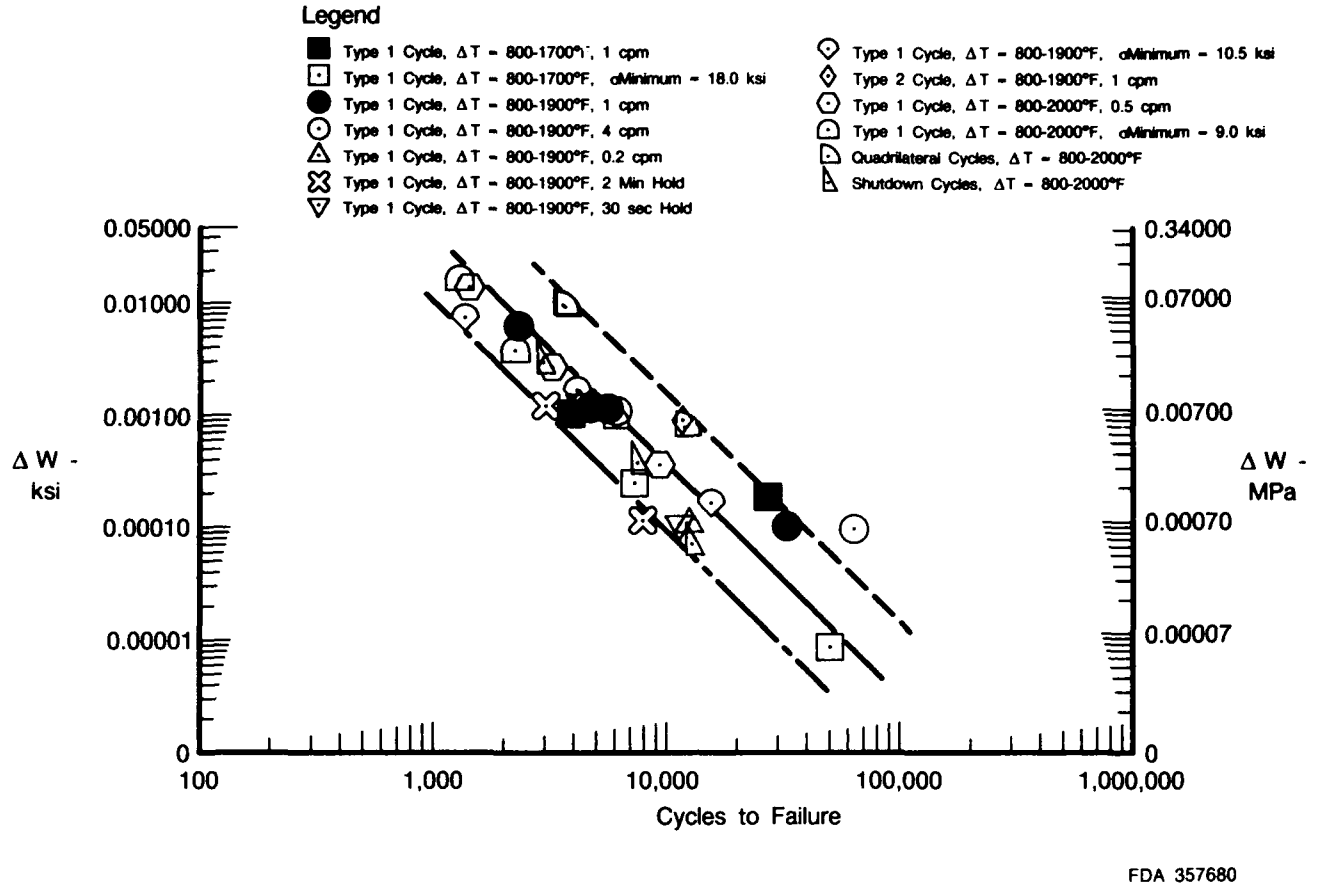

Figure 169. Effective Hysteretic Energy Damage Function Versus Cycles to Failure for Overlay Coated (PWA 286) PWA 1480 [001], Observed Tensile Stress

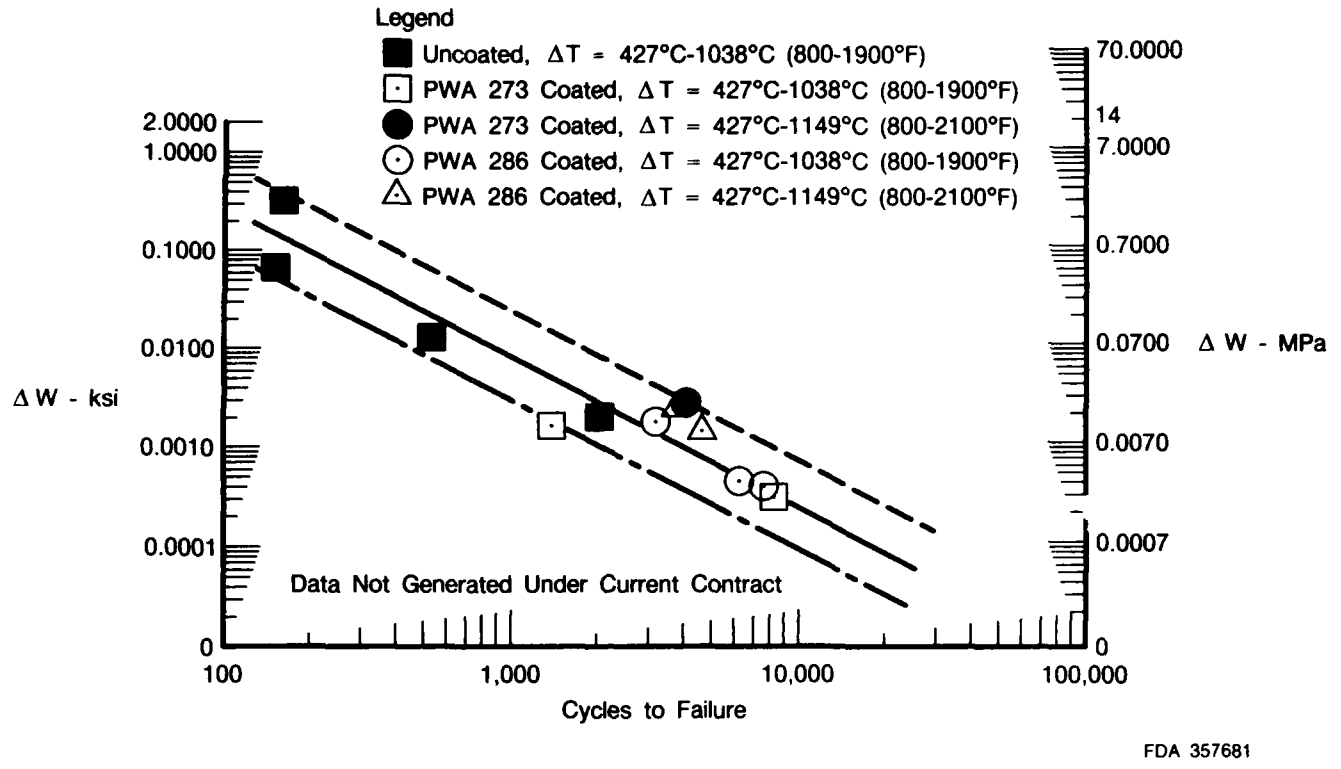

Figure 170. Effective Hysteretic Energy Damage Function Versus Cycles to Failure for PWA 1480 [111] With Various Coatings, Observed Tensile Stress

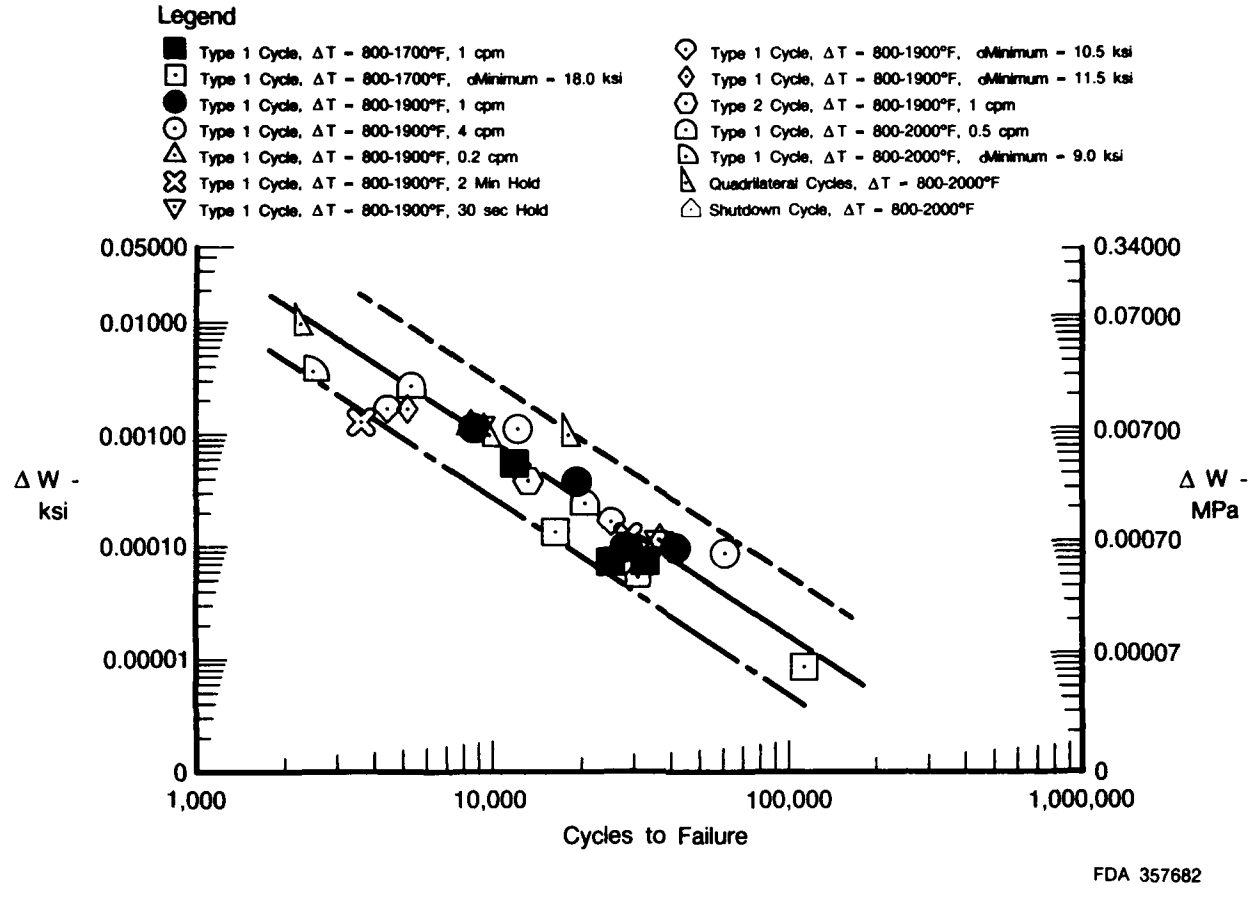

Figure 171. Effective Hysteretic Energy Damage Function Versus Cycles to Failure for Uncoated PWA 1480 [001], Constitutive Tensile Stress

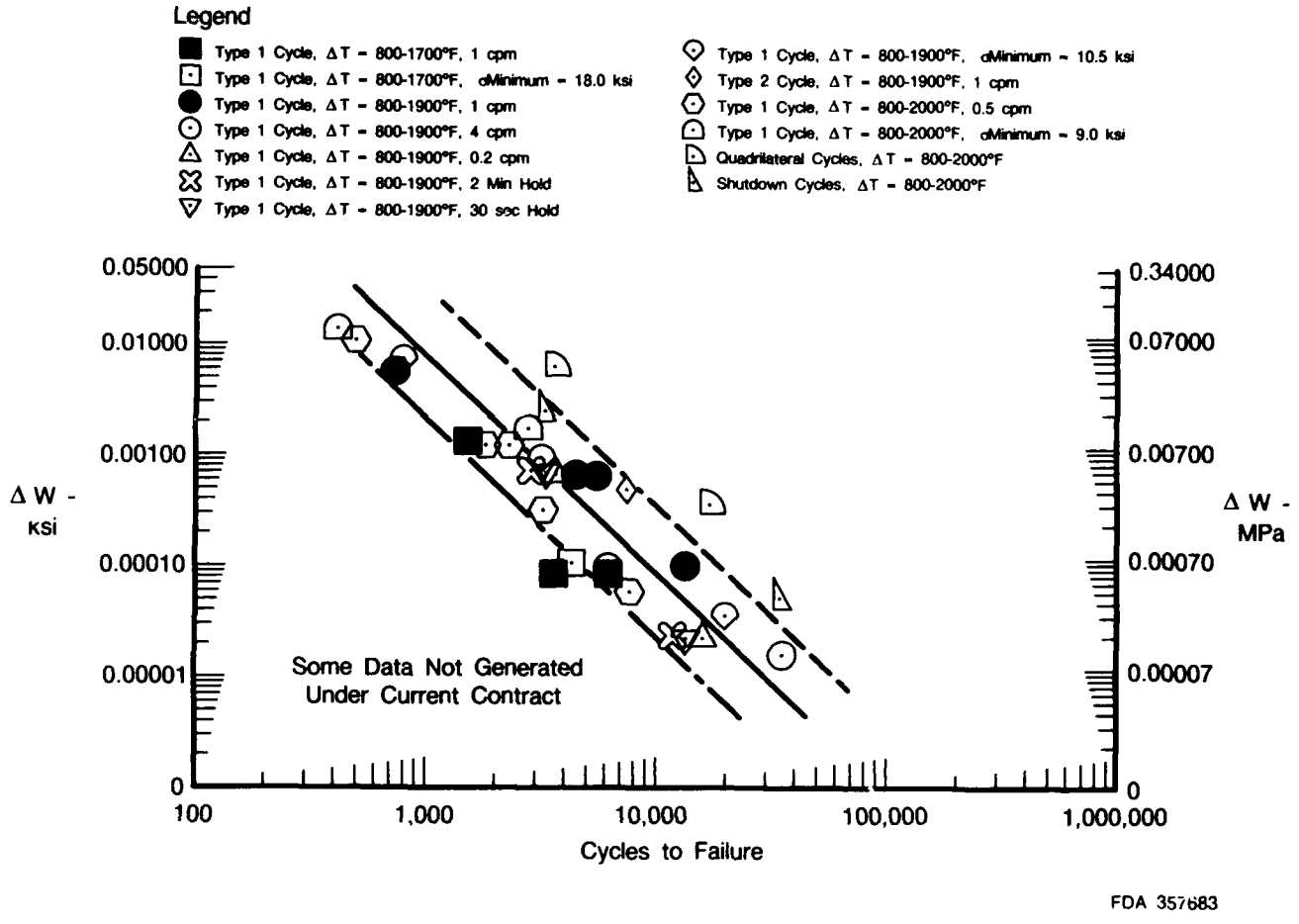

Figure 172. Effective Hysteretic Energy Damage Function Versus Cycles to Failure for Aluminide Coated (PWA 275) PWA 1480 [001], Constitutive Tensile Stress

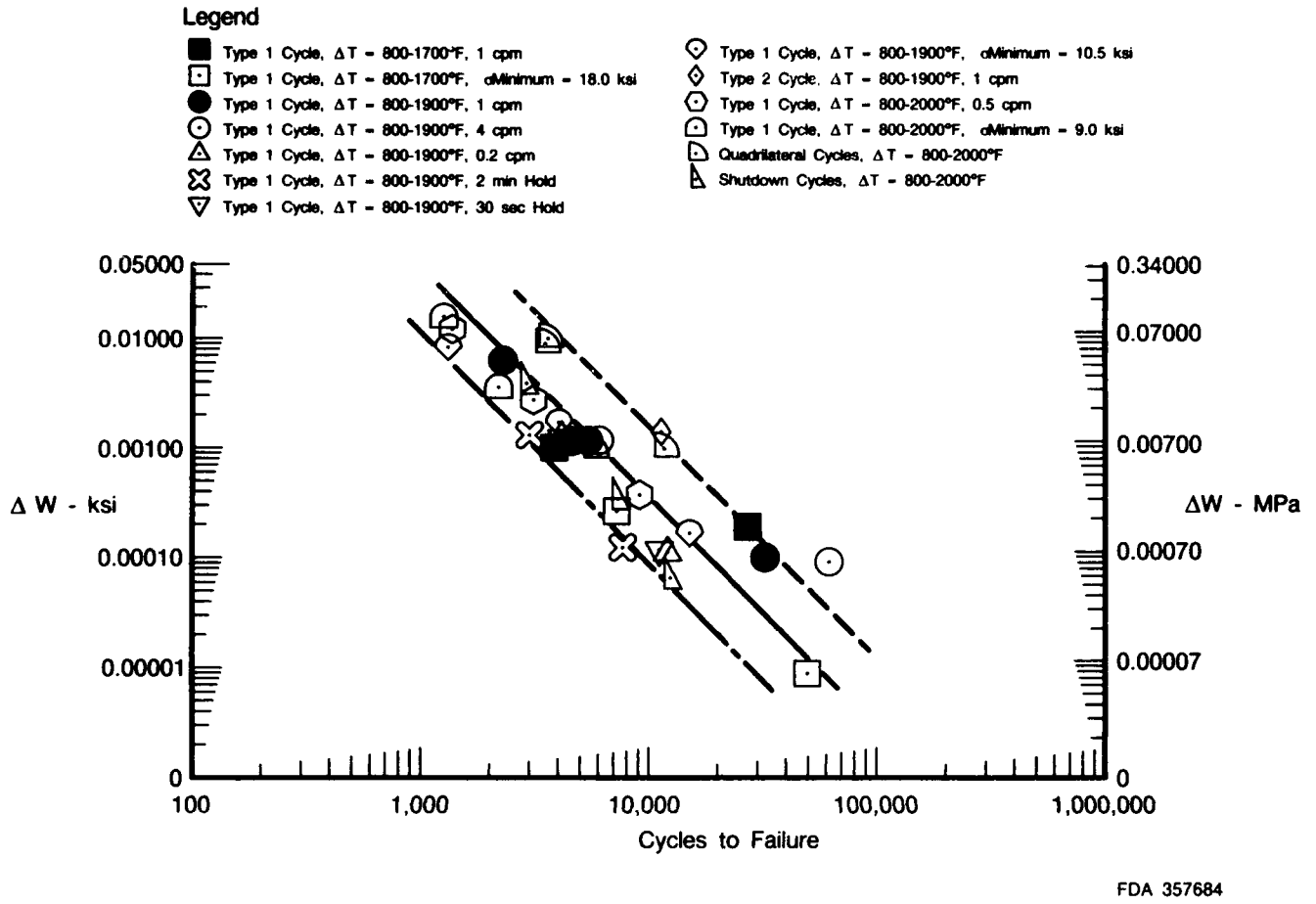

Figure 173. Effective Hysteretic Energy Damage [illegible] on Versus Cycles to Failure for Overlay Coated (PWA 286) PWA 1480 [001], Constitutive Tensile Stress

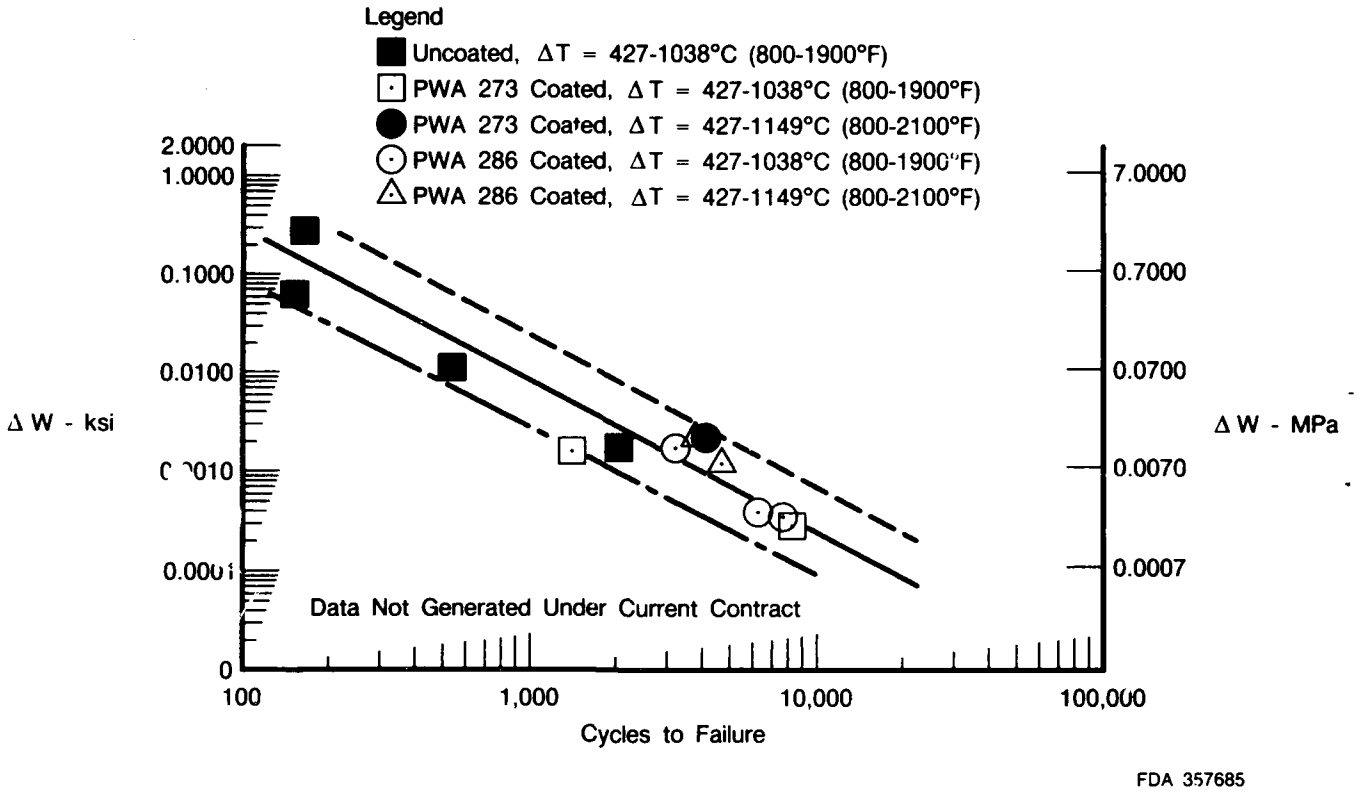

Figure 174. Effective Hysteretic Energy Damage Function Versus Cycles to Failure for PWA 1480 [111] With Various Coatings, Constitutive Tensile Stress

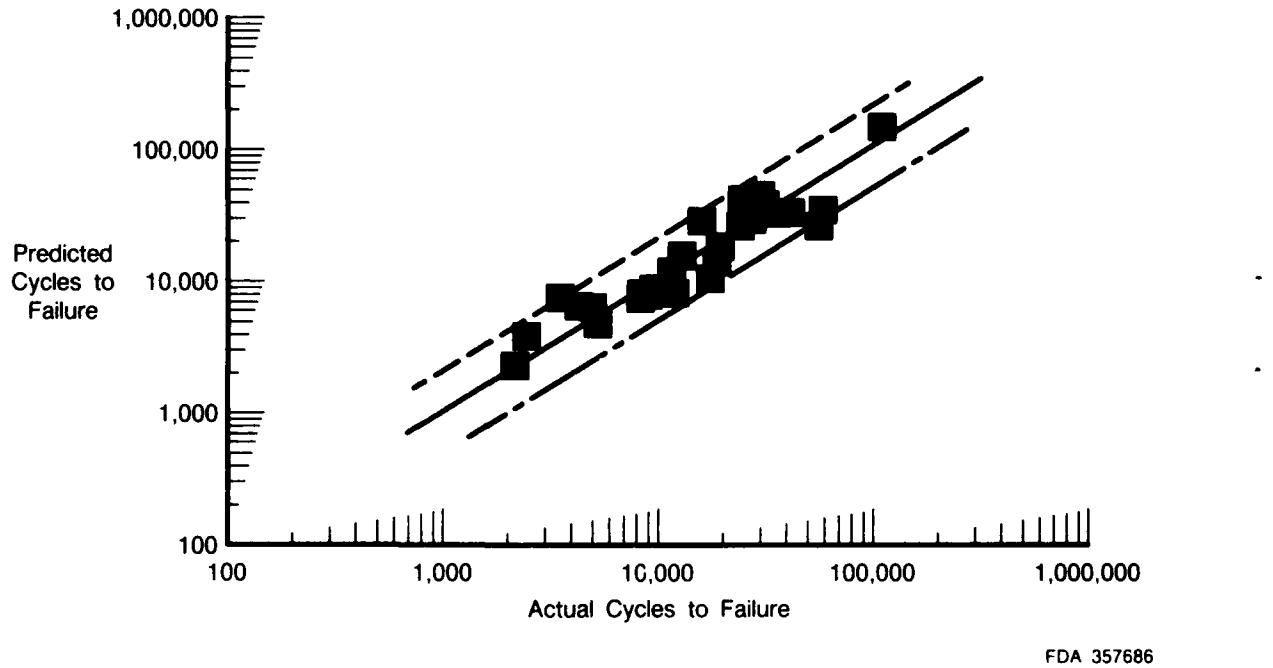

Figure 175. Actual Life Versus Predicted Life for Uncoated PWA 1480 [001] Observed Tensile Stress

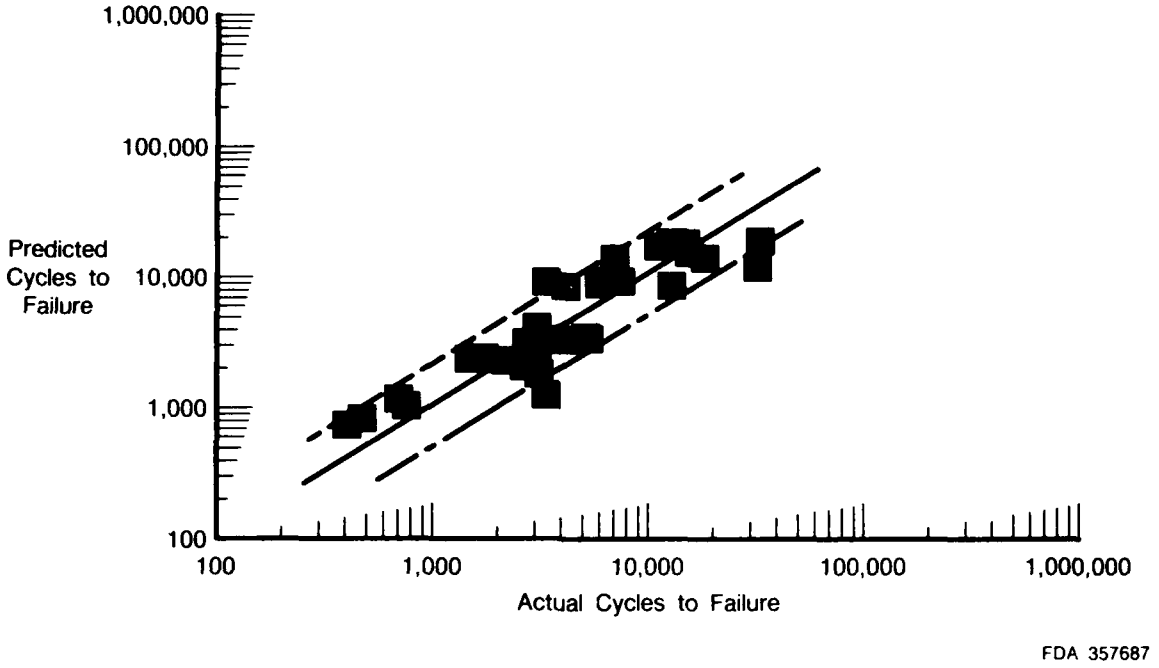

Figure 176. Actual Life Versus Predicted Life for Aluminide Coated (PWA 275) PWA 1480 [001], Observed Tensile Stress

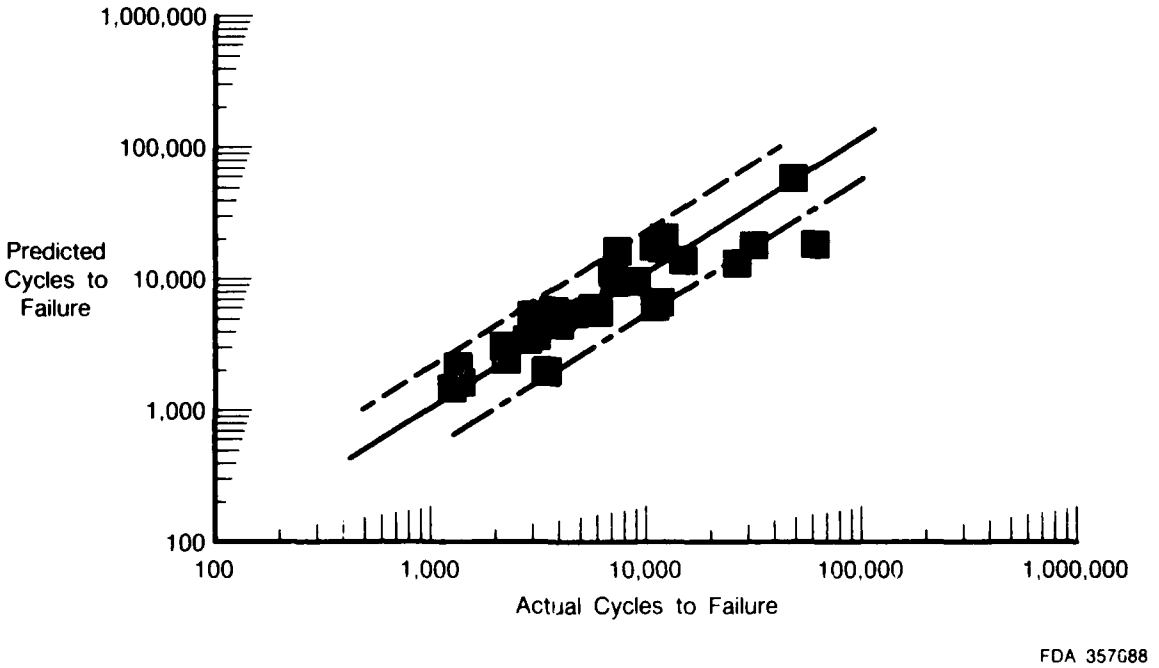

Figure 177. Actual Life Versus Predicted Life for Overlay Coated (PWA 286) PWA 1480 [001], Observed Tensile Stress

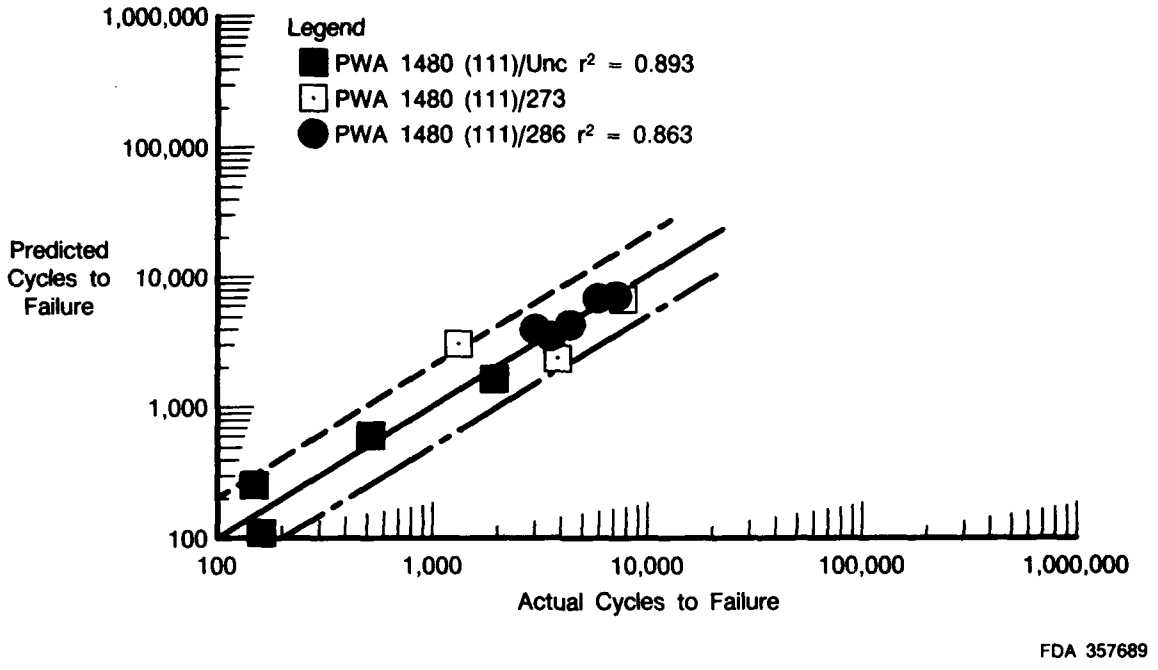

Figure 178. Actual Life Versus Predicted Life for PWA 1480 [111] With Various Coatings, Observed Tensile Stress

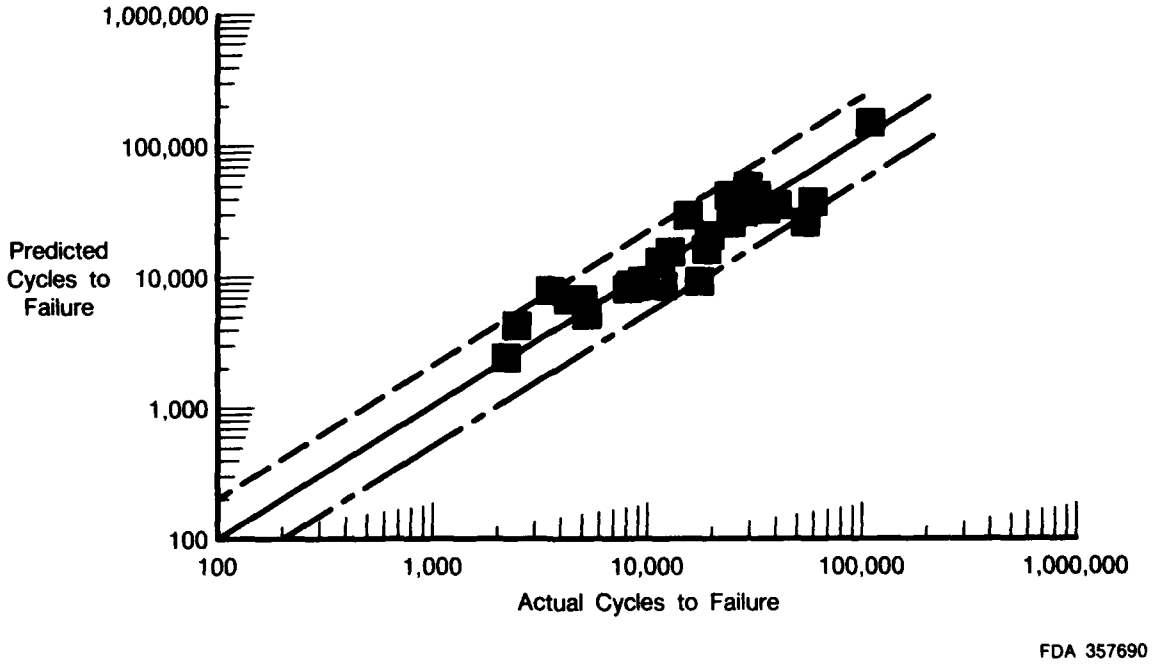

Figure 179. Actual Life Versus Predicted Life for Uncoated PWA 1480 [001] Constitutive Tensile Stress

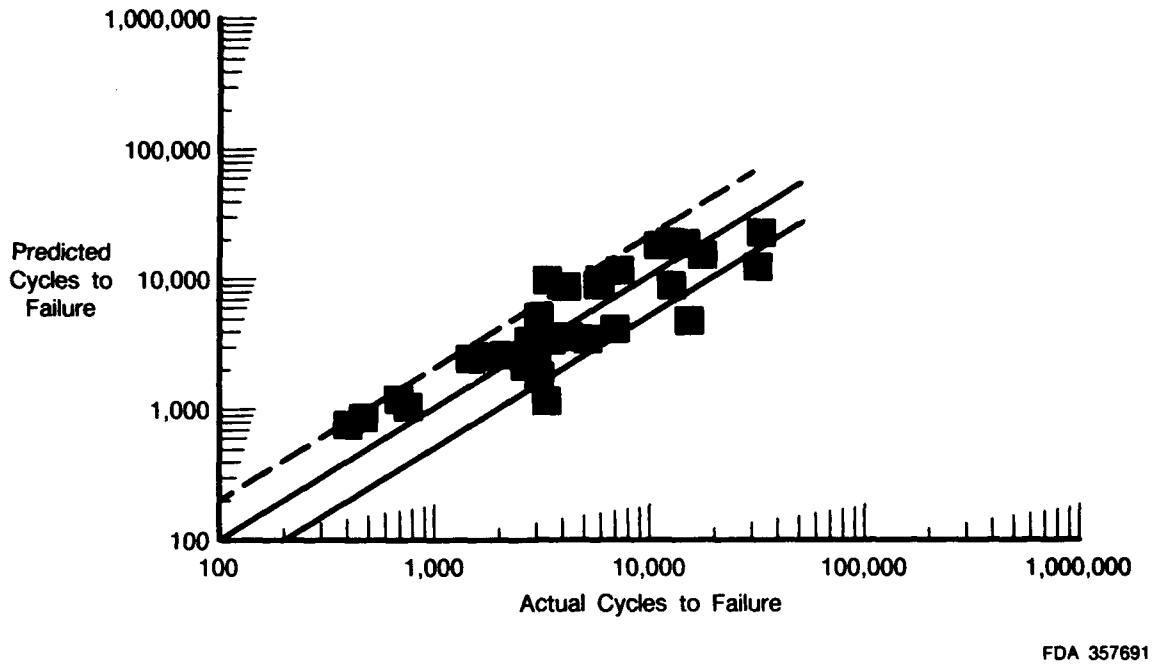

Figure 180. Actual Life Versus Predicted Life for Aluminide Coated (PWA 275) PWA 1480 [001], Constitutive Tensile Stress

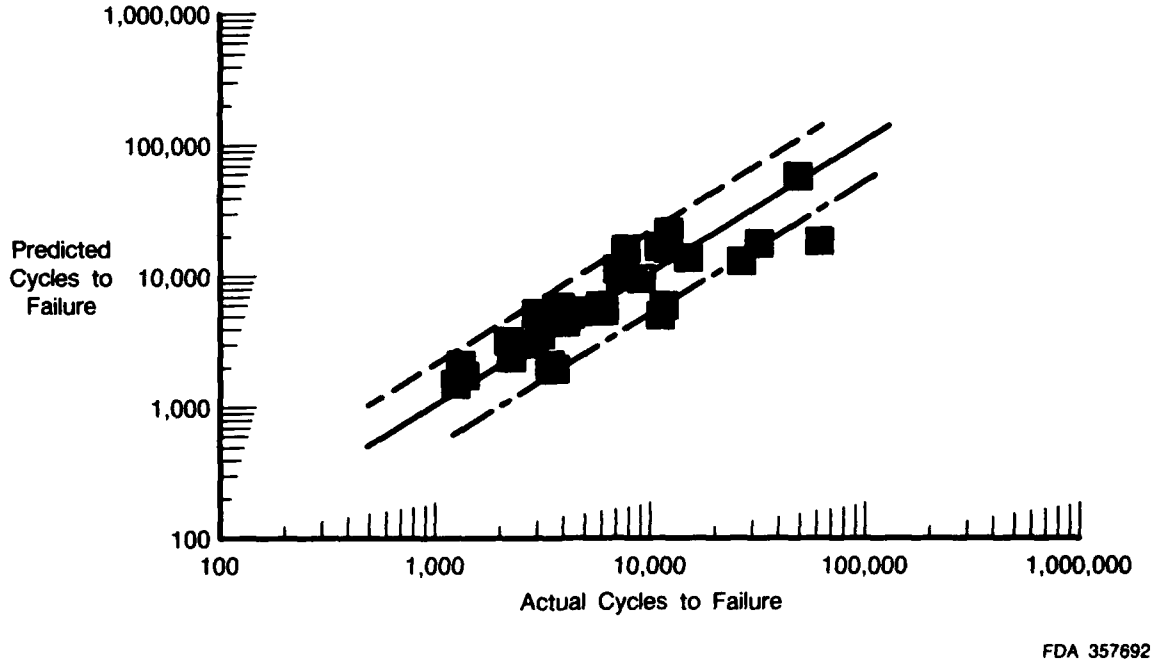

Figure 181. Actual Life Versus Predicted Life for Overlay Coated (PWA 286) PWA 1480 [001], Constitutive Tensile Stress

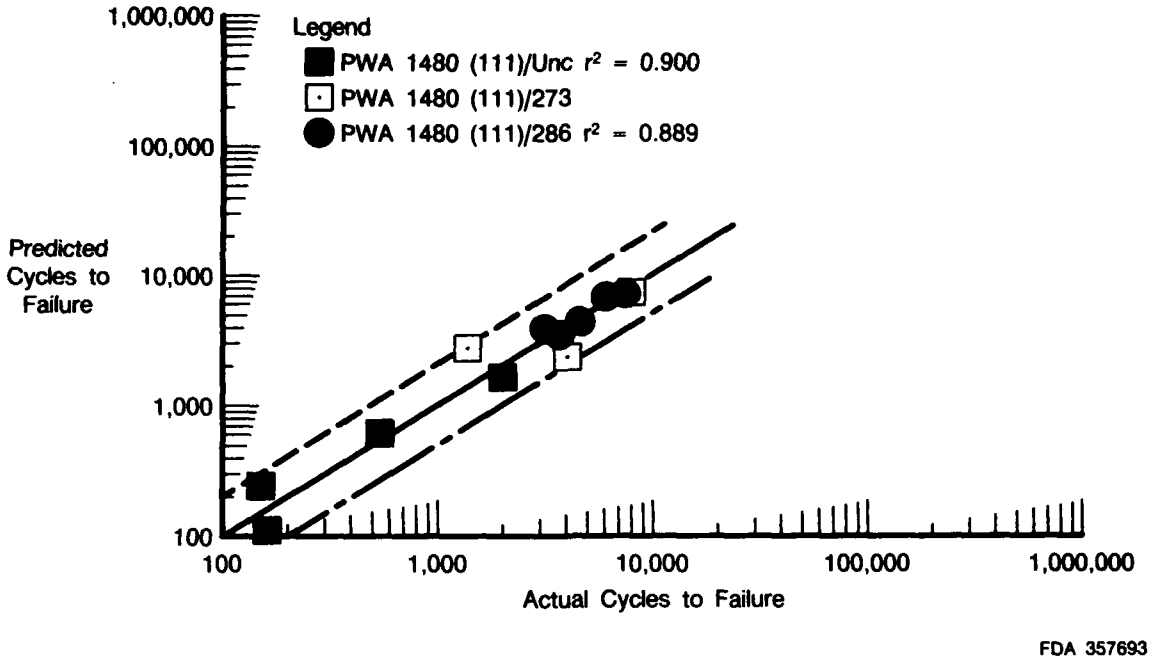

Figure 182. Actual Life Versus Predicted Life for PWA 1480 [111] With Various Coatings, Constitutive Tensile Stress

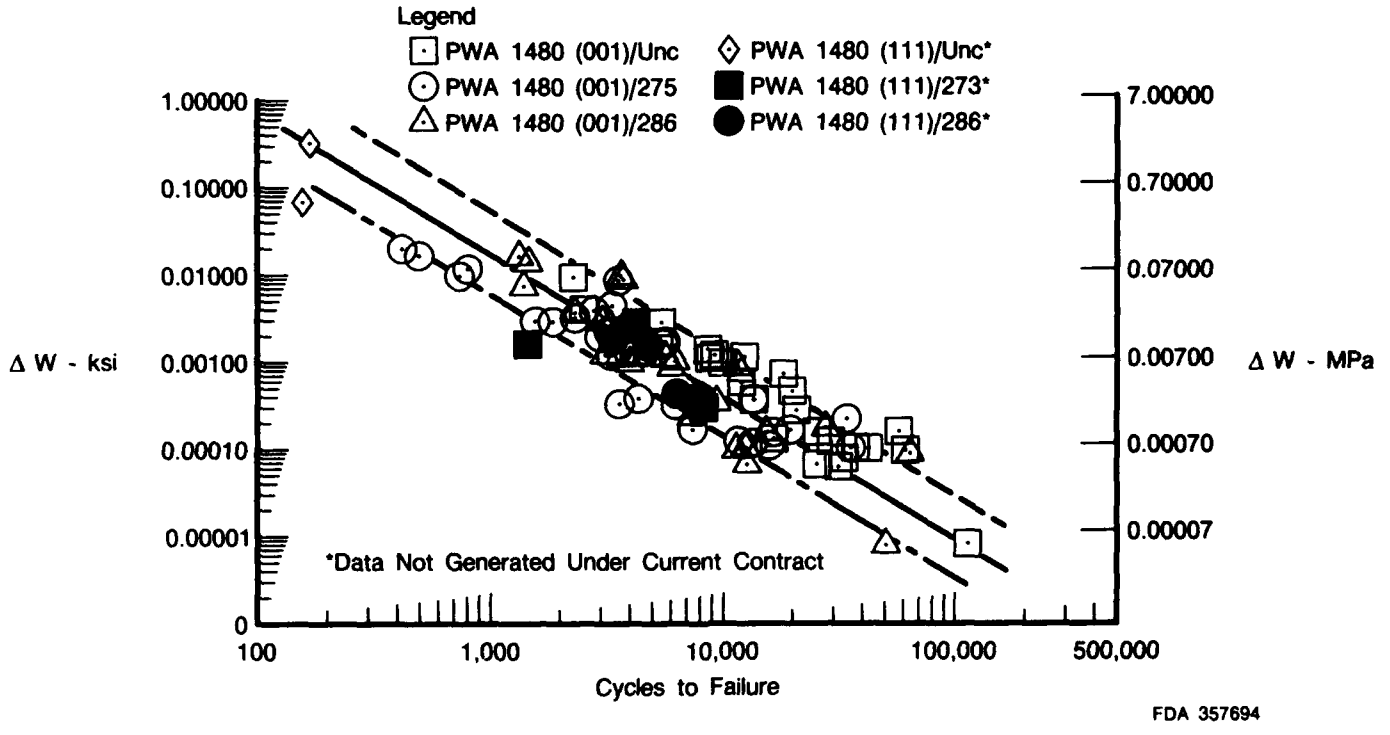

Figure 183. Effective Hysteretic Energy Damage Function Versus Cycles to Failure for PWA 1480 With Various Coatings and Orientations, Observed Tensile Stress

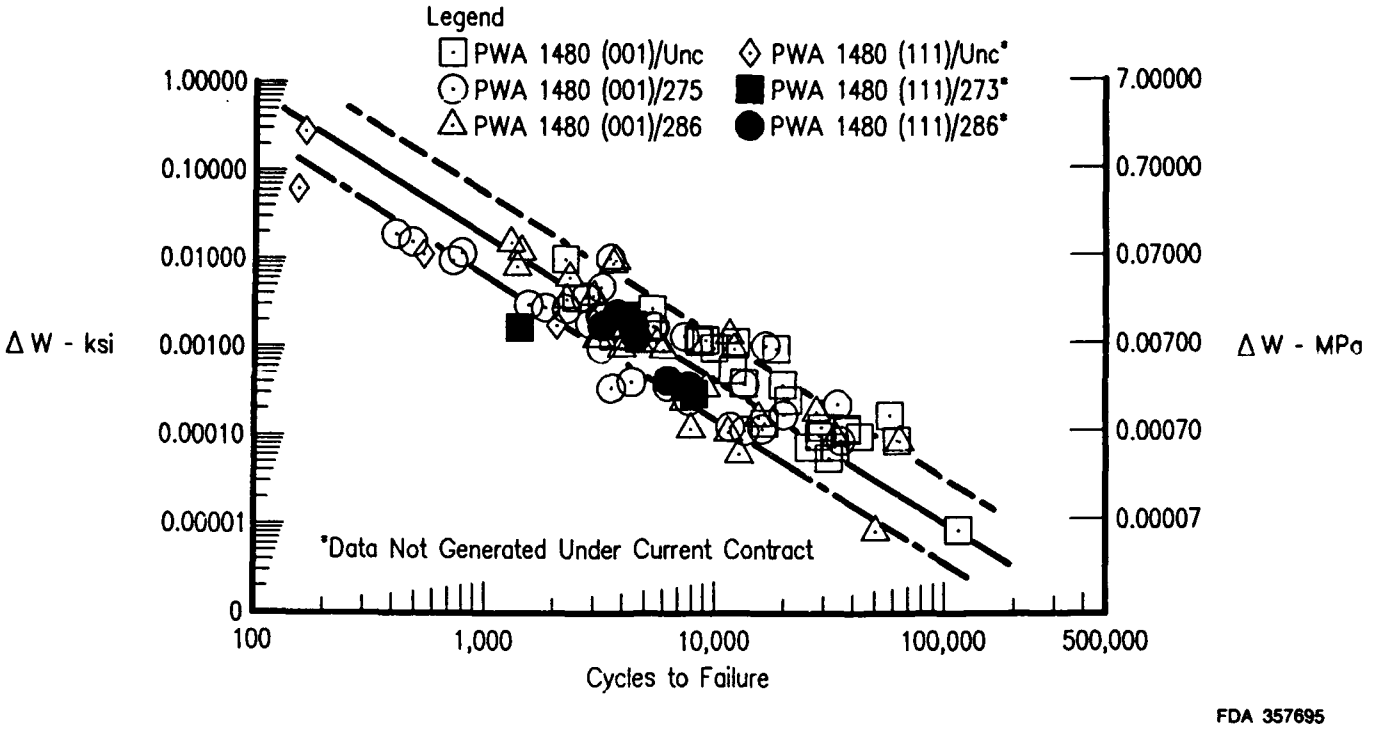

Figure 184. Effective Hysteretic Energy Damage Function Versus Cycles to Failure for PWA 1480 With Various Coatings and Orientations, Constitutive Tensile Stress

2.6 MODEL DEMONSTRATION

In order to demonstrate the predictive capabilities of the hysteretic energy model, two quadrilateral TMF cycles were selected by the Air Force project manager (Figures 185 and 186). The first demonstration cycle, Demo 1 in Figure 185, has a temperature range from 649°C (1200°F) to 1093°C (2000°F), a strain range of 0.8 percent and a 60-second hold time at 982°C (1800°F). The second cycle selected, Demo 2 in Figure 186, has the same temperature and strain ranges as Demo 1 but has a 60 second hold time at 1093°C (2000°F).

Each of the demonstration cycles were run on uncoated PWA 1480 to verify the stresses predicted by the simplified constitutive technique. The life prediction model was specifically not designed to be a constitutive excercise, and therefore the observed test stresses were required to make a life prediction.

Life predictions for the coated and uncoated material were made using both the stresses observed in the testing of the uncoated material and calculated by the simplified constitutive model. The predictions for the fatigue lives for the uncoated and coated material are given in Table 16.

After the predictions were made, the coated material was tested for both of the demonstration cycles. The actual cycles to failure are also listed in Table 16, to directly compare to the life predictions. Figure 187 shows the actual life versus the predicted life for the demonstration tests. The predicted life generally falls within $\pm 2X$ limits and does not exceed $\pm 2.5X$ limits. A comparison of the actual stresses at the half life for each of the tests is compared to the stresses predicted by the simplified constitutive technique in Figure 188. Table 17 contains the actual stresses and predicted stresses for the demonstration tests. Limits of ± 10 ksi are shown around the ideal line.

The stress range is accurately predicted for both the Demo 1 and Demo 2 cycles. This is because the stress range is strongly dependent upon the modulus of the material and is not significantly affected by hold times or cycle shape. A reasonable estimate of the stress range can be obtained from either the modulus at the mean temperature of the cycle or the secant modulus and the total strain range. The stress range for both of these demonstration cycles are predicted to be the same. This is a valid prediction because they have the same temperature and strain limits and, therefore, should have similar stress ranges.

The tensile stress and the mean stress are predicted higher than the actual stresses observed in the test. The mean stress is a combined measure of the stress range and the tensile stress. Therefore, any comments pertaining to the tensile stress also pertain to the mean stress. The simplified constitutive model predicts the same tensile stress for both of the demonstration cycles. In actuality, the tensile stresses for the two cycles are different because of the hold times at different temperatures. In testing the 60-second hold at 1093°C (2000°F) for the Demo 2 cycle does not cause as much stress relaxation as the same hold at 982°C (1800°F) for the Demo 1 cycle. This is because the load is very low (approximately 0 MPa (0 ksi)) while the specimen is at 1093°C and stress relaxation requires some minimum stress level in order to occur. The Demo 1 cycle relaxes to a higher tensile stress than the Demo 2 cycle because there is a larger stress being applied at the temperature where the hold occurs. The simplified constitutive model views these two cycles as being very similar. Because of the two holds, the only difference between the cycles is the small relaxation in stress seen by the Demo 1 cycle. After the first time through the loop, the demonstration cycles become locked into the same loop. The program then uses the hysteretic energy balance to cause the loops to reach the final stress levels. Because the loops are essentially identical, the results of this balancing procedure produce the same stress levels. That is, regardless of where the hold is in the quadrilateral cycle, the tensile stresses are predicted in the same manner. A more complex constitutive technique could improve on this tensile stress prediction.

The observed test tensile stresses, in general, are lower than the predicted tensile stresses. This is because the hysteretic energy balance does not precisely duplicate the stress relaxation seen in the actual test. In one case (S/N 25) the actual tensile stresses were larger than the predicted values. This was caused by intermittent problems with the strain control on this test. Compressive strains were occasionally induced by control problems during the cycle causing larger amounts of stress relaxation. This caused the cycle to relax to a higher tensile stress. Despite the higher tensile stress, the specimen failed at a similar number of cycles to the same test with lower tensile stress (S/N SP2).

The Demo 2 cycles had typically lower tensile stresses than the Demo 1 cycles. According to the hysteretic energy model, this should result in longer lives. Despite the lower tensile stresses seen by the Demo 2 cycles, they had typically shorter lives than the Demo 1 cycles. This decrease in life for the Demo 2 cycle may be due in part to additional damage caused by the hold at the maximum temperature. The hold at an intermediate temperature, as in the Demo 1 cycle, apparently does not cause as much environmental damage as a hold at a higher temperature. A "time-at-temperature" term could account for this effect, but this influence was not found to be important enough to warrant extensive testing during this program. A "time-at-temperature" term could be investigated to account for damage caused by the amount of time at each temperature of the cycle.

Overall, the demonstration tests showed adequate life prediction capability for the model, suitable for design systems and component life prediction use.

TABLE 16. Life predictions for the PWA 1480 (001) Model Demonstration

Coating/Cycle Type	*Predicted Life using Constitutive Stresses –Cycles*	*Predicted Life using Test Stresses –Cycles*	*Actual Life –Cycles*
Uncoated			
Demo 1	5402	5685	8661
Demo 2	5402	5934	5165
PWA 275			
Demo 1	3605	3936	8792
			6199
Demo 2	3605	4255	6177
			3954
PWA 286			
Demo 1	3908	4079	9752
			8903
Demo 2	3908	4229	6070
			5504

R20505/13

TABLE 17. Actual and Predicted Stresses for the PWA 1480 001 Model Demonstration

	Stress Range		Tensile Stress		Mean Stress	
	Actual	Predicted	Actual	Predicted	Actual	Predicted
Coating/Cycle	MPa (ksi)	MPa (ksi)	MPa (ksi)	MPa (ksi)	MPa (ksi)	MPa (ksi)
Uncoated						
Demo 1	652.9 (94.7)	666.7 (96.7)	406.7 (59.0)	444.0 (64.4)	80.7 (11.7)	111.0 (16.1)
Demo 2	639.6 (100.6)	666.7 (96.7)	378.5 (54.9)	444.0 (64.4)	31.7 (4.6)	111.0 (16.1)
PWA 275						
Demo 1	666.7 (96.7)	666.7 (96.7)	429.5 (62.3)	444.0 (64.4)	96.5 (14.0)	111.0(16.1)
	703.3 (102.0)	666.7 (96.7)	457.1 (66.3)	444.0 (64.4)	105.5 (15.3)	111.0 (16.1)
Demo 2	630.9 (91.5)	666.7 (96.7)	335.1 (48.6)	444.0 (64.4)	20.0 (2.9)	111.0 (16.1)
	714.9 (103.7)	666.7 (96.7)	413.7 (60.0)	444.0 (64.4)	56.5 (8.2)	111.0 (16.1)
PWA 286						
Demo 1	623.3 (90.4)	666.7 (96.7)	395.8 (57.4)	444.0 (64.4)	84.1 (12.2)	111.0 (16.1)
	697.1 (98.5)	666.7 (96.7)	586.1 (82.0)	444.0 (64.4)	226.1 (32.8)	111.0 (16.1)
Demo 2	701.9 (101.8)	666.7 (96.7)	392.3 (56.9)	444.0 (64.4)	41.4 (6.0)	111.0 (16.1)
	746.0 (108.2)	666.7 (96.7)	417.8 (60.6)	444.0 (64.4)	42.7 (6.2)	111.0 (16.1)

R20505/13

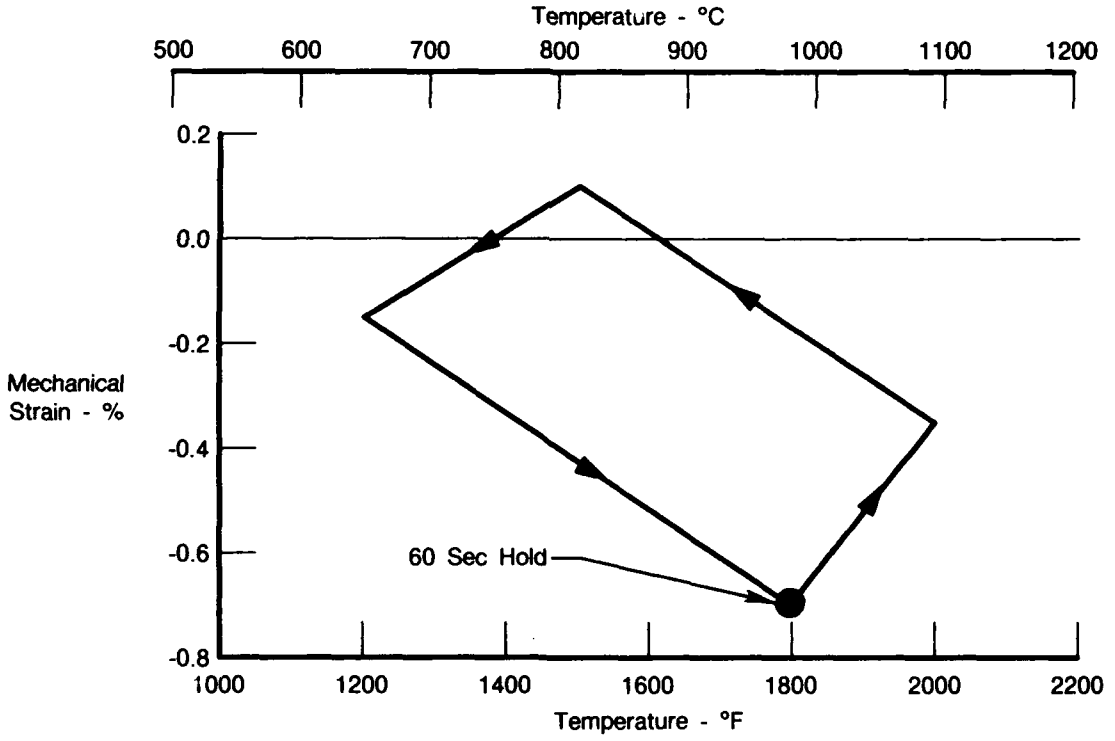

FDA 359396

Figure 185. TMF Model Demonstration Cycle 1 — Quadrilateral with Hold at Minimum Strain

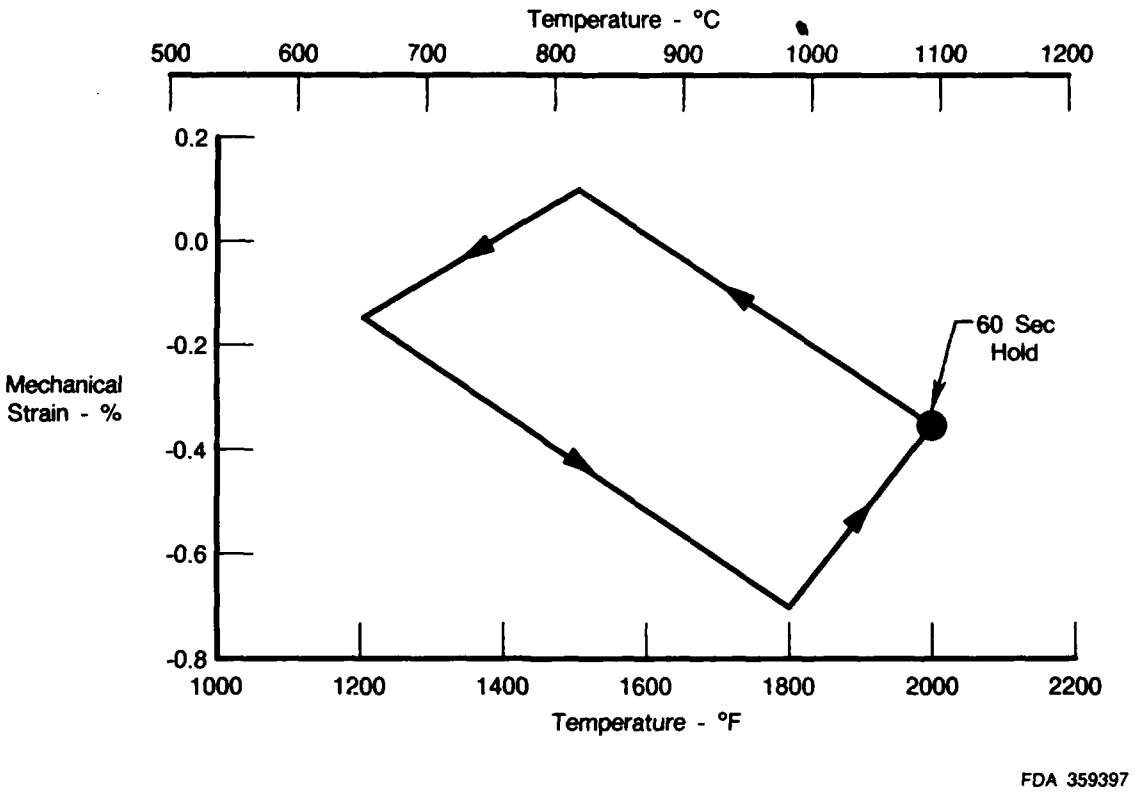

Figure 186. TMF Model Demonstration Cycle 2 — Quadrilateral with Hold at Maximum Temperature

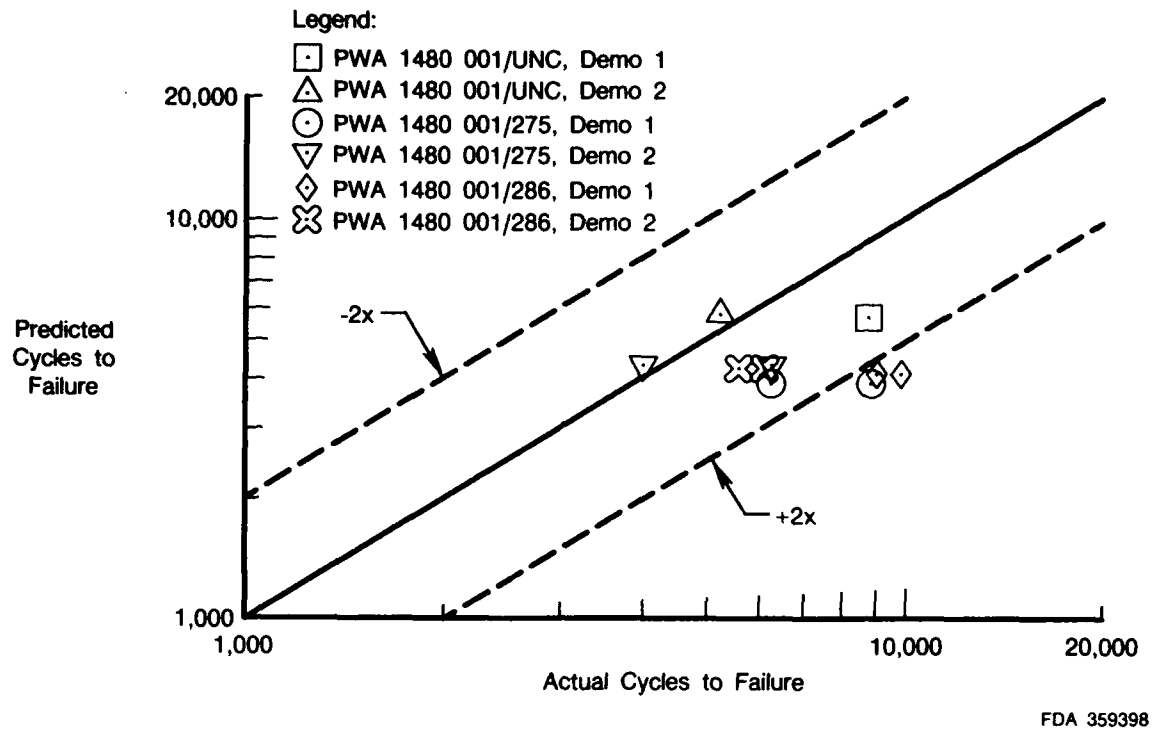

Figure 187. Demonstration Cycles: Actual Life Versis Predicted Life

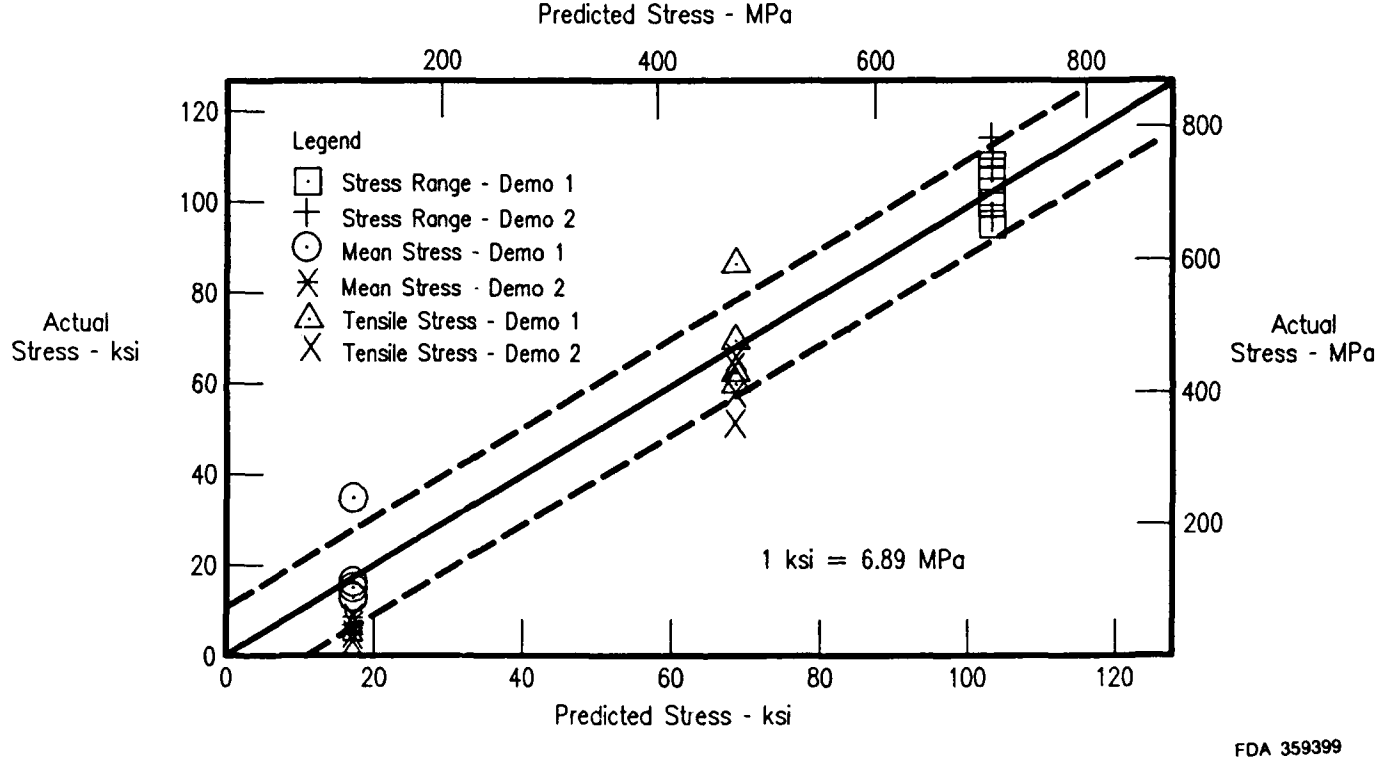

Figure 188. Actual Versus Predicted Stresses for the Demonstration Cycles (Simplified Constitutive Technique)

SECTION 3.0

DISCUSSION OF RESULTS AND RECOMMENDATIONS

The life prediction model developed under Task V of this contract was found to predict thermal mechanical fatigue (TMF) cycles to failure generally within $\pm 2.0X$ for the cycle types that were tested. A discussion of the model and recommendations for future use and development of the model follows.

3.1 MODEL CHARACTERISTICS

This life prediction model is based on the hysteretic energy of the substrate material and the coating. The hysteretic energy of the substrate requires estimates of the tensile stress and the inelastic strain. The coating hysteretic energy term is based on an elastic-perfectly plastic constitutive calculation of the coating hysteresis behavior caused by the thermal mismatch between the coating and the substrate.

The hysteretic energy calculation is most strongly dependent on the determination of the inelastic strain. Determining the inelastic strain is difficult for several reasons. Young's Modulus, E, decreases with temperature and is not constant; therefore, the fraction of the total strain range that is inelastic is difficult to determine. More importantly, inelastic strain for a typical TMF cycle is extremely small and can not be measured accurately from test data. Earlier investigations used the inelastic strain of the mean temperature of the cycle (Reference 6) as an estimate of the inelastic strain for the TMF cycle. The Incremented Inelastic Strain technique, used by this model, essentially averages the inelastic strains associated with a particular total strain range for every 56°C (100°F) temperature increment of the cycle. The inelastic strains at each temperature use Ramburg-Osgood regressions of fully reversed strain controlled isothermal fatigue data evaluated at that temperature. The inelastic strain at a particular temperature can be determined from the stress range. Because the stress ranges of interest can be very low, small variations in the slope of the Ramburg-Osgood stress-strain regressions can result in large variations in the value of the inelastic strain. The cyclic stress-strain regressions must therefore encompass the largest accurately measureable range of inelastic strain possible, and the data analyzed as a family for all temperatures.

The minimum data requirements for the Incremented Inelastic Strain technique are for the substrate material at the orientations of interest as follows:

- Young's modulus versus temperature
- Ramburg-Osgood regressions of fully reversed strain controlled isothermal fatigue (cyclic stress-strain) for various temperatures
- TMF cycle strain and temperature endpoints.

The calculation of the substrate hysteretic energy is also dependent on the value of the peak tensile stress. In the life prediction model, the tensile stress can be determined from two methods. The first method is a direct calculation of the tensile stress from the mean stress and the stress range in the input file. This allows the user to input estimates of the mean stress and the stress range from other predictive techniques or from actual test observations. The second method, developed in this program, is a Simplified Constitutive technique, the details of which have been discussed in Section 2.5. The simplified constitutive technique uses temperature incrementing instead of strain incrementing. The temperature increments are small (5.6°C (10°F)), allowing a more accurate estimate of the stress-strain loop because the modulus calculation is over a smaller increment.

Stress relaxation is used to simulate the actual relaxation of the cycle to its stabilized position. This allows the effect of frequency and hold time to be included in the estimate of the stresses. All of the cycles go through at least one circuit of the loop which includes this simulated stress relaxation.

Some cycles with large scale yielding in the first circuit of the hysteresis loop also yield in the second circuit of the loop. This causes the same values of stress-strain pairs to be calculated repeatedly because the same input for the stress is used after the yield stress is substituted. The Plastic Strain Balancing technique theorized that the stabilized hysteresis loop has equal tensile and compressive inelastic strains. The technique yielded very good estimates for the tensile stress and the stress range. A similar technique is applied to the hysteresis loops which have become "locked" into the same loop by yielding. This technique is based on the theory that the mechanisms which drive the hysteresis loop to its stabilized position are balanced when the loop is stabilized. It is assumed that the tensile and compressive areas of the hysteresis loop characterize these mechanisms. For loops with large amounts of yielding, these areas are easily calculated and balanced. Cycles having small hysteresis loops have large errors introduced by this method because of the small strain increments being calculated, and therefore this method does not work well for loops with little or no yielding. For this reason, the stress relaxation simulation is used for cycles with little or no yielding and the hysteresis balance is used for cycles with large yielding.

Because stress relaxation is not used while the loop is in the balancing routine, the effect of hold time and frequency is included during the first circuit of the loop. The presence of a hold time in a cycle with large yielding increases the size of the hysteresis loop at the hold point. This causes the area on that side to be larger causing the loop to move more to the opposite side and thus simulating stress relaxation. Generally this area is not very large, but it can cause the stress to be overpredicted, as in the model demonstration cycles in Section 2.6.

The data requirements for the Simplified Constitutive technique for the substrate material at the orientations of interest are as follows:

- Young's modulus versus temperature
- 0.2% offset yield strength versus temperature
- Constant strain creep-stress relaxation data at various temperatures where stress relaxation is prominent
- TMF cycle strain and temperature endpoints, and frequency and hold times.

The hysteretic damage parameter for the coating is defined by the Two Bar model, which is detailed in Section 2.5. Differences in the life of the material caused by the coating can be accounted for by determining a contribution of hysteretic energy for the coating to the substrate-coating system. The primary factor in determining the coating damage parameter is the thermal mismatch strain between the substrate and the coating. The thermal mismatch strain and modulus information for the coating is used to determine a constitutive stress-strain loop for the coating. This stress-strain loop is based on elastic-perfectly plastic assumptions. The use of the difference between the tensile and compressive areas as the coating hysteretic energy parameter correlates the effect of different cycle types on coated material behavior. This is because some cycle types introduce less damage to the coating than others. Therefore, some cycles do not have a debit on the substrate life.

The two coatings that were examined in this study exhibit different amounts of control over the behavior of the substrate-coating system. The aluminide coated substrate was more strongly

affected by the its coating than the overlay coated substrate was affected by its coating. This may be because the overlay coating is more evenly ductile over the entire range of temperature than the aluminide coating. The aluminide coating is more prone to cracking at low temperatures than the overlay coating, thus forming more crack initiation in the substrate and reducing the life. It was therefore expected that the aluminide coated data is more strongly affected by the behavior of the coating hysteresis loops than the overlay coated data. The overlay coated data are more affected by the substrate hysteretic energy. In fact, the overlay coated data correlates better without the coating term than with the coating term, but the difference is not significant.

The scaling factors which were used to combine the substrate and coating hysteretic damage reflect the trends described above. A first run at the scale factor is the ratio of the coating area to the substrate area. Additionally, the stronger control of the aluminide coating over the aluminide coated data is reflected by increasing the coating damage term through a scale factor. The overlay behavior is represented by reducing the coating damage term.

The data requirements for the Two Bar model are as follows:

- Young's modulus versus temperature for the coating
- Yield strength versus temperature for the coating
- Mean coefficient of thermal expansion for the coating and the substrate
- TMF cycle strain and temperature endpoints.

The data required for the first scale factor to combine the coating hysteretic damage and substrate hysteretic damage are the cross sectional areas of the coating and the substrate. The second scale factor is based on the behavior of the regressions of the substrate hysteretic energy and the effective hysteretic energy (combined coating and substrate damage using the area ratio only) versus life. If there is a marked improvement in the correlation of the coated data using the effective hysteretic energy, then the effect of increasing or decreasing the coating damage term through the scale factor is examined. The scale factor typically does not improve the correlation coefficient (R squared) by more than 0.02 or 0.04. The scale factor for the coating can be obtained using this iterative technique, or it can be omitted by setting it equal to 1.0.

3.2 LIFE PREDICTION MODEL RESULTS

The parameters which most strongly affected the thermal mechanical fatigue behavior in this test program included maximum temperature, mean stress, hold times, coating type, and cycle type. Frequency and environment did not have the expected strong effects for the test types conducted in this program and therefore, an environmental degradation term could not be separated and included in the model. An experimental degradation term may be needed for other materials.

The maximum temperature of the cycle had the effect of decreasing the TMF life with increasing maximum temperature. This can be attributed to the higher mean stresses caused by increased stress relaxation at higher maximum temperatures. The hysteretic energy based on the substrate only, correlates the uncoated data very well (Figure 147) but some obvious effects can be seen in the coated data (Figures 148 and 149). The substrate hysteretic damage of the coated data have maximum temperature segregation which is very prominent for the aluminide coated data. This is shown in the layering of the data by temperature, with 1093°C (2000°F) data on the top layer and the 927°C (1700°F) data on the bottom layer. The overlay coated data has less conspicuous temperature segregation than the aluminide coated data. This maximum temperature segregation is not apparent for the uncoated material. Therefore, the effect is apparently a coating related behavior. When the two bar coating damage model is applied, the maximum temperature effect is no longer present (Figures 168 and 169).

Mean stress strongly affects TMF behavior. The tests with higher mean stresses had decreased TMF lives. The substrate hysteretic damage accounts for this effect by using the tensile stress in the hysteretic damage term. Some additional effect of mean stress is also accounted for by the octahedral normal stress factor used to normalize crystallographic orientation effects. This is because the octahedral normal stress factor uses the secant modulus which has some resultant effect on the mean stress. For the uncoated data, there is an outlying point which has an offset minimum stress to induce a higher mean stress (Figure 147). This point appears to be part of the overall scatter of the testing, as it becomes closer to the $\pm 2.0X$ limits after the application of the octahedral normal stress factor.

Cycle type also strongly affects TMF behavior, largely by affecting the mean stress and inelastic strains which result. Life for quadrilateral cycles appears to be coating controlled for the aluminide coating (compare Figures 148 and 168), but not so much for the overlay coating (compare Figures 149 and 169). One quadrilateral cycle remains outside of the $\pm 2.0X$ scatter band after the application of the two bar model for the aluminide coated PWA 1480. This can be attributed to experimental scatter. In-phase (Type 2) cycle and out-of-phase (Type 1) cycle lives of various maximum temperatures and frequency were predicted very well for both uncoated and coated data. The shutdown cycles (Type 1 cycle with a constant strain excursion to room temperature) are well behaved for the uncoated and overlay coated data, but one point fell outside the $\pm 2.0X$ limit for the aluminide coated data (Figure 168). The two bar coating damage parameter did not account for this difference which is attributed to experimental scatter.

The effect of hold time and frequency as it changes the mean stress through stress relaxation is accounted for in the model. In most cases the substrate hysteretic energy term absorbs the effect of time at temperature manifested as stress relaxation, but not the effect that time at temperature has on metallurgical properties; i.e., oxidation, diffusion, and microstructural changes. The effect of time at temperature was not quantifiable for the tests that were run in this program, but could account for some of the test data points that lie outside of the $\pm 2.0X$ limits.

The differences in the regression lines of the substrate ΔW versus life for the uncoated and coated material is accounted for by the two bar model. When all of the data are combined for the various coatings and orientations using the final model, the data generally falls within the $\pm 2.0X$ limits. The coating damage term collapses the effect of maximum temperature on the aluminide coated data, but it does not improve the correlation of the overlay coated data. Substrates of differing crystallographic orientations are also correlated by the final model by using the octahedral normal stress factor. Uncoated and coated data of the [111] orientation fall within the $\pm 2.0X$ life limits when compared to data of [001] orientation. This shows that the octahedral normal stress factor works well in correlating TMF data of differing orientations.

3.3 MODEL TESTING REQUIREMENTS

The minimum recommended testing requirements for the life prediction model for new coating-substrate systems is presented in Table 18. The life prediction model requires monotonic properties, isothermal fatigue behavior, and TMF behavior. The majority of the tests are for monotonic properties and isothermal fatigue. A limited number of TMF tests are required to establish the hysteretic energy versus TMF life regression constants. The tests for the substrate are indicated for one crystallographic orientation only, and the substrate tests would have to be repeated at other orientations.

Ideally, the monotonic tests (modulus, yield stress, and thermal expansion coefficient) would have individual values at 56°C (100°F) intervals from room temperature to 1093°C (2000°F), but the minimum number of required tests to establish the shape of the curves could be used. The individual values at the smaller temperature increments would then be interpolated and used in the model.

The creep-stress relaxation data should be obtained at the lowest temperature where creep is observed to the maximum temperature at 56°C (100°F) increments. For PWA 1480, the minimum creep temperature was around 871°C (1600°F). The data should then be regressed giving stress as a function of both time (in seconds) and temperature.

The constant strain isothermal fatigue should be obtained from room temperature to 1093°C (2000°F). The temperature interval size should be decided according to the inelastic strain behavior of the material. Most high strength nickel-based materials have little variation in cyclic stress-strain behavior from room temperature to around 427°C (800°F). Therefore, isothermal fatigue tests do not have to be conducted at small intervals at low temperatures. At higher temperatures, more tests should be conducted. Each of the lines should then be regressed using the Ramburg-Osgood technique to define inelastic strain in terms of stress range.

The TMF tests to establish the regression constants for the life prediction model should include the effects of temperature, mean stress, frequency, hold times and cycle type. At least two different maximum temperatures should be tested at three strain ranges using out-of-phase cycles to define baseline results. To establish the effects of mean stress, two offset minimum stresses associated with two temperatures should be tested at two strains for each temperature using Type 1 cycles. Two alternate frequencies and two hold times should be tested at two strain ranges using Type 1 cycles. Quadrilateral cycles at two strain ranges should be tested to compare to Type 1 results to determine cycle type effects. Other generic mission cycle types could be substituted for quadrilateral cycles depending upon user applications.

TABLE 18. Life Prediction Model Testing Requirements

Property	*Conditions*	*Uncoated Substrate*	*Coating*	*Coated Substrate*
Modulus	RT to 1093°C (RT to 2000°F)	X	X	0
0.2% Offset Yield Stress	RT to 1093°C (RT to 2000°F)	X	X	0
Thermal Expansion Coefficient	RT to 1093°C (RT to 2000°F)	X	X	0
Constant Strain Creep-Stress Relaxation	871 to 1093°C (1600 to 2000°F)	X	0	0
Constant Strain Isothermal Fatigue	RT to 1093°C (RT to 2000°F)	X	0	0
Thermal Mechanical Fatigue	T_{min} to T_{max1} Type 1, Freq= f_1	3	0	3
	T_{min} to T_{max2} Type 1, Freq= f_1	3	0	3
	T_{min} to T_{max1} Type 1, $\sigma_{min} = \sigma_1$	2	0	2
	T_{min} to T_{max2} Type 1, $\sigma_{min} = \sigma_2$	2	0	2
	T_{min} to T_{max1} Type 1, Freq= f_2	2	0	2
	T_{min} to T_{max1} Type 1, Freq= f_3	2	0	2
	T_{min} to T_{max1} Type 1, Hold= h_1	2	0	2
	T_{min} to T_{max1} Type 1, Hold= h_2	2	0	2
	Quadrilateral Cycle	2	0	2

R20506/9

3.4 RECOMMENDATIONS

The hysteretic energy based life prediction model has some deficiencies which were illustrated by the model demonstration. Significant improvements to the model could be made as follows:

1. Time at Temperature Term — A term which includes the damage energy caused by the amount of time that the part spends at high temperature. This may be an oxidation related process which may be quantified by more tests having holds at different points of the TMF cycle. This could improve the prediction of Type I cycles and Quadrilateral cycles with and without hold times.

2. Two Bar Model — The Two Bar model may be improved by relating the coating stress to the substrate stress and determining the effect of the coating behavior on the substrate hysteretic energy directly. A combination of the hysteretic damage for the coating and the substrate would not be necessary.

3. Fracture Mechanics Extension of the Model — The hysteretic energy term is based on elastic behavior of the material which is related to cyclic fracture energy and therefore related to stress intensity and the J integral. This model could later be adpated to crack propagation models.

4. Constitutive Model — A more comprehensive constitutive model would improve the stress prediction of this model for the calculation of the hysteretic energy. The results of advanced constitutive research, such as the NASA HOST program, could be used with this model.

SECTION 4.0

CONCLUSIONS

The experimental testing performed for this program revealed critical parameters which affect the thermal mechanical fatigue (TMF) behavior of coated and uncoated PWA 1480. These parameters included mean stress, maximum temperature, hold times, coating type, and cycle type. Frequency and environment did not have as significant an effect as the other parameters. The effects of these critical parameters on TMF behavior are described below.

Higher mean stresses decrease the life, as was expected. Higher maximum temperatures also decreased the TMF life by decreasing the strength capabilities of the material and by increasing the mean stress through stress relaxation. Hold times at the maximum temperature had a similar effect of increasing the mean stress through stress relaxation, thus decreasing the TMF life. An environment effect during the hold times was investigated but could not be separated as a distinct effect. These effects causing higher stress were taken into account by the life prediction model primarily through the hysteretic energy calculation of the substrate material which is based on both the tensile stress and the inelastic strain.

The presence of a coating on the PWA 1480 also reduced the TMF life. In general, the aluminide coating (PWA 275) degraded the TMF behavior more than the overlay coating (PWA 286) at the thicknesses that were investigated in this program. The life degradation of the coating is incorporated in the life prediction model through the Two Bar model. A coating damage term is determined and linearly combined with the substrate hysteretic damage term to produce an "effective" hysteretic damage parameter for the coating-substrate system.

The cycle type strongly affects the TMF behavior of coated and uncoated PWA 1480. Quadrilateral cycles had typically longer lives than standard out-of-phase cycles for similar strain ranges. They also see much more compressive damage, characterized by severe coating damage and spallation at higher strain ranges. The effect of cycle type was also accounted for in the model by determining the substrate hysteretic damage for each leg of the cycle separately and by including the compressive hysteretic energy of the coating in the coating damage term.

It should be noted that the hysteretic energy model used in the life prediction program is strongly dependent upon accurate determination of the inelastic strain of the substrate material. The calculation of the inelastic strain by the incremented method provides an average of the inelastic strains associated with the total mechanical strain range at each 56°C (100°F) increment. This "average" inelastic strain allows the interaction of the maximum temperature of the cycle and temperature range to be included in the model. The inelastic strain is weighted toward the high temperature end of the cycle.

The life prediction model based on the hysteretic energy approach was able to predict the TMF life for the cycles that were tested generally within ± 2.0X (Figure 183). The cycles selected to demonstrate the model were also predicted to within ± 2.0X with three of the eight tests falling just outside the 2.0X limits. It can be concluded that this model predicts the thermal mechanical fatigue life for coated blade materials within reasonable limits.

LIST OF REFERENCES

(1) Pejsa, P. N., and B. A. Cowles, "Thermal Mechanical Fatigue Life Prediction for Advanced Anisotropic Turbine Alloys," *Transactions of ASME: Journal of Engineering for Gas Turbines and Power,* Vol 108, July 1986, pp 504-506.

(2) Soechting, F. O., "Turbine Low Cycle Fatigue Design Program," Final Report — Contract F33615-81-C-2018 Air Force Wright Aeronautical Laboratories, October 1986.

(3) Cowles, B. A., J R. Warren and F. K. Haake, "Evaluation of the Cyclic Behavior of Aircraft Turbine Disk Alloys," NASA CR-165123, NASA-Lewis Research Center Contract NAS3-21379, August 1980.

(4) DeLuca, D. P. et al, "Fatigue and Fracture of Advanced Blade Alloys," Final Report AFWAL-TR-84-4167, AFWAL/MLLN Contract F33615-82-C-5109, February 1985.

(5) Ostergren, W. J., "A Damage Function and Associated Failure Equations for Predicting Hold Time and Frequency Effects in Elevated Temperature, Low Cycle Fatigue," *Journal of Testing and Evaluation,* JTEVA, Vol. 4, No. 5, September 1976, pp 327-339.

(6) Pejsa, P. N., "Development of Hysteretic Energy-Based Model for Simple TMF Mission Cycle Life Prediction," Pratt & Whitney ME&T Report No. 25723, February 22, 1984.

(7) Morrow, J. D., "Cyclic Plastic Strain Energy and Fatigue of Metals," *Internal Friction, Damping, and Cyclic Plasticity,* ASTM STP No. 378 American Society for Testing and Materials, 1965.

(8) Palmgren, A., *Ball and Roller Bearing Engineering,* Translated by G. Palmgren and B. Ruly, SKF Industries, Philadelphia, PA, 1945, pp 82-83.

(9) Miner, M. A., "Cumulative Damage in Fatigue," *ASME Journal of Applied Mechanics,* Vol. 12, September 1945, pp A-159-164.

(10) Gemma, A. E., B. S. Langer, and G. R. Leverant, "Thermo-Mechanical Fatigue Crack Propagation in an Anisotropic (Directionally Solidified) Nickel-Base Superalloy," *Thermal Fatigue of Materials and Components,* ASTM STP 612, A. Spera and D. F. Mowbray, Eds., American Society for Testing and Materials, 1976, pp 199-213.

(11) Meyer, T. G., D. M. Nissley, and G. A. Swanson, "High Temperature Constitutive and Crack Initiation Modeling of Coated Single Crystal Superalloys," Pratt & Whitney NASA Contract NAS3-23939, (unpublished).